The Influence of Particle Type and Process Conditions on Electrodeposited Composite Coatings

by

Roberto Morana

A Doctoral Thesis

Submitted in partial fulfilment of the requirements

For the award of

Doctor of Philosophy of Loughborough University

January 2006

Supervisor: Dr. G.D. Wilcox

Institute of Polymer Technology and Materials Engineering

Loughborough University

Synopsis

Composite materials are usually multi-phase materials, made up from two or more phases, which are combined to provide properties that the individual constituents cannot. This technology represents an economical way to improve product performances avoiding the use of expensive materials. Composite materials can be obtained as films by means of the electrolysis of electroplating solutions in which micrometre- or submicrometre-size particles are suspended: variable amounts of these particles become incorporated in the electrochemically produced solid phase, to which they impart enhanced properties. The main aims of the present work contributing to this thesis are the study of different parameters influencing the electroco-deposition process in order to promote and improve the applicability of such a technology in the high speed electroplating industry.

Following a comprehensive review on the electroco-deposition of composite coatings, the phenomena have been analysed moving from a microscopic point of view i.e. the role of the metal ions present in the electrolyte and adsorption on the inert particles and their interactions with the growing metal layer, to a macroscopic point of view i.e. the electrolyte agitation, its influence on particle motion and all the issues related to the presence of particles in an electrolyte during electroplating. In particular the inert particle influence in terms of geometry, dimension and chemical nature (spherical polystyrene particles *vs.* irregular alumina particles with different dimensions), the metal matrix influence (nickel, copper and zinc), the influence of electrolyte agitation (using a Rotating Cylinder Electrode cell system) and the influence of the coating thickness on particle content in the final coating, using different deposition times, have been examined.

The importance of the particle shape has been highlighted showing how incorporating irregular geometries gave higher particle incorporation densities than regular geometries. The influence of the substrate finishing in terms of imperfections has been related to the particle incorporation rate showing how small surface imperfections enhanced the incorporation of particles. Different hydrodynamic regimes have been analysed resulting three different regimes being discerned:

laminar, transitional and turbulent. The consequence, in terms of particle incorporation levels, has been found showing how the amount of particles in the coating changed from one regime to another. Different rate-determining steps were related to the hydrodynamics: when the regime is laminar, particles were incorporated as agglomerates and the process was under particle transfer control, whilst in the turbulent zone, the rate determining step was the velocity of reduction of the ions adsorbed on the particle surface.

Keywords: electrolytic deposition, composite coatings, electroco-deposition, rotating cylinder electrode, electrolyte agitation, image analysis, alumina, polystyrene, centrifugal forces.

Acknowledgements

I wish to express my sincere gratitude to my supervisor, Dr. G.D. Wilcox for his kind help, guidance and constant encouragement throughout the course of the research programme.

I would also like to express my gratitude to Loughborough University, EPSRC and Corus (Ijmuiden – The Netherlands) for providing financial support to this project. Thanks are also due to I. Portegies Zwart, J. Miedema, K. Schnetz, M. Huisert and all the people I've met during the time spent in Corus (Ijmuiden – The Netherlands) for their encouragement, assistance, collaboration and for the kind hospitality they have offered to me.

In addition, much is owed to my colleagues and the technical staff within the department for their support.

Roberto Morana

January 2006

Dedicated to the girl with the blue hair, she knows, and to my Dad.

Table of notation

Symbols

a	Particle density in eq. 4.6
a_p	Particle radius, μm
A	Parameter related to the gravitational forces in eq. 4.27, or parameter related to gravitational force in eq. 4.32
B	Volume percentage of embedded particles, or parameter related to the diffusion flux in eq. 4.27, or parameter related to particle diffusion in eq. 4.32
b	Rate of agitation in eq. 4.6
c_i	Concentration of a ionic species *i* in bulk electrolyte, mol dm^{-3}
$C_{p,b}$, *or* C_p^{∞}	Concentration of particles in bulk electrolyte, mol dm^{-3}
$C_{p,s}$	Concentration of particles at cathode surface, mol dm^{-3}
C_s	Concentration of electroactive species adsorbed on the particle surface, mol l^{-1}
D	Diffusion coefficient, $cm^2\ s^{-1}$
D_p	Particle diffusion coefficient, $cm^2\ s^{-1}$
E	Equivalent weight
E_i	Electrode potential, J mol^{-1}
E_e	Equilibrium potential, J mol^{-1}
ΔE	Change in potential
f	Friction coefficient
F	Faraday constant, 96490 C mol^{-1}
F_D, *or* F_d	Diffusional force, J $mol^{-1}\ cm^{-1}$
F_{adh}	Force of adhesion, N
F_{shear}	Hydrodynamical force due to the various shear flows, N
F_{stagn}	Hydrodynamical force due to the stagnation point flow, N
F_{total}	Net force acting on a particle, N
g	Acceleration due to the gravity, m s^2
H	Variable related to bath agitation
$\vec{i}$	Unit vector
i_0	Exchange current density, A dm^{-2}
j	Current density, A dm^{-2}
j_p, *or* J_p	Particles flux, mol $cm^{-2}\ s^{-1}$
J	Diffusion flux, mol $cm^{-2}\ s^{-1}$
k	Certain amount of ions, or static coefficient of friction
k^*	Variable depending on the intensity of the particle-cathode interaction
k_B	Boltzmann's constant
k_p	Driving force for particle co-deposition
K_0	Standard electrochemical reaction rate constant
K	Total amount of ions
m	Mass of a particle, g
N^*	Collision rate of particle co-deposition
N_A	Avogadro's number
N_p	Number of particles arriving at the cathode surface

p	Probability of a particle crossing the diffusion layer, or fluid pressure in annulus
p_0	Uniform pressure of the fluid in annulus when the system is at rest
Q	Coulombs
q	Adsorbed charge density
r	Particle radius, μm
r_p	Particle radial position in cylindrical coordinates
R	Gas constant, 8.314 J K^{-1} mol^{-1}, or distance from cathode axis
R_i	Number of particles immobilised
R_r	Number of particles removed
S_b	Bond strength per unit area
T	Temperature, K
t	Time, sec
v_θ	Fluid tangential velocity in annulus, cm s^{-1}
v_R	Radial tangential velocity in annulus, cm s^{-1}
v_∞	Contribution to particle velocity due to fluid motion, cm sec^{-1}
V_p	Particle adsorption rate, mol s^{-1}
V_P	Total volume of particles in the final coating, cm^3
$V_{m,M}$	Molar volume of the metal film
V_{metal}	Volume of deposited metal matrix, cm^3
w	Rotation rate of the electrode, sec^{-1}
W	Work done to transport a mole of species, J mol^{-1}, or grams of substance
W_p	Weight of one particle, g
x	Distance from the cathode, cm
$x_{d,l}$	Diffusion layer thickness, μm
x_V	Volume fraction of particles in the final coating
z	Charge on the metal ion
Z	Valency of an ionic species

Greek

α'	Loose adsorption surface coverage
β_p	Constant in eq. 4.2
β_m	Tafel constant for metal deposition
δ	Diffusion layer thickness, μm
ϕ	Experimental term in eq. 4.11
η	Overpotential
η_a	Anodic overpotential
η_c	Cathodic overpotential
μ	Chemical potential, J mol^{-1}, or dynamic viscosity g m^{-1} sec^{-1}
ν	Absolute viscosity m^2 sec^{-1}
ν_0	Constant in eq. 4.2
ω	Cathode angular velocity, rpm
ϑ	Strong adsorption surface coverage
ρ	Density of a particle, g cm^{-3}
ρ_0	Uniform density of the fluid in annulus when the system is at rest, g cm^{-3}
ξ	Parameter related to the distance from cathode axis

ψ	Potential in eq.2.7, defined as the work to be done to bring a unit positive charge from infinity to the particular point, J mol^{-1}

Abbreviations

AAS	Atomic absorption spectrometry
ACR	Anode circumference rotation
AZTAB	4-Ethylazobenzene-4'- (oxyethyl) trimethylammonium bromide
CE	Current efficiency
CECD	Conventional electroco-deposition
CETAC	Hexadecyltrimethylammoniumchloride
CMCD	Compositionally modulated composite deposits
CR	Cathode rotation
DC/PC	Direct current / Pulsed current
DSC	Differential scanning calorimetry
EDTA	Ethylenediamine tetra acetic acid
EDX	Energy dispersive X-ray spectroscopy
EIPET	Electrode-ion-particle-electron-transfer model
EIS	Electrochemical impedance spectroscopy
FEG-SEM	Field emission gun scanning electron microscope
HA	Hydroxyapatite
IR	Infrared spectroscopy
IRRAS	Infrared reflection absorption spectroscopy
OFHC	Oxygen-free high conductivity
RCE	Rotating cylinder electrode
SCE	Saturated calomel electrode (+0.242 mV with respect to the standard hydrogen electrode at 25 °C)
SEM	Scanning electron microscope
PTFE	Poly-tetra-fluoro-ethylene
PS	Polystyrene
PZC	Point of zero charge
TEPA	Tetraethylene pentamine

List of Figures

Table of contents

1. Introduction to composite materials and composite coating technologies

Composite materials are usually multi-phase materials, made up from two or more phases, which are combined to provide properties that the individual constituents cannot. This technology represents an economical way to improve product performances avoiding the use of more expensive materials. Composite materials can be obtained as films by means of the electrolysis of electroplating solutions in which micrometre- or submicrometre-size particles (typically particulates of oxides, carbides and nitrites, graphite or organic particles like polystyrene (PS) and Poly-tetra-fluoro-ethylene (PTFE)) are suspended: variable amounts of these particles become incorporated in the electrochemically produced solid phase, to which they impart enhanced properties. Comparing the process with others able to produce composite materials (i.e. metal spraying, dipping techniques, vacuum processes), electroco-deposition provides the significant advantage of avoiding heat-treating of the parts and thus thermal damage to the components. It is a technique able to successfully coat complex geometrical forms with high uniformity of thickness with the reduction of waste often associated with the other processes.

Electroco-deposition can be traced back to the earlier days of conventional electroplating (the formation of rough deposits for conventional electrodeposition, in fact, were always attributed to the presence of particulate impurities in the electrolyte), but the first composite coatings produced with the purpose of gaining a certain benefit were by FINK AND PRINCE [1] in 1928, when they deposited a self-lubricating copper coating containing graphite. Since the late 1960s, there has been a marked increase in the interest in composite electroplating technology, with electroless composite coating-technology gaining popularity from the early 1970s [3]. For a long period of time, the work carried out in this field was aimed almost entirely to the production of wear- and corrosion-resistant coatings, self-lubricating layers and dispersion-strengthened coatings mainly for the aerospace industry. From the 1990s to the present day, however, the electrochemical preparation of composite materials was no longer limited to the electroplating of metal coatings, but new applications have been envisaged and this has drawn the attention of the investigators

to new matrix materials, i.e. electronic conductors other than metals, which can be grown by an electrochemical method from an appropriate deposition bath [153].

The use of the electroco-deposition provides several advantages for modern industry, not least of which is the limited investment needed to convert conventional electrolytic production cells and strip plating plants. As a consequence of this, another important advantage is that it is possible, as for conventional electroplating processes, to process parts continuously. The only serious difference to take into account is the presence of suspended particles in the electrolyte. The process parameters associated with conventional electroplating such as current density and electrolyte agitation are also of fundamental interest in electroco-deposition. However, the inclusion of a particulate phase in the electrolyte poses the need for further analysis to optimise process performance. If the electroco-deposition is to be applied to a high speed electroplating scenario (such as the electroplating of steel strip) then a fundamental appreciation of the effect of particle size, particle geometry, chemistry and the forces acting on particles in such a plating process, are of great importance.

Thus the main aim of the present work is the study of different parameters influencing the electroco-deposition process in order to promote and improve the applicability of such a technology in the high speed electroplating industry. The phenomena have been analysed moving from a microscopic scenario i.e. the role of the metal ions present in the electrolyte and adsorption on the inert particles and their interactions with the growing metal layer, to a macroscopic one i.e. the electrolyte agitation, its influence on particle motion and all the issues related to the presence of particles in an electrolyte during electroplating.

In particular the inert particle influence in terms of geometry, dimension and chemical nature (spherical polystyrene particles *vs.* irregular alumina particles with different dimensions), the metal matrix influence (nickel, copper and zinc), the influence of electrolyte agitation (using of a Rotating Cylinder Electrode cell system) and the influence of the coating thickness on particle content in the final coating, using different deposition times, have been examined and the results discussed in depth.

All these parameters have been studied evaluating their influence on the coatings produced in terms of coating morphology (SEM analysis), particle content evaluation (image analysis), and correlation between particle content and electrolyte agitation levels.

In addition, a fundamental analysis has been made evaluating the forces acting on particles when they are approaching the cathode surface. This has been achieved using rotating cylinder cathodes with different diameters in order to isolate the effect of centrifugal forces.

2. Electrodeposition: production of electrolytic coatings

Electrodeposition is an extremely important technology. It covers often inexpensive and widely available base materials with electroplated layers of different metals with superior properties extending their use to applications which otherwise would have been prohibitively expensive [4,7]. Electrodeposited coatings may be applied for appearance, protection, improved surface properties, or engineering, or mechanical properties [8]. On the other hand it is probably one of the most complex unit operations known because of the unusually large number of critical elementary phenomena or process steps that control the overall system [5]. Table 2.1 shows an overview of the several parameters involved in the process.

System components	Factors influencing metal distribution	Electrodeposit
Tank	Geometric	Metal distribution
Electrodes	Electrochemical	Composition
Electrolyte composition	Incidental	Structure
Process conditions		Properties
Current		

Table 2.1 – Metal distribution relationships in electrodeposition [6].

Electrodeposition as an industrial activity has been practiced for over 150 years, one of the first applications having been the electroforming of printing plates [9]. Subsequently, electrodeposition gained major importance as a cheap and versatile surface finishing process for decorative applications and for corrosion and wear protection. Typical examples include chromium plated automobile trimmings, gold plated brass jewellery, nickel-plated steel, gold plated electrical contacts or hard chromium plated bearings. Traditionally the automotive industry has been a big user of electrodeposition [10]. While this industry used large integrated plating facilities, specialised shops of relatively small size performed much of the plating for other applications. Indeed, a characteristic of traditional plating has been its fragmentation to which several factors may have contributed. On one hand, before strict

environmental regulations came into effect, the investment needed to start a commercial plating activity was relatively modest. Furthermore, the availability of fully formulated commercial plating electrolytes reduced the development efforts needed to start production. Success of a plating operation then depended mostly on the skill and ingenuity of the electroplater. Because electroplating depended largely on empirical know-how and involved handling of aggressive chemical and solutions, it did not fit well into mechanical production lines and many manufacturing industries preferred to subcontract plating operations to specialists.

At the end of the last century though, the electroplating industry was undergoing fundamental changes, which are likely to continue in the future [7]. Firstly, due to the more severe regulations concerning the emission and final disposal of heavy metal ions and chemicals, the electroplating industry today needs advanced water recycling and purification schemes that drastically increase investment costs. Environmental pressures also require that certain established plating processes be substituted by more environmentally friendly technologies that often require closer and better scientific understanding. A well-known example is the replacement of cadmium coatings for corrosion protection by other metal or alloy coatings, hexavalent chromium widely used for the passivation of zinc and in chromium plating has come under attack, as well as lead-containing electroplated solder alloys. On objects that are in contact with human skin, notably jewellery and watches, traditional nickel barrier coatings must be replaced, because nickel causes allergic reactions in some people[7].

A second driving force for change is the emergence of electrodeposition as a large scale manufacturing process involving fully automated high throughput installations. Examples are found in the steel industry and in the electronics manufacturing industry. In these and in other applications, electrochemical processes compete with dry processes and to be competitive they must exhibit the same degree of reliability and control. Interestingly, the principles governing scale up and scale down of electrodeposition processes are perhaps better understood at present than those of competing plasma deposition processes.

Finally, the general trend towards globalisation modifies the market conditions for the electroplating industry and creates new types of partnership between the manufacturing companies and their subcontractors with ever higher demands on technical competence, cost effectiveness and product reliability.

During the last part of the 1990s, electroplating, historically considered a "black art" [11], has evolved into an exciting field of high technology with numerous new applications and challenges in micro and nanotechnology. The dramatic pace of progress in information technology and its enormous impact on human society is common knowledge. Perhaps not so well known is the fact that electrodeposition and related electrochemical processes have had a decisive impact on the development of computer technology [12]. Fundamental research carried out by electrochemists, electrochemical engineers and materials scientists made these developments possible. Continuing research will permit these advances to be sustained in the future.

2.1 Fundamentals of electrodeposition

An electrochemical cell is made up of a solution (the electrolyte), in which different species and metal ions are dissolved, and two electrodes (see Fig.2.1).

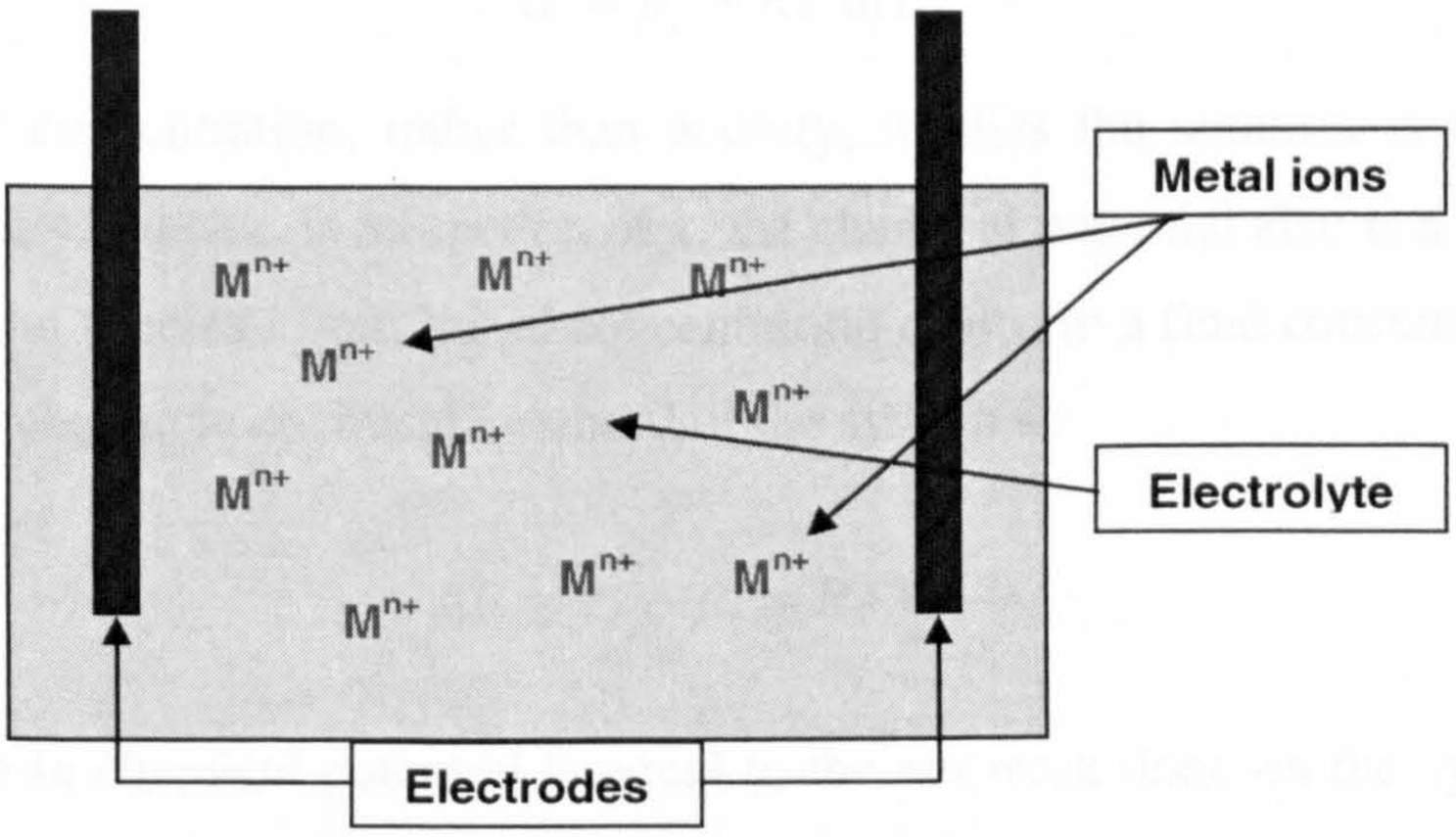

Figure 2.1 - Schematic of an electrochemical cell.

Metal ions produce a drift, or flux, when they move more in a certain direction than in others. As metal ions have a mass and bring a charge, a flux of them in a preferred direction results in the transport of matter and a flow of charge.

Three main reasons why metal ions become a flux inside an electrolyte:

- where there is a difference in concentration in different regions of the electrolyte, the resulting concentration gradient produces a flux of ions (*diffusion*);
- if there are differences in electrostatic potential at various point in the electrolyte, then the resulting electric field produces a flow of charge in the direction of the field (*migration or conduction*);
- if a difference of pressure or density or temperature exists in various part of the electrolyte, then the liquid begins to move as a whole or parts of it move relative to other parts (*hydrodynamic flow*).

The present discussion is restricted to the transport processes of diffusion and conduction and their interconnection (the laws of hydrodynamic flow are not particular to the flow of electrolytes; they are characteristic of the flow of all fluids).

2.2 Ionic drift under a concentration gradient: diffusion

In an electrolytic solution, the concentration c_i of an ionic species i, is assumed to vary with the direction x. The situation can be considered in terms of chemical potential (μ) of i:

$$\mu_i = \mu_i^0 + RT \ln c_i \qquad \textbf{Eq. 2.1}$$

The use of concentration, rather than activity, implies the solution is assumed to behave ideally. Since c_i is a function of x, the chemical potential also is a function of x. If a mole of species i from initial concentration c_I at x_I to a final concentration c_F at x_F, then the change in chemical potential of the system is:

$$\Delta\mu = \mu_F - \mu_I = RT \ln \frac{c_F}{c_I} \qquad \textbf{Eq. 2.2}$$

The change in chemical potential is equal to the net work done on the system in an isothermal, constant-pressure reversible process. Thus the work W done to transport a mole of species i from x_I to x_F is:

$$W = \Delta\mu \qquad \textbf{Eq. 2.3}$$

From the analogous situation in mechanics (the negative of gravitational potential energy defines the gravitational force) one would expect that the negative of the gradient of the chemical potential would act formally like a force. Further, just as the

gravitational force results in the motion of a mass, the chemical-potential gradient results in the net motion, or transfer, of the species *i* from a region of high chemical potential to a region of low chemical potential. This net flow of the species *i* down the chemical-potential gradient is diffusion, and, therefore, the gradient of chemical potential may be looked upon as the diffusional force F_D:

$$F_D = -\frac{d\mu_i}{dx} \qquad \textbf{Eq. 2.4}$$

The macroscopic description of the transport process of diffusion is, qualitatively speaking, simple. The gradient of chemical potential resulting from a non-uniform concentration is equivalent to a driving force for diffusion and produces a diffusion flux. The quantitative cause-and-effect relation between the driving force F_D and the flux J_i is given by the Fick's first law of steady-state diffusion:

$$J_i = -D\frac{dc_i}{dx} \qquad \textbf{Eq. 2.5}$$

where D is termed the *diffusion coefficient.*

Fick's first law tells one how the concentration gradient is related to the flux under steady-state conditions; it says nothing about how the system goes from equilibrium to steady-state when a diffusion source or sink is set up inside or at the boundary of the system, Thus, it says nothing about how the concentration changes with time at different distances from the source or sink. In other words, Fick's first law is inapplicable to non-steady-state diffusion. For this, one has to go to Fick's second law:

$$\frac{\partial c}{\partial t} = D\frac{\partial^2 c}{\partial x^2} \qquad \textbf{Eq. 2.6}$$

which relates the time and space variations of the concentration during diffusion.

Once Fick's second law is solved (the solution of is facilitated by use of Laplace transform, which convert the partial differential equation into an easily integrable total differential equation), the concentration of diffusing species as a function of time and of distance from the diffusion sink when a constant normalized flux is switched on at t=0 is obtained.

2.3 Ionic drift under an electric field: conduction

With the aid of an external source, a potential difference is now applied across the electrodes. How does this applied potential difference affect the ions in the solution? The potential (defined as the work to be done to bring a unit positive charge from infinity to the particular point) in the solution has to vary from the value at one electrode ψ_I to that at the other electrode ψ_{II}. The electrolytic solution is therefore a region of space in which the potential at a point is a function of the distance of that point from the electrodes. The work to be done to bring a test ion in the solution from the point x_1, where the potential is ψ_1, to another point x_2 of potential ψ_2 is:

$$W = \psi_1 - \psi_2 \qquad \textbf{Eq. 2.7}$$

When this work is divided by the distance over which the test charge is transferred, the force per unit charge, or the *electric field X*, is obtained:

$$X = -\frac{\psi_1 - \psi_2}{x_1 - x_2} \qquad \textbf{Eq. 2.8}$$

where the minus sign indicates that the force acts on a positive charge in a direction opposite to the direction of the positive gradient of potential.

In the absence of an electric field, the ions are in random motion within the electrolyte and the net flux is zero. Under the influence of an electric field the net flux of ions is not zero. They experience a force directing them towards the electrode that is charged oppositely to the charge on the ion (see Fig.2.2). The positively charged electrode is called the anode, whilst the opposite one is called the cathode.

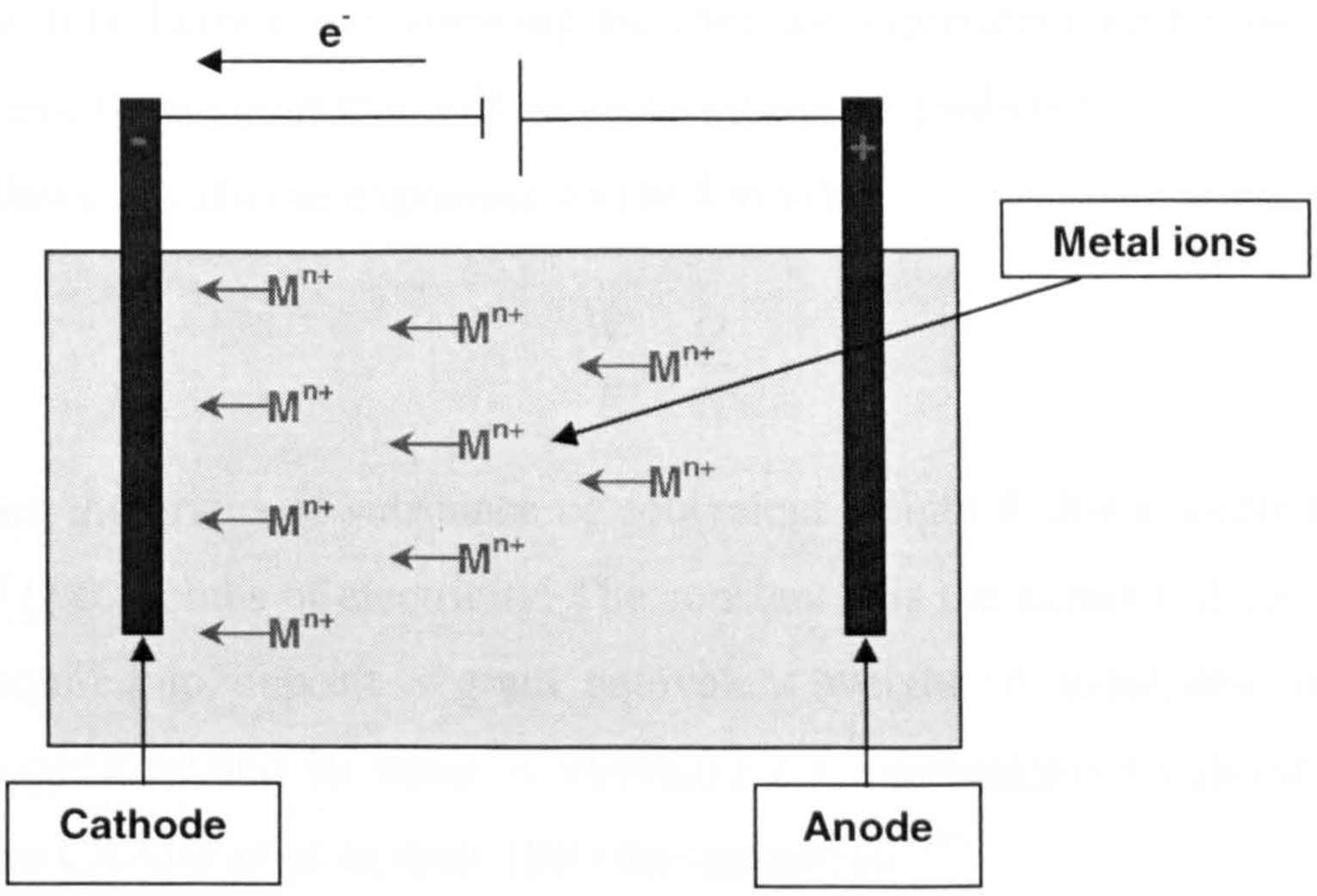

Figure 2.2 - Schematic of an electrochemical cell when an external source supplies current to the cell.

Electrodeposition is a process that involves the transfer of a metal ion through an energy barrier. This energy barrier exists at the interface between a submerged metal and an electrolyte [13].

The passage of a unidirectional current through a solution is associated with the movement through it of charged particles, ions. The electrodes are the terminals; they lead the current into the solution. One of them supplies ions into the solution (anode), while the other one (cathode) allows them to deposit on its surface, receiving an electrodeposited film. This is due to electric field generated between the two electrodes.

Faraday proposed the laws that describe the process in 1833 and they can be stated as follows [8]:

1. the amount of chemical change (e.g. electrodeposition) produced by an electric current is proportional to the quantity of electricity that passes;
2. the amounts of different substances liberated by a given quantity of electricity are proportional to their equivalent weights (the chemical equivalent of an element is its atomic weight divided by the valence change involved in the reaction).

In particular these laws can predict that, by measuring the quantity of electricity flowing in the cell, a measure of the amount of chemical change that will thereby be

produced will be known and, knowing the chemical equivalent weight of the species under process, the amount that will be involved can be predicted.

Faraday's laws can also be expressed by the formula:

$$\frac{W}{E} = \frac{Q}{F} \qquad \textbf{Eq. 2.9}$$

where W are the grams of substance of equivalent weight E that is deposited by the passage of Q coulombs of electricity. The constant F is the number of coulombs that will be required to deposit a gram equivalent weight of substance, it is called *Faraday's constant* and its value is 96490.0 ± 2.4 international Coulombs per mol, according to CRAIG *et al.* in their 1960 determination [14].

It has been suggested that four different zones exist in an electroplated metal-substrate system, Fig.2.3 shows these zones.

The substrate is the base material. The substrate interface is a very important zone; in fact, characteristics such as adhesion and tenacity between substrates and coatings are relevant for a successful electrodeposition. Finally the coating itself: it can be compact or porous and must provide properties that the substrate does not exhibit when in contact with the external environment.

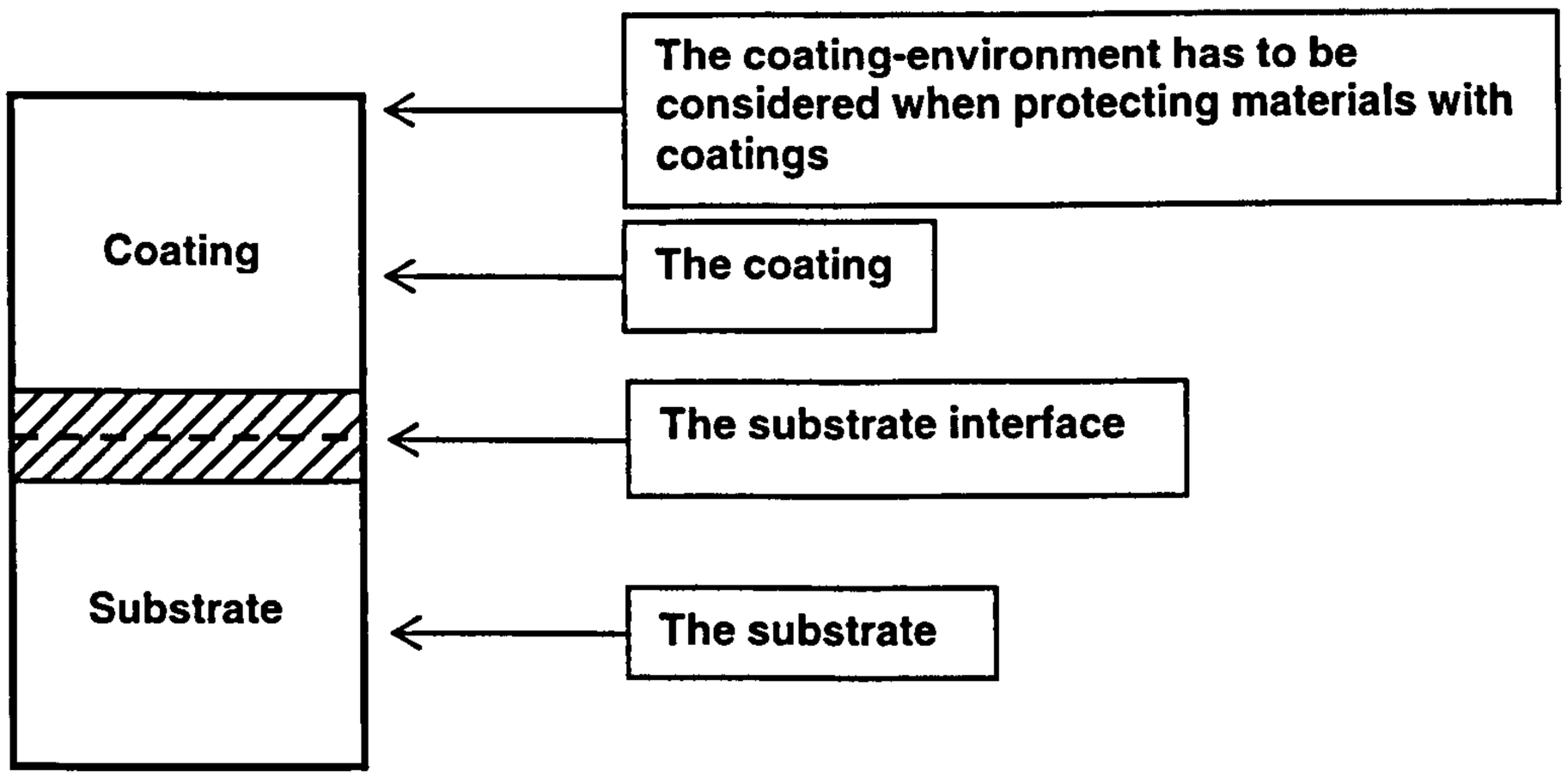

Figure 2.3 - Typical electroplated metal-substrate zones [6].

2.4 Current efficiency

Often the amount of metal deposited, involved in an electroplating process, calculated by Faraday's laws is nor equal to that evaluated experimentally. This is due to the failure to take into account all the electrochemical reactions involved. In

the usual electroplating situation the main interest is in the amount of metal deposited at the cathode or dissolved at the anode, and any other possible processes occurring at the same time, e.g. hydrogen evolution at the cathode, which could represent a waste of electricity and a reduction in the efficiency of the process. Hydrogen evolution could also damage the coating, and, furthermore, influence the hydrodynamics in the vicinity of the electrode surface. If ferric ion (Fe^{3+}) is present in the electrolyte, it may be reduced at the cathode to the ferrous ion (Fe^{2+}), thus using some of the current supplied without visible gas evolution or metal deposition. The reverse reaction may take place at the anode. In fact, a solution containing both Fe^{3+} and Fe^{2+} may be electrolysed indefinitely without any change in its composition: the reactions $Fe^{3+} + e^- = Fe^{2+}$ and $Fe^{2+} = Fe^{3+} + e^-$ simply balance each other. Other reducible ions may also cause low cathode efficiencies without hydrogen evolution. If nitrate ions are present in the solution, they are easily reduced to lower valences, such as nitrite, nitrogen or ammonia, at the expense of metal deposition.

Thus the *current efficiency (CE)* for an electrodeposition process is stated as:

$$CE = \frac{actual}{theoretical} \times 100\% \qquad \textbf{Eq.2.10}$$

where *actual* is the mass of metal deposited or dissolved, measured gravimetrically, and *theoretical* is the corresponding mass predicted from Faraday's laws assuming that there were no side reactions. Anode or cathode efficiency is current efficiency as applied, respectively, to the anode or cathode reaction [8, 13]. A cathodic current efficiency of less than 100% means that only a part of the energy supplied to the cell is spent in the deposition process. Part of it is sustaining other processes that often are not welcome.

2.5 Current distribution

In electroplating the thickness of the electrodeposited coating is of more interest than the total amount of material deposited (in terms of both the average thickness and the distribution of the deposit on the cathode). The average thickness depends on the amount of metal deposited and the area over which this deposit is spread, while its distribution depends upon how evenly the deposit covers the cathode. The *current density* (current in amperes per unit area of electrode) is the parameter correlated

with these aspects. The current, apart from a few ideal cases, is not uniform over the surface of an electrode. The manner in which it distributes itself over an electrode in practical cases is quite complicated, usually not easily calculable from geometry. Current tends to concentrate at edges and points, and unless the resistance of the solution is extremely low (lower than in any practical scenario), it flows more readily to parts near the opposite electrode rather than to the more distant parts. Because of this, the thickness of the deposit is not uniform over the surface. This effect is often not fully appreciated and usually minimized by the choice of cell design aiming to decrease the difference between the high and the low current density areas [13].

In the absence of metal deposition, the current distribution obtained is called the *primary current distribution*. It depends only on Ohm's law; it can be calculated from potential theory (although calculations are complex and difficult) and can be measured by probes on a large scale, or on a scale up to 1000 ml by means of conducting paper. It depends only on the geometry of the system and it is not affected by the properties of the electrolyte, including its conductivity. When anode and cathode are very close together and one or the other of them is of irregular profile (is rough), primary current density distribution is far from uniform. As the electrodes are moved farther apart, the distribution becomes more uniform, but the greatest uniformity achievable by separating the electrodes is reached at fairly small distances, and further separation achieves little improvement.

As soon as metal deposition commences, the current distribution is changed to the *secondary* distribution. Activation polarization shows its effects immediately, and as soon as electrolysis has proceeded for any significant time, concentration polarization also becomes a factor and increases with time up to some steady-state value. Both types increase with current density and hence act to improve the current distribution. Secondary current distribution is always more uniform than primary. The relative influence of Ohmic resistances and of polarization depends on the scale of the system: the greater the roughness of the electrode profile, the greater the relative importance of Ohmic resistance, and the closer the secondary to the primary distribution.

The distribution of metal deposit is also affected by the variations of cathode current efficiency with the current density. In a bath in which the cathode efficiency falls rapidly as cathode current density increases, the excess deposited on edges and projections (region of high current density) will not be as great as would be expected from current distributions alone. Finally, the use of levelling agents in the electrolyte can provide improvements in thickness distribution of the coating. These agents (usually organics) are able to inhibit the growth of dendritic structures, improving the thickness uniformity of the deposit.

2.6 Other potential effects

When no external current is supplied to an electrochemical cell, the system is said to be at *equilibrium* and the potential between electrodes is called the *equilibrium potential* E_e. It is a dynamic equilibrium, in the sense that metal ions are discharged and metal atom are ionised, but these two effects cancel each other, so there is no net-change in the system. The small currents involved are called exchange currents. To obtain a metal deposition the system must be moved away from equilibrium applying an external current. The difference between the electrodes' potential (E_i) when current is flowing trough the cell and E_e is called overpotential η:

$$\eta = E_i - E_e \qquad \textbf{Eq. 2.11}$$

This overpotential can have several causes, such as:

- during the passage of current the activities (related to the concentration) of the reactants near the electrode change (they decrease near the cathode) and this causes concentration overpotential;
- overpotential may be required to overcome various kinetic barriers (e.g. the energy required by an electron to jump across the metal/electrolyte interface) to the reaction and this causes activation overpotential;
- some reactions of crystallization on the electrodes surface can have high activation energies and this causes crystallization overpotential.

Another overpotential, the so-called ohmic drop, is required to overcome the resistance of the electrolyte, and it can be calculated from the Ohm's law [8,18].

2.7 Effect of temperature

Temperature is a critical variable in most practical plating bath and, for best results, must usually be controlled within plus or minus 2 °C from the "optimum". An increase in temperature increases the rate of diffusion, the ionic mobility and therefore the conductivity of the bath. It also increases the rate of evaporation, rate of hydrolysis of bath constituents and the rate of deposition of additives. Most compounds become more soluble with increasing temperature, but there are exceptions. These opposing effects make it difficult or impossible to predict the best temperature of operation for any given bath, which therefore must be determined experimentally. Thus heating or cooling coils are necessary for most plating setups. Passage of current through the resistance of the bath produces a heating effect and, unless this is balanced by evaporative cooling, temperature control is required.

3. Electroco-deposition: production of electrolytic composite coatings

The continuous phase in a composite is referred to as the matrix, whilst the other phase (or phases) provides reinforcement. Composite materials can often be found in the form of fibre, whisker or platelet-reinforced materials, particulate composites such as dispersion-strengthened alloys and cermets, laminates and sandwich materials. Metallic composites can be produced by various methods such as:

- powder metallurgy: based on the mixing of metallic and non-metallic powders, which are pressed and sintered to form products;
- metal spraying: based on the melting of metallic powders that are sprayed onto surfaces by a gas stream, with composites being obtained by adding inert particles into the powder blend;
- internal oxidation and co-precipitation: composites containing very finely dispersed oxides produced by the selective oxidation of metals and alloys, while composites produced by the co-precipitation method require a mixture containing an easily reducible metal salt and colloidal oxide dispersion. Reduction of the metal salt produces a mixture of very fine metal and oxide powders that can then be processed by a conventional powder metallurgy technique.

Composite electroco-deposition is a process in which metal matrix composite coatings are obtained by electroplating from a suspension of small particles, which are co-deposited with the electroplated metal. A scheme of the process can be seen in Fig. 3.1. Usually the metal matrix gives properties such as corrosion resistance and physical strength to the coating, whilst the second phase can give a low friction coefficient (e.g. graphite, PTFE or oil containing capsules), a high wear resistance (e.g. silicon carbide, tungsten carbide or diamond) or a high surface hardness (e.g. alumina, silica or zirconia).

Composite electrodeposition can be traced back to the early days of conventional electroplating. The formation of rough deposits was attributed to the presence of impurities in electrolytes, which were co-deposited during electrolysis. This phenomenon was not widely reported as being advantageous until 1928, when FINK

AND PRINCE [1] deposited a self-lubricating copper coating, containing graphite. Twenty years later AQUESSE [2] filed a patent, which allowed the useful life of coated cutting tools to be increased by the co-deposition of a hard second phase. Since the late 1960s, there has been a marked increase in the interest in composite electroplating technology, with electroless composite coating-technology gaining popularity from the early 1970s [3].

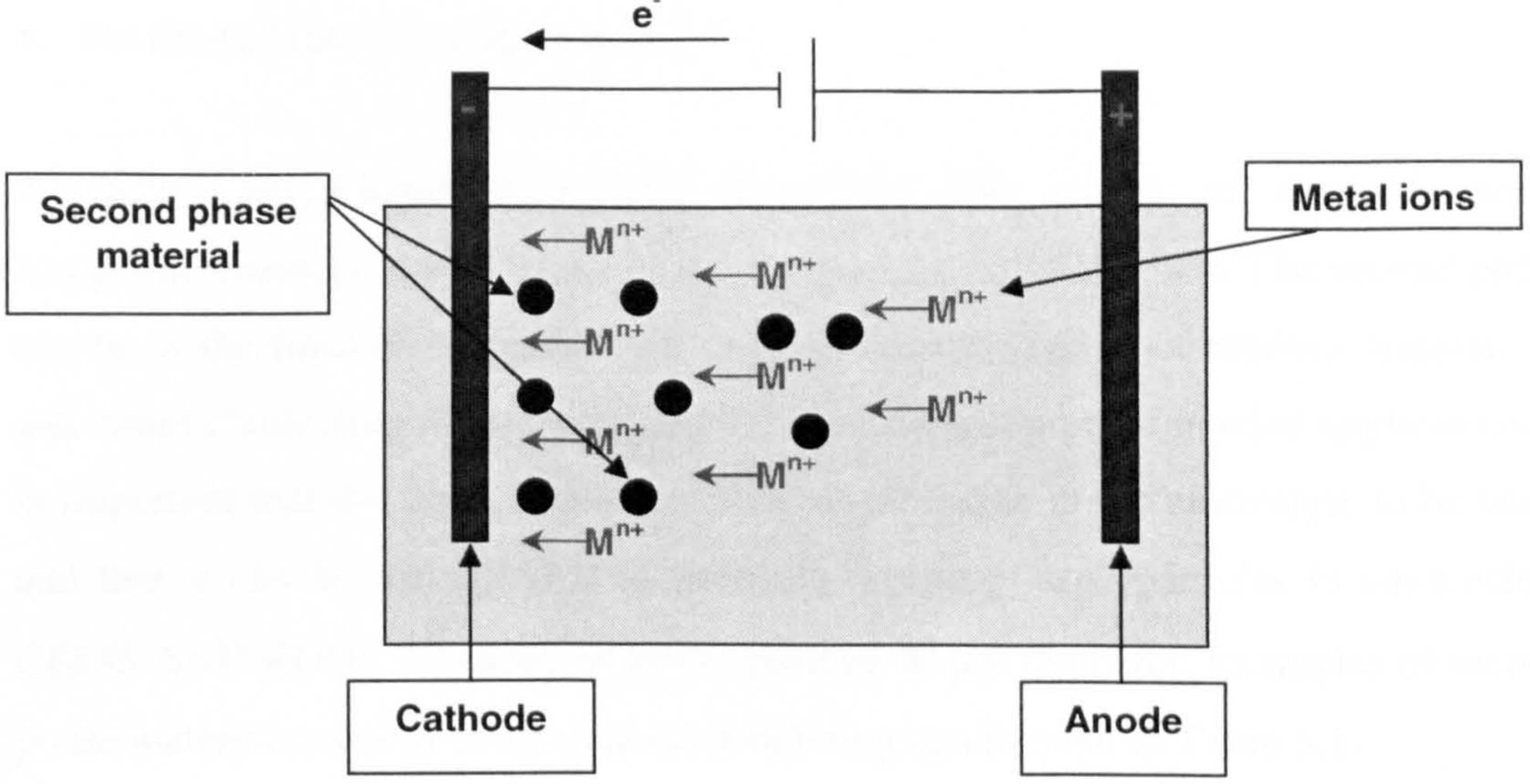

Figure 3.1 - Schematic of the electroco-deposition process.

The main advantages of electrolytic and electroless composite deposition are as follows:

- only a limited investment is necessary to adapt conventional electroplating cells;
- ability to process parts continuously;
- a wide range of composites can be obtained by selecting different types of inert particles like metal oxides, metal carbides or organic compounds;
- control of the production conditions permits smooth deposits with dimensions as required, resulting in minimal post-treatment;
- no heat-treating of the parts is required, and thus thermal damage of the components to be coated is avoided;
- when compared to metal spraying, more complex geometrical forms can be coated successfully, but highest uniformity of thickness is obtained by electroless plating;
- reduction of waste often encountered in dipping or spraying techniques;
- this process avoid drawbacks associated with high temperature and vacuum processes (such as with sputtering and chemical vapour deposition). The

electroco-deposition is carried out in an electrolyte and, for a large number of processes, high temperatures are not required.

The main limitations of electrolytic and electroless composite deposition are as follows:

- the particle size of the second phase;
- the limited rate of co-deposition.

As with conventional electrolytic deposition, the matrix of electrodeposited composite coatings can be in the form of a pure metal or an alloy. The second phase can be in the form of a powder or a fibre (either oriented or of random orientation) and either conducting or non-conducting, depending upon the intended application. It is important that the second phase material is insoluble in the electrolyte to be used, and that it can be wetted. Due to problems keeping large particles in suspension, CELIS AND ROOS [15] stated an upper limit of 40 μm diameter. Examples of second phase materials used in composite electroplating can be seen in Table 3.1.

Elements	Al, B, Cr, Fe, Mo, Ni, Si, Ta, Ti, W, Zr Incorporated as Oxide, carbide, nitride, sulphide, sulphate, carbonate, phosphate, or as pure compounds
Other second phase materials	Glass, graphite, diamond, synthetic materials (e.g. PTFE), Powder metal alloys (e.g. Ni-Al, Ni-Al-Ti)

Table 3.1 – Examples of second phase materials used in composite electroplating [15].

The most commonly used matrix metals are nickel, copper, zinc and cobalt [16]. There are several techniques used to form electrolytic composite coatings:

- the conventional suspension techniques, in which particles are continuously kept in suspension, chemically or mechanically, allowing the formation of a composite coating on the cathode during electroplating;
- the sedimentation technique, in which particles are periodically distributed by vigorous agitation and allowed to sediment again on a horizontal surface during electroco-deposition. This has the advantage that higher incorporation rates can

be achieved when compared with normal suspension techniques. Also, by periodic agitation/sedimentation, it is possible to get layered deposits;

- the brush electroplating technique [17], in which current is passed through an adsorbent material, which has been soaked in electrolyte containing both metal salts and solid particles. This technique has not received widespread investigation in the literature.

To maintain the inert particles in suspension, unless suitable surfactants are employed, some kind of agitation has to be employed. CELIS AND ROOS [15] mentioned two suitable techniques: the "plate pumping" process, that uses a vibrating perforated plate at the bottom of the plating cell, and the "liquid/air" process, where electrolyte is circulated using a peristaltic pump. In the second case, air is also used to give a greater degree of agitation, however, care is needed to prevent flotation of the particles and "dead corners", as sedimentation of particles will occur. The first technique is more effective than the second one, especially if air is added. However, air can introduce problems to materials being an oxidant, and it also increases the ohmic drop in the electrolyte promoting higher production costs.

The several parameters that influence the electroco-deposition process can be divided into three categories: features related to the electrolyte, to the hydrodynamics of the system, and to electrolysis effects (including bath type, pH, current density, temperature, bath agitation, type and concentration of particles and addition agents present in solution). Fig. 3.2 shows the general effects of electroplating parameters on the electrolytic co-deposition of particles.

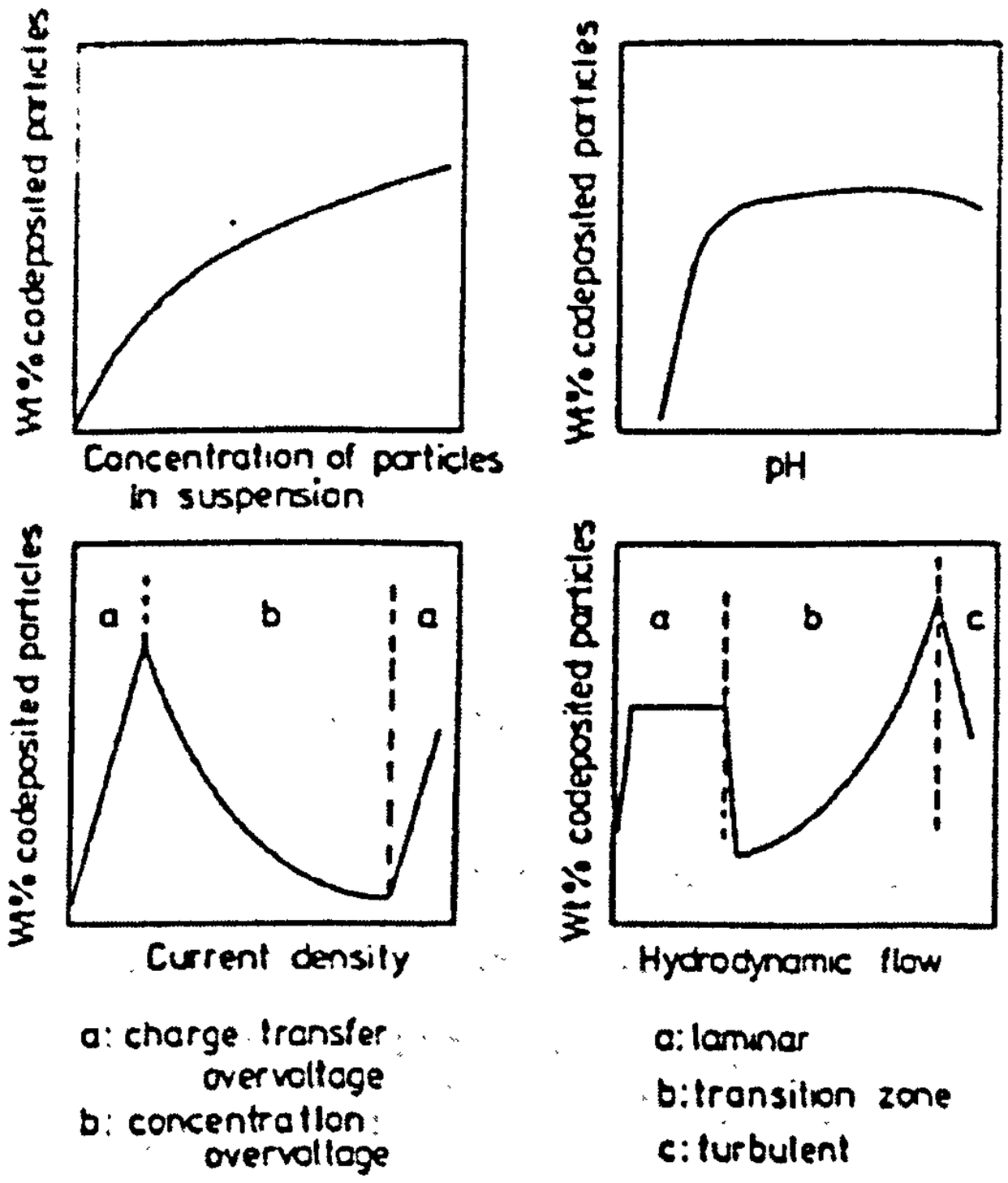

Figure 3.2 - General effects of electroplating parameters on the electrolytic co-deposition of particles [19].

3.1 Effect of bath and pH

Generally the electrolytes used for depositing composite coatings are of a similar composition to those used to deposit conventional coatings, except for the addition of the particles themselves and some addition agents used to promote the co-deposition. An electrolyte is usually chosen for its ability to deposit the matrix metal, but the metal type will generally affect the amount of co-deposition obtained. For example, BRANDES AND GOLDTHORPE [20] found that alumina could be deposited with copper and nickel from conventional electrolytes, but not from a typical chromium bath. They also found that the type of electrolyte used to obtain a given matrix metal would affect the co-deposition rate. The inclusion of alumina in copper, for example, from sulphate electrolytes was found to be less than that obtained from alkaline cyanide based baths. Earlier studies of HOFFMAN AND ERNST [21] stated that co-deposition of alumina does not occur from sulphate or fluoroborate baths, whilst a little occurs in a basic pyrophosphate bath. The authors found the highest possible co-deposition rate in a formate bath.

In the same period WILLIAMS AND MARTIN [22] found that the amount of co-deposited silica fibres increases with the increase of the CuCN content of a cyanide copper system.

BAZZARD AND BODEN [23], in their studies on nickel/chromium co-deposition, suggested that an electrolyte used for the formation of composite coatings must demonstrate good micro-throwing power to ensure that uniform metal deposition occurs over the entire cathode surface and, additionally, it must be capable of depositing into spaces between the particles as the deposit is built up.

Recent investigations, carried out by HIRATO *et al.* [24], stated that the deposition of silica is easier if a non-aqueous electrolyte is used, in their case $AlCl_3$-dimethylsulphone electrolyte obtaining Al/SiC composite coatings. Silica did not codeposit from acid copper sulphate solutions [25]. Silica particles, that are normally hydrophilic, do not codeposit because a layer of water, strongly bound to the silica surface, negates particle contact with the cathode surface.

Variation in pH seems to yield differing results. SAUTTER [26] found that, for Ni/Al_2O_3 coatings, for pH greater than 2, there was very little effect on the particle co-deposition content, whilst for pH lower than two there was a sharp decrease. Also other researchers, such as CELIS AND ROOS [15], found similar results, but they found this dependent upon the type of second phase particle present as well: in fact molybdenum disulphide and tungsten disulphide systems showed an increase in co-deposition if pH was decreased and the same was found with nickel/silicon carbide [27]. YEH AND WAN [28], during their work on the effects of ion adsorption on the co-deposition of SiC from a Watts type nickel bath, explained this phenomenon. They found that SiC powders catalysed the adsorption of hydrogen ions and significantly increased hydrogen evolution at pH less than or equal to 2. They concluded that the powder content of the deposited layer and the current density for nickel reduction were both notably decreased at pH < 2 when SiC particles were present in the electrolyte. HAYASHI *et al.* [29] also found that the bulk solution pH itself was affected by the presence of alumina particles. They stated that the surface of alumina is generally covered by OH^- groups which, when placed into a solution,

dissociate or adsorb H^+. When the amount of OH^- and H^+ are equal, the solution pH corresponds to the point of zero charge (PZC) for these particles. In the pH range below the PZC, excess H^+ will be adsorbed onto the particle surface (that is why the deposition is not promoted at these pH values), whilst for pH values above the PZC, particles adsorb excess OH^- or release H^+. Similar results have been found by BONINO *et al.* [30] in their work on the co-deposition of Co_3O_4 with nickel from a Watts bath; the introduction of particles in the electrolyte influences the pH. This change depends on the acid-base properties of the particles and indicates the magnitude of the H^+ exchange on their surface.

Studying different aspects of the electroco-deposition of Al_2O_3 with Cr-Ni alloys BERKH *et al.* [31] found that the coating deposition rate initially increases with the pH between 0.5 and 1. For pH values between 1 and 3 it is more or less constant. For pH values higher than 3, precipitation in the bulk electrolyte was observed.

3.2 Effect of current density and temperature

Current density coupled with particle concentration in solution, is the most widely investigated parameter. In their review, HOVESTAD AND JANSEN [32] stated that two distinct current density dependencies can be found in the literature: firstly, current density has a little or no effect on the amount of second phase deposited and secondly, particle content shows one or more maxima when plotted against current density.

In their 1982 review, CELIS AND ROOS [15] noted a general trend of decreasing co-deposition as current density was increased, while an increase was found for nickel/SiC composites. They concluded that either effect could be obtained depending on the system. Other studies found the maxima mentioned above: TiO_2 and SiC particles deposited from nickel sulphamate baths [33], Al_2O_3 deposited from an acidified copper sulphate solution [34] and V_2O_5 particles co-deposited with nickel from a fluoroborate bath show this behaviour [35]. Studying the production of electrodeposited metal/fluoroplastic composite coatings SAKSIN *et al.* [36] found that the rate of co-deposition for these polymeric particles decreased with increasing current density.

NARYAN AND NARAYANA [37], studying electrodeposited chromium-graphite composite coatings, and HOVESTAD *et al.* [38], studying the electroco-deposition of zinc and polystyrene in the presence of surfactants, stated that current densities had little effect on the co-deposition rate.

Recently, KERR *et al.* [39] reported that it was possible to increase the particulate content of a nickel/PTFE composite by pulsed electrodeposition. They found that using a DC current density of 3 A dm^{-2} it was possible to codeposit 6.9 vol% PTFE, while using pulsed current, giving a mean current density of 3 A/dm^2, it was possible to codeposit 12 vol.% PTFE with improved dispersion of the particles throughout the matrix. On the contrary, SIMMONS [40] found that pulsed current density had little effect on the percentage of co-deposited PTFE present in zinc/PTFE composite coatings. He found similar results also for zinc-cobalt/PTFE composites. However, when deposition was carried out at a mean current density of 0.625 A/dm^2, the percentage of co-deposited PTFE present in these coatings showed a dependency on duty cycle (i.e. as the duty cycle was increased, the percentage of co-deposited PTFE decreased).

GYFTOU *et al.* [41] used pulsed current condition to produce nickel matrix composite coatings containing SiC particles of two different sizes (namely 1 μm and 20 nm) from a Watts solution. They observed that the application of pulse current resulted in deposits with more uniform particle distributions than those obtained under DC conditions. They stated that the microhardness was not only increased by the presence and the reduced size of the particles, but also by the current conditions (i.e. duty cycle and pulse frequency). The microhardness of the deposit had been improved by further thermal treatment.

Not only is particle content dependent upon current density, but also current density itself is affected by the presence of particles within the electrolyte. BUELENS *et al.* [42] carried out cathodic polarisation trials on copper and gold electrolytes containing alumina particles; they stated that the shape of the plots obtained were similar to those obtained without any alumina, but the presence of inert particles was said to shift the curves to a higher cathodic current density for the same overpotential. Similar results have been found for other metal/particle systems [26, 43-47].

SUZUKI *et al.* [45], in particular, investigating the cathodic polarisation behaviour of Ag/Al_2O_3, discovered that the addition of particles to an electrolyte reduced the cathodic current density at low overpotential, while the opposite was true at higher overpotential. The latter was explained with the reduction of the diffusion layer thickness by the presence of particles in solution. At low overpotential, the authors postulated that the alumina particles actually adsorbed onto the cathode, suppressing silver deposition.

SIMMONS [40], investigating the cathodic polarization behaviour of zinc/PTFE, showed that neither PTFE nor the surfactant required to disperse the polymer underwent any significant electrochemical reduction during polarization. However, PTFE did cause the current density/potential relationship for an acid electrolyte to become increasingly displaced, where a more cathodic potential was required to obtain a given current density. The limiting current for zinc deposition also became lowered when PTFE was present in the electrolyte. HWANG AND HWANG [48], however, found that particle content had no effect on the polarisation curves.

BANOVIC *et al.* [148] studied the co-deposition of nickel with alumina. Starting from a morphological study of the composites produced, they found that, for samples deposited below 1 A/dm^2, the nickel matrix was extremely smooth, whilst above this current density, some structure could be observed within the matrix which became larger as the current density was increased. The authors attributed this structure within the matrix to the growth and coalescence of the depositing nickel around the particles. Since the alumina particles are electrically insulating, the nickel matrix cannot electrodeposit onto them, but instead, must deposit around them. Therefore, it is the difference in the rate of coalescence of the depositing nickel layer on top of the particle at the various current densities that gives this appearance, as schematically illustrated in Fig. 3.3. At the higher current densities, the nickel metal deposits are being incorporated faster than they can diffuse across the surface. This results in growth of nickel around the particle becoming rough and the formation of a ridge, as seen schematically in Fig. 3.3 (c). At the lower current densities, the coating deposits at a much slower rate, thus allowing surface diffusion to occur and a smoother appearance to be attained.

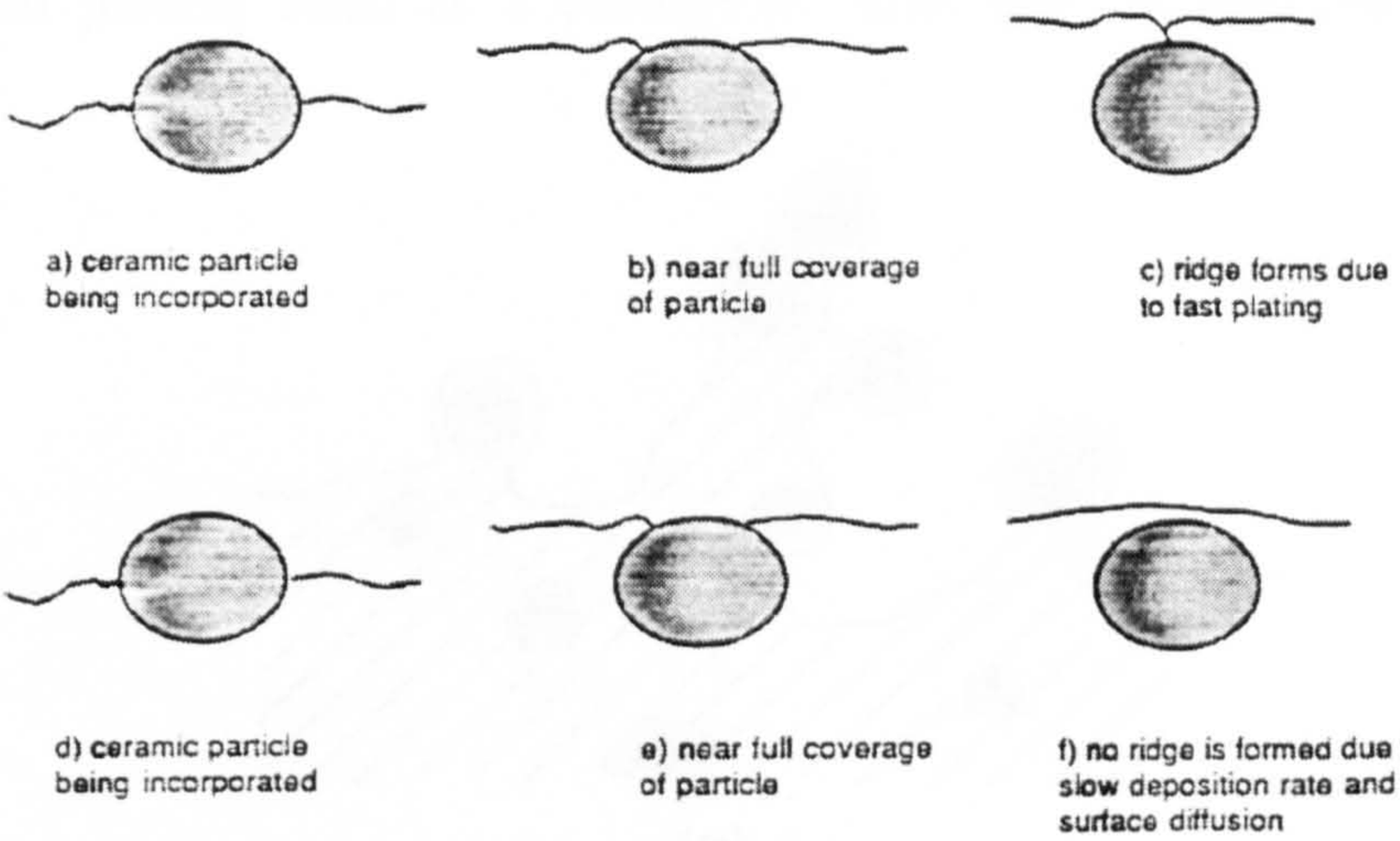

Figure 3.3 - Schematic illustrating the different surface morphologies of the electro-composites deposited at different current densities. A high plating rate (current density) is observed in (a), (b), and (c). A slower plating rate is found in (d), (e), and (f) [148].

Temperature appears to have different influences depending on the system: varying temperature had little, or no effect on the particle content for Ni/Al_2O_3 [26, 49], while the particle content of a Cr/graphite composite showed a steady increase, up to a maximum, as the temperature was raised to 50°C [37]. The reverse was found for Cr/Al_2O_3 where there was a decrease in co-deposition up to a temperature of 50°C [50]. A peak particle content was reported at 50°C for Ni/V_2O_5 [35].

3.3 Type, concentration, shape and size of second phases

Generally, increasing the particle content of an electrolyte increases the volume percentage of particles found in the deposit until a maximum is reached. However, the percentage of embedded particles depends partly upon the electrolyte composition and partly on the type of particles added. An example can be found in the work by GRECO AND BALDAUF [51], which noted that three times as much TiO_2 than Al_2O_3 could be deposited with nickel for the same conditions. Also for conducting particles relatively large amounts of entrapment can be obtained, while for non-conductive particles it is more difficult [17].

In their work on nickel/chromium composite electroplating, BAZZARD AND BODEN [23] found that co-deposition of conductive particles can be problematic because of the dendritic growth on their deposits, caused by the fact that an

incorporated particle acted as a conductive "high spot" in the coating for the deposition.

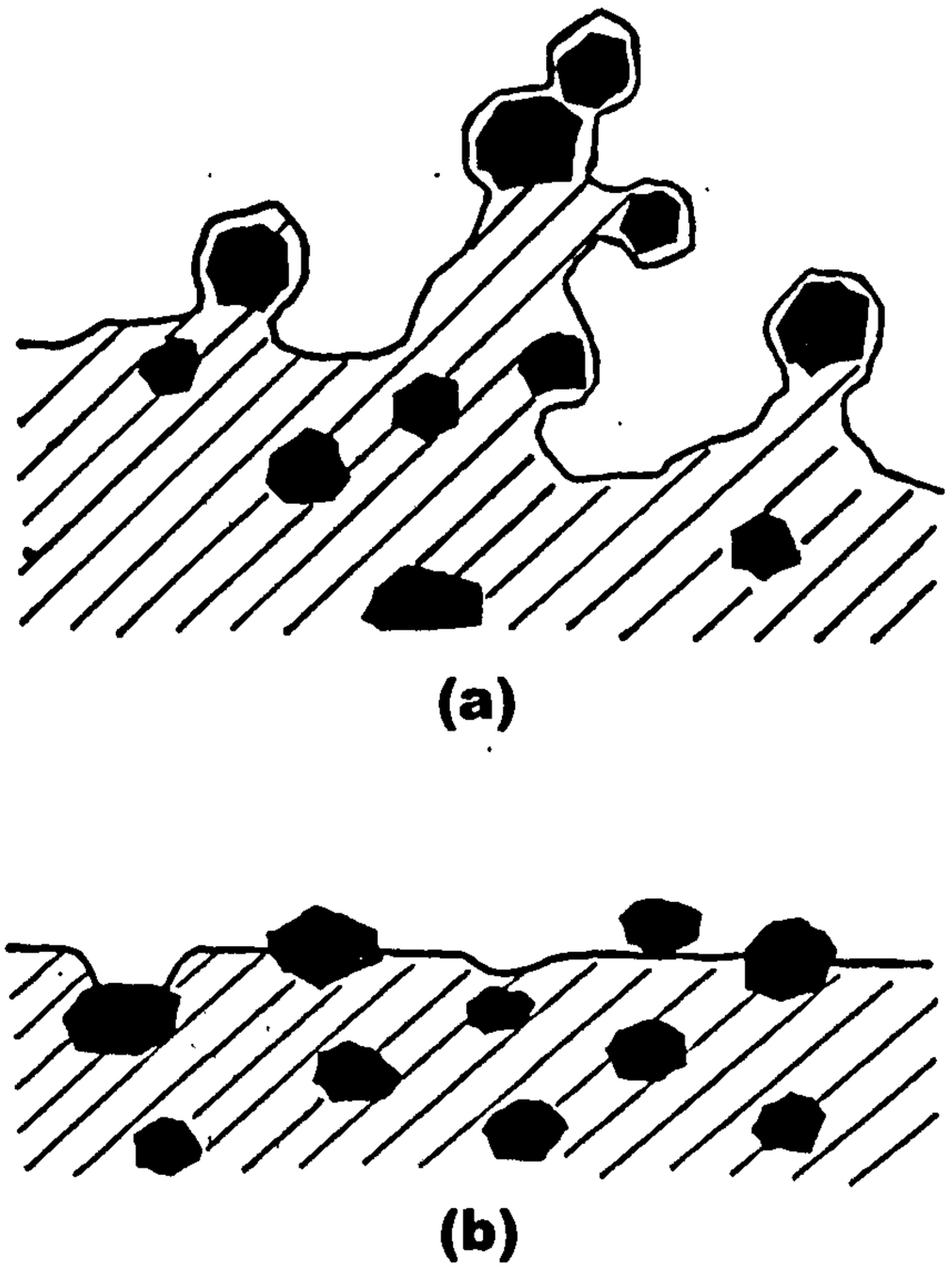

Figure 3.4 - Typical surface profile of composite coatings: a) containing conducting particles; b) containing non-conducting particles [52].

Similar findings have been reported by others [52-54], who stated that semi-conductive and conductive particles (e.g. chromium carbide, zirconium diboride, graphite) tended to form surface nodules, whereas non-conductive particles (e.g. silicon carbide, alumina) did not. STANKOVIC [54], in particular, noted that particle type and current density has greater influence over coating morphology than particle size. However, SOVA [55] did not find any of the nodulation previously mentioned in his trials on the co-deposition of zirconium particles with a nickel-cobalt alloy. The reason was that the zirconium particles were covered with a very thin stable layer of oxide, so that they behaved more like inert non-conductors.

CHEN *et al.* [56], studying the co-deposition of copper with alumina, stated that particle structure plays an important role. The hexagonal structured α–alumina can be readily co-deposited, while spinel cubic structured γ–alumina was reported to show no co-deposition (γ-alumina can be partially or totally converted to α-alumina after heating at 1125°C). ROOS *et al.* [57], however, disagreed with these results,

stating that γ-alumina can be deposited as well as α-alumina, but in much smaller amounts. This was found to be due to the different amount of ions adsorbed on the particle surfaces. The ionic cloud around the particle plays two different roles on the co-deposition rate: it could help the attraction towards the cathode if a positive charge is present at the particle surface (and giving time for the particle to be engulfed by the growing metal layer) but, on the other hand, it can interfere with the diffusion layer. CHEN *et al.* [56] also noted that titania behaves in similar way to alumina, with rutile being the most favoured deposited form, anastase did not codeposit at all.

The influence of suspended sub-micrometre diameter alumina particles on polarization during electroco-deposition with copper at a rotating cylinder electrode has been studied by STOJACK AND TALBOT [58]. The authors stated that particle incorporation behaviour, as a function of increasing current density, can be divided into several general regions: initially a region where incorporation increases sharply reaching a maximum value, followed by a sharp decrease in incorporation, then a region where incorporation is relatively constant, and lastly another decrease as mass-transport-limited conditions are approached. The regions wherein the amounts of incorporation sharply increase or decrease with current density are more sensitive to particle size, crystallographic phase and even to the particle manufacturing process. When the incorporation increases the rate-determining step for co-deposition appears to be the reduction of metallic ions adsorbed onto the alumina particles. The peak in particle incorporation was found to coincide with the point of zero charge (PZC) of copper in an acid copper plating solution. The results are shown in table 3.2. Essentially, VERELEST *et al.* [49] draw the same conclusion for Ag/Al_2O_3 composite coatings.

Particle identification	Current density / mA/cm^2	Particle incorporation / wt %
0.3 µm α-Al_2O_3	20	0.7
0.3 µm α-Al_2O_3	24.5	0.9
0.3 µm α-Al_2O_3	35	0.5
1 µm α-Al_2O_3	20	0.7

Table 3.2 - Co-deposition of α-Al_2O_3 at 20 mA cm^{-2}, 120 g l^{-1} loading and using a rotating cylinder electrode at 1000 rpm [74].

Recently, NOWAK *et al.* [59] used the electrochemical impedance spectroscopy (EIS) technique for an in situ investigation of the electrolytic co-deposition of Ni/SiO_2 and Ni/SiC composite coatings. They tried to clarify why silica particles hardly codeposit in comparison to silicon carbide particles. They stated that the presence of SiO_2 and SiC particles influences the metal deposition process in different ways: SiC particles are embedded in the growing layer because of an apparent decrease in the electrode surface area, probably due to blocking off of part of the surface by partly engulfed particles, while in the case of SiO_2 particles no blocking has been observed. EIS has also been used by BENEA *et al.* [60] to study the influence of silicon carbide nanoparticles on nickel electroplating. Particles affected the nickel reduction as outlined by the displacement of the polarization curve to a lower reduction potential and by the presence of a lower charge-transfer resistance. They also stated that the surface morphology of nanostructured composite layers is different compared to a pure nickel coating. The effect of SiC particles was to increase the number of nucleation sites with a reduction in crystal growth, resulting in smaller grain size of the nickel matrix.

MASALKI *et al.* [61] determined the equivalent circuit for the nickel electrocrystallisation process from a Watts bath containing SiC as shown in Fig. 3.5. The authors added a surfactant (sodium dodecylsulphate) and a brightening agent (2-butyne-1,4-diol and saccharine) to the electrolyte. In the equivalent circuit proposed, R1 amounts to 13 Ω and is related to the electrolyte resistance, R3 is related to the charge transfer resistance and ranges between 6 and 80 Ωcm^2 depending on the

electrolyte composition, R4 is the desorption resistance and ranges between -20 and 4 Ωcm^2 depending on the electrolyte composition, C2 is the double layer capacitance and ranges between and 25 and 70 Fcm^2 depending on the electrolyte composition, finally C5 is the pseudo-capacitance of adsorbed intermediates and ranges between -2.4 and -0.1 Fcm^2 depending on the electrolyte composition.

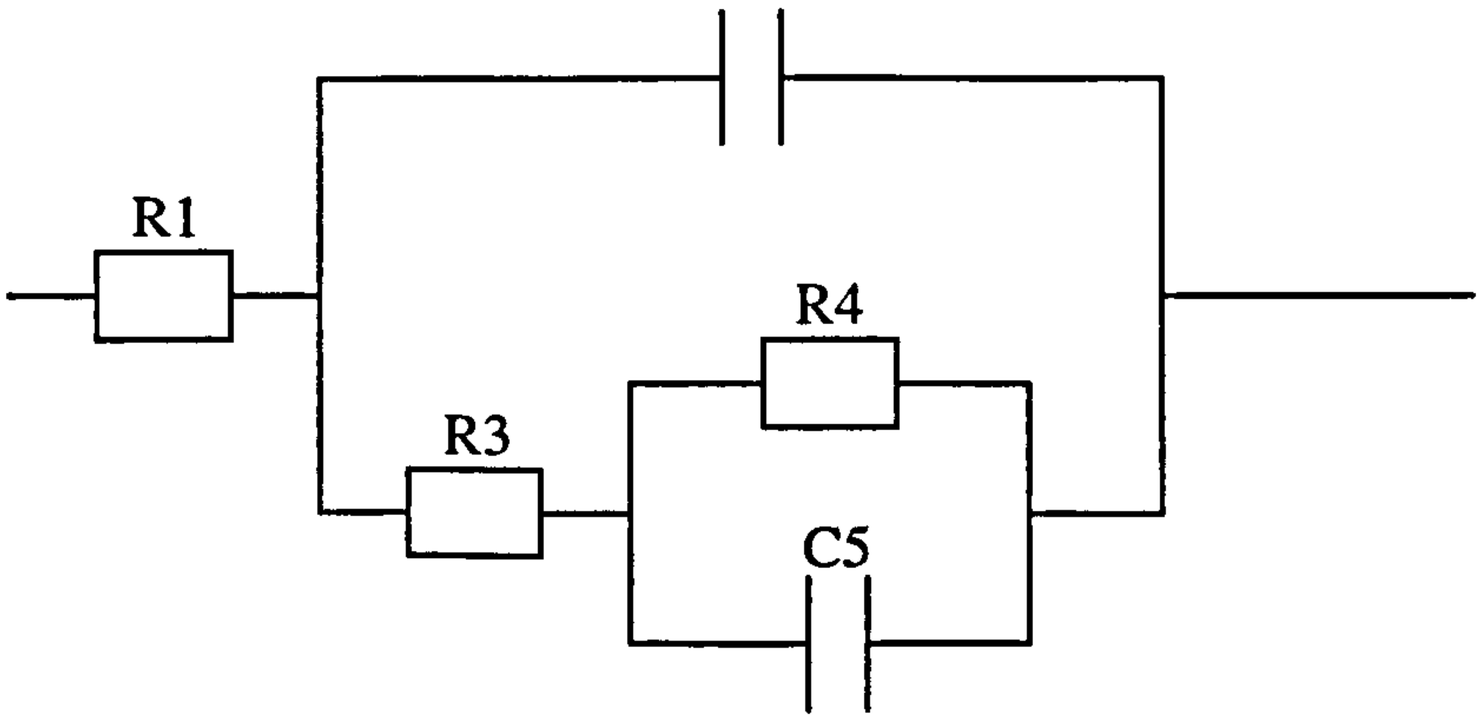

Figure 3.5 - An electric equivalent circuit for the nickel electrcrystallisation process from a Watts bath containing SiC [61].

KONDO *et al.* [62] proposed two different ways for the deposition of SiO_2 into a (001) oriented zinc electrodeposit: (a) by particles lining up along the laterally growing macrosteps on the (001) and (b) by randomly dispersed particles on the (001). They proposed that the sidewalls of particles are incorporated into the macrosteps at the edge of (001), whilst the bottom of randomly dispersed particles are incorporated into the (001) probably by atomic steps.

BOZZINI *et al.* [63, 75, 76] found that when B_4C micrometre sized particles are added to an electrodeposition bath containing $KAu(CN)_2$ and citrates, a decrease or increase of the cathode overvoltage is observed depending on the deposition current density (overvoltage decrease for low current density range, while the opposite for high current density range). They related this phenomenon to the morphology of the deposit (surface roughness) and to the hydrodynamic conditions prevailing at the cathode surface. They stated the hydrodynamic effects were minor. The observed overvoltage variations were dominated, according to the authors, by the competition of two morphological effects. These were in addition to the usual polarisation increase with current density increase and were a reduction of the overvoltage due to the increase of the effective cathode area because of the formation of "humps" and

an enhancing effect due to the reduction of effective cathode area because of the screening effect of ceramic particles.

In 2001 SURVILIENE *et al.* [64] studied the influence of the presence of oxides (MoO_2 and TiO_2) on the electrodeposition of chromium. They found a lower rate for the formation of composite Cr-MoO_2 and Cr-TiO_2 compared with that of a Cr coating. They suggested this is related to the adsorptive capacity of MoO_2 and TiO_2 and desorption of their hydrides from the electrode surface. They showed that highly dispersed particles of MoO_2 might be used to reduce hydrogenation of the substrate, because MoO_2 acts as an inhibitor of hydrogen adsorption in the substrate, and its efficiency increases with increase in MoO_2 concentration. Moreover, both the oxides have an effect on such coating properties as hardness, ductility, internal stresses and high temperature resistance. Despite the large range of sizes employed, the authors found out that particle type (in terms of "chemical" nature) and current density had a greater influence over coating morphology than particle size.

Support for the importance of the particle nature rather than particle sizes comes from CHEN *et al.* [56]. They stated that the co-deposition of alumina with copper is easier if α-Al_2O_3 is co-deposited rather than γ-Al_2O_3. This was found to be more important than the particle sizes.

There are few investigations regarding the effect which particle shape has on co-deposition. Of course particle shape would affect adsorption onto the cathode, adsorption of ions onto the particle themselves and suspension stability. GRECO [65], in a review, noted those composites containing discontinuous fibres are far more difficult to produce then particulate composites.

Different results have been reported for the influence of particle size. BAZARD AND BODEN [23] found that they could increase the co-deposition rate of chromium in a nickel matrix by increasing the particle size, as did CHEN *et al.* [56] in their work on copper/alumina. SUZUKI AND ASAI [66], however, found that the opposite occurs with Ag/Al_2O_3, while VERELEST *et al.* [49] have stated that the effect of particle size on co-deposition is very small. Recently GARCIA *et al.* [67, 149] investigated Ni-SiC composites. They co-deposited SiC particles of three different sizes (namely 5, 0.7 and 0.3 μm) with nickel from a Watts' bath. They found that for

a given number density of particles in the plating solution, the number of particles in the coating increases with increasing particle size. This aspect should be better investigated in the future.

STANKOVIC AND GOJO [54] performed a similar investigation, but they also tested the influence of different particle types rather than just different particle dimensions. Table 13.2 shows the particles analysed by these authors together with their main dimensions.

Kind of particle	Main diameter (μm)
α-Al_2O_3	0.3
SiC	2.3
MoS_2	6.1
Graphite	5.4

Table 3.3 - Size of particles used by STANKOVIC AND GOJO in their investigations [54].

3.4 Agitation of the electrolyte

Agitation plays two important roles in composite electrodeposition: it is used to maintain particles in suspension and to aid their transportation in the electrolytic cell. Some workers have used both agitation and blending before experiments, to break up agglomerates. This is necessary to obtain homogeneous deposits containing a fine dispersion of particles [32]. BAZARD AND BODEN [23], however, had some success with the sedimentation technique used to codeposit chromium into a nickel matrix. They were able to produce coatings possessing a good particle distribution and smooth surface finish by adopting the following process: the electrolyte was agitated for a short period of time, then left for the particles to settle onto a horizontally placed flat cathode, prior to the application of current.

FOSTER AND CAMERON [52] studying the influence of cathode vibration on co-deposition rates found that under DC conditions, with no vibration, very few particles were co-deposited, whereas with cathode vibration only, small particles were included in the deposit. By using intermittent cathode vibration and pulsed

electrodeposition, they noted a wide size distribution of co-deposited particles. The co-deposition of finer particles during continuous electrode vibration was believed to demonstrate the existence of attractive force interactions between the particles and cathode during the initial stages of composite coating formation. KALANTARY *et al.* [68, 69] investigated another kind of vibratory agitation, using the plate pumping technique mentioned briefly by CELIS AND ROOS [15] in their 1982 review. This type of agitation was reported to be particularly suitable for the production of composite coatings, since it is especially good at holding fine particles in suspension without swirling or gross turbulence.

Early workers [23, 53] found that increasing bath agitation led to a larger amount of particles becoming incorporated. However, it was also noted that too much agitation tended to remove particles from the cathode surface before they could become incorporated. This has since been confirmed by a number of workers studying agitation effects on particle co-deposition using rotating electrode techniques. For example, MASUKO AND MUSHIAKE [70, 71] found that for Ni/Al_2O_3, the alumina content of the resulting coatings, as well as the size of the particles embedded in the coating, decreased with increasing rotation speed.

Using a rotating disc electrode, CELIS *et al.* [42, 72], investigated hydrodynamic effects on both copper and gold composite coatings containing alumina. Their results for the copper system can be summarised in Fig. 3.6. Under laminar flow conditions (up to about 400 rpm) the amount of co-deposited alumina remained constant, but at the start of the transition zone there was an obvious decrease in the amount of the alumina present. As rotation speed was further increased, the amount of embedded alumina was found to increase again, to give a maximum prior to reaching turbulent flow conditions, after which there was a dramatic decrease in particle incorporation. Additionally, particle agglomeration was observed once non-laminar flow was achieved, indicating that such conditions should be avoided in order to optimise mechanical and physical properties of the coating.

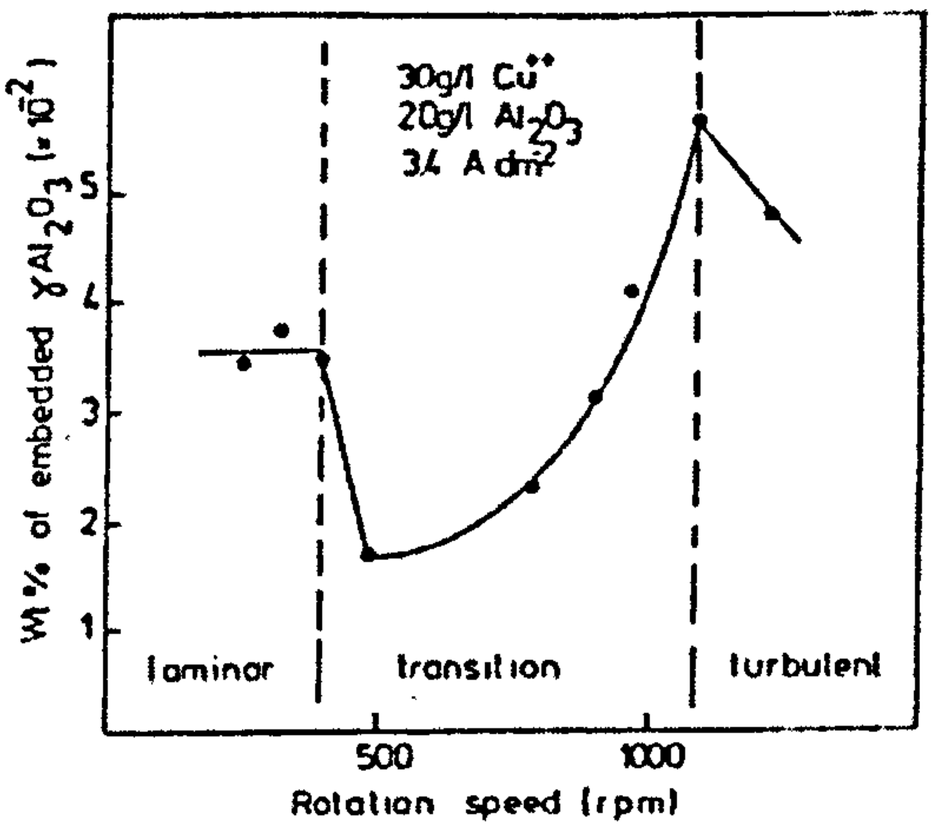

Figure 3.6 - Effects of rotation speed on the weight percentage of alumina particles co-deposited with copper [42].

HOVESTAD *et al.* [32, 38] studied the influence of cathode rotation speed for the co-deposition of zinc with polystyrene. Fig. 3.7 shows their result. As can be seen, results were strongly dependent on the particular system used. As the particle concentration was decreased in the electrolyte and the surfactant concentration was increased, the particle concentration in the electrodeposited coating decreased with the increasing cathode rotation speed.

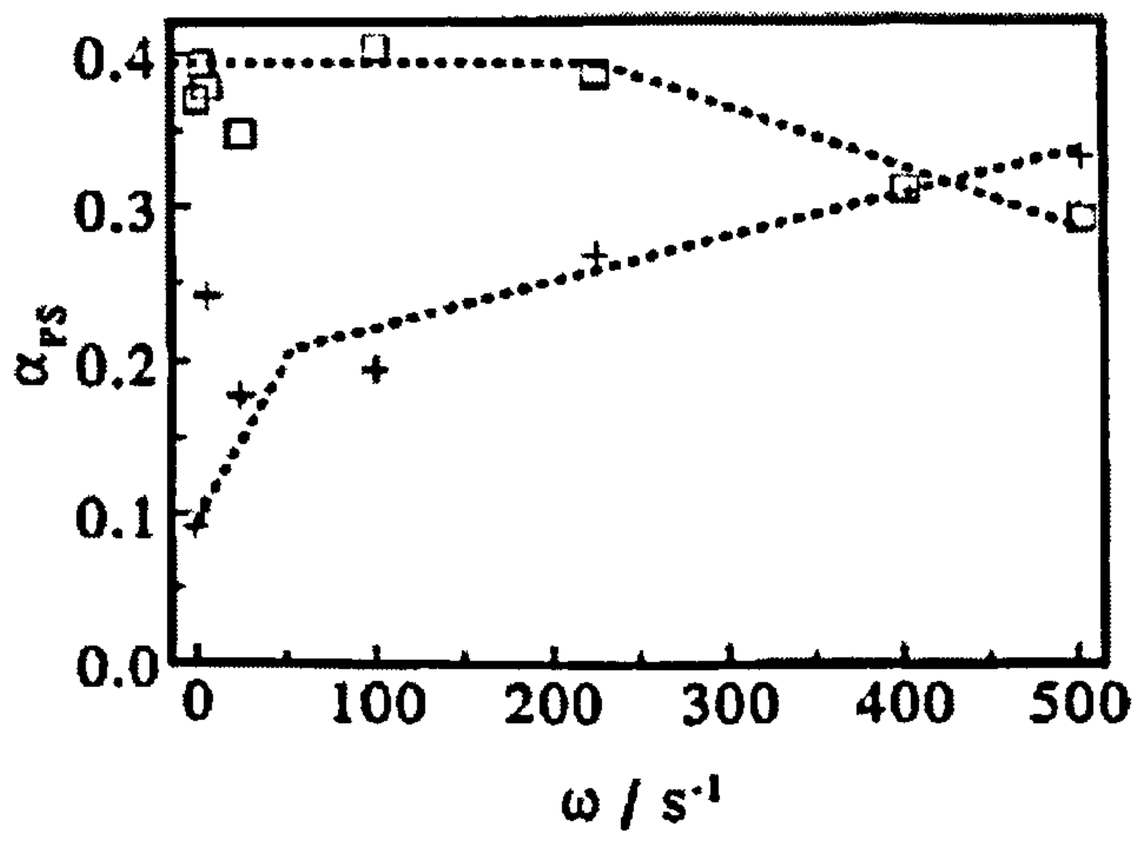

Figure 3.7 - Volume fraction of co-deposited PS particles against the electrode rotation speed at a current density of 0.5 kA m^{-2} and: +) PS particle volume fraction in electrolyte of 0.054 and a concentration of surfactant (cetylpyridinium chloride) of 0.02 mol kg l^{-1}; □) PS particle volume fraction in electrolyte of 0.02 and a concentration of surfactant (cetylpyridinium chloride) of 0.2 mol kg l^{-1} [32].

The same authors also found out that the probability for a particle to be incorporated in a metal growing layer is strongly related to the cathode surface roughness. The authors stated that the friction force, which prevents a particle from being removed

from the surface before being incorporated depended on the local surface roughness around the particle. A particle adsorbed in a recessed area had a much larger probability of becoming included than one adsorbed on a flat surface. Particularly if particles are able to move along the surface to recessed areas due to shearing forces or Brownian motion, a rough surface will lead to a higher amount of incorporated particles. The authors observed that changes in deposit appearance and surface morphology correlate with changes in PS co-deposition. Therefore it was proposed that a change in surface roughness, due to the change in the free surfactant concentration in their system, was responsible for the differences in PS co-deposition. Fig. 3.8 shows a schematic of the different morphologies of zinc-polystyrene electrodeposits obtained by HOVESTAD *et al.* [32].

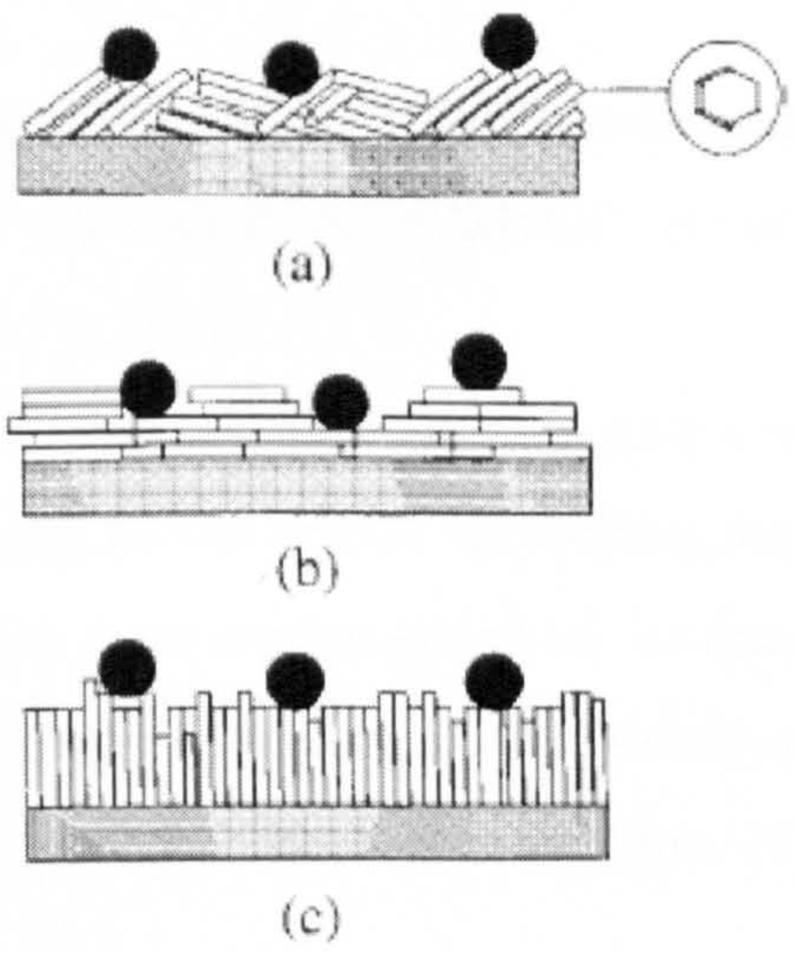

Figure 3.8 - Growth morphologies of zinc deposits: (a) intermediate type; (b) basal type; (c) vertical type. Black spots represent polystyrene particles [32].

The only data available in the literature about the influence of the hydrodynamic regime on the co-deposition process when alumina is used as second phase material was the work, carried out by STOJAK AND TALBOT [58] in 1999, on the electroco-deposition of copper with alumina on a rotating cylinder electrode. The authors performed electroco-deposition at different cathode rotation rates and at different current densities. Results are shown in Fig. 3.9.

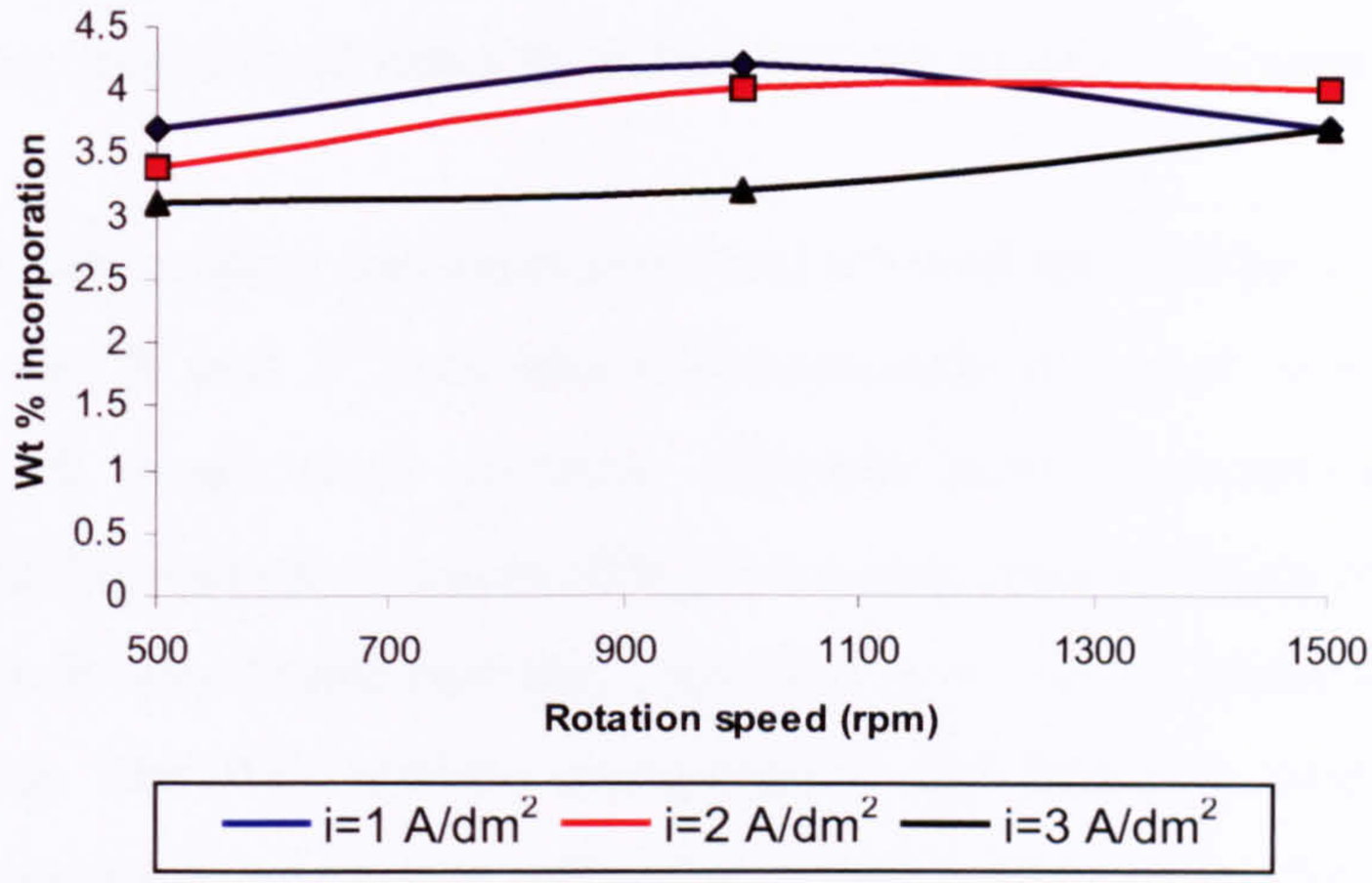

Figure 3.9 - Particle incorporation vs. cathode rotation speed for copper alumina electroco-deposition at three different depositing current densities and 120 g l^{-1} particle loading [58].

A new experimental approach for Ni/WC electroco-deposited composite coatings has been recently proposed by SOMBATSOMPOP *et al.* [73]. The details of all components are shown in Fig. 3.10:

- direct current motor (1) and (2): the motor (1) with a maximum speed of 130 rpm functioned as the driving power source for rotating the cathode around the anode, and the motor (2) with a maximum speed of 30 rpm functioned as the driving power source for cathode self-rotation, both vertically and horizontally;
- spur gears (3) and (4): they serve the function of self-rotating the cathode vertically;
- straight bevel gears (5) and (6): they serve the function of self-rotating the cathode horizontally;
- cathode holder (7): it holds the cathode and conducts electricity to the cathode through the short shaft;
- anode (8);
- cathode (9): holding frame holds the cathode and functions as the base for the motor;
- test specimen (cathode) (10).

The authors compared their results in terms of thickness distribution and uniformity, WC particle incorporation and hardness with those obtained by conventional

electroco-deposition techniques, conventional electroco-deposition with the electrolyte being stirred at all times by a magnetic stirrer or with a liquid-air process.

The new composite coating apparatus proposed allowed the cathode to rotate around itself both in the X and Y axes and simultaneously to rotate around the anode circumference. It could work in three different ways: conventional electroco-deposition (CECD), cathode rotation (CR) and anode circumference rotation (ACR) (see Fig. 3.11). It was found that this apparatus was able to assist in an efficient solution stirring. The WC particle incorporation and hardness were found to be dependent on the mode of coating technique, whereas the coating thickness profiles were not. The coating thickness distribution across the specimen was not uniform, showing very high coating thickness at the edge and low near the centre. The coating thickness distribution in all the coating techniques increased at low current density (around 4-6 A/dm^2) and then decreased at higher current density. The CECD technique was found to be more sensitive to current density than the CR and ACR techniques. The ACR technique gave the best thickness distribution while the CR was recommended when relatively high thickness was required.

The thickness of the coating by the CR technique increased at low self-rotating velocity and decreased at higher values. With the ACR technique, the thickness was found to increase also with increasing cathode velocity around the anode. However, at high cathode self-rotation velocity, the coating thickness tended to decrease with increasing cathode velocity around the anode. The current density did not affect the particle content and average hardness with all the techniques used. The ACR technique was recommended when requiring high particle incorporation in the coating and high coating hardness.

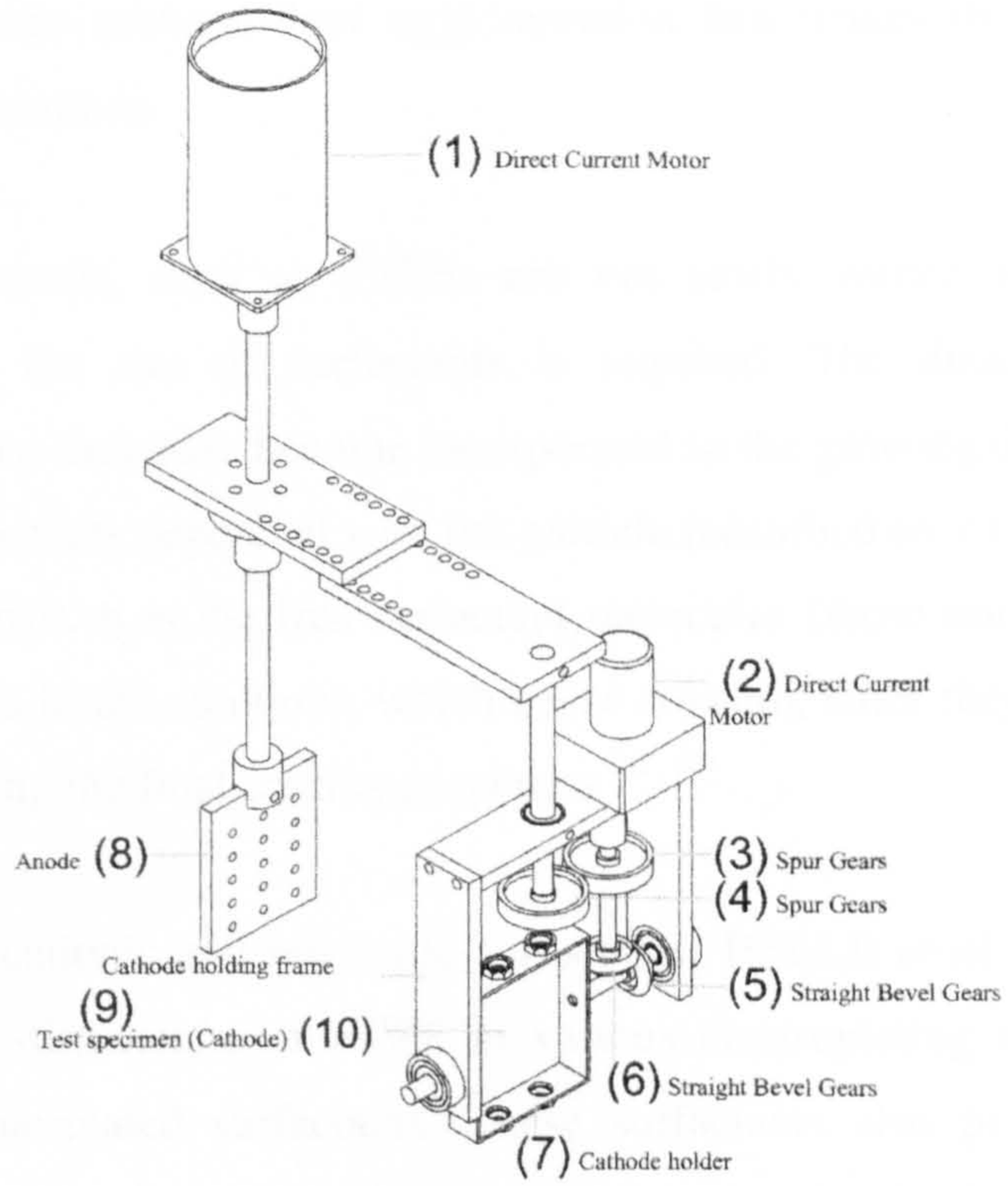

Figure 3.10 - Design of new electrodeposited composite coating system [73].

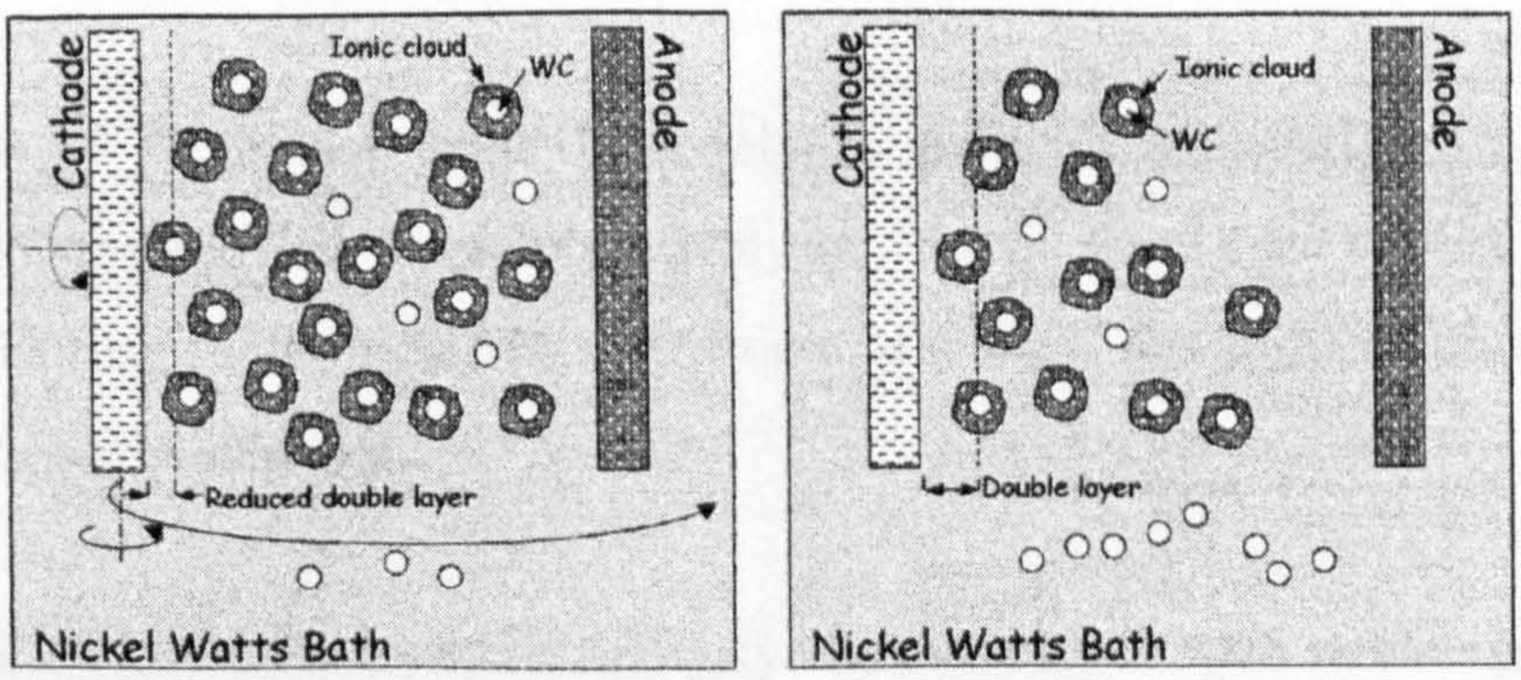

Figure 3.11 - Deposition mechanism for Ni-WC composite coatings for the cathode rotating and the anode circumference rotating techniques in comparison with that for a conventional electroco-deposition coating technique [73].

3.5 Effect of surfactants present in the electrolyte

In their study on alumina and graphite electroco-deposition with copper, FINK AND PRINCE [1] had problems with graphite agglomeration. They therefore utilised surfactants (gelatin and tannin) to increase the wettability of their particles. Usually this is not a problem for inorganic particles, but advantages can be gained from the use of surfactants; cationic surfactants, for example, give particles a net positive

charge, which can prevent their agglomeration and makes them electrostatically attracted to the cathode.

Organic compounds, such as PTFE, are not easily wetted using conventional techniques, so the use of surfactants is required. The disadvantage of using surfactants is that they may become incorporated in the growing deposit. Usually the amount of surfactants deposited with the particle (adsorbed on it) is small and hardly affects the deposit. It is the free surfactant molecules (those not adsorbed onto the particle and free in the solution), which cause concern, since they may deposit with the metal, altering the final coating properties [77, 78].

By combining cationic and non-ionic surfactants, HELLE *et al.* [77-80] were able to produce stable dispersions of PTFE in various electroplating solutions, using, in these cases, fluorinated surfactants. These surfactants also produced a dramatic increase (up to 50 volume percent) in particle content for particles such as SiC and diamond.

SAKSIN *et al.* [36] co-deposited fluoropolymer particles with matrices of zinc and nickel from standard acid sulphate electrolytes. Dextrin was added to the zinc bath in order to stabilise the particles in suspension. However, the deposits obtained were coarse and poorly adherent.

HOVESTED *et al.* [38] showed that polystyrene particles formed stable agglomerates when added to a zinc sulphate electroplating baths. The authors found that the addition of cetylpyridinium chloride, a cationic surfactant, prevents aggregation and enhances polystyrene co-deposition. Other surfactants (e.g. cetyltrimetylammonium bromide, cetyltrimetylammonium chloride, sodium dodecylsulphate) also increase suspension stability, but diminish polystyrene co-deposition, irrespective of their charge. Hence, the surfactant charge does not affect polystyrene co-deposition. CHANG AND LEE [81] were able to produce Ni/Al_2O_3 deposits from bright nickel baths containing up to 33% in volume of particles, while using bath particulate concentrations one or two orders of magnitude lower than other published works.

MEGURO et al. [82] demonstrated that the use of non-ionic surfactants ($C_{16}H_{33}$-O-$(CH_2CH_2O)_nH$, $C_{22}H_{45}$-O-$(CH_2CH_2O)_nH$, $C_{18}H_{35}$-O-$(CH_2CH_2O)_nH$ and $C_{18}H_{37}$-CO-O-$(CH_2CH_2O)_nH$, where n indicates the mole number of oxyethylene units included in the surfactant) and silane coupling agents increased the suspension stability of β-SiC in a commercial nickel sulphamate electrolyte. Additionally, for a given particulate concentration in solution, the rate of co-deposition was doubled.

Recently SHRESTHA *et al.* [83] stated that, compared to other surfactants so far reported, the co-deposition of SiC with nickel is enhanced by using a cationic surfactant, 4-Ethylazobenzene-4'- (oxyethyl) trimethylammonium bromide (AZTAB), containing an azobenzene group. The authors proposed that this enhancement is related to the reduction of AZTAB at the cathode surface during the deposition of nickel. With such a surfactant they produced a composite coating with 62% by volume of SiC.

BENEA *et al.* [60] noticed that the addition of sodium dodecylsulphate improved uniformity and the amount of dispersed SiC particles in a nickel matrix, but they didn't provide a mechanism for this action.

3.6 Addition agents present in solution

Often, in order to improve the coating characteristics (for example reduce internal stress, level the deposit or change the lustre of the deposit), organic and inorganic species are added to electrolytes. These additions can also have an influence on composite systems.

TOMASZEWSKY *et al.* [84] stated that different brighteners can have different effects, but generally they increased co-deposition. GRECO AND BALDAULF [51] confirmed this result and stated that wetting agents, in particular, were beneficial in increasing the amount of co-deposited particles.

The addition of small quantities of anti-pitting agent was found to increase the particle content of a Ni/Cr_3C_2 composite, but on further additions, co-deposition was dramatically decreased [53]. Organic additives, such as TEPA and EDTA have been

found to promote particle co-deposition with copper [34, 85-86], while urea, a common brightening agent, has proven to be detrimental to the deposition of Al_2O_3 with nickel [19]. Inorganic additives, particularly the soluble salts of the monovalent cations thallium (Tl^+), rubidium (Rb^+), caesium (Ce^+) and ammonium (NH_4^+) were especially good at promoting the deposition of fine insoluble inorganic powders with copper from sulphate baths. It was believed [85] that these cations, or the organic additives mentioned previously, did not codeposit with the powders to any appreciable extent, but could become adsorbed on the particle surface making it positively charged. The cathode could therefore attract the particles and insoluble non-conducting powders could be deposited from plain sodium-, potassium-, or other alkali metal sulphate baths.

3.7 Bath ageing

Ageing of composite electrolytes seems to affect only certain metal/particle systems. Upon ageing of a copper/alumina bath, the percentage of Al_2O_3 co-deposited decreased for an electrolyte pH of less than one. LAKSHMINARAYANAN *et al.* [87] attributed this to the presence of impurities in the electrolyte due to the partial dissolution of oxides in the solution.

This ageing process could be reversed by increasing the electrolyte pH through the addition of $Cu(OH)_2$. No ageing occurred for solutions having a $pH \geq 2$. No ageing effects were found for the co-deposition of Al_2O_3 with nickel, silver or copper, whilst copper/SiC demonstrated significant ageing [88]. Other work [50] has reported that there were no apparent ageing effects for up to 18 days for Cr/Al_2O_3, unless co-deposition was carried out at 30 A/dm^2. At this current density and a bath loading of 20 g/l alumina, a maximum co-deposition rate was noted after ten days ageing. Bath ageing for up to eight days had no apparent effect on the co-deposition of Cr/graphite [37] composite electrodeposits.

3.8 Particle pre-treatment

In 1982, NARAYAN AND CHATTOPADHYAY [50] stated that problems associated with the co-deposition of alumina with chromium can be overcome by coating the particles with nickel, or by dry grinding them prior to mixing with the electrolyte.

The first method, however, proved problematic since the coated particles proved unstable in the electroplating solution. Using dry ground Al_2O_3 powder it was shown that increasing the bath load of Al_2O_3 increased its content in the coating at all the current density investigated.

In order to codeposit fluid-containing nano-spheres with nickel, ALEXANDRIDOU *et al.* [89] found out that it was necessary to remove residual by-products of their synthesis by washing in distilled water. If this procedure was not carried out, the resulting deposits had a highly cracked morphology. In fact, it was found that careful washing of the microcapsules was a prerequisite for avoiding agglomeration of the microcapsules in the plating bath.

3.9 Effect of electrodeposit crystal growth

In 1987, SUZUKI AND ASAI [66], studying the co-deposition of alumina with silver from a thiocyanate electrolyte, stated that, if low overpotentials or low particle loadings were used, the deposits formed consisted of large silver crystals with Al_2O_3 being preferentially co-deposited at the grain boundaries. Upon increasing the bath particulate concentration and/or overpotential, they found that the alumina particles could also be co-deposited at the crystal faces. Additionally, grain growth of the silver crystal was suppressed by the presence of the alumina particles.

3.10 Brush electroplating

EHRHARDT [17] demonstrated that it was possible to deposit composite coatings using the brush plating technique. Coatings of Ni/Al_2O_3, Ni/SiC and Cr/Al_2O_3 were successfully deposited using this technique at current densities of up to 50 A/dm^2. Limited success was obtained with a high-speed cobalt electrolyte containing alumina. Operating parameters such as brush rotation speed and electrolyte flow were reported to have little effect on coating quality. However, it was important to avoid localised overheating of the electrolyte, especially when operating at high current densities.

3.11 Magnetic charging of particles

TACKEN *et al.* [90] found that magnetised nickel particles could be satisfactorily co-deposited with zinc. Particles were maintained in suspension only by agitation, and increased bath loading produced composites containing with higher contents of the codeposited material. The authors, prior to forming the composite coating, in order to obtain a better understanding about the role the steel substrate played in the process, deposited pure zinc layers of varying thickness. It was found that as the zinc layer-base thickness increased, nickel co-deposition was reduced as a result of weakened magnetic attraction forces. The authors expected that a particle gradient would be set up within the coating as film thickness increased. No clustering of the particles or dendritic growth was observed, as with other work on conducting particles, possibly due to magnetic dipole interactions between the magnetic nickel and steel cathode. It was found out that cathode current efficiency decreased with increasing nickel concentration in the electrolyte. Three possible causes were suggested:

- hydrogen is more readily evolved from nickel particles present in the coating;
- some of the nickel particles contacting the surface will evolve hydrogen and grow a layer of zinc before dislodging from the surface and re-dispersing into the electrolyte;
- conducting particles meeting the surface will be charged and, due to their capacitance, discharge in the electrolyte when the contact particle-electrode is broken.

The authors concluded that this technique offers a variety of possibilities, since it could easily be applied to any ferromagnetic metal (e.g. iron or cobalt) or compound (e.g. Fe_3O_4 or Fe_3Si), with the prerequisite that the substrate material must also be ferromagnetic. Particles that do not demonstrate ferromagnetic behaviour, such as alumina, could also be co-deposited using this technique, provided that they were coated with a suitable material prior to magnetisation. Electroless nickel would be ideally suited as a coating material in such a situation.

4. Mechanism of electrolytic co-deposition

Early work on composite plating technology suggested three possible mechanisms for the co-deposition of solid particles in a metal matrix:

- electrophoresis: proposed in 1962 by WHITHERS [91], who stated that electrophoretic motion of positively charged particles towards the cathode could be responsible for their co-deposition;
- mechanical entrapment: suggested by WILLIAMS AND MARTIN [22] in 1964. Particles are transferred to the cathode by bath agitation, which controls the amount of particles at the cathode surface. Co-deposition is governed by the duration time of particles on the cathode and by metal deposition rate;
- adsorption: in 1967 BRANDES AND GOLDTHORPE [21] stated that particles can be adsorbed onto the cathode due to Van der Waals attractive forces. Once adsorbed onto the cathode surface, the particles are incorporated into the growing metal matrix.

In 1974 SYKES AND ALNER [92, 93] made measurements of the streaming potentials of alumina in different electrolytes and studied the influence of particle concentration on the co-deposition rate. They stated that the zeta potential of alumina in Watts nickel or copper sulphate plating baths is very small and negative. They concluded that, for such a reason, electrophoresis could not be a driving force for electroco-deposition, because negatively charged particles can be incorporated as well as positively charged ones. TOMASZEWSKI [84, 85, 94] found that the presence of particles with negative charges on their surface had an unfavourable effect on the adsorption of nickel ions. Amorphous silica particles, used in his study, having such negative charges on their surface, showed poor adsorption of nickel ions and poor inclusion in the nickel matrix.

Interest in the mechanism of composite electroplating has lead to the development of models to predict the rate of particle co-deposition. Among the first of these was the model proposed by BAZZARD AND BODEN [23] in 1971, which stated that particles suspended in the electrolyte by adequate agitation constantly collide with the cathode. Particles remaining in contact for sufficiently long time will become

electroplated with a thin layer of metal and consequently embedded in the growing metal layer. However, the effects of electrolysis parameters such as pH, temperature, bath composition and hydrodynamics were not considered.

4.1 Model of Guglielmi [18, 95]

In 1972 GUGLIELMI [95] offered a model based on a two-stage adsorption process:

1. loose adsorption stage (physical in nature): particles become loosely adsorbed onto the cathode surface. Particles are still surrounded by a cloud of adsorbed ions, the ionic cloud;
2. strong adsorption stage (field assisted and electrochemical in nature): particles loose their ionic cloud, giving rise to strong adsorption on the cathode.

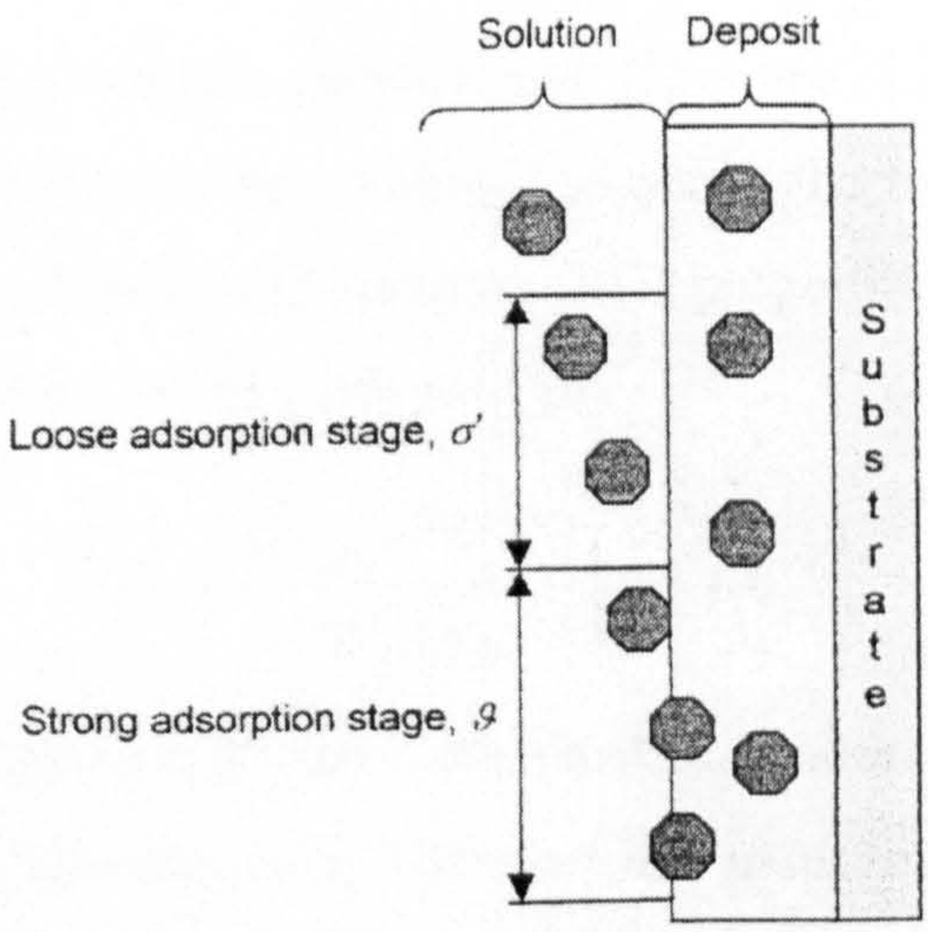

Figure 4.1 - Co-deposition mechanism based on a two-stage adsorption process [95].

During these steps, the growing metal layer engulfs the adsorbed particles. The first stage was described by a Langmuir adsorption isotherm, where the loose (α') and strong (ϑ) adsorption surface coverage and particle concentration of the bulk solution (C_p^{∞}) were related by a variable depending on the intensity of the particle-cathode interaction (k^*), as shown in the equation below:

$$\alpha' = \left(\frac{k^* C_p^{\infty}}{1 + k^* C_p^{\infty}} \right) (1 - \vartheta) \qquad \textbf{Eq. 4.1}$$

Guglielmi considered the second stage and suggested the strong adsorption rate (V_p) was linear dependent upon α', as shown in the equation below:

$$V_p = \alpha' \nu_0 e^{\beta_p \eta_c} \qquad \textbf{Eq. 4.2}$$

where η_c was a term used for cathodic overpotential to account for the field dependence as previously mentioned, while ν_0 and β_p are constants. Faraday's law can express the rate of metal deposition. Current density (j) is related to overpotential by the Butler-Volmer equation, and after accounting for the available cathode area for metal deposition, can be written in Tafel form, as shown below:

$$j = (1 - \vartheta)\, j_0 e^{\beta_m \eta_c} \qquad \textbf{Eq. 4.3}$$

where j_0 is the exchange current density and β_m is the Tafel constant for metal deposition. These equations can be combined to obtain the following, assuming that the volume percentage of embedded particles (B) is proportional to strong adsorption coverage (ϑ) and is much less than 100 percent:

$$\frac{C_p^{\infty}}{B} = \frac{M_m j_0 e^{(\beta_m - \beta_p)\eta_c}}{nF\rho_m \nu_0}\left(\frac{1}{k^*} + C_p^{\infty}\right) \qquad \textbf{Eq. 4.4}$$

where k^*, ν_0 and β_p depend upon the metal/particle system under investigation and have to be determined experimentally. Therefore this model cannot be used to predict the co-deposition behaviour of a particular system. Despite this shortcoming, the model has successfully been used to describe co-deposition for the following systems: Ni/SiC, Ni/TiO_2, Cu/(α and γ)Al_2O_3, Cr/graphite, Ag/Al_2O_3, Cu/SiC and Cu/P. It has not, however, been so successful in describing Cr/Al_2O_3, Ni/Al_2O_3 or Zn/phenolic resin. A weakness of this model is that the Langmuir adsorption isotherm is only valid for the adsorption of molecules, and may not be applicable to the relatively large particles used in composite electroplating. Also, the use of Tafel's law for reduction of metal ions implies that only charge transfer conditions are considered. CELIS AND ROOS [15] presented evidence of this shortcoming for Cu/Al_2O_3 in a review concluding that there is a considerable increase in the amount of alumina co-deposited, as current density is increased while copper ions undergo charge transfer control. When concentration overpotential control takes over, the alumina content was found to fall with increasing current density. Once the cathodic

overpotential was sufficiently large to reduce other ions onto the particles (e.g. hydrogen), higher co-deposition rates were obtained. They also stated that the second adsorption step was rate determining. Additionally, other important parameters such as particle size and type, agitation, bath constituents or bath ageing were neglected by GUGLIELMI's model.

4.2 Model of Narayan and Chattopadhy [50]

In 1982 NARAJAN AND CHATTOPADHYAY [50] electrodeposited Cr-Al_2O_3 composite coatings discovering that only when alumina particles were coated with nickel or dry ground before mixing in the conventional hexavalent chromium bath, did codepositon take place. They also found that Guglielmi's model is not valid for this system and proposed a mechanism consisting of three steps:

1. the alumina particles have a surface charge, which may be modified because of the adsorption of certain species from the plating bath;
2. particles are transported towards the cathode because of hydrodynamics and electrophoretic effects;
3. particles are entrapped in the growing chromium layer.

Alumina particles, which are initially negatively charged, move towards the cathode because of hydrodynamics and eventually electrophoresis too. Near the cathode hydrogen ions (H^+) are produced by chromium deposition and become strongly adsorbed on alumina surfaces. This adsorption would either neutralize or reverse the particles' polarity and promote the migration towards the cathode. At the surface H^+ ions are reduced and hydrogen is evolved as gas. However, the authors did not produce a formula to predict the particle content but they considered some parameters, such as the nature of the particles involved, neglected by Gulgielmi's model.

4.3 Model of Kariapper and Foster [19, 33]

KARIAPPER AND FOSTER [33] investigated the role of adsorbed metal ions. They concluded these ions play a double role:

- metal ions cause particles to be electrostatically attracted to the cathode.

- metal ions reduced at the cathode cause a strong physical bond between the particle and cathode surface.

They also investigated the significance of agitation and stated:

- agitation influences the forces acting on particles resting on the cathode surface;
- particle collision with the cathode increases with increased agitation rate.

Their model expressed the rate of particle co-deposition (V_p) by the following equation, where N^* is the collision rate of particles suitable for co-deposition:

$$V_p = \frac{N^* k^* C_p^\infty}{1 + k^* C_p^\infty} \qquad \textbf{Eq. 4.5}$$

where the intensity of the particle interaction (k^*) was assumed to be dependent on the electrostatic attraction on the adsorbed charge density (q) and on the change in potential near to the cathode (ΔE). The physical bond strength ($S_b i^2$) was determined by the contact area between metal and particle at a given current density, where (S_b) is the bond strength per unit area. In this model, k^* is also assumed to be dependent upon mechanical factors, such as particle size and density (a), and the rate of agitation (b). The particle/cathode interaction is then calculated from the expression below, where k' is a constant:

$$k^* = k'\left(q\Delta E + S_b i^2 - ab\right) \qquad \textbf{Eq. 4.6}$$

Practical use for this model appears complicated, because there are certain incorporated factors that cannot be easily measured or estimated.

4.4 Model of Celis, Roos and Buelens [19, 96]

This model was first proposed in 1987 as an attempt to address the shortcomings of GUGLIELMI's model. Co-deposition is now broken down into five steps, as shown in Fig.4.2:

1. an adsorbed double layer forms around each particle in the bulk of the solution;
2. the particles are transferred to the hydrodynamic boundary layer by forced convection;
3. the particles reach the cathode surface by diffusion;
4. free and adsorbed ions are reduced;

5. when a fraction of the ions originally adsorbed onto the particle are reduced, that particle becomes entrapped in the growing electrodeposit.

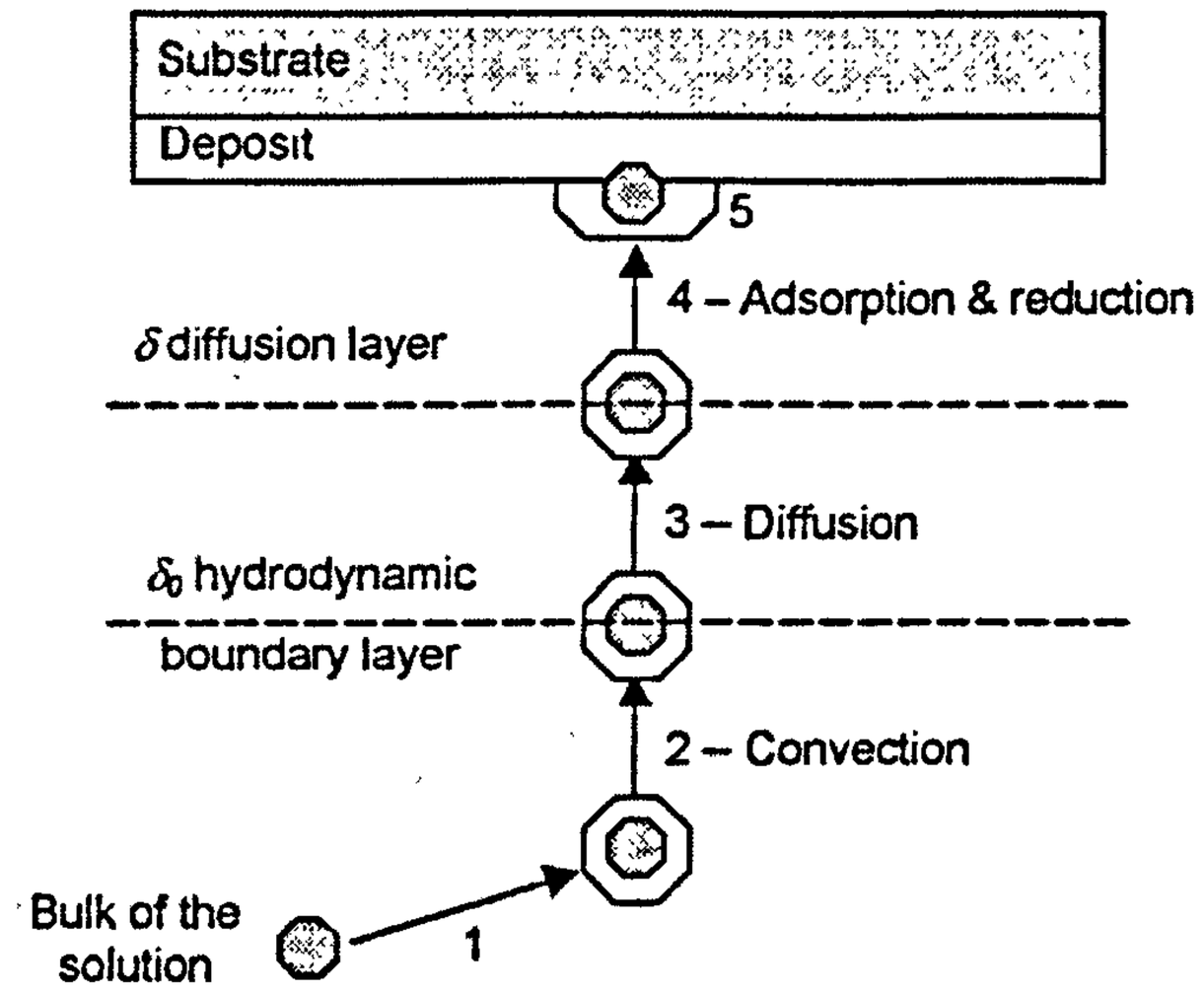

Figure 4.2 - Co-deposition mechanism based on a five-stage adsorption process suggested by Celis, Roos and Buelens [96].

The basic assumption of this model is that a certain amount of ions (k) on the particle out of a total amount of ions (K) must be reduced at the cathode for the particle to become captured. This allows for a certain residence time of a particle on the cathode surface necessary for it to become entrapped in the growing metal layer. Therefore not all particles coming into contact with the cathode will be deposited. This assumption was also made in GUGLIELMI's model, described earlier.

This model uses a statistical approach where the volume percentage of co-deposited particles (B) can be expressed as a function of the weight of one particle (W_p), number of particles arriving at the cathode surface (N_p) and the probability of a particle crossing the diffusion layer (p). The remaining bracketed terms are derived from Faraday's law and give the weight increase due to metal deposition per unit time and surface area:

$$B = \frac{W_p N_p p}{\left(\frac{M_m j}{nF}\right) + W_p N_p p} \times 100 \qquad \textbf{Eq. 4.7}$$

The term p, above, depends upon the probability ($p_{(k/K,i)}$) that at least k out of K adsorbed ions are reduced. If p_i is the chance that one ion is reduced at a current density j, then ($p_{(k/K,i)}$) can be expressed as a binomial distribution thus,

$$p_{(k/K,i)} = \sum_{z=k}^{K} C_z^K \left[1 - p_i\right]^{K-z} p_i^z \qquad \textbf{Eq. 4.8}$$

In order to calculate p_i, it is assumed that there is no distinction between free and adsorbed ions so that both can be treated as equal with respect to transport and reduction processes.

$$p_i = \frac{j}{nFC_m^\infty + \frac{j\delta^2}{2D_m} + j} \qquad \textbf{Eq. 4.9}$$

where C_m^∞ and D_m refer to the bulk concentration of metal ions and diffusion coefficient of these ions respectively, whilst δ is the diffusion layer thickness. An additional term (H) is introduced in order to account for bath agitation and other hydrodynamic effects,

$$p = Hp_{(k/K,i)} \qquad \textbf{Eq. 4.10}$$

making the probability as follows: for laminar flow condition $H=1$ while for highly turbulent flow $H=0$.

The number of particles arriving at the cathode (N_p) is found from the reduction rate of metal ions. This is related to the number of ions crossing the diffusion layer per unit time and per unit of surface area (N_m) and the type of overvoltage control,

$$N_p = N_m \frac{C_p^*}{C_m^*}\left(\frac{j_{tr}}{j}\right)^\phi \qquad \textbf{Eq. 4.11}$$

where C_p^* and C_m^* are, respectively, the number of particles and metal ions in bulk solution, whilst j_{tr} is the transition current density from charge transfer to concentration overvoltage control. The experimental term ϕ is defined as follows: under charge transfer overvoltage control $\phi = 0$ because ion reduction is rate determining; under concentration overvoltage control $\phi = 0$ because ionic diffusion is rate determining. Volume percentage of co-deposited particles can be found by

combining the previous formulae. However, terms k, K and ϕ must be determined experimentally, so, similar to GUGLIELMI's model, this model cannot predict particle content without the need for experimental investigation.

4.5 Model of Valdes [19, 97]

In 1987 VALDES [97], examined the difficulties other workers were having in obtaining a good description of the particle-cathode interactions during electrolytic co-deposition. He proposed the use of a concept frequently used for non-electrochemical system, the "perfect sink" model. This corresponds to infinitely fast reaction kinetics, i.e. assumes that all particles arriving within a critical distance of the electrode surface are irreversibly and instantaneously captured. The model was developed for co-deposition occurring at a rotating disc electrode, taking account of the various ways in which particles can be transported (i.e. Brownian diffusion and convection). The convection term accounts for all forces and torques acting on a particle, such as hydrodynamic migration, electromigration and diffusion migration. Along with expressions for the local electric field, and local electrolyte concentration, a coupled set of transport equations was obtained. However, this model was found to be of little use, since it predicts maximum co-deposition at the limiting current density, which is in contradiction with experimental findings.

Therefore, another model was proposed based on the generally accepted assumption that the reduction of adsorbed ions is the rate-determining factor for particle co-deposition. This second model, the electrode-ion-particle-electron transfer (EIPET) model, accounts for the electrochemical nature of colloidal particle deposition. This led to the formation of a Butler-Volmer type expression for particle deposition, in which charge transfer overpotential becomes the main driving force for particle co-deposition (k_p):

$$k_p = k^0 C_s n\left[\exp\left(\frac{-VZF}{RT}\eta_a\right) - \exp\left(\frac{(1-V)ZF}{RT}\eta_a\right)\right] \qquad \textbf{Eq. 4.12}$$

where (k^0) is a standard electrochemical reaction rate constant, (C_s) is the concentration of electroactive species adsorbed on the particle surface, (η_a) is the charge-transfer overpotential and (Z) is the valency of the ionic species. This model

is reportedly able to predict the peak shown in experimental data when particle co-deposition rate is plotted against current density. However, it should be noted that little work has been carried out to prove the validity of this model for "real" co-deposition systems.

4.6 Model of Hwang and Hwang [48]

This model is similar to that proposed by GUGLIELMI [18, 95] except that three different current density ranges were identified, with the rate of particle co-deposition being determined by the electrode reactions of adsorbed species on the particles. The three current density ranges for this reduction of adsorbed ions are classified thus:

1. low current density, where only H^+ are reduced;
2. intermediate current density, where H^+ reduction rate has reached its limiting value and metal is reduced;
3. high current density where the reduction rate for both metal ions and H^+ is at its limiting value.

This was an improvement over GUGLIELMI's model, but assumptions were made without any validation. The first of these assumes that the reduction of ions adsorbed on to particles differs from that of free ions in solution. Also, the efficiency of metal deposition was thought to be independent of current density, while for adsorbed ions three different regimes were distinguished.

4.7 Model of Fransaer, Celis and Roos [98]

In 1992 FRANSAER, CELIS AND ROOS proposed a model for the electrolytic co-deposition of spherical particles with metals on a rotating cylinder electrode based on a trajectory analysis of the particle deposition, including convective mass transport, geometrical interception and migration under specified forces coupled to a surface immobilization reaction. Based on the knowledge of the flow around an electrode and taking into account all the forces acting on a particle, the trajectory of that particle can be determined from the motion equation. If the criterion of particle attachment, once in contact with the electrode, is assumed (the most simple one would be that all particles stick to the electrode upon contact), the co-deposition rate

can be determined. Fig 4.3 shows a perspective diagram of the various coordinates used to describe the trajectory of particles in the electrolyte during the co-deposition process.

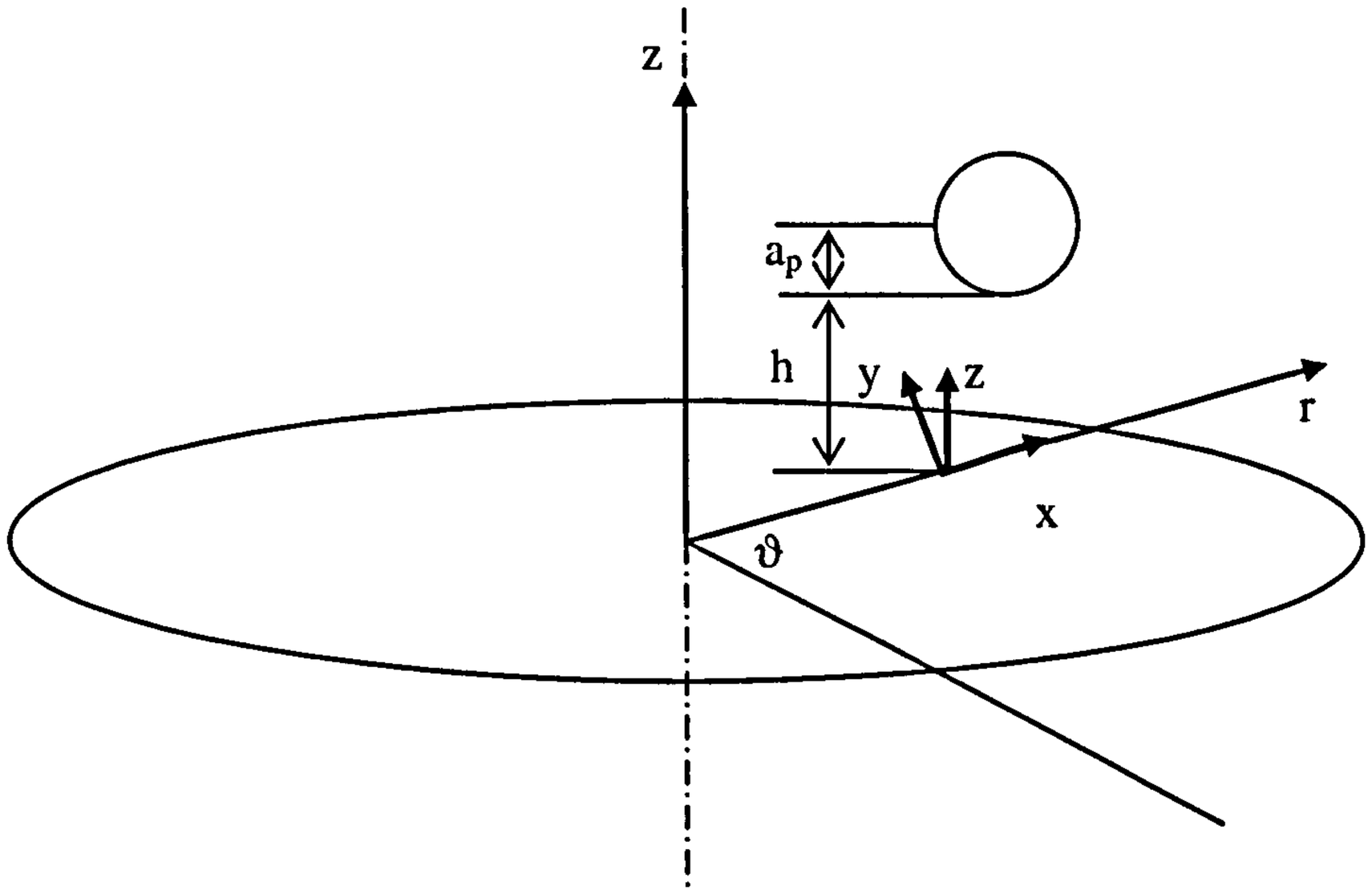

Figure 4.3 - Perspective drawing of the various coordinates used in the description of the trajectory analysis: x, y and z are the Cartesian coordinates; θ and r are the cylindrical coordinates; a_p is the particle radius and h is its distance from the x-y plane [98].

If the particle is large (>1μm), its Brownian motion can be neglected and the momentum balance on the particle can be used to predict particle trajectory. As long as the particle concentration is low and the particle size is much smaller than the rotating cylinder electrode and the thickness of the hydrodynamical boundary layer, it is possible to make the following assumption: the flow field is undisturbed by the presence of particles, except in the immediate vicinity of a particle and when a particle is more than several particle diameters away from the electrode, the particle centre moves along undisturbed fluid streamlines. In the bulk of the solution, besides the hydrodynamic forces, the forces acting on the particles are as follow: gravity, buoyancy and the electrophoretic force. In particular the electrophoretic force has been found to have a monotonic increase as the particle-to-surface separation decreases.

Another parameter they took into account is the contribution of London-Van Der Wals forces between the instantaneous dipoles that the particle forms and the dipoles induced in neighbouring atoms of the electrode and vice-versa. Once the particle is

approaching the electrode surface, the double layer of the particle and electrode overlap. The double layers, due to the high concentration of the electrolyte, are greatly compressed. This means that double layer forces are not effective in bringing particles to the electrode. However, their role in the adhesion force cannot be ruled out. The behaviour of particle in the immediate vicinity of the cylinder will be characterized by a reaction term R which is thought to consist of two terms: $R=R_i+R_r$, respectively the particle immobilization term R_i and the removal rate R_r. The advantage of incorporating the reaction term in the trajectory equation is that, because of the presence of removal forces, a condition of perfect sink (all particles contacting the cylinder become irreversibly captured) can be avoided and the specific interactions can be accounted for in a more realistic way. In real systems, surface roughness and non-uniform surface charge distributions of particle and electrode produce significant tangential forces, which locally act on the particles. This is the reason why particles remain on the electrode surface in the presence of hydrodynamic shearing. Whilst the modelling of the specific normal forces has been carried out with some success, the tangential forces are much less defined. To model these short-range tangential forces, the authors assumed that the tangential force immobilising a particle is proportional to the normal adhesion force. If the hydrodynamic shearing forces are balanced by interactions in a narrow region of the particle-wall contact, a force balance on the particle can be set up (Fig.4.4).

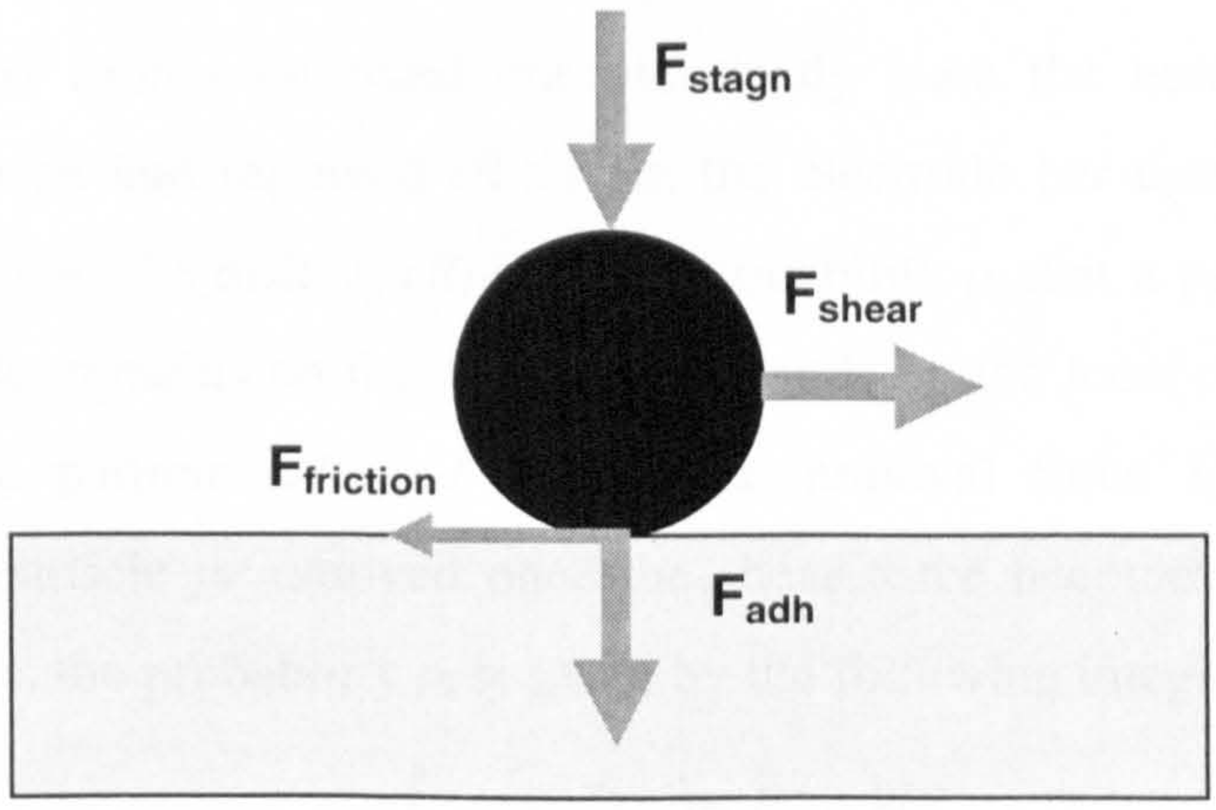

Figure 4.4 - Scheme for the various forces acting on a particle near a plane surface [98].

F_{adh} is the force of adhesion; F_{stagn} and F_{shear} are the hydrodynamical forces due to the stagnation point flow and the various shear flows. The critical shear force needed to remove a particle is given by:

$$F_{shear} = k\left(F_{adh} + F_{stagn}\right) \qquad \textbf{Eq. 4.13}$$

where k is the static coefficient of friction (friction theory is adopted, which assumes that the tangential force localising the particle is given by the normal force times the friction coefficient k). The authors calculated the shear and stagnation forces from the previous analysis of the forces acting in the bulk of the solution. Near the rotating cylinder electrode, the total shear force was found as follows:

$$\vec{F}_{shear} = 6\pi\mu a\left\{v_{lin}^{x}\tilde{F}_{lin} - a_p v_{par}^{x}\tilde{F}_{par}\right\}\vec{i}_x + 6\pi\mu a_p^2 r_p v_{lin}^{y}\tilde{F}_{lin}\vec{i}_y \qquad \textbf{Eq. 4.14}$$

where μ is the dynamic viscosity [g m^{-1} s^{-1}], a_p the particle radius, v_{lin} and v_{par} the absolute viscosity [m^2 s^{-1}] pertaining the to the linear shear flow and to the parabolic (quadratic) shear flow, r_p the particle radial position in cylindrical coordinates, $\vec{i}_x$ and $\vec{i}_y$ unit vectors in Cartesian coordinates (see Fig. 4.3 for the various coordinates used in this description). Eventually the adhesion force is given by:

$$F_{adh} = \frac{6\pi\mu a_p^2}{k}\sqrt{\left\{v_{lin}^{x}\tilde{F}_{lin} - a_p v_{par}^{x}\tilde{F}_{par}\right\}^2 + \left\{v_{lin}^{y}\tilde{F}_{lin}\right\}^2} - 6\pi\mu a_p^3 v_{stagn}\tilde{F}_{stagn} \qquad \textbf{Eq. 4.15}$$

After a review of literature, the static coefficient of friction k, [99], has been assumed to be 1. The possibility that the friction coefficient will be different in the case of different systems (authors chose the codepositon of polystyrene with nickel as a reference system) cannot be ruled out. At steady state the number of particles immobilised (R_i) on and removed (R_r) from the electrode per unit time equals the flux j_p of particles to the disk: $j_p=R_i-R_r$. The probability p_i that a particle, in contact with the electrode, remains on the electrode, depends on the local ratio of the forces immobilising the particle $k(F_{adh}+F_{stagn})$ to the removal force F_{shear}. Since it is assumed that a particle is removed once the shear force becomes greater than the total normal force, the probability p_i is given by the following integral:

$$p_i = \frac{\int_{F_{shear}}^{\infty}\left(f_{adh}(F) + F_{stagn}\right)dF}{\int_{0}^{\infty}\left(f_{adh}(F) + F_{stagn}\right)dF} \qquad \textbf{Eq. 4.16}$$

where $f_{adh}(F)$ is the differential distribution of the adhesion force of a particle on the electrode. The denominator normalizes the probability, while the numerator is the probability that the normal force is greater than the shear force. The distribution

$f_{adh}(F)$ arises because the adhesion force between a particle and the electrode depends on the local physical and geometrical imperfections and on the size of the particle. The probability p_i is a function of position, time, the size of the particle, the current density, the fluid flow velocities and it should be looked upon as the instantaneous probability that a particle remains on the electrode. Since particles passing nearby exert random forces on particles residing on the surface, an immobilized particle may be removed at a later instant. The first instant is, however, the most critical since in later instances metal grows around the particle, leading to a lowering of the tangential removal forces and a concomitant increase in the normal adhesion. The probability that a particle in contact with the electrode will codeposit is given by the time average (p_i) of the instantaneous probability p_i. Using Eq. 4.16 the immobilization rate R_i is given by $j_p p_i$ and $R_r=j_p(1-p_i)$.

Concluding, the authors stated that a particle remains on an electrode if the ratio of the normal to tangential forces acting on the particle when it first hits the surface is favourable. If this condition is satisfied, a particle brought into contact with the electrode has enough footholds to remain on the electrode and be engulfed by the growing metal. In the centre of a RCE, tangential forces are absent and the rate of co-deposition is controlled solely by the mass transfer of a particle towards the rotating electrode with due account of surface blockage and hydrodynamic shielding. The analysis and calculations carried out by the authors indicate that the trajectory method is an adequate basis for studying the electrolytic co-deposition of particles on a RCE. The comparison of experimental results with theoretical predictions proves the predominance of the tangential shearing forces and, in general, of the fluid flow velocities on the co-deposition of particles. The experiments also point out that the lack of useful descriptions for the tangential forces localising the particles is the most pronounced difficulty in developing useful theories on electrolytic co-deposition. This difficulty arises because the all models proposed for the normal force assume a spherical isotropic particle on a flat surface, while tangential forces only emerge if geometrical and physical heterogeneities are taken into account. The need for an adequate representation of the randomness of particles and electrode is thus obvious.

In their recent work, BOZZINI *et al.* [63, 75] used a similar approach to study the hydrodynamic actions leading to the electrodepositon of AuCu/B_4C composite coatings using a rotating cylinder electrode. They interpreted the entrapping actions, which lead to embedding of particles in the growing cathode and to selection of their diameters, in terms of the balance of forces acting on the particle lying in the boundary layer.

4.8 Model of Vereecken, Shao and Searson [100, 101]

Recently VEREECKEN, SHAO and SEARSON [100, 101] have carried out analyses on the electrolytic codepositon of particles. They showed that the kinetics of nanometre size particle incorporation into a growing film can be described by a model that takes into account both the diffusion forces as well as the gravitational force acting on the particle. They considered a single rigid particle in a homogeneous solvent. The net velocity v of the particle is proportional to the total force F_{total} acting on the particle [102].

$$F_{total} = fv \qquad \textbf{Eq. 4.17}$$

where f is defined as the friction coefficient, which according to Stoke's law is given by $f = 6\pi\eta r$, where η is the viscosity of the solution [g cm^{-1} s^{-1}] [102]. The force on the particle has two components. The first is due to the diffusion force F_d, which was taken by Einstein to be the negative of the chemical potential gradient [102]:

$$F_d = -\nabla\mu \qquad \textbf{Eq. 4.18}$$

The second component is related to the gravitational force F_g acting on the particle:

$$F_g = mg = \frac{4\pi r^3}{3}\rho g \qquad \textbf{Eq. 4.19}$$

where m is the mass of the particle, g is the acceleration due to gravity and ρ is the density of the particle. Gravitational force is strongly dependent on the particle size. For an ideal solution, the chemical potential gradient is given by:

$$-\nabla\mu = \frac{k_B T}{c}\nabla c \qquad \textbf{Eq. 4.20}$$

where k_B is Boltzmann's constant, T is the temperature and c is the particle concentration [mol cm^{-3}].

For deposition at an electrode that is downwards facing, as shown in Fig.4.5, the gravitational force is opposed in direction to the diffusion force due to the concentration gradient.

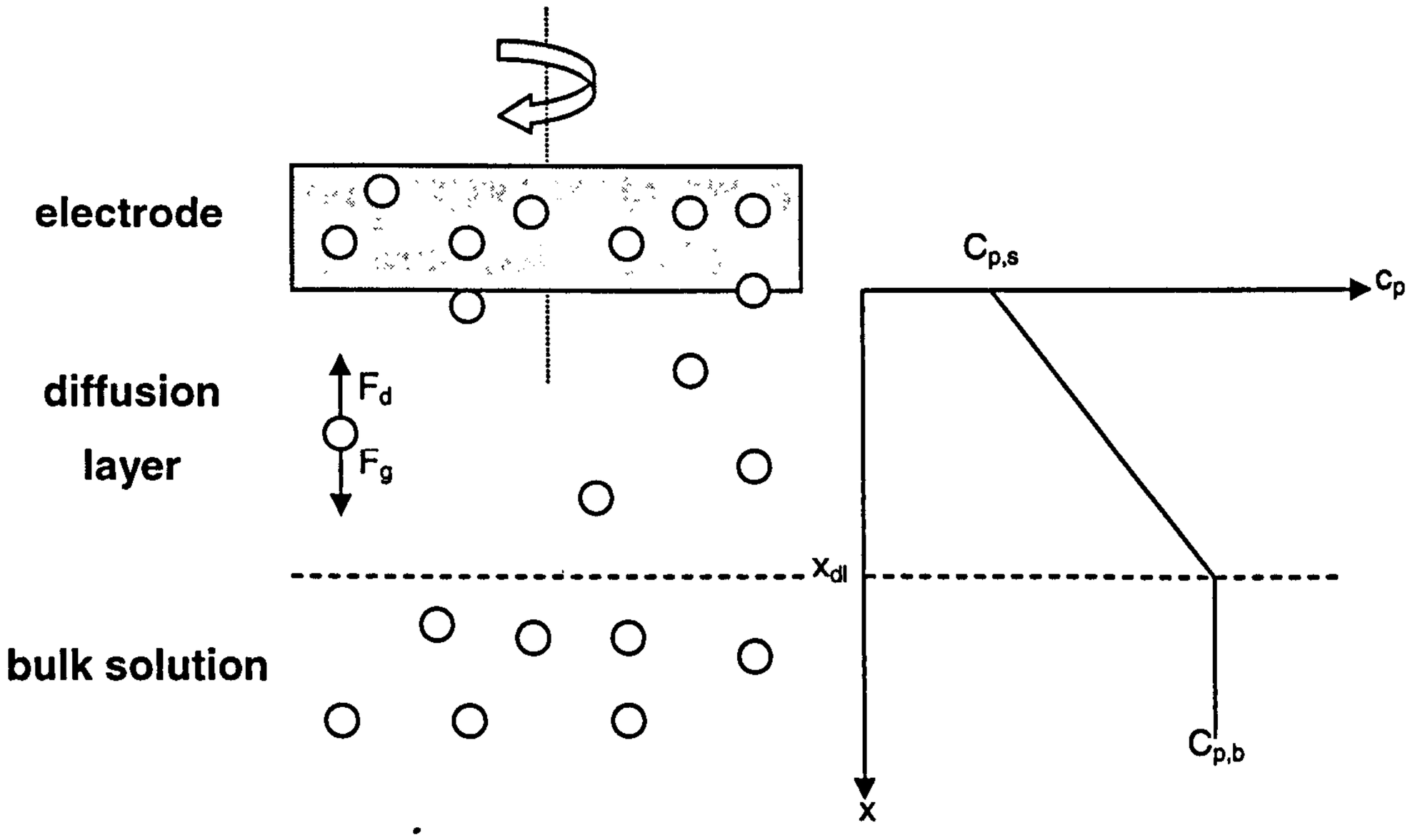

Figure 4.5 – On the left schematic illustration showing the particle diffusion force and gravitational force when the rotating disk electrode faces down. On the right particles concentration profile. $C_{p,b}$ is the particle concentration in the bulk of the solution, while $C_{p,s}$ is the particle concentration at the disk surface. x_{dl} is the diffusion layer thickness [100, 101].

The total force exerted on the particle is given by:

$$F_{total} = F_d - F_g \qquad \textbf{Eq. 4.21}$$

Combining Eq. 4.18, 4.19, 4.20 and 4.21, Eq. 4.17 can be rewritten as:

$$F_{total} = \frac{k_B T}{c}\nabla c - \frac{4\pi r^3}{3}\rho g = 6\pi\eta r v \qquad \textbf{Eq. 4.22}$$

The particle flux $J_P = cv$. Substituting for the velocity from Eq.4.22 we obtain:

$$J_P = \frac{k_B T}{6\pi\eta r}\nabla c - \frac{2\rho g r^2}{9\eta}c \qquad \textbf{Eq. 4.23}$$

Comparison with Fick's first law shows that $\frac{k_B T}{6\pi\eta r}$ is the particle diffusion coefficient D_P [102]. The Nernst diffusion layer model can express the particle flux towards the surface [103]:

$$\nabla c = \frac{(c_{p,b} - c_{p,s})}{x_{dl}} \qquad \textbf{Eq. 4.24}$$

where $c_{p,b}$ is the bulk particle concentration, $c_{p,s}$ is the particle concentration at the electrode surface and x_{dl} is the diffusion layer thickness. The particle flux, considering that $(c_{p,b} + c_{p,s})/2$ is the average particle concentration within the diffusion layer, can be written as:

$$J_P = D_P \frac{(c_{p,b} - c_{p,s})}{x_{dl}} - \frac{\rho g r^2}{9\eta}(c_{p,b} + c_{p,s}) \qquad \textbf{Eq. 4.25}$$

The diffusion layer is given by [104]:

$$x_{dl} = 1.6\upsilon^{1/6} D_P^{1/3} w^{-1/2} \qquad \textbf{Eq. 4.26}$$

where w is the rotation rate of the electrode (s^{-1}). Substituting Eq.4.26 into Eq.4.25 gives:

$$J_P + 2Ac_{p,b} = (A + B)(c_{p,b} - c_{p,s}) \qquad \textbf{Eq. 4.27}$$

where A and B are defined as:

$$A = \frac{\rho g r^2}{9\eta} \qquad \textbf{Eq. 4.28}$$

$$B = 0.62 D_P^{2/3} \nu^{-1/6} w^{1/2} \qquad \textbf{Eq. 4.29}$$

The parameter A is related to the gravitational forces whereas B is related to the diffusion flux. For a given particle size and solvent, A is a constant and B is a function of rotation rate. The particle flux can also be written in terms of the volume fraction x_V of particles in the film [100]:

$$J_P = \frac{3V_{m,M}}{4\pi r^3 z F N_A} \frac{x_V}{1 - x_V} i \qquad \textbf{Eq. 4.30}$$

where $V_{m,M}$ is the molar volume of the metal film, z is the charge on the metal ion, N_A is Avogadro's number and i is the deposition current density (assuming 100% current efficiency). The particle flux can be experimentally determined from Eq. 4.30 as long as the volume fraction of particle in the film is $x_V/(1-x_V)=V_P/V_{metal}$ where V_P is the total volume of particles in the film and V_{metal} is the volume of the deposited metal matrix. Combining Eq. 4.25, 4.26 and 4.30 gives an expression for V_P/V_{metal} as a function of the rotation rate w and current density i:

$$\frac{V_P}{V_{metal}}=\frac{4\pi r^3 zFN_A}{3V_{m,M}i}\left[\left(0.62D_P^{2/3}\upsilon^{1/6}w^{1/2}\right)\left(c_{p,b}-c_{p,s}\right)-\frac{\rho g r^2}{9\eta}\left(c_{p,b}+c_{p,s}\right)\right] \qquad \textbf{Eq.4.31}$$

When the metal deposition becomes fast enough so that all the particles that reach the electrode surface are incorporated in the metal matrix (*i.e.* particle incorporation probability p=1), the particle surface concentration $c_{p,s}$=0. In this case, particle incorporation becomes limited by particle diffusion to the layer, and Eq.4.31 can be rewritten as:

$$\frac{V_P}{V_{metal}}=\frac{4\pi r^3 zFN_A}{3V_{m,M}i}(B-A)c_{p,b} \qquad \textbf{Eq. 4.32}$$

This equation illustrates that particle incorporation is dependent on particle diffusion through term B, and particle deceleration due to the gravitational force through term A. When particle incorporation is under diffusion control, the particle surface concentration is zero and the significance of the gravitational term can be illustrated by plotting the magnitude of A and B vs. particle size, as shown in Fig.4.6. As can be seen, the particle gravitational force is close to the diffusion force when the particle becomes larger than 100 nm, $A/B \leq 0.03$ and gravitational force can be ignored.

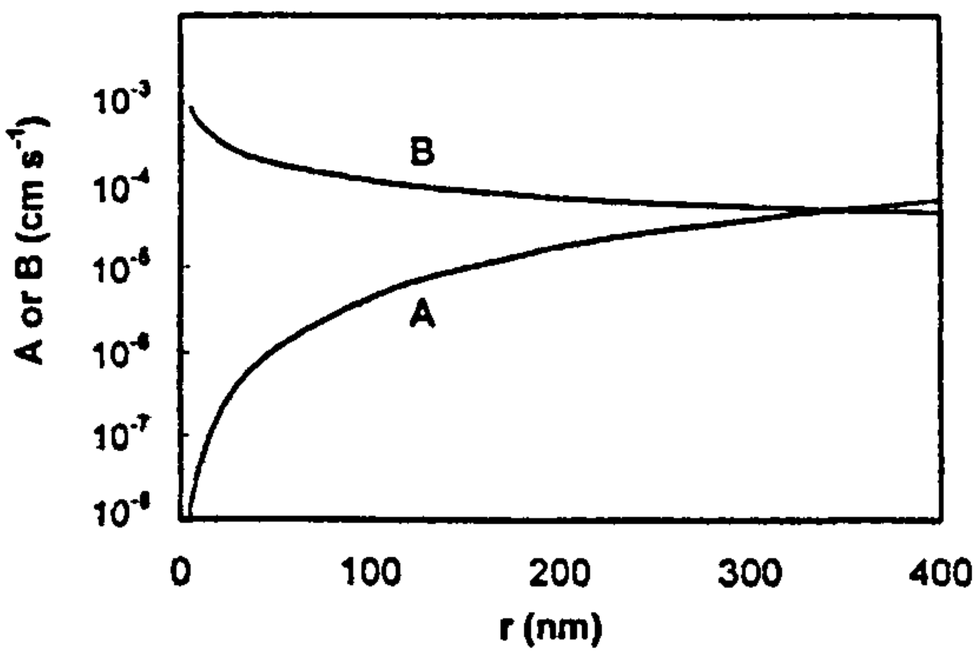

Figure 4.6 - A plot of parameters A and B in Eq. 4.31 *vs.* particle radius r [101].

5. Properties and industrial uses of composite coatings

As mentioned previously, one of the advantages of composite coatings is the improvement in physical properties that can be achieved even as far as providing new coating characteristics. Advantages of composite deposition can be summarised as [15, 32, 105]:

- high performance coatings can now be applied to materials such as titanium, aluminium, lower-cost steels, ceramics and polymers, where, with previously used techniques, this was either difficult or impossible. The benefits of this capability are of special interest to aerospace applications where lighter, more durable or less expensive materials are required and are made practical with such surface treatments;
- replacement of environmentally harmful coating processes, such as electroplated chromium can be achieved with suitable composite coatings;
- the production of higher productivity manufacturing equipment with greater speeds, less wear and less maintenance-related downtime trough the use of high performance coatings on critical surfaces;
- even more demanding service conditions can be endured requiring, for instance, less wear and lower friction.

5.1 Self-lubricating coatings

As with wear resistant coatings, self-lubricating coatings will reduce the coefficient of friction and associated wear resistance of two sliding bodies. From this point of view the embedded particles must have some level of inherent lubricity. Suitable second phase materials include graphite, molybdenum disulphide, barium sulphate and synthetic polymers such as PTFE [15, 85, 105]. Nickel/PTFE coatings have been used in Japan on moulds due to their non-stick properties. Metal/PTFE composite coatings also show poor wetting characteristics with water, so they are particularly beneficial for use in condenser pipes. An insulating water film will not cover such coated pipes and an increased thermal efficiency for the condenser can be obtained [77, 79]. Other work on metal/fluoropolymer coatings by SAKSIN *et al.* [36] claimed that wear, heat and corrosion resistance could be increased by a factor of ten, but no supporting evidence was given.

DONAKOWSKY AND MORGAN [106] co-deposited graphite within a zinc matrix using a barrel plating technique. These coatings were developed as a possible replacement for electrodeposited cadmium used on threaded fasteners. Standard acid electrolytes, based on either sodium or potassium chloride, were employed with the additions of between 5-75 g/l refined colloidal graphite (2 μm particle size). No surfactants were added and the particles were held in suspension purely by solution agitation. The potassium chloride bath was reported to give the most lustrous deposits, but was not adopted on the grounds that coating brightness was not important, and sodium chloride is cheaper. Tribological performance, assessed by the torque-tension method, was said to be comparable to that of cadmium (either chromated or un-chromated). By increasing the graphite content of these coatings, the coefficient of friction could be reduced even further. Neutral salt-spray testing revealed that zinc/graphite offered inferior resistance to electrodeposited cadmium, even when a chromate conversion coating was applied. However, no comparison was drawn with conventional zinc deposits.

ALEXANDRIDOU *et al.* [89] have produced self-lubricating coatings by the co-deposition of oil containing microcapsules with nickel. As the metal and capsules are progressively worn away, liquid lubricant is released, thus maintaining a low coefficient of friction.

5.2 Wear resistant coatings

The wear resistance of coatings can be improved by codepositing hard second phase materials such as silicon carbide (SiC), tungsten carbide (WC) or diamond.

Typical industrial applications are:

- copper/SiC for electrical contacts;
- copper/WC coatings with good erosion resistance and anti-arc properties;
- nickel/SiC and cobalt/Cr_3C_2 used as bearing coatings for the automobile and aircraft industries;
- nickel/diamond coatings used on saw blades [78].

One of the most well known examples of the use of nickel/SiC coatings is in components of the Wankel-rotary engine [39, 78]. These coatings contain approximately 5% SiC. However, special care had to be exercised in the selection of contacting materials, since these coatings are highly abrasive. Nickel shows wear resistant properties even if co-deposited with alumina [81], and the extent of wear resistance has been found to increase with increasing alumina content in the composite coating.

The electrolytic cobalt/Cr_3C_2 composites (trade name *Tribomet T104C*™) have been adopted on an industrial scale in the UK to combat wear on aircraft engine components [107]. These coatings offer exceptional fretting wear resistance over a wide range of temperatures (20 °C-800 °C).

SACHIAN *et al.* [108] produced zinc composite coatings containing SiC and/or Al_2O_3 from alkaline electrolytes. Coating hardness was greatly influenced by the percentage of embedded particles, up to a maximum of 5-6%, where after the coatings became brittle. These composites offer improved wear resistance and frictional properties when compared to conventional zinc deposits, with a marginal improvements in corrosion resistance. Another point of note is that the coating structure (e.g. grain size) was believed to have been modified by the co-deposition of particles and some of the organic conditioning agents.

With nickel/Al_2O_3 coatings the wear resistance was found to increase with the Al_2O_3 content in the coating [81]; a composite containing 22 vol.% Al_2O_3 gave improvements in wear resistance of up to three times that for AISI 316 stainless steel and six times that of conventional electrodeposited Watts nickel. Wear resistance of the nickel/diamond composites was also influenced by the size of the occluded particles, and was highest when synthetic or natural diamonds of 3-6 μm diameter were used [109]. Smaller or larger diamonds gave reduced wear resistance. Similarly, but for the Ni/SiC system, MATHIS *et al.* [27] found that smaller particles (<10 μm) offered better wear resistance than larger ones (>20 μm). This was because the larger particles tended to pull out of the matrix material more easily.

The same system (Ni/SiC) has been studied by GARCIA *et al.* [67]. They evaluated the friction and wear behaviour of these composites in uni- and bi-directional sliding tests against corundum balls, obtaining the best wear resistance with Ni/SiC composite coatings containing 4-5 vol.% submicrometre SiC particles.

WAN *et al.* [110] compared Cu/$MoSi_2$ and Cu/Al_2O_3 coatings in terms of hardness and wear rate. Hardness was found to increase with increasing particle content in the deposit, due to the dispersed phase obstructing movement of dislocations and plastic flow in the matrix. The authors concluded that wear rate was independent of particle hardness, since composites containing the softer $MoSi_2$ particles gave the lowest wear rate.

Results of an investigation to assess the performance of aluminium bronze coatings and molybdenum coatings both filled with PTFE and deposited on steel substrates in rolling line contact have been presented by AKDOGAN *et al.* [111]. The authors' results show that both types of coating studied have outstanding wear and surface fatigue resistance. Under pure rolling conditions, the aluminium bronze coating was found to be more wear resistant than the molybdenum coating. However, after $1.2 \cdot 10^6$ load cycles under the normal load of 36 N and 98 N, both coatings did not suffer any serious surface damage.

GUO AND ZHU [112] produced a composite coating containing 1.35 wt.% CeO_2, 5.46 wt.% W, 3.82 wt.% B, 15 wt.% SiC and nickel. They found the addition of CeO_2 enhanced the hardness and wear resistance of the coating remarkably. The authors showed the hardness and wear resistance of the coating increased with a rise in heat treatment temperature, and the hardness reached the optimum value at 400 °C, whilst the coating had the best wear resistance at 500 °C. The wear resistance they obtained is four times as high as that of chromium and the corrosion resistance was superior to that of 1Cr18Ni9Ti stainless steel in various corrosive media (except for nitric acid).

5.3 Corrosion resistant coatings

In order to prevent corrosion of a metal substrate zinc flake paints are successfully employed, but similar effects can be obtained by the inclusion of particles within

electrodeposited metal coatings. Several kinds of sub-micrometre particles have been investigated for this reason, such as Al_2O_3, $BaSO_4$, Si_3N_4, V_2O_5 and Cr_2O_3; their incorporation has been shown decrease the corrosion of metal considerably [32].

By the deposition of microporous chromium layers, caused by the presence of non-conducting particles in the underlying nickel layer, the corrosion resistance of traditional nickel-chromium layered systems can be improved. Corrosion of the nickel layer occurs over an increased area, resulting in a smaller depth of attack. Zirconium carbide particles are beneficial in improving corrosion resistance of chromium in sulphurous atmospheres [105]. Ni/Al_2O_3 and Ni/SiC coatings offer better oxidation resistance than conventional nickel in oxygen-enriched atmospheres. Zinc/chromium hydroxide composites are reported to offer considerably enhanced corrosion performance in salt-spray test (264 hours to red rust) when compared to commercial bright zinc 8 µm deposits (96 hours). Similar effects were obtained for zinc/Al_2O_3 composites, but to a lesser extent [113].

Epoxy resin or calcium phosphate, when co-deposited with zinc, act as corrosion inhibitors [39]. BAPU AND YUSUF [35] stated that the presence of V_2O_5 in a nickel matrix confers improved protection on steel against corrosion in NaCl medium. On the contrary, recent work carried out by ERLER *et al.* [114] shows deterioration in corrosion resistance for Ni composite coatings with nano-particles of oxide ceramic (alumina and TiO_2). The observation was carried out using salt spray tests and potentiodynamic measurements of corrosion current density when particles were co-deposited. This behaviour might be explained by an accelerated diffusion of chloride ions along the interface between nickel and incorporated particles.

Composite coatings can also provide adhesion between coatings and subsequent lacquer or paint layers with a consequent improvement in corrosion performance. Zinc and copper, co-deposited with polymer (e.g. PTFE), are typical examples in this sense [78].

HIRAMATSU *et al.* [115] investigated the paint adhesion characteristics of zinc/silica composites and managed to obtain coatings offering very good resistance in salt spray tests. This high corrosion performance was obtained by treating the composite

coating with a silane-coupling agent prior to applying the spray-coated melamine type paint, because of the ability of this agent to form chemicals bonds with both silica and melamine type paints, therefore promoting adhesion between the coating and paint layer. This system was said to offer far better adhesion and corrosion protection than phosphate type coatings normally used to aid paint adhesion on zinc.

SOVA [55] used Ni-Co-Zr-Cr ternary alloys to prevent high temperature degradation of the underlying carbon-fibre composite substrate. Direct electrolytic co-deposition of ternary or quaternary chromium based alloys is very difficult due mainly to the different deposition potentials of the co-deposited metals as well as the electrolyte instability. The author achieved deposition of a four-component alloy system in two stages by co-deposition of zirconium in a Ni-Co matrix alloy and either under or over coating chromium; the four components are then alloyed by diffusion at about 1000 °C under vacuum.

5.4 Dispersion strengthened coatings

By dispersing small particles in a metallic matrix a strengthening effect based on the Orowan theory can be expected, with an improvement in mechanical properties up to the melting temperature of the metallic matrix. However, the particles might cause a slight reduction in other properties.

For nickel composites containing alumina, titania, silica or zirconia, and chromium composites containing alumina [50], the coating hardness was found to increase with increased particle content. The opposite was found for nickel/graphite composites, where hardness was decreased as particle content was increased, probably due to the low shear strength which graphite possesses, allowing easy deformation.

Co-deposition of oxides or carbides with either nickel or copper was found to improve mechanical properties such as room temperature yield strength or ultimate tensile strength. STANKOVIC AND GOJO [54] found that they could dramatically increase the tensile strength of copper by its co-deposition with alumina. Copper/silicon carbide composites, on the other hand, showed an initial sharp rise in tensile strength up to a particle content of approximately 2 wt.%, followed by a sharp

decline, reaching a minimum at around 4 wt.% SiC. This minimum in tensile strength is still higher than for conventional copper coatings. The authors also investigated coating hardness stating that co-deposition of hard abrasive particles tended to yield composites having increased hardness, while softer particles (e.g. MoS_2, $BaSO_4$ and graphite) had the opposite effect.

GRECO AND BALDAUF [51] stated that alumina particles gave greater increases in strength than titania particles if included in a nickel matrix because of the finer particle size and uniform distribution of alumina through the matrix.

Recently MANNA *et al.* [116] deposited nanocrystalline aluminide particles ($NbAl_3$ and Cu_9Al_4) along with copper onto a copper substrate. They proposed that co-deposition of $NbAl_3$ is more effective in enhancing the hardness. However, co-deposition beyond a limit adversely affects the electrical conductivity. They determined the optimal conditions for co-deposition to enhance hardness without adversely affecting conductivity and predicted co-deposition could be a suitable technique for developing a surface composite microstructure with uniform distribution of nanocrystalline alumide particles.

Besides the particle size distribution, the mechanical properties of the coatings are influenced by the grain size of the metal matrix. Recently, ZIMMERMAN *et al.* [117] tested the mechanical properties of a nanocrystalline Ni matrix (grain size 10-15 nm) reinforced with sub-micrometre size SiC particulates (average particle size: 0.4 μm) up to 10.5 vol.% produced by pulsed electrodepsotion. They found a substantial improvement in hardness, yield and tensile stress compared with conventional Ni/SiC composites with a matrix grain size in the micrometre range. The authors measured tensile strengths up to four times that for conventional polycrystalline Ni and twice that for conventional polycrystalline Ni/SiC of comparable SiC content. The tensile and yield strengths of the nanocomposite coatings with SiC content less than 2 vol.% were higher than those for pure nanocrystalline Ni of comparable grain size. The authors also found out an unexpected increase in tensile ductility when compared to pure nanocrystalline nickel. At higher SiC content (>2 vol.%) the strength and the ductility were found to decrease to the detriment of the nanocomposite. This was thought to be due to particle clustering in the coating.

5.5 Heat-treatable metal/alloy coatings

Composite coatings may be heat-treated for different reasons. Upon heat-treatment, as-plated or hot/cold rolled, composite coatings retain higher strength than conventional coatings up to the highest annealing temperature (a uniform particle distribution is necessary to obtain maximum hardness after annealing).

VERELST *et al.* [49] noticed that, prior to heat-treatment, nickel/alumina composites had similar microstructures to conventional nickel deposits. After annealing at 800 °C for one hour, the grain size of the composite coatings had not increased appreciably, but the microstructure had changed, with the annealed grains showing fewer defects. This demonstrated that dispersed alumina inhibits grain growth. The annealed composite did, however, show a marked decrease in mechanical properties, such as yield strength (a drop of 300 MPa was obtained, while for pure nickel the drop because of the annealing was about 150 MPa). Also GRECO AND BALDAUF [51] found that nickel/alumina and nickel/titania composites showed a reduction in mechanical properties (hardness, ultimate tensile strength and yield strength) when heat-treated at temperatures of 650 °C, but percentage elongation was hardly effected. No phase changes were found for these coatings.

Composite deposits can also be heat-treated in order to obtain coatings that are not easily produced by other methods, such as the production of a "stainless steel" coating by the heat-treatment of an iron-nickel alloy containing chromium particles [47]. Other alloys produced using this method are zinc-nickel (nickel particles in a zinc matrix) alloys by the heat-treatment of zinc/nickel composites [90], and Ni-Co-Zr-Cr- diffusion alloys (see section 5.3) [55].

Another interesting example of the heat-treatment of composite coatings is the ability to sinter the "white layer" of a metal/PTFE composite (film of loosely bound PTFE particles present on the coating surface) to provide a good adherent top layer of polymer with excellent dielectric properties and high corrosion resistance [79].

5.6 Multi-layer composite coatings

One of the earliest references to such coatings was the work by KARRIAPPER AND FOSTER [33]. They were able to produce compositionally modulated composites of Ni/Al_2O_3, Ni/SiC and Ni/TiO_2 by the use of DC conditions accompanied by periodic reverse plating (the specimen was alternately polarized at 900 mV cathodically and 200 mV anodically with different cycle times). They found that short cycle times of periodic reverse current (10 ms) produced deposits with few or no particles present, whilst longer cycle times (30, 100 ms) prevented co-deposition of larger particles. This was attributed to the fact that for small cycle times, particles were repelled by anodic conditions near the cathode, whilst, for short cycle times, the particles had discharged sufficiently to be inert to field changes in their vicinity.

HELLE AND WALSH [78] stated that it was possible to produce compositionally modulated composite coatings by varying parameters such as current density, temperature, surfactant level and type, and the degree/type of agitation.

HELLE [77, 79-80] also stated that it is possible to deposit metal in the white layer formed on metal/PTFE composite coatings. This would allow an additional layer of composite material to be co-deposited from a conventional electrolyte.

It is therefore possible, by selecting carefully the operating parameters, to produce coatings having a modulated particle composition, referred to as compositionally modulated composite deposits (CMCD) by KERR *et al.* [39].

5.7 Liquid-containing microcapsule composite coatings

KENTEPOZIDOU *et al.* [118] investigated the possibility of the deposition of water-containing microcapsules with nickel. The capsules were synthesised by means of an interfacial polymerisation process, which involves the condensation polymerisation of two complementary monomers, each of which is soluble in one phase of a two-phase dispersion system. Upon reacting and the subsequent evaporation of the solvent, these monomers create a thin polymeric shell around the fluid phase to be encapsulated. Composition of the liquid core was reported to show a notable

influence on the capsule quality, and subsequent dispersion stability in aqueous solutions.

Dispersion stability was also related to the reactivity of surface groups on the capsules with the electroplating bath constituents (i.e. ions, surface active agents, polymeric species, as well as pH and temperature). These surface groups on the microcapsules arise from the polymeric wall material itself and the stabiliser used for its preparation. Additionally, due to the microporosity of these capsules, any ions present in the core solution may interact with the dispersion medium. Stabilisers present on the surface of the capsules act as bath contaminants, producing cracked deposits. This was overcome by washing the particles and using a different emulsifier (in order to solve the lack of suspension stability of the water-containing capsules) capable of improving the hydrophobic nature of the capsules, and preventing their agglomeration in solution. These surfactants were also used to aid dispersion of the water-containing capsules and were found to significantly improve their co-deposition with nickel. Two possible alternative uses of such coatings are in the synthesis of metal foams, and production of surface films capable of providing their own conversion coatings top layer [40] (i.e. self-chromating coatings).

In 2002 FAURE *et al.* [16] co-deposited new particles, called spherulites, into a zinc hydroxide layer by electrolytic co-deposition. These are colloidal particles able to encapsulate a rich variety of compounds (pigment, polymer and oxides) and can, therefore, provide unique properties to the composite depending of the encapsulated compound i.e. pigment for decorative purpose or polymers for antisticking properties. The spherulites are multilamellar vesicles, which differ from the classical ones by the persistence of the lamellae down to their core. They are usually produced by shearing a lamellar phase without excess solvent.

5.8 Electrode materials

In the work carried out by NONAKA *et al.* [119, 120], various hydrophobic composite electrodes were produced for the electro-reduction of organic compounds. Composites of zinc/tetrafluoroethylene oligomer and zinc/fluorocarbon (CF_n) were deposited from simple sulphate electrolytes, while tetrafluoroborate baths were used

to form the zinc/fluorinated pitch and lead/PTFE composites. Coatings of nickel containing fluorinated pitch were also produced, using sulphamate baths. In all cases, surfactants were added to the electrolytes to aid co-deposition.

In 1992, IWAKURA *et al.* [121] produced electrodes prepared by simultaneous electrodeposition of Ni and RuO_2 on a Ni substrate from an electrolyte containing a suspension of RuO_2 under vigorous stirring condition. These electrodes have been found to have excellent characteristic as active cathodes for hydrogen evolution in hot concentrated alkaline solutions.

5.9 Medical composite coatings

DASARATHY *et al.* [122] proposed that hydroxyapatite (HA), a popular bio-ceramic based on calcium phosphate, could be co-deposited with metal. Initial trials appeared successful, with the deposition of a cobalt/HA composite onto titanium alloys. Although substrate adhesion was not sufficiently high, the authors concluded that the results demonstrated the viability of the technology and the other biocompatible meta-alloy matrices could result in superior bond strength for use on medical implants.

5.10 Coatings for the electronics industry

Copper is widely used on glass fibre-reinforced epoxy, particularly for printed circuit board manufacture. Adhesion is usually promoted by application of a rough copper oxide layer having a critical composition. If submicrometre particles of phenolic resin are incorporated within a copper layer, adhesion can be obtained directly to the metal and several disadvantages of the copper oxide layer can be avoided [78].

WAN *et al.* [110] found the electrical resistivity of Cu/$MoSi_2$ composites was less than Cu/Al_2O_3 composites with similar particle contents. This was thought to be due to the superior conductivity of $MoSi_2$. The improved wear properties, stated previously, and low resistivity make Cu/$MoSi_2$ ideal for use on electrical contacts.

5.11 Nuclear coatings

Fissile materials like UO_2 and Pu have been co-deposited with nickel for possible use as nuclear fuel elements, while neutron absorbing materials such as boron and its compounds could also be deposited with nickel for use as reactor control materials [105].

5.12 Anti-fouling coatings

Anti-fouling coatings can be produced by codepositing silicone or polysilane particles with copper [39].

5.13 Applications in textile machinery

Usually, coatings applied to several mechanical parts involved in the cotton textile industry are expected to improve production efficiency and to decrease the relevant costs. The quality of cotton products is one of the most crucial parameters in the development of the textile industry and is closely associated with the mechanical and tribological properties of the coated machinery parts. Mechanical parts involved in this process require smooth surfaces with reduced porosity, increased hardness and wear resistance.

In 2000, GYFTOU *et al.* [123] investigated the possibility of using nickel matrix composite coatings containing silicon carbide micro-particles, prepared under pulsed plating conditions, for such a purpose. They stated that certainly Ni/SiC coatings, produced under specific conditions, do not substantially harm cotton products, even if their contact imposes intensive friction stresses. This property combined with an enhanced wear resistance of the coating itself, could lead to an extensive list of applications in textile machinery parts. Coating of spare parts, frequently replaced during cotton treatment processes, is expected to yield appreciable financial profits. Therefore, low cost coatings with good mechanical properties and sufficient wear resistance, which do not damage the textile products, are ideal for many applications in textile machinery.

5.14 Production of electroless composite coatings

Electroless coatings are produced by the chemical reaction of metal salts and a reducing agent; therefore, no external power supplies are needed as for electrolytic deposition. Since the baths used for electroless deposition are closely dependent upon surface area in their operation, they are regularly filtered to remove any insoluble contaminants that may lead to autocatalytic decomposition of the solution, and/or imperfections in the deposit. Typical baths contain a number of different additives, such as complexing agents, buffers, brighteners and stabilisers, in order to control the speed of metal deposition and to avoid solution decomposition. Electroless coatings can be applied to many substrate types, such as metals, alloys, or non-conductors with excellent thickness uniformity, even on complex shaped components.

Electroless composite deposition was first patented by METZGER [124, 125], and was based on a nickel-phosphorous matrix. Other matrix metals deposited in this way include copper, cobalt and nickel-cobalt. The solutions used are often very similar to those used in conventional electroless deposition, except for the amount of stabiliser added. This is to counteract decomposition of the bath, since the presence of particles breaks the cleanliness "rules" of conventional electroless baths. Often, periodic separation of the solids allows filtration of the bath to remove any impurities. Silicon carbide particles are mainly used, but others commonly added include alumina, titania, diamond, zirconia, boron nitride, boron carbide, molybdenum disulphide, chromium carbide and PTFE. These are all either totally insoluble or slightly soluble in the baths used.

FELDESTEIN [126] *et al.* stated that with some types of particulate matter, only certain specific forms have found use, i.e. the polycrystalline form of diamond and the platelet form of alumina. They also stated that it was possible to codeposit more than one particle type from the same solution, producing a greater range of opportunities for end use. Generally, the percentage of entrapped particles increases with increased bath content and increased temperature. Temperature also increases matrix deposition rates, although the addition of particles causes deposition rates to be reduced.

GROSJEAN *et al.* [127, 128] prepared and characterized electroless Ni/SiC composite deposits. These kind of coatings combine anti-corrosion properties (due to the presence of nickel), with mechanical and tribological performances (due to the presence of SiC). The authors analysed the mechanism of wear from observations of the wear scars and their characterization using two-dimensional and three-dimensional profilometry. Results showed that increasing the size or the deposition rate of SiC particles incorporated lead to an increase in both the hardness of the films and friction coefficient when sliding against a steel ball.

Luminescent particles (europium doped yttrium vanadate) have been co-deposited with electroless nickel by DAS *et al.* [129]. These particles have potential application as indicators and for product authentication. The corrosion protection characteristics of the nickel coating, was lost due to the presence of the luminescent particles, microhardness remained almost unchanged while the surface roughness increased with increase in the level of particle incorporation.

6. Flow behaviour

In this section the flow around the rotating cylinder and the dispersed particle in the electrolyte is analysed. This is in order to understand which kind of forces are acting on particles while they are immersed in the electrolyte due to the rotation of the cylinder electrode. The following theory is limited to initially incompressible fluids and laminar flow. At high rotation speeds (turbulent flow) particles can reach the cathode surface, but the agitation does not let them rest on it for enough time to become incorporated, resulting in poor incorporation levels. The transition between laminar and turbulent flow is a really unstable zone in terms of co-deposition characterization (see chapter 12) and is not considered in this chapter.

6.1 Flow around a RCE [130-132]

Fig. 6.1 shows a schematic of the rotating cylinder electrode (RCE) cell. Fluid is in the annulus between two concentric cylinders with external radius R and internal r=*k*R (*k* is the ratio between internal and external cylinder diameters, *k*<1). The outer cylinder is stationary, while the inner is rotating with an angular velocity of ω.

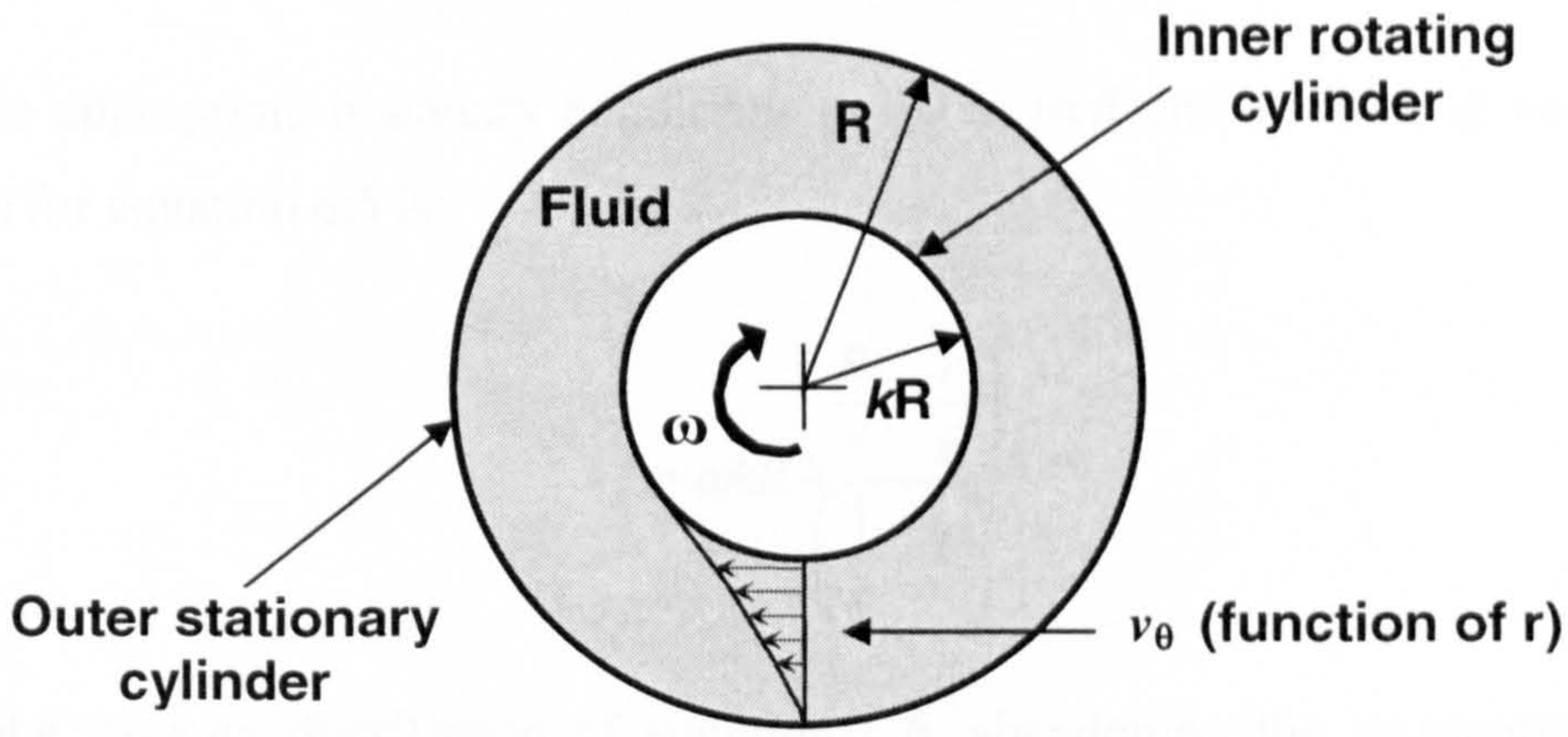

Figure 6.1 - Tangential laminar flow of an incompressible fluid in the space between two cylinders; the inner one (with radius *k*R) is moving with an angular velocity ω. The outer cylinder radius is R. v_θ is the fluid tangential velocity [130].

In the portion of the annulus the fluid flows in a circular pattern. Reasonable postulates for the velocity and pressure are:

$$v_\theta = v_\theta(r) \qquad \textbf{Eq. 6.1}$$

$$v_R = 0 \qquad \textbf{Eq. 6.2}$$

$$p = p(r) \qquad \textbf{Eq. 6.3}$$

where v_θ and v_R are the tangential and the radial components of velocity, while p is the pressure of the fluid. It is expected that p depends on r (which is the distance between the cylinder rotational axis and the point under consideration, thus $k\mathrm{R} \leq \mathrm{r} \leq \mathrm{R}$) because of the centrifugal forces.

For these postulates all the terms in the equation of continuity are zero and the components of the equation of motion simplify to:

r-component $$-\rho\frac{v_\theta^2}{r} = -\frac{\partial p}{\partial r} \qquad \textbf{Eq. 6.4}$$

θ-component $$0 = \frac{d}{dr}\left(\frac{1}{r}\frac{d}{dr}(rv_\theta)\right) \qquad \textbf{Eq. 6.5}$$

Where ρ is the fluid density.

Equation 6.4 shows how the centrifugal force affects the pressure and equation 6.5 gives the velocity distribution.

With the appropriate boundary conditions ($v_\theta=0$ at $r=R$ and $v_\theta=\omega kR$ at $r=kR$), the solution for equation 6.5 is:

$$v_\theta = \omega kR\frac{\left(\frac{R}{r}-\frac{r}{R}\right)}{\left(\frac{1}{k}-k\right)} \qquad \textbf{Eq. 6.6}$$

Using the velocity distribution of equation 6.6, abandoning the assumption of an incompressible fluid, applying the same boundary conditions and assuming that the fluid density ρ is known as a function of p, we can now perform the integration of Eq. 6.4. The result is [132]:

$$\frac{p-p_0}{\rho_0 k^2\omega^2R^2}\left(\frac{1-k^2}{k}\right)^2 = \frac{1}{2}\left(\xi^2-\frac{1}{\xi^2}\right)-2\ln\xi-1-\frac{1+k^2}{4}+\frac{1+2k^2}{1-k^2}\ln k \qquad \textbf{Eq. 6.7}$$

where ρ_0 and p_0 are the uniform density and pressure of the fluid when the system is at rest and ξ is defined as $\xi(r)=\frac{r}{R}$. This function is shown graphically in Fig. 6.2.

It is clear that as long as the fluid is far from the rotation axis, the pressure acting on it increases with respect to the pressure of the fluid when the system is at rest. This means that if particles are present in the fluid, they experience a radial pressure that increases as the distance from the rotation axis increases.

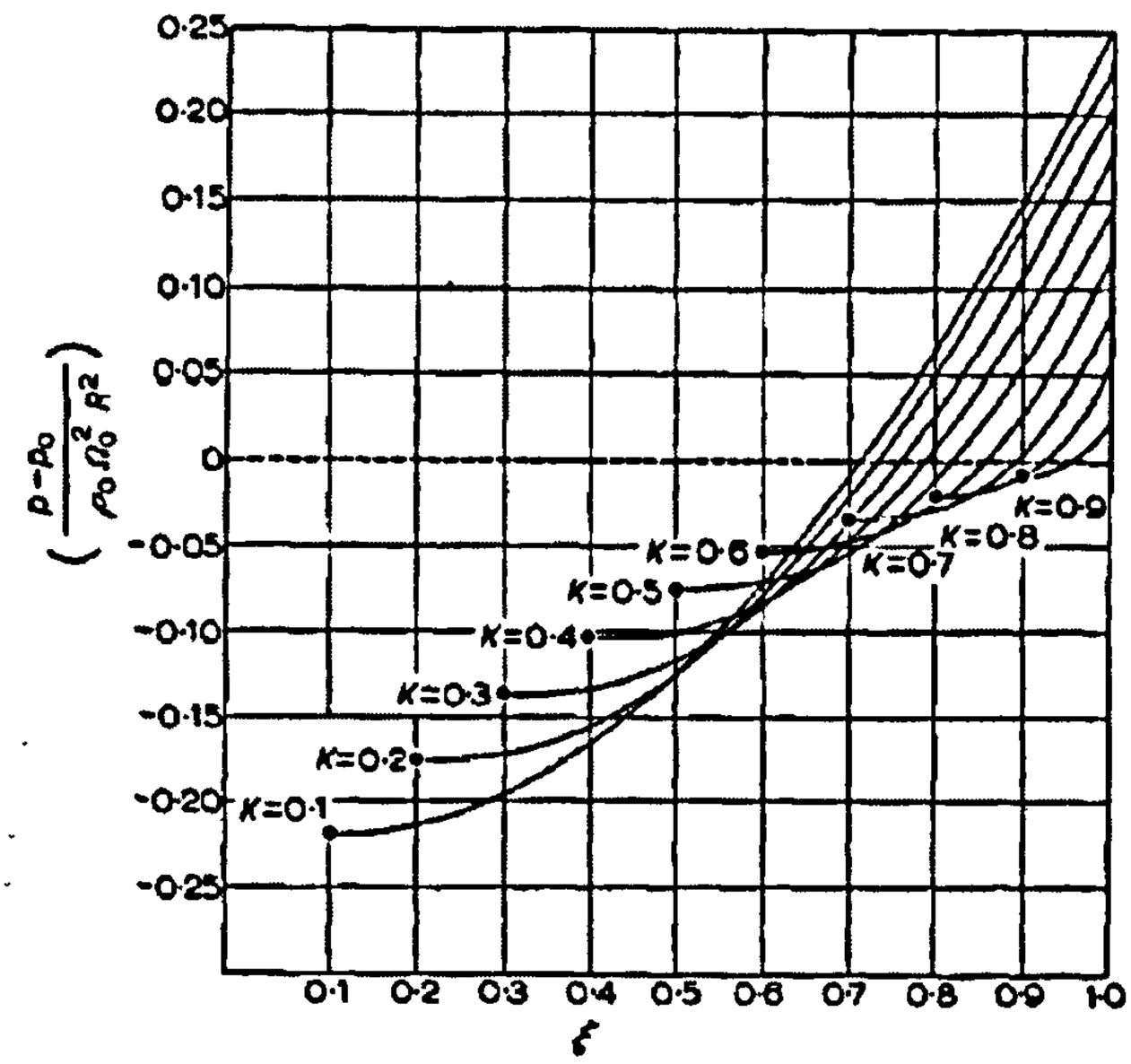

Figure 6.2 - Steady-state pressure *vs.* distance from the cylinder axis with the parameter *k* (ratio between internal and external cylinder diameters) of fluid around a RCE [132].

The theory illustrated is strictly valid for small values of angular velocity ω. However, when ω reaches a critical value ω_{crit}, the fluid develops a secondary flow, which is superimposed on the primary (tangential) flow and which is periodic in the axial direction. A very neat system of toroidal vortices, called *"Taylor vortices"*, is formed (see Figs. 6.3 and 6.4). The loci of the centres of these vortices are circles, which are located on the common axis of the cylinders. This is still laminar flow, but certainly is not consistent with the postulates made at the beginning of the section.

When the angular velocity is increased further, the loci of the centres of the vortices become travelling waves (see Fig. 6.4); that is, the flow becomes, in addition,

periodic in the tangential direction (the angular velocity of the travelling waves is approximately $\frac{1}{3}\omega$).

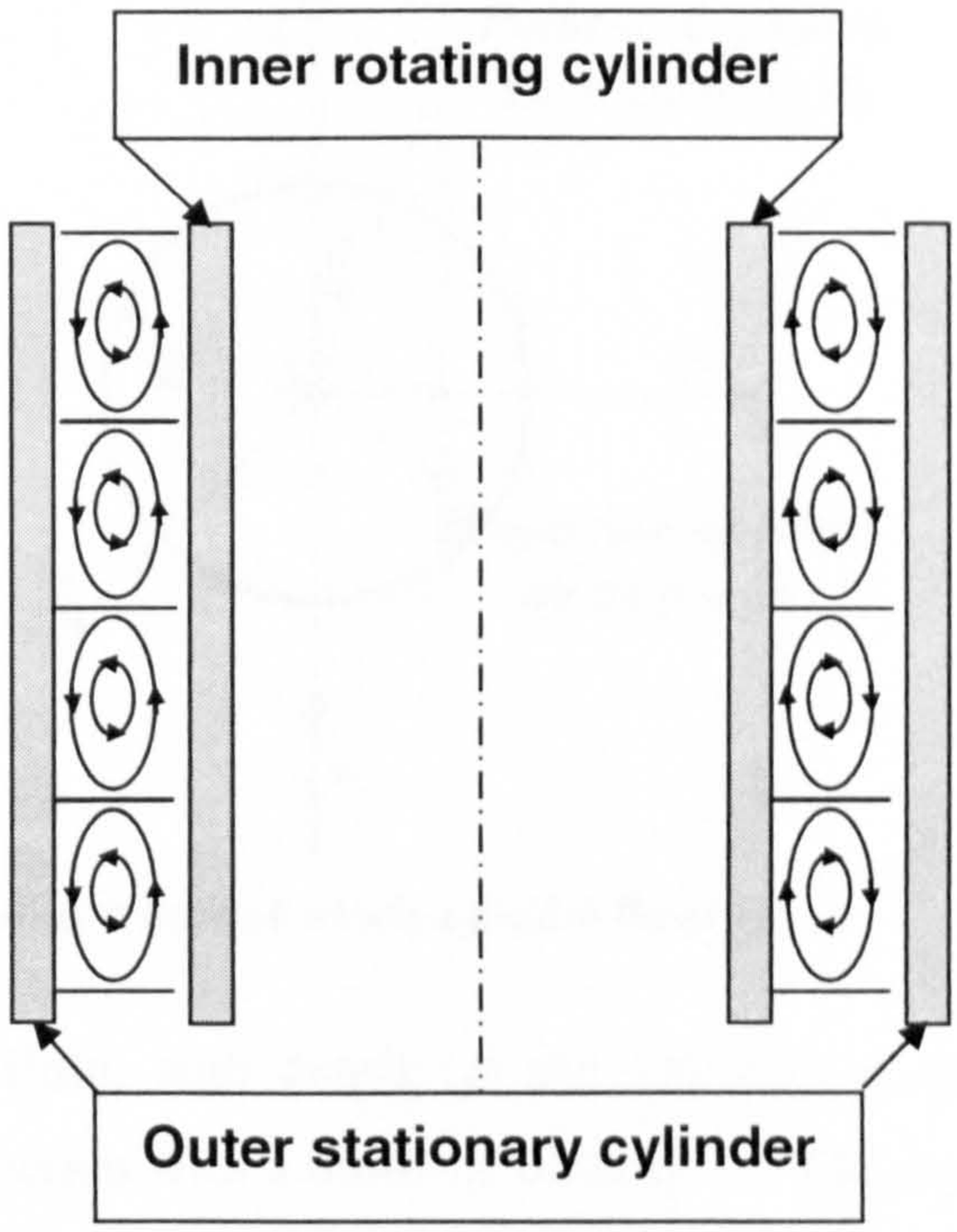

Figure 6.3 - Counter rotating toroidal vortices, called *Taylor vortices*, observed in the annular space between two cylinders [130].

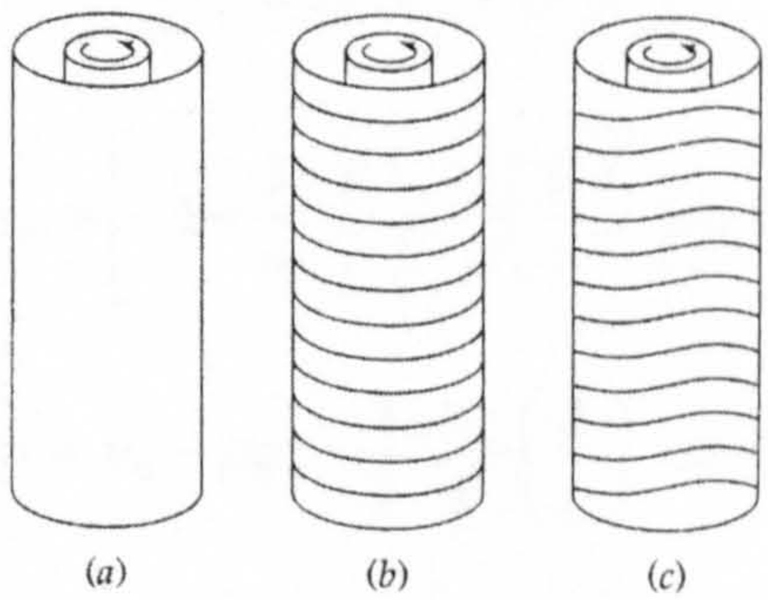

Figure 6.4 - Sketches showing the phenomena observed in the annular space between two cylinders: (a) purely tangential flow; (b) singly periodic flow (Taylor vortices); (c) doubly periodic flow in which an oscillating motion is superposed on the Taylor vortices [130].

When the angular velocity is further increased, the flow becomes turbulent.

6.2 Flow around a dispersed particle in the electrolyte of a RCE system [130]

Fig. 6.5 shows a schematic of the flow of an incompressible fluid around a spherical particle of radius *R*.

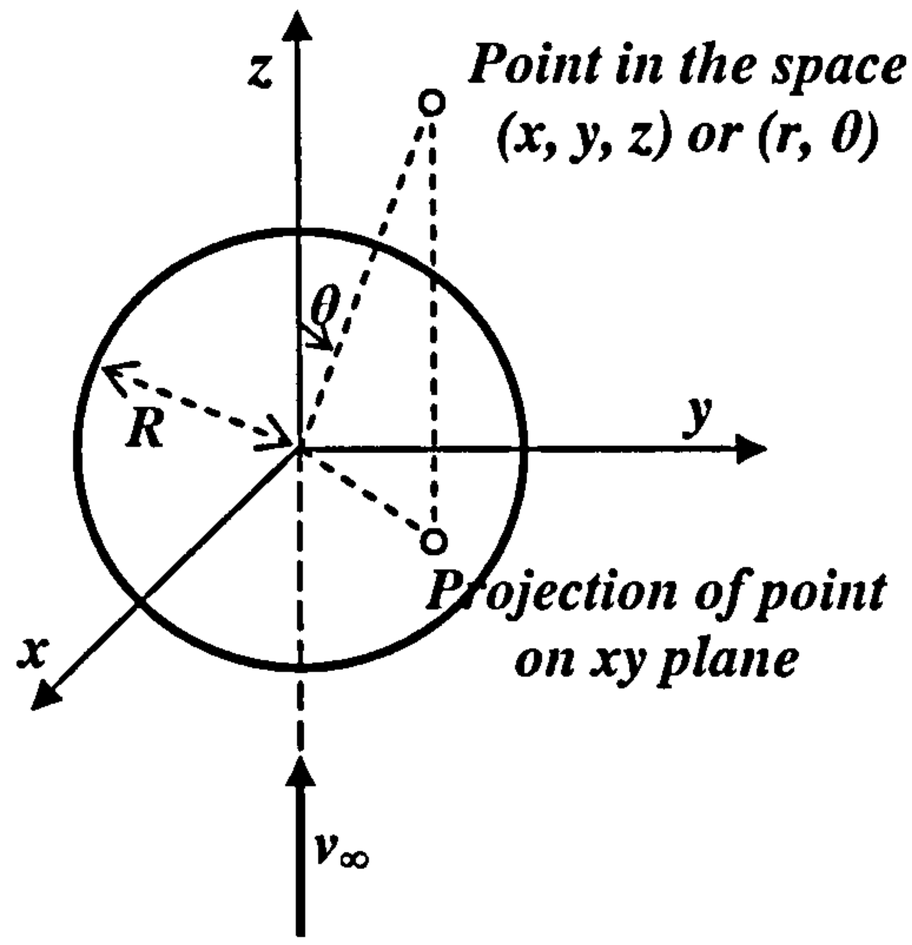

Figure 6.5 - Sphere of radius *R* around which a fluid is flowing.

In this example the fluid, with density ρ and viscosity μ, approaches the sphere vertically in the z-direction with a uniform velocity v_∞. The regime is assumed to be laminar. The radial velocity v_r, the tangential velocity v_θ, and pressure p distributions for this creeping flow are:

$$v_r = v_\infty\left[1-\frac{3}{2}\left(\frac{R}{r}\right)+\frac{1}{2}\left(\frac{R}{r}\right)^3\right]\cos\theta \qquad \textbf{Eq. 6.8}$$

$$v_\theta = \left[-1+\frac{3}{4}\left(\frac{R}{r}\right)+\frac{1}{4}\left(\frac{R}{r}\right)^3\right]\sin\theta \qquad \textbf{Eq. 6.9}$$

$$p = p_0 - \rho g z - \frac{3}{2}\frac{\mu v_\infty}{R}\left(\frac{R}{r}\right)^2\cos\theta \qquad \textbf{Eq. 6.10}$$

In Eq. 6.10 the quantity p_0 is the pressure in the plane $z=0$ far away from the sphere. The term $-\rho g z$ is the hydrostatic pressure resulting from the weight of the fluid, and the term containing v_∞ is the contribution from the fluid motion. Equations 6.8, 6.9 and 6.10 show that the fluid velocity is zero at the surface of the sphere. Furthermore, in the limit as $r \to \infty$, the fluid velocity is in the z direction with uniform magnitude v_∞.

7. Quantitative analysis of composite coatings

The production of composite coatings requires a stable formulation able to produce the desired composite and a reliable method of qualitative and quantitative detection of second phase particles in the coating. So it is of interest to find a method, which allows us to control the quality of the coating produced. Literature reviews suggest that considerable work has been carried out in this direction, and a number of methods have been proposed.

The weight per cent of embedded particles has been determined by several authors [57, 133-134] gravimetrically. After dissolution of the deposit (often in nitric acid) the slurry is filtered and the residue is weighed. The main objection to this procedure is that, often, particles used are soluble in the chemical used for the dissolution as claimed by HOFFMAN [135] and CHEN [56].

7.1 The gravimetric method

For more accurate determination of particle contents in coatings, ROOS *et al.* [57] used Atomic Absorption Spectrophotometry (AAS) to evaluate the alumina content in the Cu/Al_2O_3 composite coatings they produced. After dissolution of a Cu/Al_2O_3 deposit and fusion of Al_2O_3 with sodium carbonate, the aluminium content is determined by AAS. This method appears to be independent of the particle size of the alumina and of its solubility in the reagent used. The big limitation is that organic compounds cannot be determined by AAS analysis.

A variation of this method was introduced by BAPU AND MOHAN [136]: the coated sample (in this case Ni-PTFE) was weighed before and after selective dissolution of the composite coating. The metal mass of the matrix was obtained by AAS and then the inclusion rate of PTFE can be deduced. The volume percentage of PTFE was evaluated as follows:

1. Volume of nickel in composite $(V_1) = \dfrac{\text{mass of nickel}}{\text{density of nickel}}$

2. Volume of PTFE in the composite $(V_2) = \dfrac{\text{mass of PTFE}}{\text{density of PTFE}}$

3. Total volume $V = V_1 + V_2$

4. Volume percentage of PTFE = $\frac{V_2}{V} \times 100$

7.2 The gravimetric method after filtration [137]

Using this method the composite coating is dissolved by selective etching. The resulting solution is filtered to obtain the mass of particles. The weight of the composite coating is determined by the difference between the sample before and after dissolution of the composite coating. This method does not take into account the possible eventual dissolution of both particles and filters in the reagent used.

7.3 The method of particle counting with an image processing software [138-143]

This method has been developed by BOZZINI [138-139] to determine the inclusion rate of diamond particles in a Ni-P-diamond coating by observation of sample cross-sections with Scanning Electron Microscopy (SEM). It involves selectively etching the composite matrix. The particles are then counted from micrographs of cross-sections.

7.4 The morphometric analysis [144]

Łosiewicz *et al.* [144] used this method to determine the percentage volume fraction of TiO_2 and PTFE in Ni-P-TiO_2 and Ni-P-TiO_2-PTFE composite coatings.

The principle of morphometric analysis is based on a programme which can make a digital conversion of a "living" image of the layer surface observed under a microscope by means of a digital camera and appropriate computer card. From the "living" image the area in the optical plane containing subjectively the largest quantity of phase/phases observed is chosen. Computer analysis of the digital image yields a chance to display that image as a luminance with 256 grey shades. It also allows the selection of the required phase/phases with a precise grey shade from the observed area. In this way the selected object with an identical brightness threshold

are marked in one colour and cut out from the "frozen" image and then subjected to the morphometric measurements.

An example of the micrographs used in this analysis is shown in Fig. 7.1.

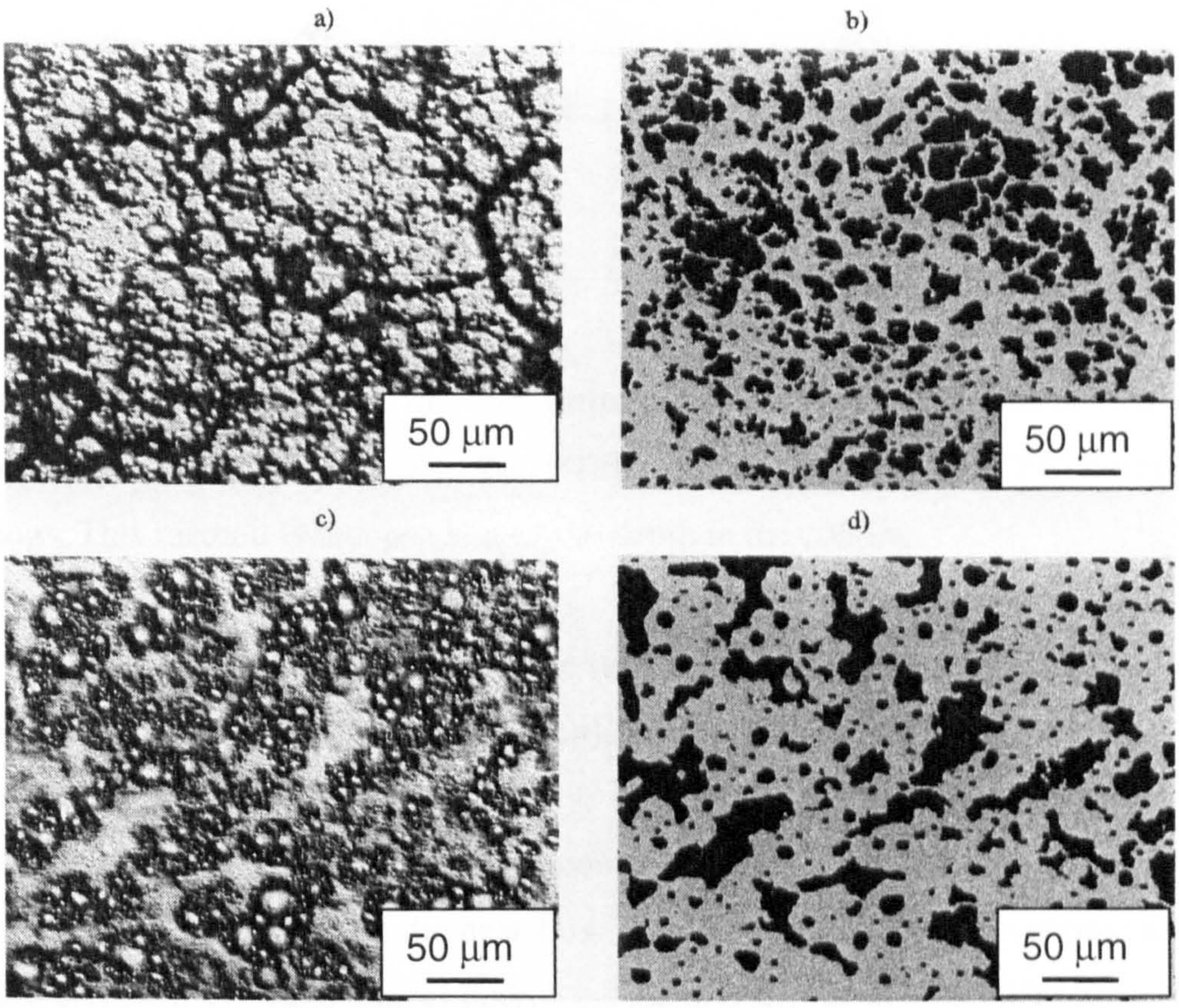

Figure 7.1 - Surface morphology of the Ni-P-TiO2 layers (a, c) and appropriate micrographs (b, d) used for the morphometric analysis by ŁOSIEWICZ *et al.* [144].

7.5 Infrared Reflection Absorption Spectroscopy (IRRAS)

SERHAL *et al.* [133-134] produced Au-Co-PTFE composite coatings by electrocodepostion. Initially they determined the inclusion rate of PTFE particles in the coating using Infrared Spectroscopy (IR). The fluoropolymer, which presents strong absorption bands, can be characterised by this technique. EDS analysis and other methods have been used to confirm the presence of PTFE and to validate the method. IR analysis was conducted by specular reflection (IRRAS). The authors used a suspension made up of PTFE particles with a wetting agent (to maintain particles in suspension). After filtration and separation of the solid mass (PTFE) from the liquid, particles were washed, dried and applied to a pure gold coating. The infrared

spectrum of the pure coating was recorded as a reference before application of PTFE. The spectrum obtained after application of PTFE was characterised by two absorption bands, which were assigned to the C-F stretching vibrations of PTFE. Similar spectra were produced by gold-PTFE composite coatings confirming the presence of PTFE. After a calibration, the authors were able to estimate the particle content in the coating. This method also allows, by successive polishing (layer by layer), to study the distribution of PTFE particles according to their depth in the composite coating.

7.6 Differential enthalpic analysis

More recently, SERHAL *et al.* [145] proposed the use of Differential Scanning Calorimetry (DSC) to evaluate the PTFE content in Au-Co-PTFE composite coatings. This method is independent of the depth in the coating.

When a material undergoes a state change such as melting, boiling, glass transition or when it reacts chemically (polymerisation), heat is either absorbed or released. The process can be initiated by gradually increasing the material's temperature. Differential scanning calorimeters are constructed to determine the enthalpies of these processes by measuring the heat flow necessary to maintain the sample and an inert reference at the same temperature. This latter is regulated by a linear process.

PTFE has a characteristic DSC thermogram with very interesting energies and melting points. The authors determined these temperatures for the polymer and more particularly:

- the melting point which appeared through an endothermic effect at approximately 327 °C for PTFE;
- the heat quantity absorbed by the sample during the melting of PTFE crystallites. This heat energy is proportional to the quantity of PTFE incorporated in the composite coating.

As a matter of fact, gold is a noble metal with a melting point of approximately 1064 °C so this method allowed the authors to quantify the inclusion rate of PTFE in the coating without melting the gold.

The main goal of this method is to obtain measurements over the totality of the coating.

In the following sections the experimental work will be presented. This experimental program had the purpose to better understand the mechanisms of electrolytic co-deposition processes. To fulfil this task, the attention was focused on several parameters influencing the process, in particular:

- influence of different metal matrices:
  - ✓ this was achieved by the production of Ni, Cu and Zn composite coatings and their comparison in terms of surface morphology and amount of inert particles incorporated;
- influence of the second phase materials:
  - ✓ this was achieved by the production of PS and alumina composite coatings with the metals mentioned above. Coatings were compared in terms of surface morphology and amount of inert particles incorporated;
- influence of the hydrodynamics in the co-deposition cell:
  - ✓ this study was carried out using a RCE system. With this system, as will be shown in the following sections, it is possible to produce composite coatings at different cathode rotation speeds, thus at different levels of agitation;
- influence of the centrifugal forces acting on the particles in the electrolyte solution.
  - ✓ cathodes with different diameters were used. Particle contents were then plotted against $r\omega^2$, a parameter proportional to centrifugal forces.

After the presentation of the experimental equipments utilised and of the experimental procedures set up, in particular the evaluation of the amount of particles incorporated in the coatings, data obtained will be presented and discussed.

8. Experimental investigations

8.1 Electrolyte preparation

Composite coatings with three different metal matrices (copper, zinc and nickel) were produced. The electrolytes used were very concentrated in order to obtain a high conductivity. This was to avoid large ohmic loss of potential through the electrolyte.

The solutions detailed below were prepared using analytical grade chemicals, provided by Alfa Aesar, to the stated compositions, and deionised water. The pH was then measured using a Hanna Instruments HI-8424 digital pH meter.

8.1.1 Nickel electrolyte

- 300 g/l $NiSO_4$
- 35 g/l $NiCl_2$
- 40 g/l H_3BO_3
- pH = 3.1

8.1.2 Zinc electrolyte

- 300 g/l $ZnSO_4$
- 80 g/l Na_2SO_4
- pH = 4.4

8.1.3 Copper electrolyte

- 125 g/l $CuSO_4$
- 120 g/l H_2SO_4
- pH = 0.25

8.2 Second phase materials and suspension preparation

Different second phase materials were used, polystyrene (spherical shape) and alumina (irregular shape), in order to study the influence of different particle geometries on the process.

In order to investigate the influence of the particle size on the process, alumina particles with different particle sizes (0.02, 0.3, 1 and 3 μm) were used.

8.2.1 Alumina

Alumina particles were APS alpha/gamma-alumina powders from Alfa Aesar.

Suspensions were prepared by adding alumina particles to the solution in the cell, at the desired concentration. The mixture was covered and stirred using a magnetic stirrer for 12-24 hours, placed in an ultrasonic bath for 2 hours and cooled at room temperature. The ultrasonic bath was used in order to obtain a suspension as homogeneous as possible and to break the alumina agglomerates [58].

8.2.2 Polystyrene

The polystyrene (PS) particles (spherical with an average diameter of 1 μm) were supplied by Corus-Ijmuiden. They were produced by emulsion polymerisation with persulphate salts as an initiator and surfactants. To be able to incorporate the particles in a metal layer, these salts, styrene monomers and production surfactants had to be removed from the surface of the particles.

Before addition to the electrolyte, the polystyrene particles were repeatedly rinsed with deionised water following the procedure below:

- 150 g of PS suspension (25% by weight approx) was added to 250 ml of deionised water;
- the suspension was filtered, using a glass microfibre filter able to retain fine particles down to 0.7 μm (Whatman). The filter-cake was not allowed to dry out totally;
- the suspension was then redispersed with a magnetic stirrer for 30 minutes;
- the sequence was repeated until the conductivity of the filtrate was less than 5 μS/cm;
- a suspension of about 9% PS by weight was prepared. The PS particles were prevented from settling by using a magnetic stirrer during storage.

CETAC (hexadecyltrimethylammoniumchloride) surfactant was then added as a concentrated solution in water (Table 8.1 shows the amount of surfactant in the concentrated solution).

Surfactant	Concentration (mmol/l)	Concentration (g/l)
CETAC/isopropanol	6.25/20	2.00/1.2

Table 8.1 - Amount of surfactant in the concentrated solution provided.

To obtain a good dispersion, $40 \cdot 10^{-3}$ mmoles of surfactant for every square metre of PS-surface in the solution were used. The surfactant solution and the PS particles were mixed for 5 minutes (in order to allow surfactant adsorption on PS particle surfaces) and then were slowly added to the electrolyte at a concentration of 2 g of PS for every litre of electrolyte.

8.3 Cell design

Experiments were carried out using a Rotating Cylinder Electrode (RCE) provided by Pine Instrument Company and shown in Fig. 8.3. This cathode format was chosen because of the necessity to control the hydrodynamic regime of the system. With such a configuration it is possible to produce composite coatings at different cathode rotation speeds and hence quantifiable levels of agitation.

To investigate the influence of the centrifugal forces acting on the particles in the electrolyte solution, cathodes with different diameters (1.27, 3.8 and 8.4 cm) were used.

Fig. 8.1 shows the cell used to obtain composite coatings on 1.27 and 3.8 cm diameter cathodes. This was a nylon cylinder, in order to have an inert surface in contact with the electrolyte solution. The stationary anode, positioned flush against the inside of the cell wall to minimise flow disturbance, was 1 cm high with an inner radius of 2.4 cm and a final anode surface area of 15 cm^2. Commercial inert tape was used to cover the outside surface of the cylindrical anode foil, as well as the

submerged portion of the anode's electrical connection and support, which was also positioned flush against the cell wall.

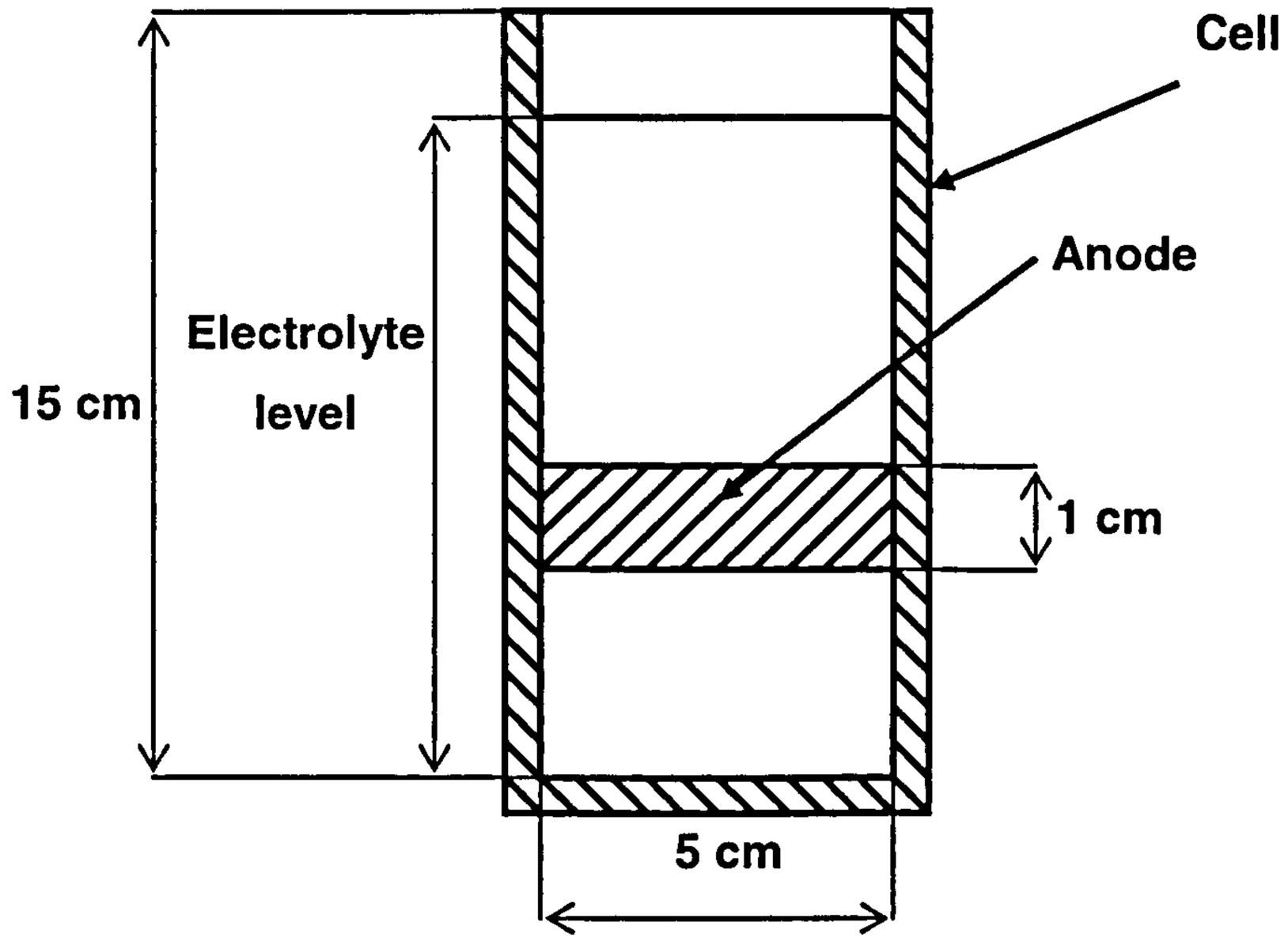

Figure 8.1 – Side view schematic of the cell design used to obtain composite coatings on 1.27 and 3.8 cm diameter cathodes. The cell dimensions are also reported in the picture.

Fig. 8.2 illustrates the rotating cathode used. It consisted of an electrode mounting shaft, a PTFE cover, a stopper and the proper cathode surface which was a removable AISI 316 stainless steel cylinder machined to an external diameter of 1.27 cm (or 3.8 cm) and 2 cm in height. The electrode surface was recessed slightly from the PTFE cover above and stopper below it, using commercial inert tape, in order to reduce the effect of the current discontinuity at the electrode edges. The final cathode surface area was 3.19 cm^2.

Fig.8.3 shows a photograph of the apparatus used to produce composite coatings on 1.27 and 3.8 cm diameter cathodes: a rotational speed controller (MSRX Speed Control, Pine Instrument Company) controlled an electric motor (AFMSRX Analytical Rotator, Pine Instrument Company) and a current generator (PL330 32V-3A PSU, Thurbly Thandar Instruments) supplied the cell with current.

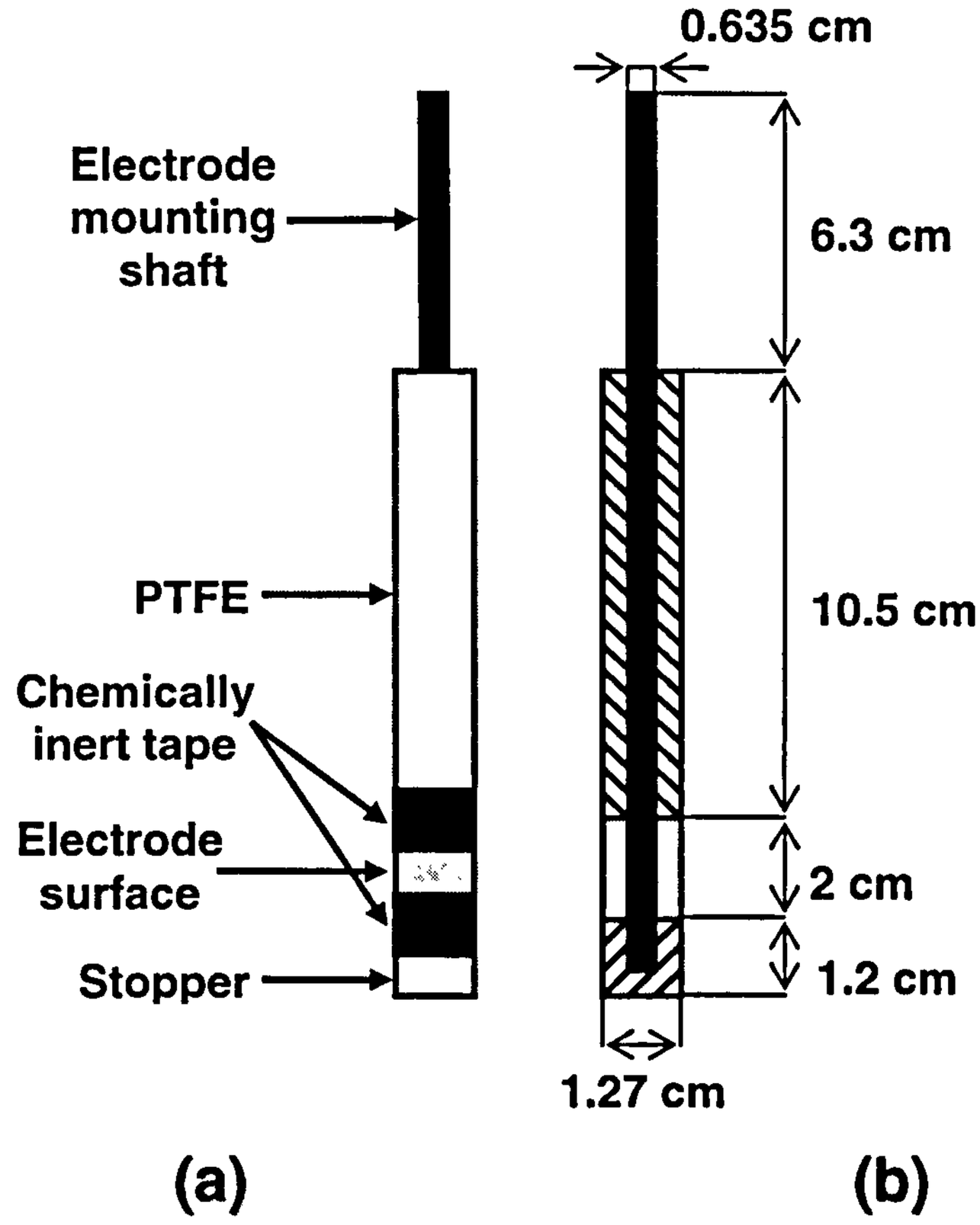

Figure 8.2 - Schematic showing rotating cathode. (a) Overall schematic. (b) Internal arrangements and dimensions.

Experiments with 8.4 cm diameter mild steel cathodes were carried out at the Corus-Centre for Packaging Technology, Ijmuiden, the Netherlands. The cell was a jacket reactor coupled with a temperature control unit. The capacity was 6 litres. A rotation speed controller controlled the rotating cathode and a current generator supplied the cell with current. Figs. 8.4 and 8.5 show photographs of the reactor and associated equipment.

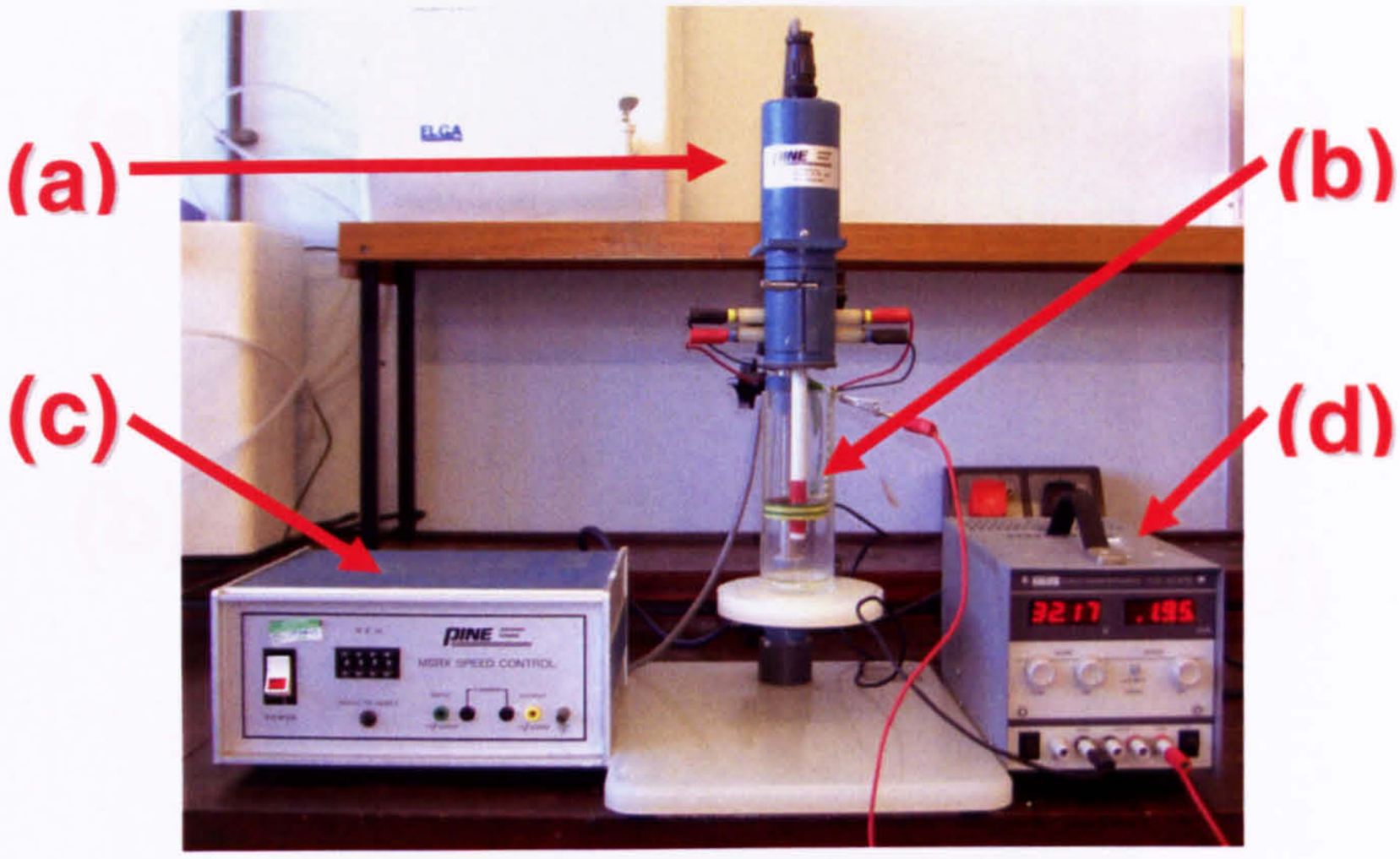

Figure 8.3 - Photograph of the apparatus used to produce electrodeposited composite coatings on 1.27 and 3.8 cm diameter AISI 316 stainless steel cathodes. (a) Electric motor. (b) Cell and rotating cathode. (c) Speed control unit. (d) Direct current supplier.

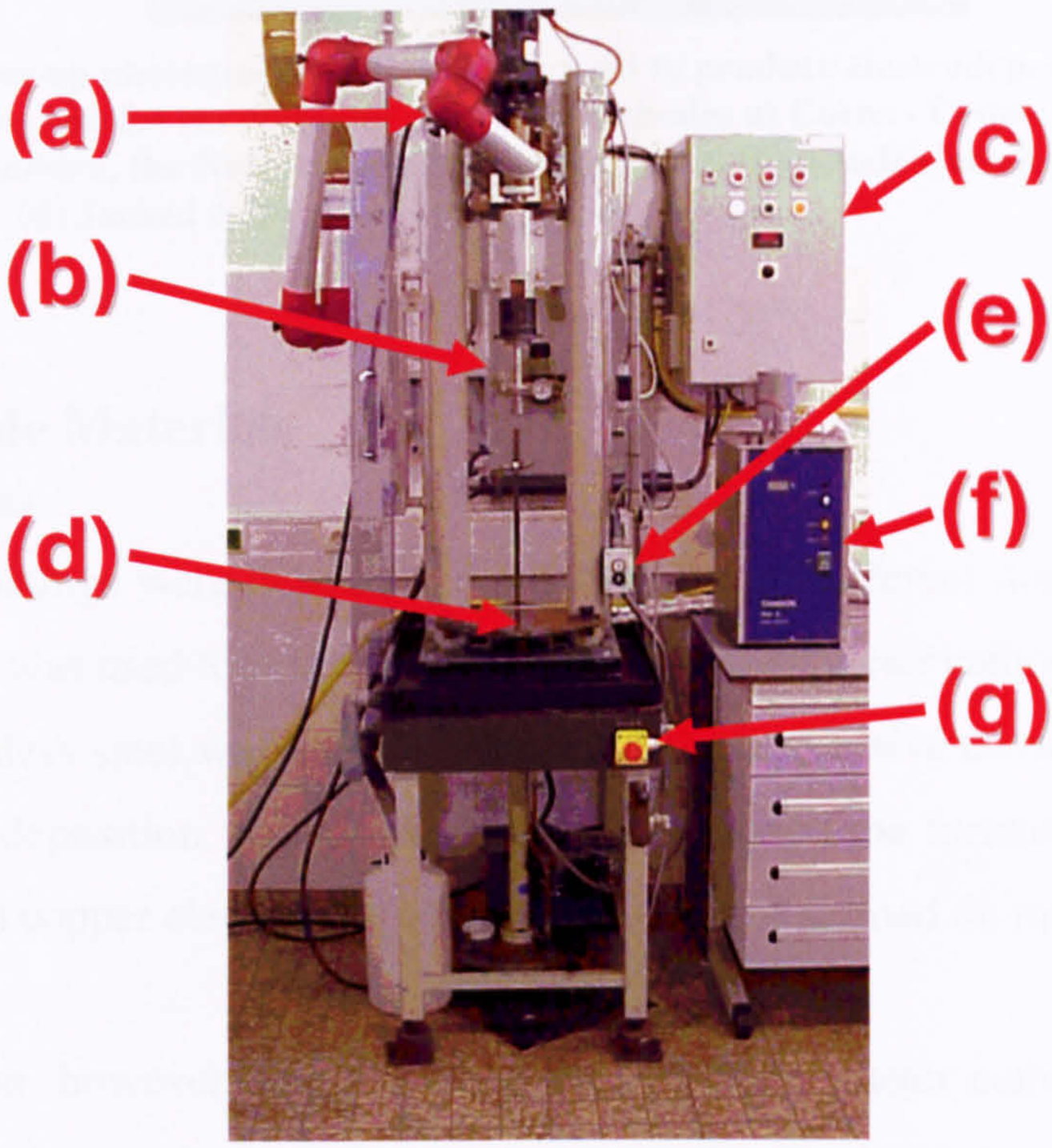

Figure 8.4 - Photograph of the reactor used to produce electrodeposited composite coatings on 8.4 cm diameter mild steel cathodes at Corus - Centre for Packaging Technology, Ijmuiden, the Netherlands. (a) Fume cape. (b) Rotating unit. (c) Speed control unit. (d) Reactor support. (e) Up and down cell support control. (f) Temperature control unit. (g) Security switch.

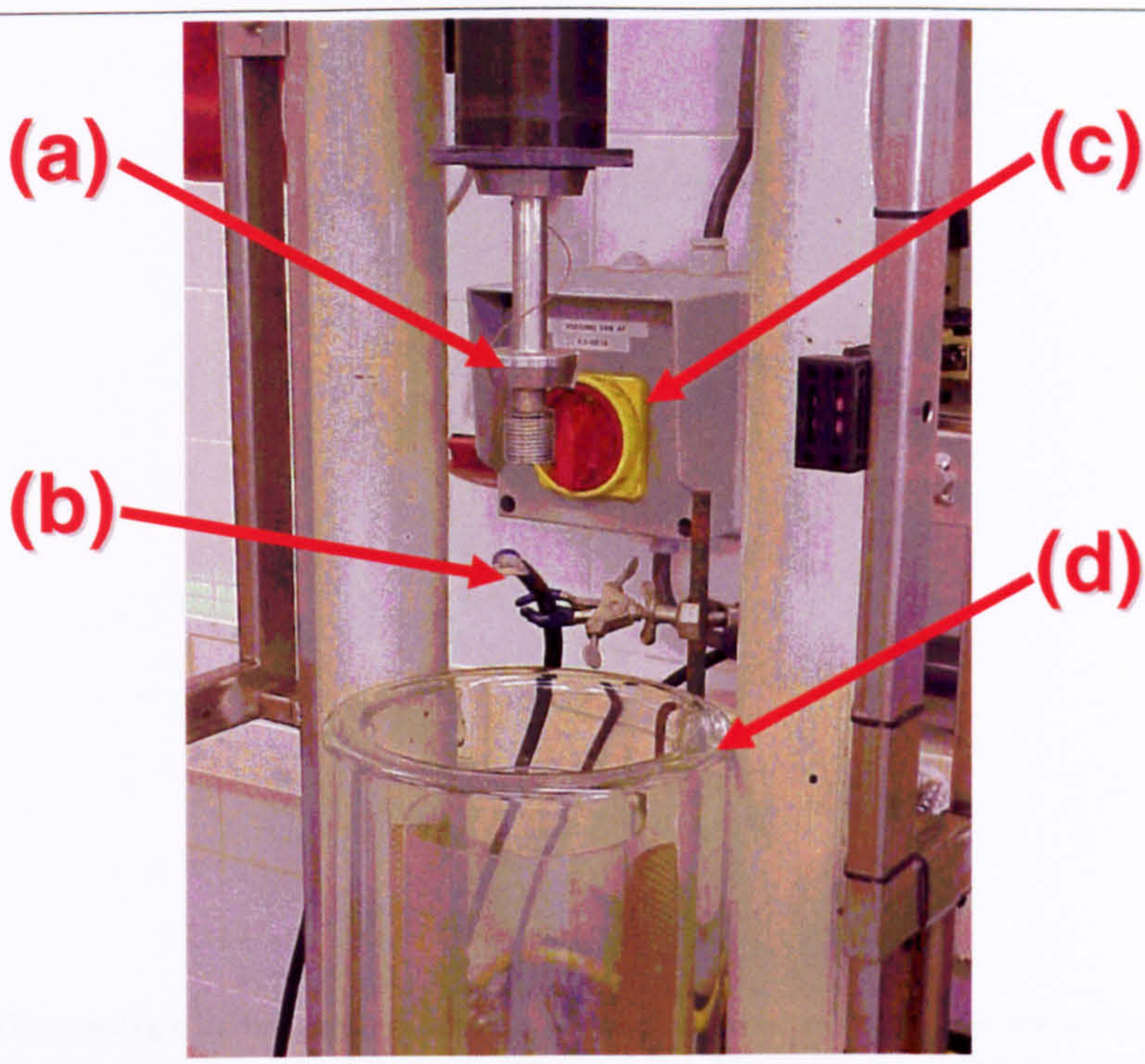

Figure 8.5 - Close-up photograph of the reactor used to produce electrodeposited composite coatings on 8.4 cm diameter mild steel cathodes at Corus - Centre for Packaging Technology, Ijmuiden, the Netherlands. (a) Rotating unit. (b) Anode electrical connection. (c) Main switch. (d) Jacked cell.

8.4 Electrode Materials

8.4.1 Cathodes

Composite coatings were deposited on cathodes with different diameters. AISI 316 stainless steel was used to make the 1.27 and 3.8 cm diameter cathode cylinders. This grade of stainless steel was chosen because of the aggressive environment in which the electroco-deposition was to take place and to avoid the formation of immersion coatings (with copper electrolytes), which would have formed on mild steel surfaces.

Mild steel was, however, used to make the 8.4 cm diameter cathode cylinder. For Cu/PS composite coatings, cylinders were pre-plated with a 1 μm nickel coating, prior to experimentation, at 500 rpm, in order to avoid the formation of immersion coatings.

Fig. 8.6 shows a photograph of the cathodes used, while Fig. 8.7 shows examples of cathodes after co-deposition trials.

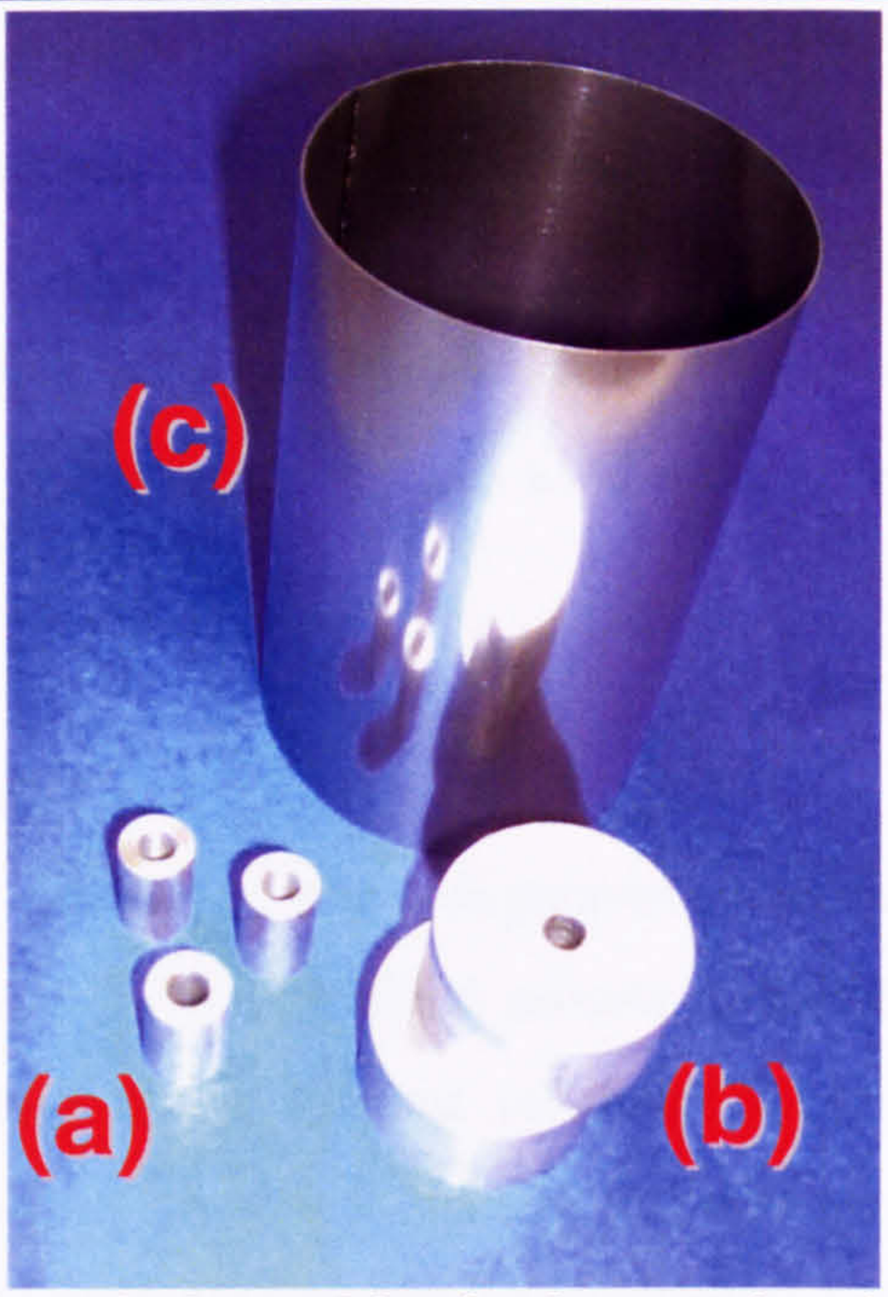

Figure 8.6 - Photograph of the cathodes used for the electroco-deposition trials. (a) 1.27 cm diameter AISI 316 cathodes. (b) 3.8 cm diameter AISI 316 cathodes. (c) 8.4 cm mild steel cathode.

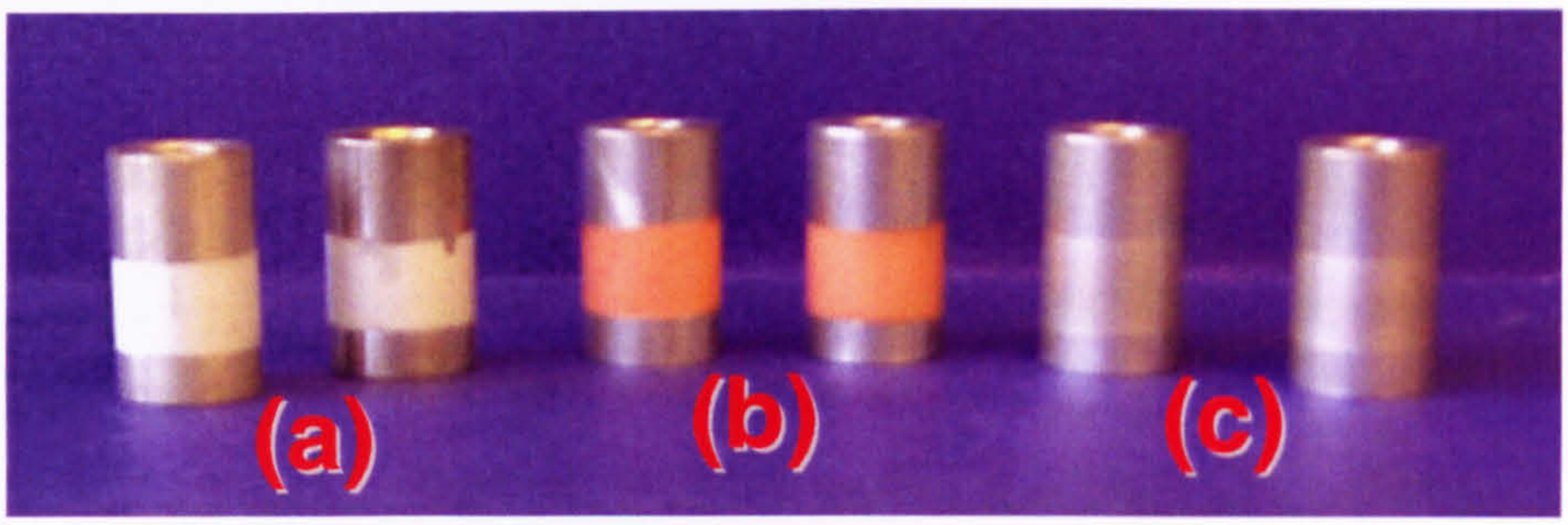

Figure 8.7 - Examples of 1.27 cm AISI 316 stainless steel electroco-deposited cathodes. (a) Zinc-alumina composite coatings. (b) Copper-alumina composite coatings. (c) Nickel-alumina composite coatings.

8.4.2 Anodes

- *Electroco-deposition of Cu-Al_2O_3 and Cu-PS coatings on 1.27 cm diameter cathodes.*

Oxygen-free high conductivity (OFHC) copper foil was used to make the stationary outer cylindrical anodes. This material was chosen due to its high purity and ability to electrochemically dissolve uniformly.

- *Electroco-deposition of Ni-Al_2O_3 coatings on 1.27 cm diameter cathodes and Ni-PS coatings on 1.27 and 3.8 cm diameters cathodes.*

Pure nickel foil was used to make the stationary outer cylindrical anodes.

- *Electroco-deposition of Zn-Al_2O_3 and Zn-PS coatings.*

Pure zinc foil was used to make the stationary outer cylindrical anodes.

- *Electroco-deposition of Cu-PS, Ni-PS and Zn-PS coatings*

Titanium clad with iridium oxides (IrO_x) was used to make the stationary outer inert cylindrical anodes.

8.4.3 Electrode treatments

Before experimentation, electrodes were degreased in dichloromethane and dried. Cylinders were then rotated at 250 rpm for 1 minute in the plating bath, after that the rotation speed was adjusted to the desired value for 20 seconds and subsequently electrodeposition was carried out at the specific rotation speed. After plating metal-PS coatings samples were rinsed with water and alcohol and then dried. They were subsequently treated ultrasonically in a water-surfactant (CETAC) solution to remove particles loosely attached to the substrate, rinsed with water and alcohol and then dried.

For the same reason, metal-alumina samples were treated ultrasonically in acetone, rinsed with water and alcohol and then dried.

8.5 Composite electrodeposition trials

The current density applied to the cell was 5 A/dm^2 for all the experiments.

For the 1.27 cm diameter cathodes the rotation speeds investigated were: 0, 100, 200, 400, 600, 800, 1000, 1250, 1500, 1750 and 2000 rpm.

For the 3.8 cm diameter cathodes the rotation speeds investigated were: 0, 150, 300, 450, 600, 700, 800, 900, 1000 and 1100 rpm.

For the 8.4 cm diameter cathodes the rotation speeds investigated were: 0, 30, 60, 140, 220, 300, 380, 460, 540, 620 and 700 rpm.

All the other operating conditions are summarised in Table 8.2.

The electrodeposition of copper on 8.4 cm diameter mild steel cathodes was also carried out at 30, 140, 300, 460 and 620 rpm for comparison with Cu-PS composite coatings.

Metal matrix	Second phase material	Second phase particle size / μm	Coating thickness / μm	Cathode diameter / cm	Temperature / °C
Nickel	Alumina	0.02	1	1.27	20°C
Nickel	Alumina	0.3	1	1.27	20°C
Nickel	Alumina	1	1	1.27	20°C
Nickel	Alumina	3	3	1.27	20°C
Nickel	Polystyrene	1 approx	2	1.27	35°C
Nickel	Polystyrene	1 approx	2	3.8	35°C
Nickel	Polystyrene	1 approx	2	8.4	35°C
Zinc	Alumina	3	3	1.27	20°C
Zinc	Polystyrene	1 approx	2	1.27	35°C
Zinc	Polystyrene	1 approx	2	8.4	35°C
Copper	Alumina	3	3	1.27	20°C
Copper	Polystyrene	1 approx	2	1.27	35°C
Copper	Polystyrene	1 approx	2	8.4	35°C

Table 8.2 - Operating conditions for electroco-deposition trials.

8.6 Cathode current efficiency studies

Electrodeposition of copper on stainless steel was carried out to evaluate the cathode current efficiency for this process. Electrode materials and their pre-treatment were the same as previously reported for alumina-copper co-deposition experimentations (see Section 8.4). The cell design used was also the same (see Section 8.3). The bath composition was: 0.5 M $CuSO_4$ + 1.2 M H_2SO_4. Fresh electrolyte was prepared for each experiment using reagent grade sulphuric acid and copper sulphate. Experiments were carried out at 1, 2, 3, 4 and 5 A/dm^2.

8.7 Morphological studies

A Cambridge 360 scanning electron microscope was used to investigate surface and cross-sectional morphology of the coatings produced and to observe the size and surface morphology of the particles used in the experimental trials. This device was

capable of displaying secondary electron and back-scattered images, either individually or in combination, for easier interpretation of surface features.

In order to take information on a nanometre-scale, a Leo 1530VP field emission gun SEM (FEGSEM) capable of nanometre resolution was used. This device was equipped with a variable pressure facility and EDAX/TSL Pegasus system allowing simultaneous electron backscattering diffraction and energy-dispersive X-ray analysis.

In order to analyse the surface morphology samples of 1.27 and 3.8 cm diameter were placed directly in the SEM chamber, whilst, for the 8.4 cm ones, a small section (1 cm^2) was removed and inserted into the SEM.

After mounting in conducting bakelite (suitable for analysis using SEM, EDX, EBSD), all cross section specimens for scanning electron microscopy were subjected to metallographic preparation. This involved mechanical polishing. The first step of grinding was carried out on the sample by hand, using water-cooled silicon carbide paper. The grit paper grade sequence was 240, 400, 800, 1200 grit. Pre-polishing was then performed on a silk napped cloth with 3 μm diamond particles and subsequent final polishing was carried out on a short nap synthetic cloth with 1 μm diamond particles.

For the analysis of the inert particulate materials used, the SEM samples were prepared by applying an adhesive tape to a standard SEM sample stub and pressing the adhesive side of the stub into the powder to be analysed. Excess powder was removed by gently tapping the sample stub. The remaining adherent powder was coated with gold prior to insertion into the SEM.

8.8 Atomic Absorption Spectrophotometry (AAS) analysis

The Inductively Coupled Plasma (ICP) unit used for the Atomic Absorption Spectrophotometry analysis was a Thermo-Jarrell-Ash AtomScan16.

The composite coating was dissolved in 10 ml of 20% by weight nitric acid. Sodium carbonate was added to dissolve the alumina following the chemical reaction:

$$Al_2O_3 + Na_2CO_3 + 2HNO_3 + 2H_2O \rightarrow 2Al(OH)_3 + 2NaNO_3 + CO_2.$$

On this solution, Atomic Absorption Spectrophotometry was carried out to evaluate the aluminium content. The solution was then diluted 1000 times and AAS analysis was carried out to evaluate the copper content. The coating composition was then calculated.

9. SEM particle characterisation

Electroco-deposition is a process strongly related to the material used as the second phase. The final properties of the coatings are significantly influenced by the nature of this particulate material used. Wear resistant coatings, in fact, can be obtained rather than self-lubricating ones just depending on the nature of the second phase employed.

In these investigations the interest was focused in how using a particular type of material influences the co-deposition process, in terms of particle content in the coating and morphological differences. Irregular ceramic particles (alumina) and spherical polymeric ones (polystyrene) were used trying to find out what influence these differences had on the final product. The dimension of the particle used could also affect the composite coatings, so alumina particles of different sizes were also tested.

To carry out such a task, the characterisation of the several types of particles used as second phase materials in the co-deposition experiments represented an important starting point.

9.1 Alumina

Scanning electron microscopy (SEM) was used to observe the size and surface morphology of the particles. Figs. 9.1-9.4 show the results.

The particle distribution seems to be uniform for particles of 0.02 μm (Fig. 9.1), but it can be seen that particles tend to agglomerate into larger structures. For the other cases the particle distribution is not so uniform. Fig. 9.2 shows alumina particles reported to be 0.3 μm in size. Particles smaller than 0.3 μm are present and in particular very small particles (less than 0.1 μm) can be seen. The same conclusions can be drawn for the 1 μm alumina particles shown in Fig. 9.3.

Fig. 9.4 shows 3 μm alumina particles. Large particles of approximately 3 μm can be seen, but they exhibit a large amount of very fine particles on their surface. Smaller particles, about 0.1 μm, are also present.

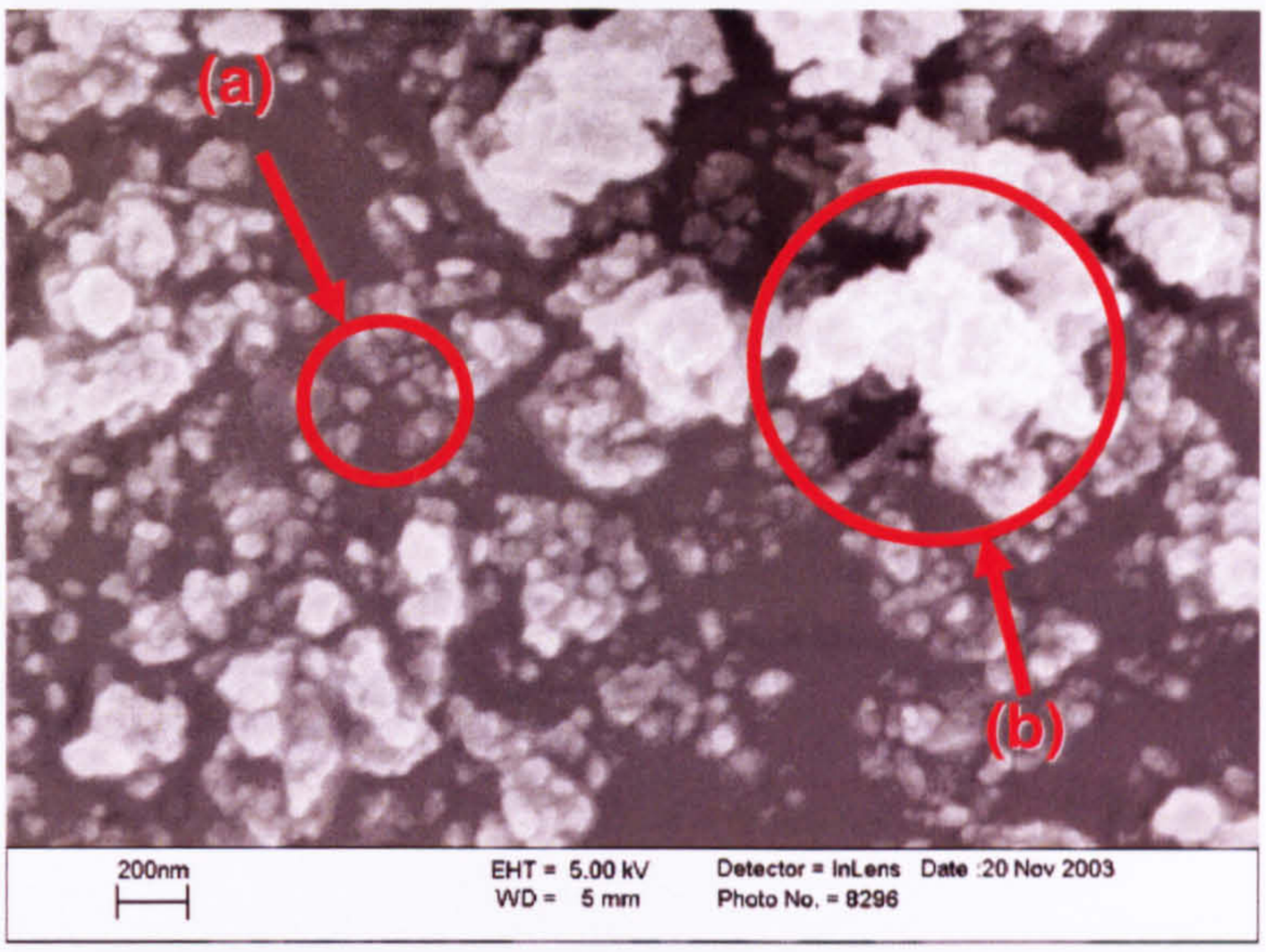

Figure 9.1 – FEGSEM micrograph of 0.02 μm alpha/gamma alumina particles. (a) Single particles. (b) Agglomerate of particles.

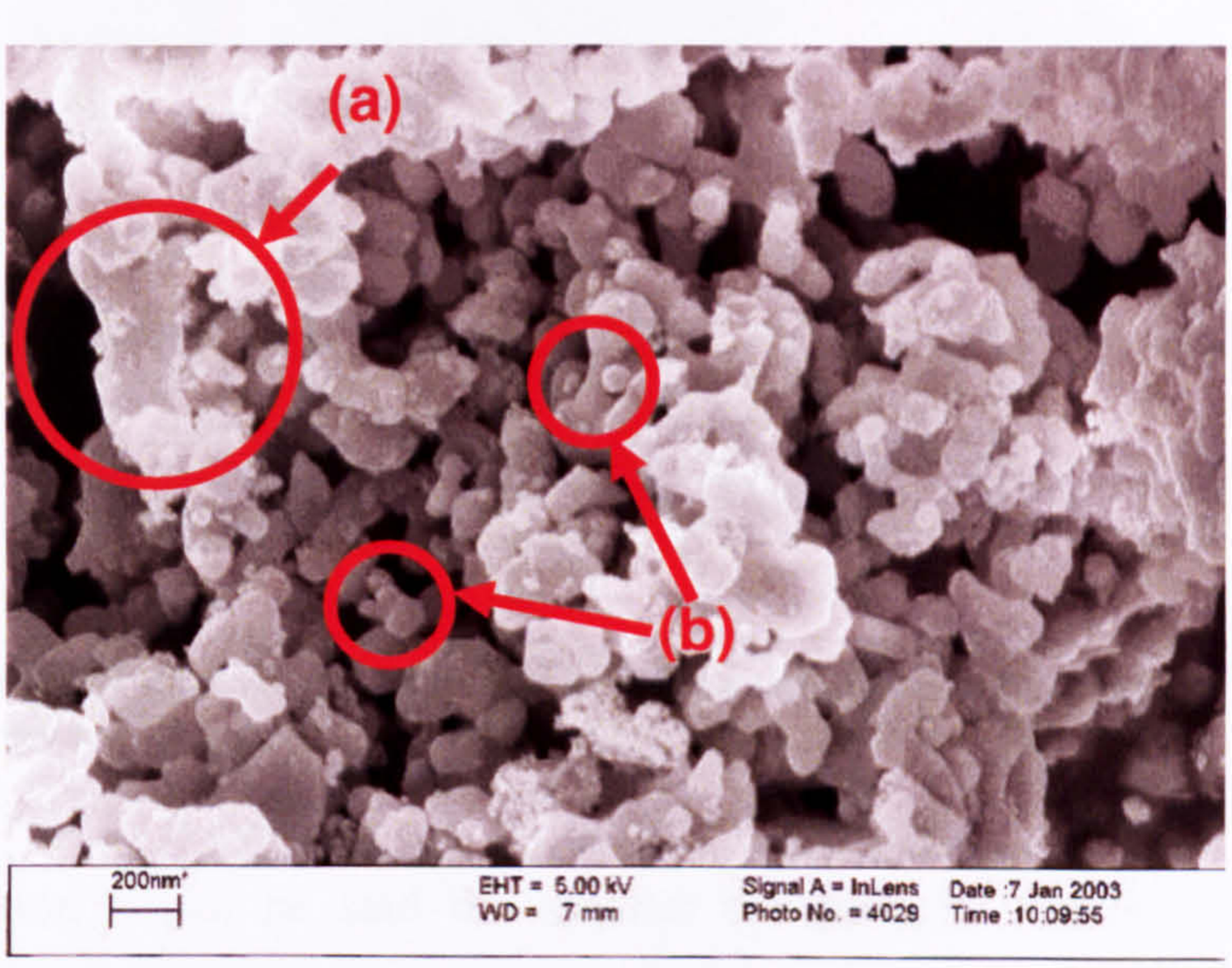

Figure 9.2 - FEGSEM micrograph 0.3 μm alpha/gamma alumina particles. (a) 0.3 μm particle. (b) Examples of particles smaller than 0.3 μm.

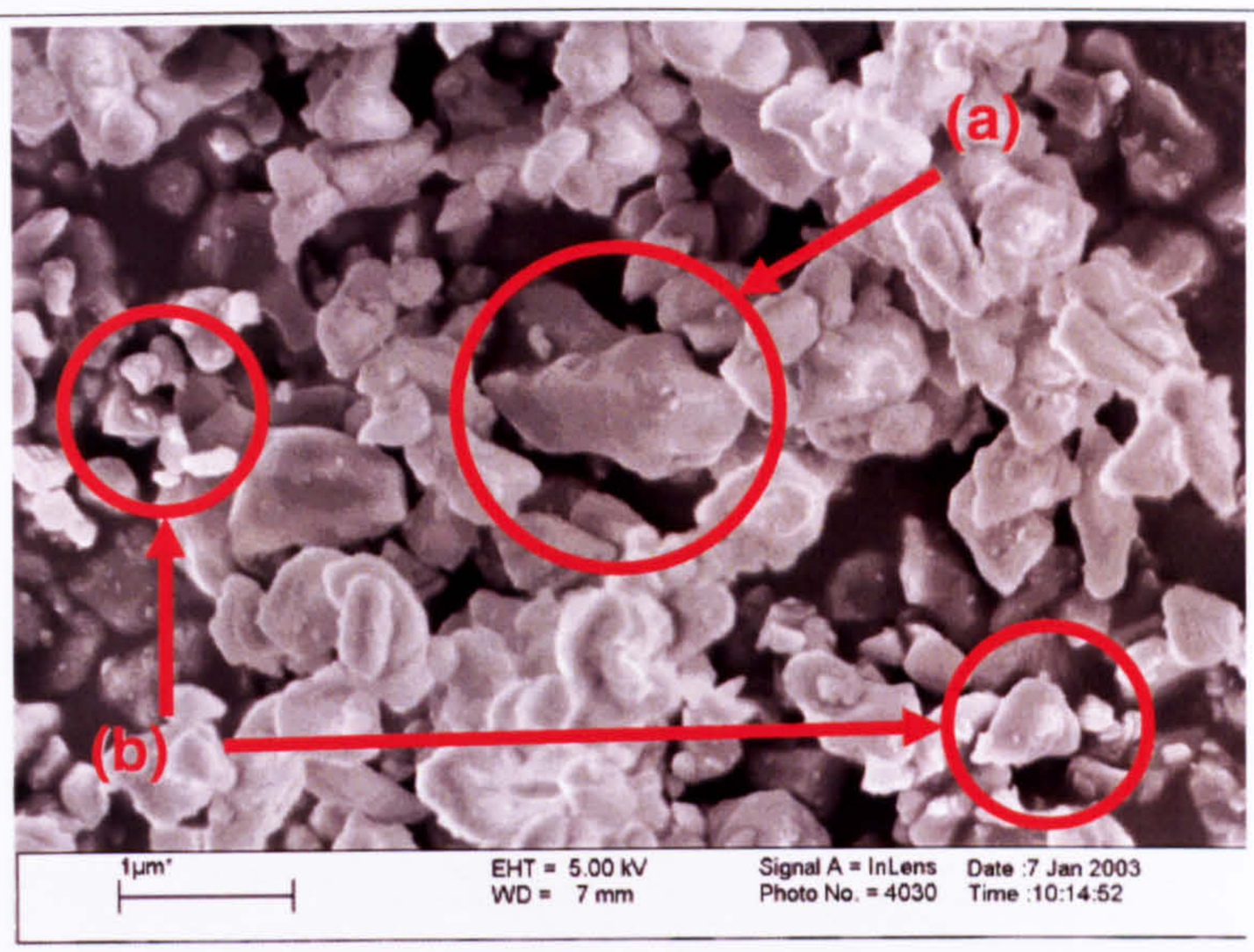

Figure 9.3 - FEGSEM micrograph 1 µm alpha/gamma alumina particles. (a) 1 µm particle. (b) Examples of particles smaller than 1 µm.

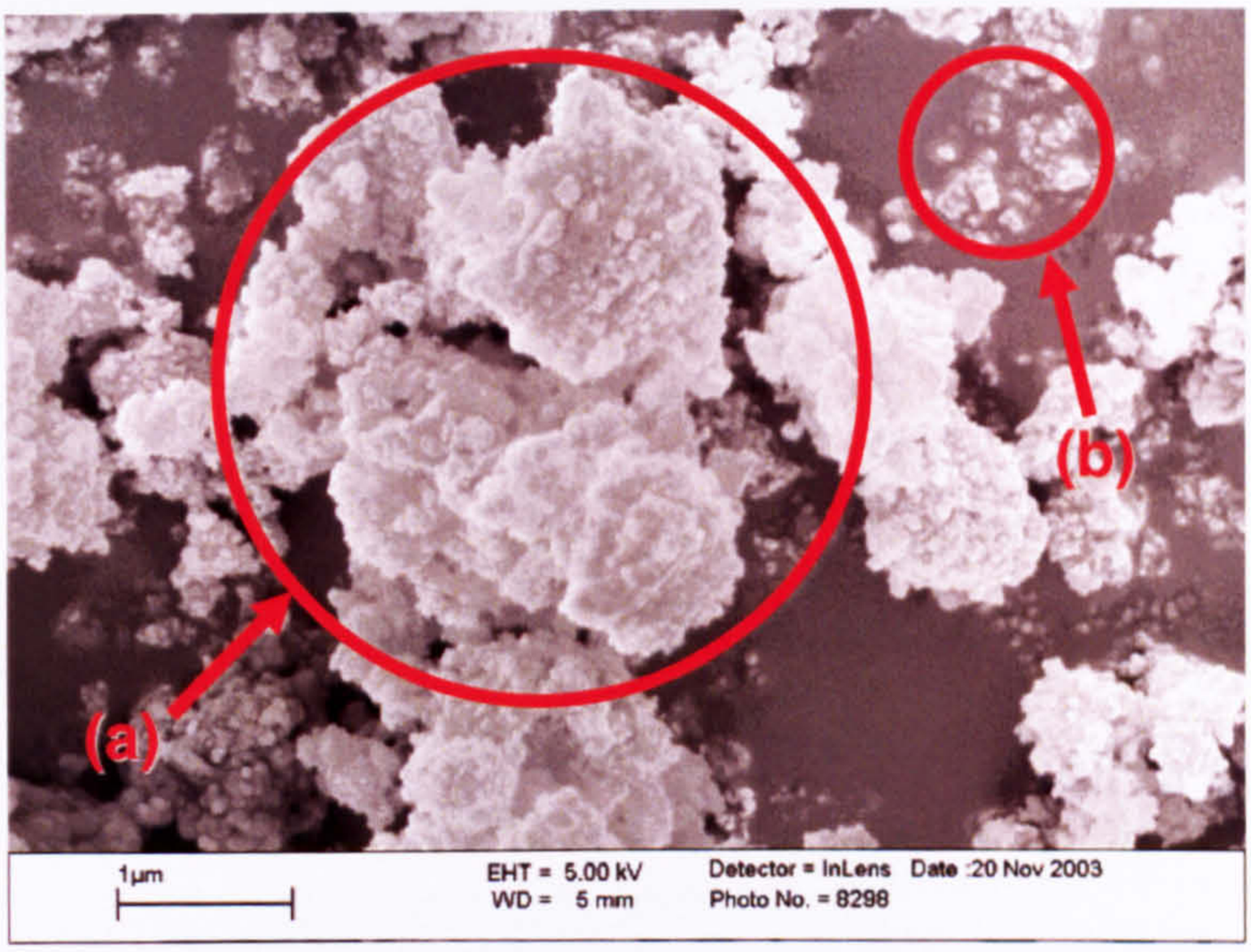

Figure 9.4 - FEGSEM micrograph 3 µm alpha/gamma alumina particles. (a) Particles of about 3 µm covered with smaller ones. (b) Particles much smaller than 1 µm.

As a conclusion it can be said the smaller the particles the better is their size distribution. This is important because particles of different mass in the electrolyte can experience different forces and particle segregation can arise inside the electrolyte during electrodeposition. This can cause the preferential incorporation of small particles instead of the desired ones and can arm the results obtained. An example of this will be shown in Chapter 12, where the hydrodynamic influence on the co-deposition process will be discussed.

9.2 Polystyrene

Fig. 9.5 shows the polystyrene (PS) particles, as previously described.

The distribution of such particles is very uniform, their shape is regular and spherical and their size, according to SEM analysis, is about 1 μm.

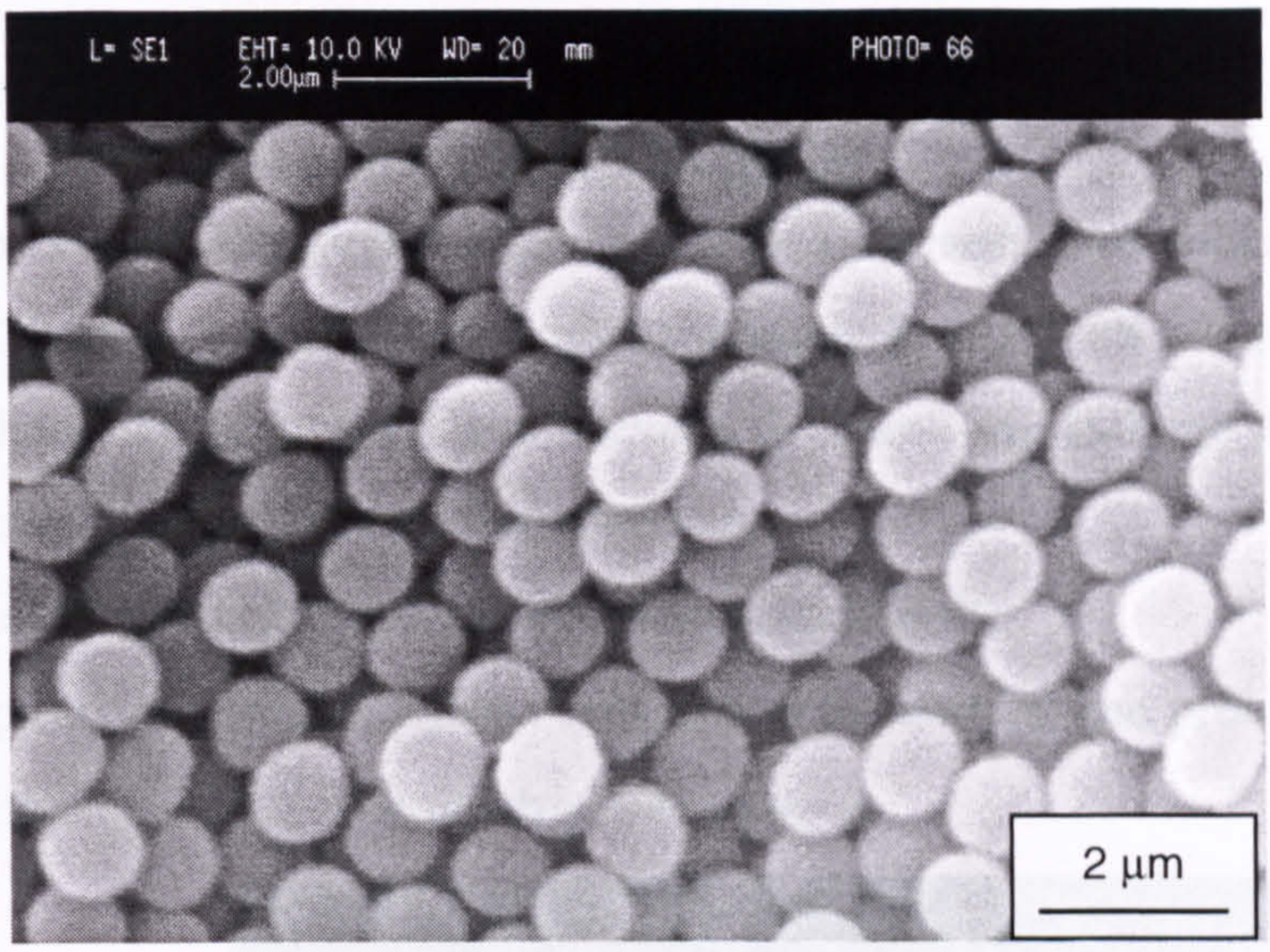

Figure 9.5 – SEM micrograph of polystyrene particles.

10. Morphological studies

All the composite coatings produced in this work were analysed by SEM microscopy in order to investigate how the presence of inert particles in the electrolyte affected their as-plated surface morphology.

10.1 Nickel-polystyrene composite coatings

Fig. 10.1 shows a backscattered electron image of a sectioned nickel-PS coating obtained at 220 rpm, 5 A/dm^2 and 2 g/l PS particle loading, on a 7.4 cm diameter mild steel cathode. The deposited layer seemed to be uniform and two different kinds of particle-related features can be characterised:

- PS particles totally incorporated into the electrodeposit;
- holes, imprints of particles loosely attached to the surface and probably lost with the ultrasonic treatment after electroco-deposition.

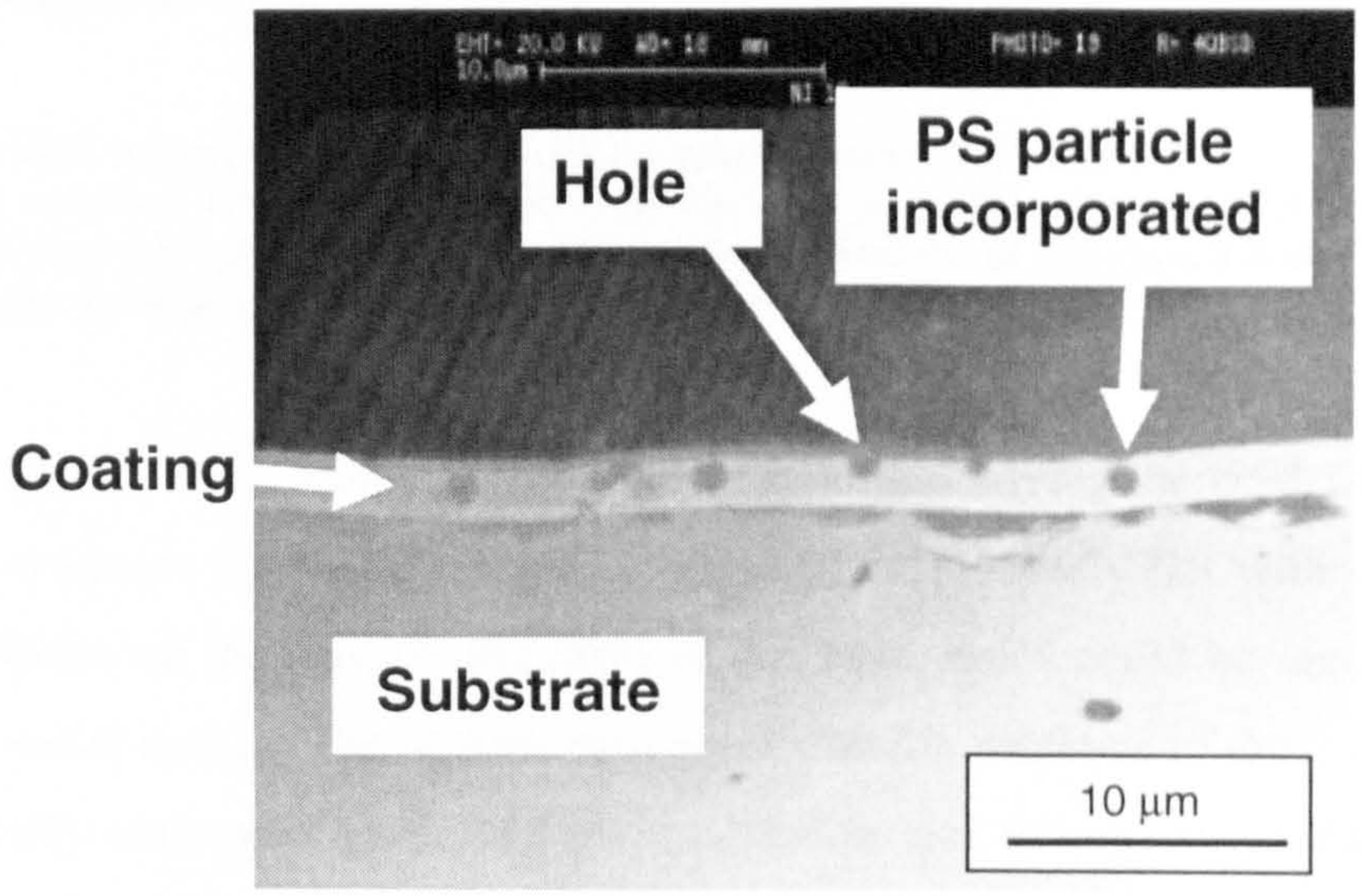

Figure 10.1 - Backscattered electron image of a 2 µm nickel-PS electrodeposit section produced at 220 rpm, 5 A dm^{-2} and 2 g l^{-1} PS particle loading, on a 7.4 cm diameter mild steel cathode. Two different kinds of features can be characterised: PS particles totally incorporated and holes.

Fig. 10.2 shows SEM micrographs of the surface of nickel-PS composite coatings obtained at 5 A/dm^2, 2 g/l PS particle loading and different cathode rotation speeds (460 and 220 rpm) on 7.4 cm diameter mild steel cathodes. The nickel matrix seemed to be homogeneous and fine-grained throughout the layer. Holes can be seen and can be distinguished from particles incorporated (showing as black in the micrographs).

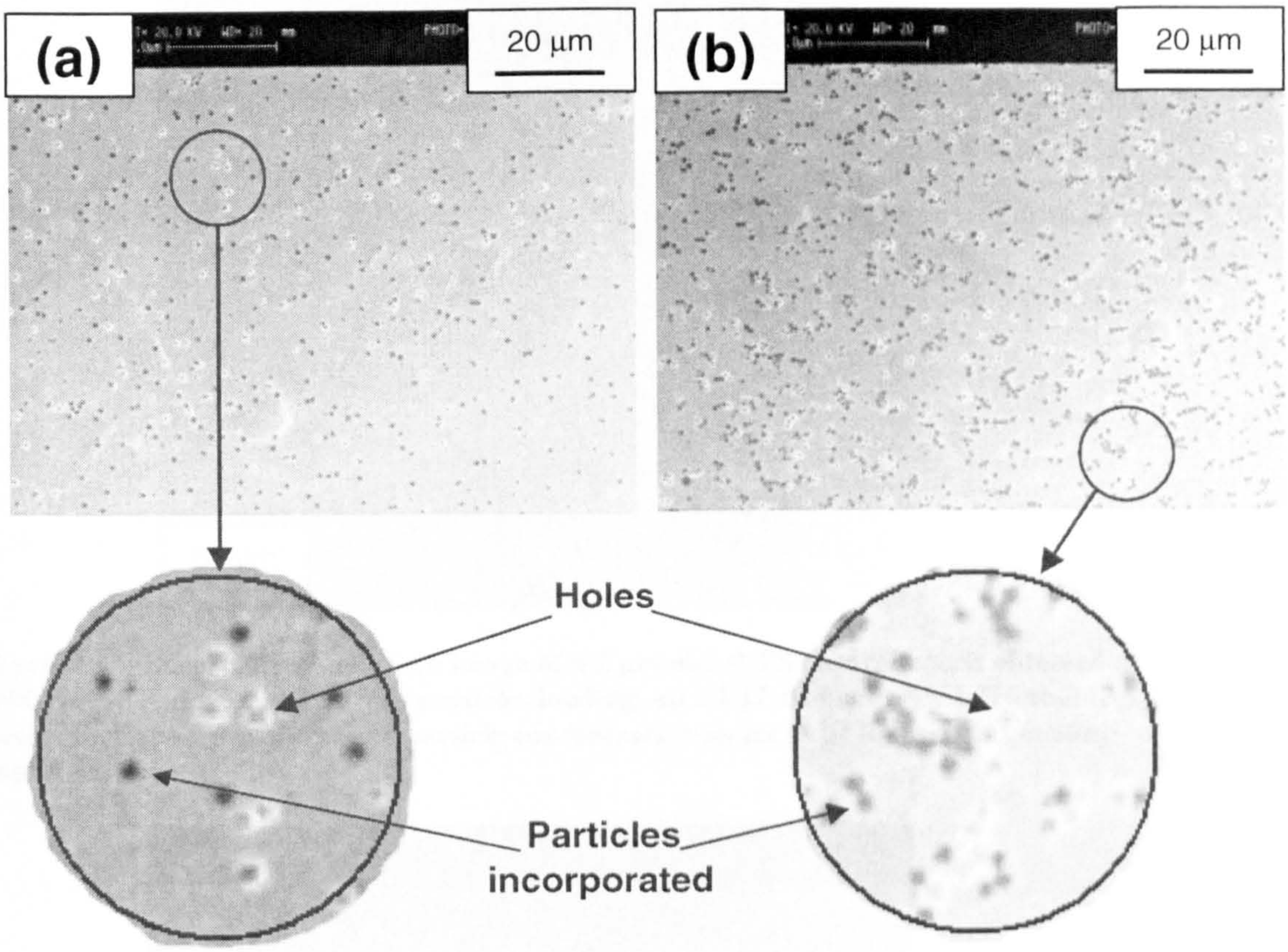

Figure 10.2 – SEM micrographs of Nickel-PS composite coatings. a) Nickel-PS electrodeposit obtained at 460 rpm, 5 A dm^{-2} and 2 g l^{-1} PS particle loading on a 7.4 cm diameter mild steel cathode. b) Nickel-PS electrodeposit obtained at 220 rpm, 5 A dm^{-2} and 2 g l^{-1} PS particle loading on a 7.4 cm diameter mild steel cathode.

BANOVIC *et al.* [147-148] found very similar behaviour studying the co-deposition of nickel with alumina. Coating surfaces appeared to be relatively flat with entrapped alumina particles on the surface and, also in this case, holes could be seen in some areas of the metal matrix. The authors also agree that the presence of these holes was due to partially entrapped particles losing adhesion and falling out of the coating subsequent to deposition.

Fig. 10.3 shows a backscattered electron image of a nickel-PS coating obtained at 1500 rpm, 5 A/dm^2 and 2 g/l PS particle loading on a 1.27 cm diameter AISI 316 stainless steel cathode. It is possible to see that near the coating imperfections (arrows) the PS concentration appeared to be higher than in the rest of the coating. This is shown more clearly, in a higher magnification micrograph (Fig. 10.4).

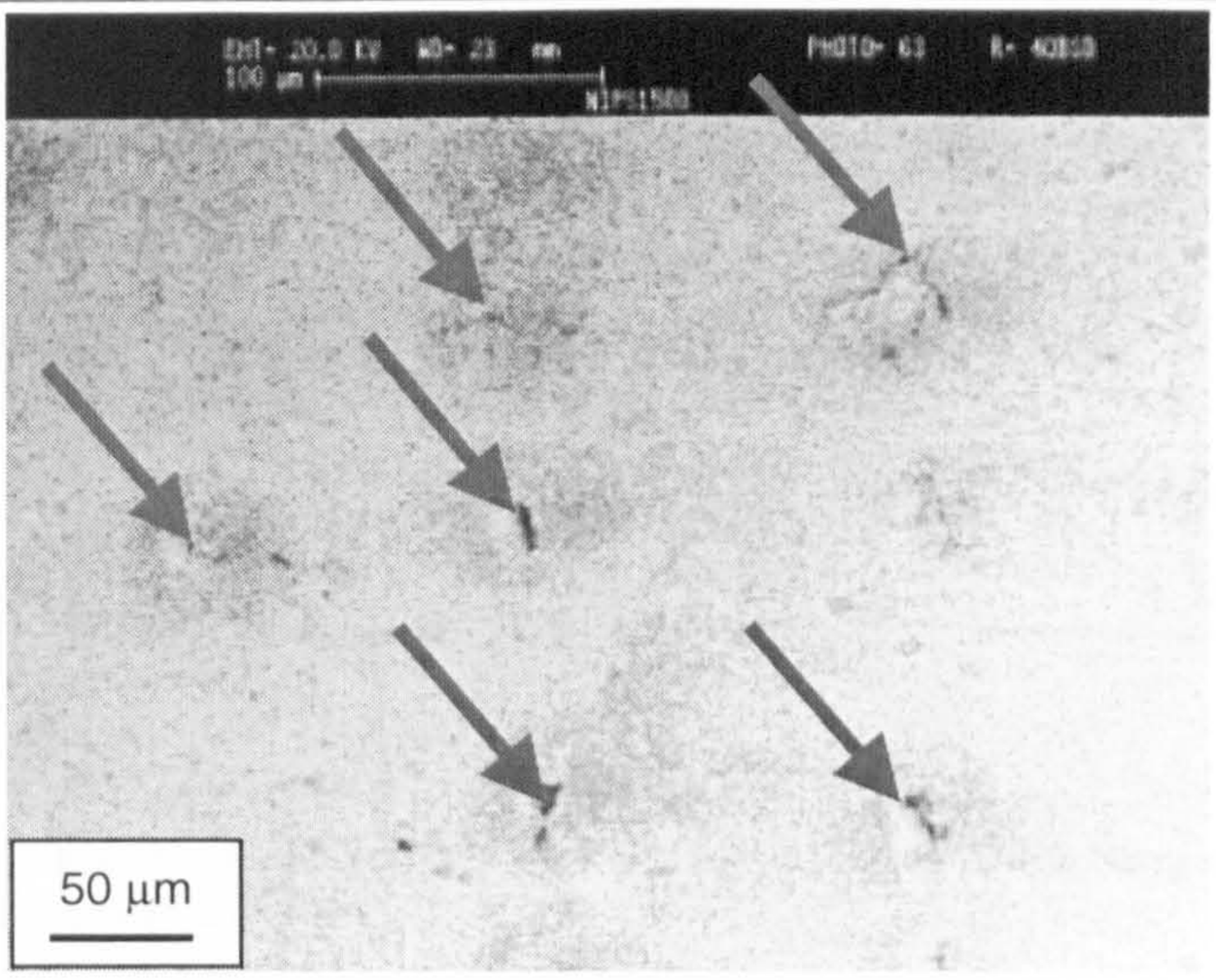

Figure 10.3 -Backscattered electron image of a 2 µm nickel-PS electrodeposit obtained at 1500 rpm, 5 A dm^{-2} and 2 g l^{-1} PS particles loading, on a 1.27 diameter AISI 316 stainless steel cathode. Arrows show how particle concentration seems to be higher near coating imperfections.

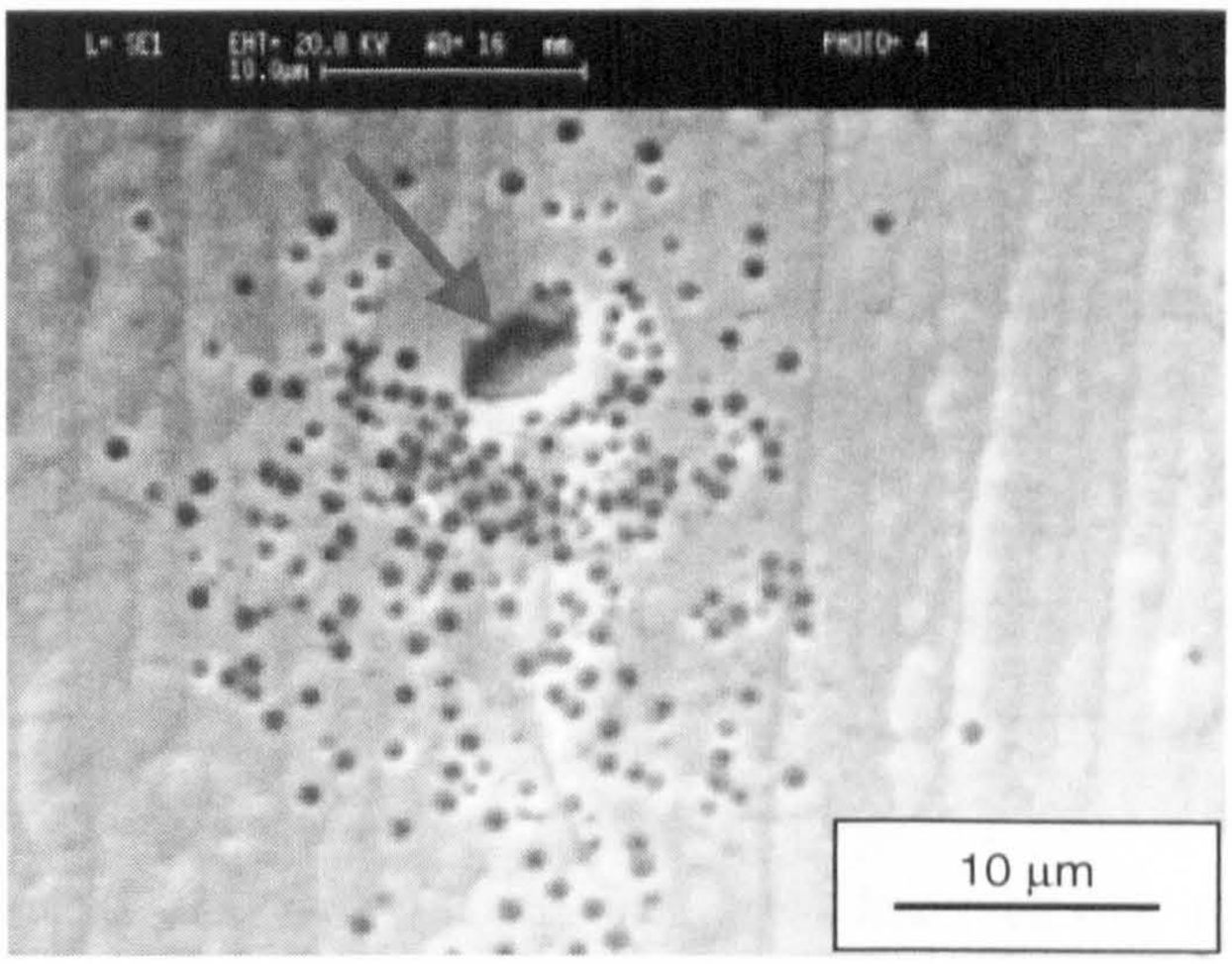

Figure 10.4 - Backscattered electron image of a 2 µm nickel-PS electrodeposit obtained at 1100 rpm, 5 A dm^{-2} and 2 g l^{-1} PS particles loading, on a 1.27 diameter AISI 316 stainless steel cathode. Arrow shows how particle concentration seems to be higher near coating imperfections.

This observation suggests that small imperfections on the coating surface influence the particle incorporation possibly with the following mechanism:

1. near the imperfection the hydrodynamic regime is locally altered reaching a higher turbulence;
2. this allows the particles to have a higher number of contacts with the surface;
3. this also allows the creation of stagnation zones where particles can stay and get incorporated into the metal growing layer (see Fig. 10.5);

4. higher turbulence also permits a higher local limiting current density as well, so the coating can grow locally faster;

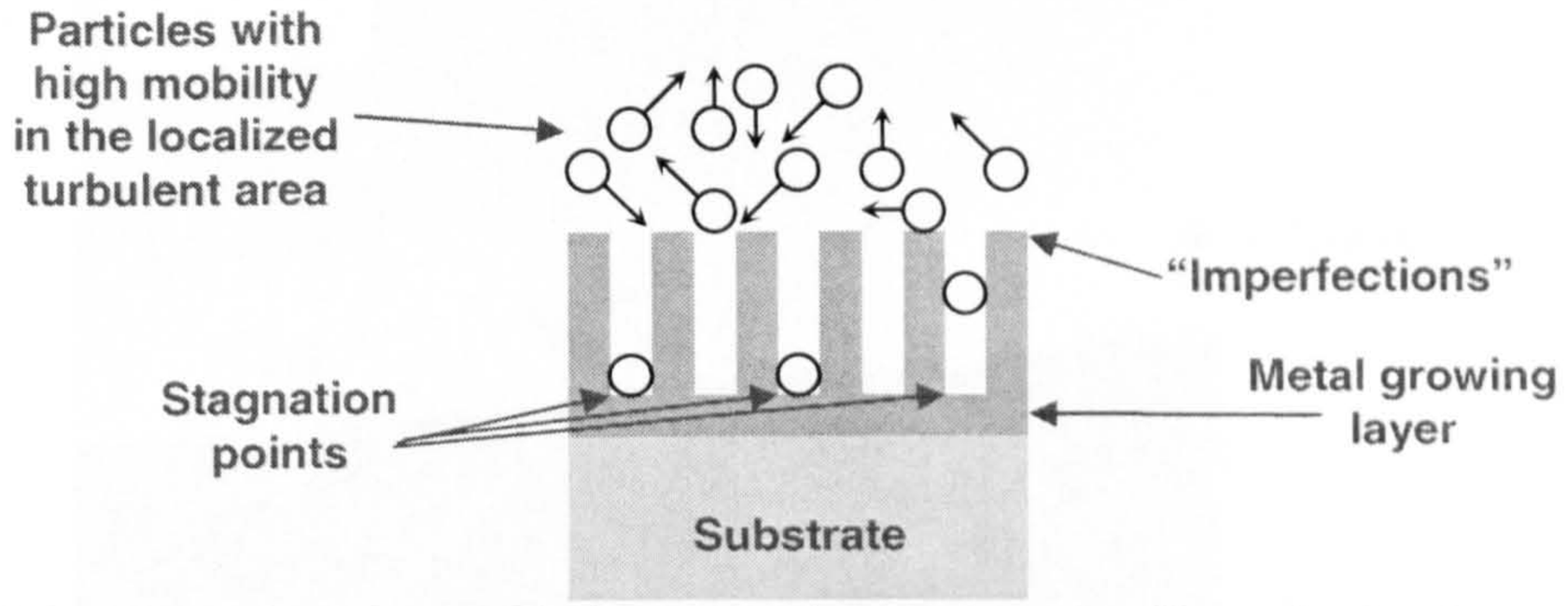

Figure 10.5 - Schematic of the particle incorporation process when "imperfections" are present on the cathode surface.

BOZZINI *et al.* [63], depositing AuCu alloy with B_4C particles, arrived at the same conclusion on the basis of a morphological analysis of their coatings. They stated that in the case of tangential flow, roughness development brings about local non-tangential components of flow, leading to enhanced incorporation of smaller particles (i.e. as the cathode in a tangential position grows rough with increase in coating thickness, its hydrodynamic conditions tend to approach the behaviour typical for the generation of stagnation points).

Figs. 10.6 and 10.7 show sectioned nickel-PS coatings, nominally 10 μm thick, produced at 60 rpm, 5 A/dm^2, 2 g/l PS particle loading and different electrode rotation speeds (60 and 300 rpm). The incorporated particles seemed to be higher in number when the electrode rotation speed was low (see Fig. 10.6). At the same time the particles seemed to coagulate in preferential areas rather than being well distributed throughout the layer. Particle agglomerations were probably due to the presence of coating imperfections and were covered, later, by the growing metal layer.

When the rotation speed was higher, particles incorporated in the coatings were less in number, but they seemed to have a better distribution in the direction parallel to the substrate (see Fig. 10.7).

However the particle distribution did not appear to be uniform in the direction perpendicular to the substrate for either of the cathode rotation rates.

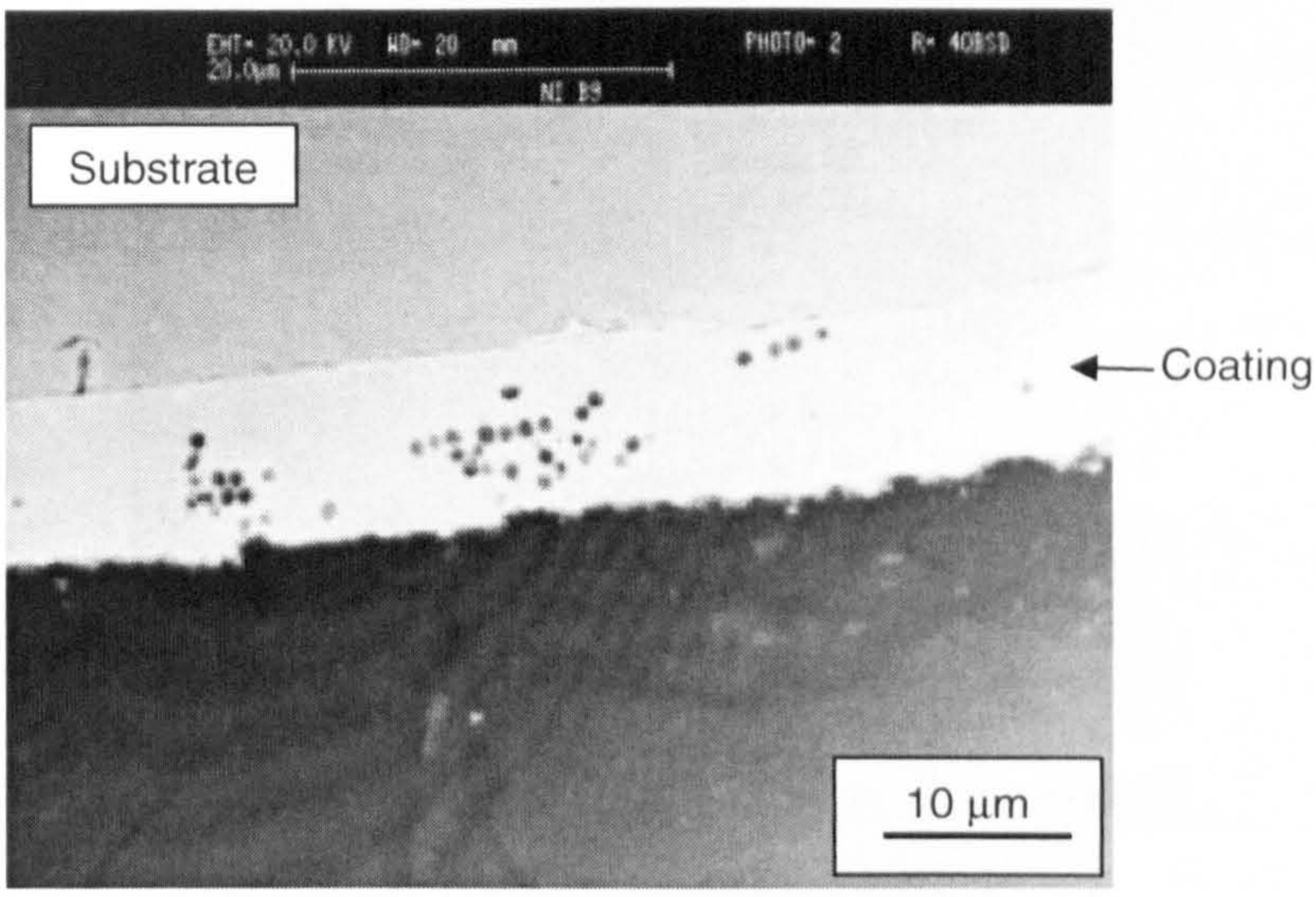

Figure 10.6 - Backscattered electron image of a 10 µm nickel-PS electrodeposit section produced at 60 rpm, 5 A dm^{-2} and 2 g l^{-1} PS particle loading, on a 7.4 cm diameter mild steel cathode.

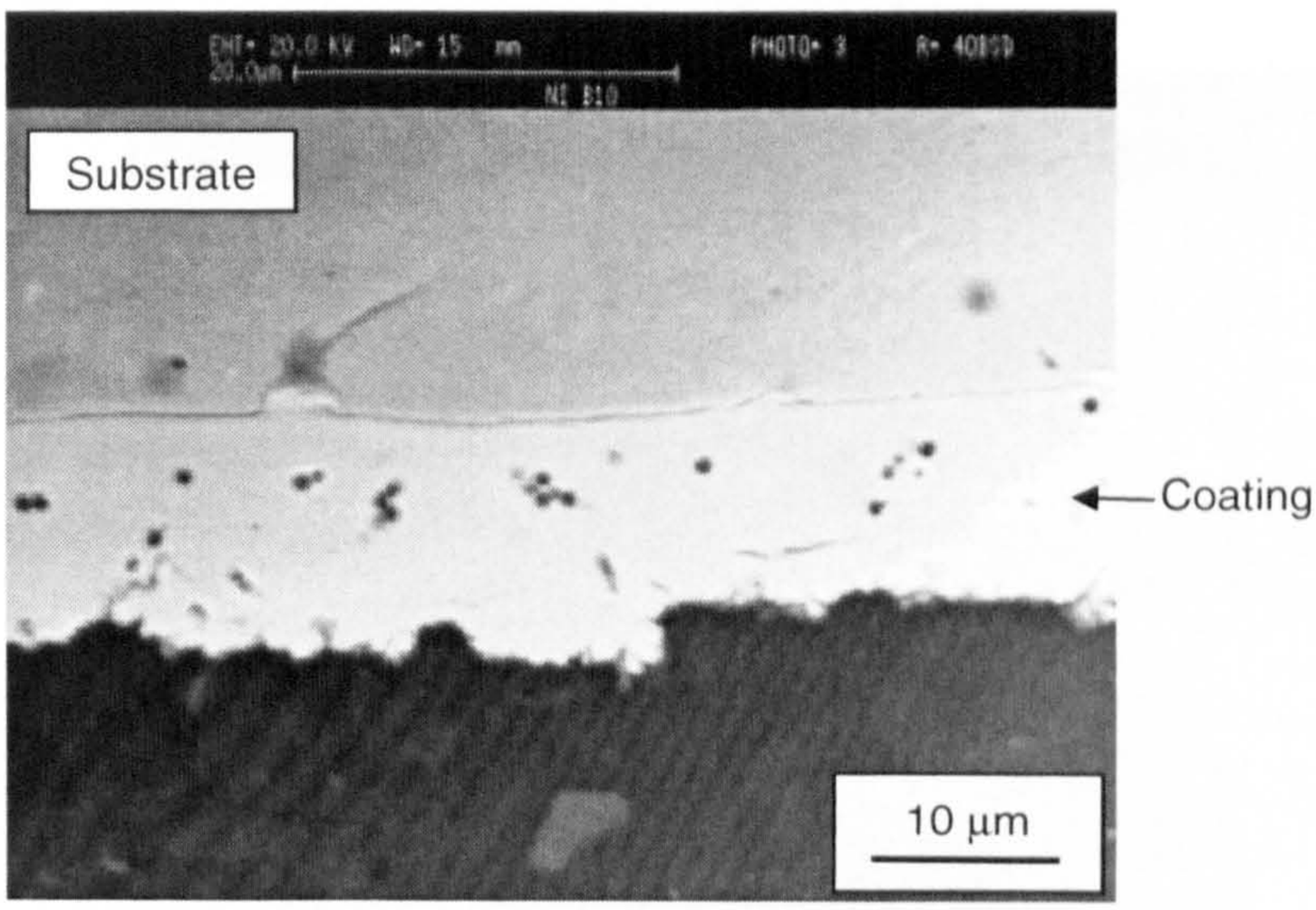

Figure 10.7 - Backscattered electron image of a 10 µm nickel-PS electrodeposit section produced at 300 rpm, 5 A dm^{-2} and 2 g l^{-1} PS particle loading, on a 7.4 cm diameter mild steel cathode.

10.2 Copper-polystyrene composite coatings

Fig. 10.8 shows a SEM micrograph of the surface of a copper-PS composite coating, obtained at 700 rpm, 5 A/dm^2 and 2 g/l PS particle loading on a 7.4 cm diameter mild steel cathode; Fig. 10.9 shows the corresponding backscattered image.

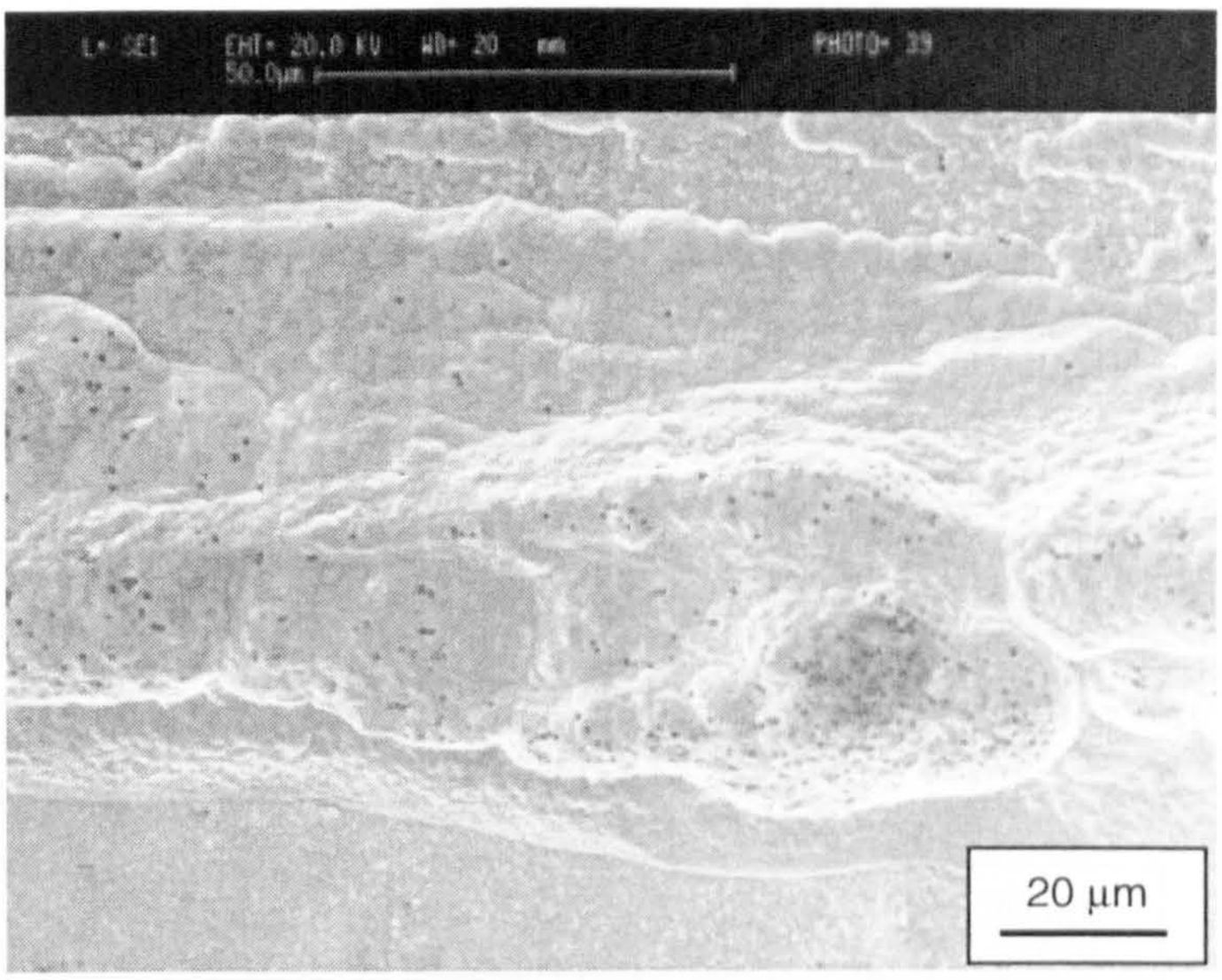

Figure 10.8 - SEM micrograph of a copper-PS electrodeposit obtained at 700 rpm, 5 A dm^{-2} and 2 g l^{-1} PS particle loading on a 7.4 cm diameter mild steel cathode.

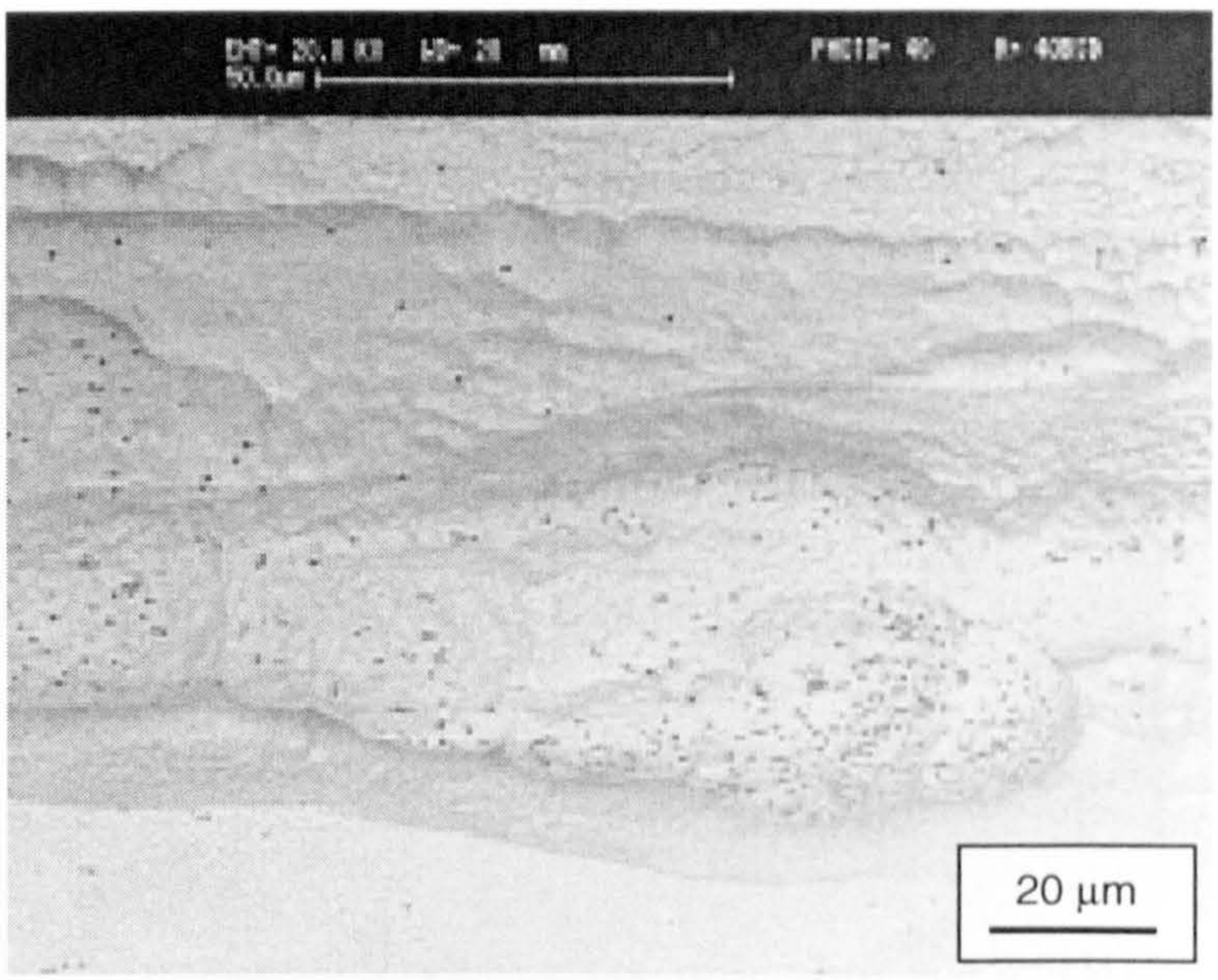

Figure 10.9 - Backscattered electron image of a copper-PS electrodeposit obtained at 700 rpm, 5 A dm^{-2} and 2 g l^{-1} PS particle loading on a 7.4 cm diameter mild steel cathode.

Copper-PS composite coatings obtained at high cathode rotation speed, on mild steel cathodes, showed "nodular striped" structures on their surface (see Figs. 10.8 and 10.9). This formation didn't occur at low cathode rotation speeds, as shown, for example, in Fig. 10.10.

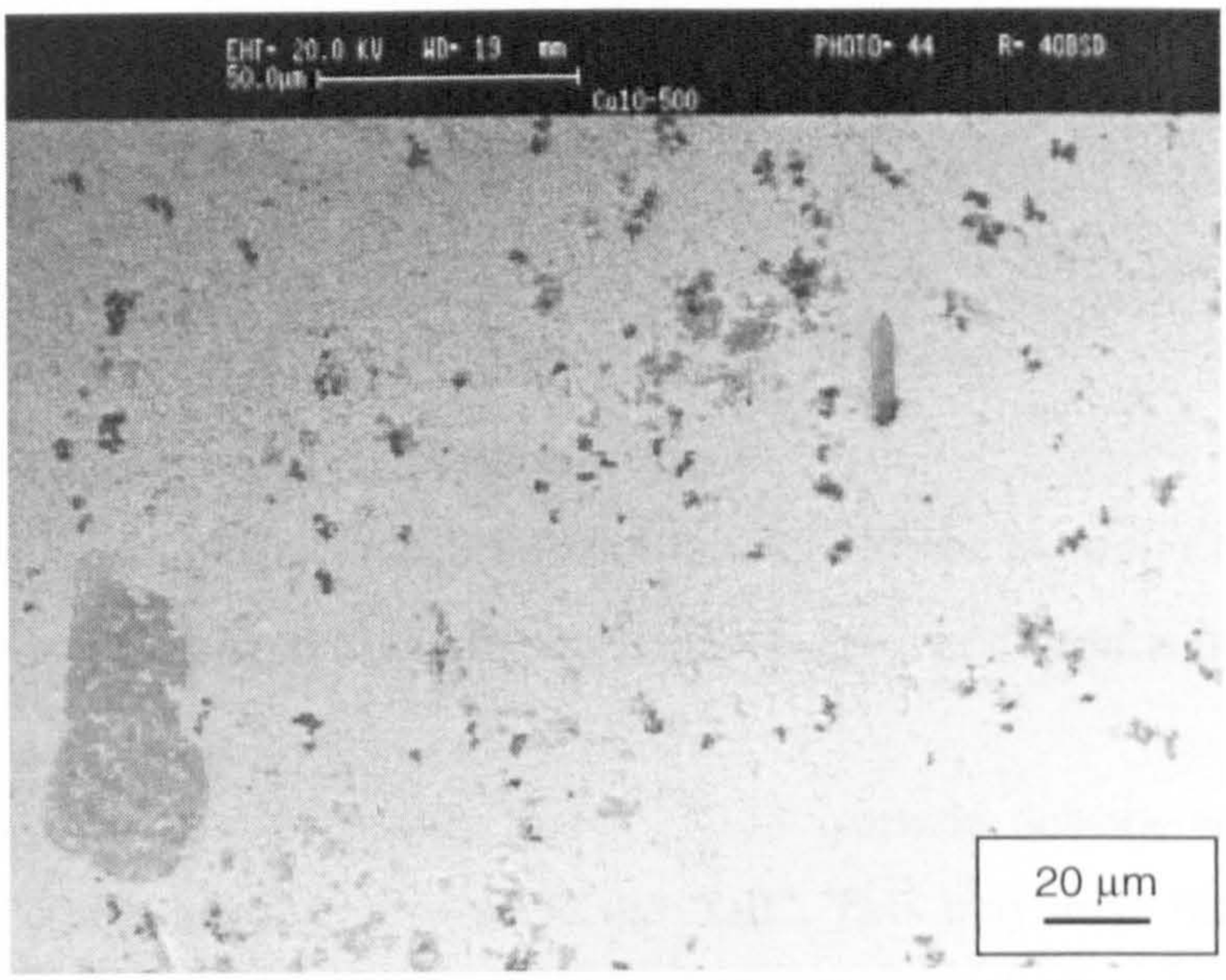

Figure 10.10 - SEM micrograph of a copper-PS electrodeposit obtained at 30 rpm, 5 A dm^{-2} and 2 g l^{-1} PS particle loading on a 7.4 cm diameter mild steel cathode.

The concentration of PS particles seemed to be much higher in the "nodular striped" structures than in the rest of the coating. This is clearly evident in Fig. 10.11.

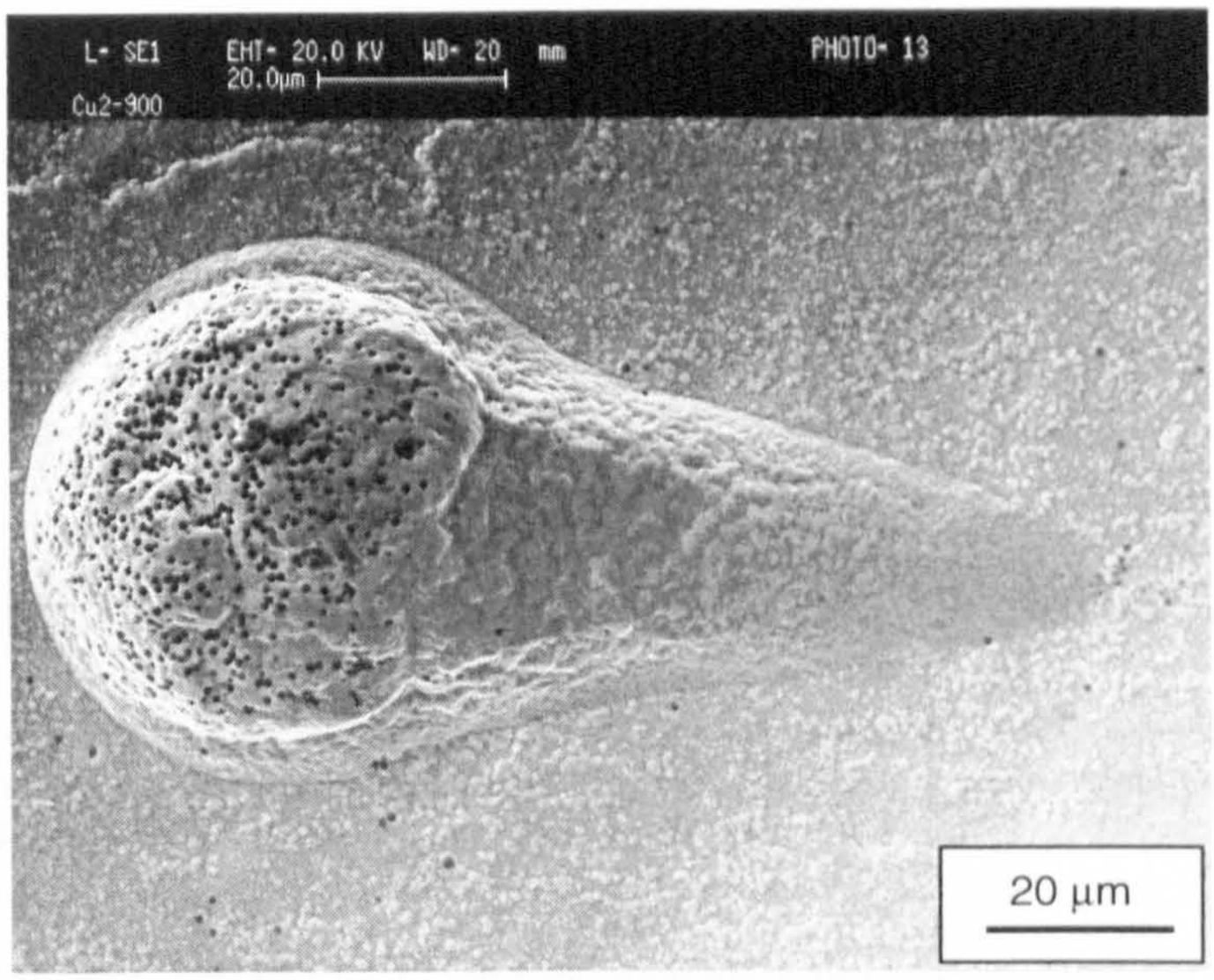

Figure 10.11 - SEM micrograph of a copper-PS electrodeposit obtained at 620 rpm, 5 A dm^{-2} and 2 g l^{-1} PS particle loading on a 7.4 cm diameter mild steel cathode.

The shape of the "comet type" nodule in Fig. 10.11 suggests that a local growth orientation has occurred in the area. Once this "preferential growth" begins, the hydrodynamics of the electrolyte in contact with the cathode surface is probably altered locally. The "comet type" nodule can grow producing the stripes shown previously because, due to the surface discontinuities formed, the current density is

higher at the "raised" growth. Another consequence is that a local remixing of the electrolyte in the vicinity of these areas is probable. This may explain the difference in the PS concentration, which was much higher on the "nodular striped" structures than in the rest of the coating:

- the turbulence is perhaps higher at these points;
- this leads to a local remixing of the electrolyte;
- more particles can make contact with the cathode surface per unit time;
- the probability of being particle incorporation in the metal layer is higher.

In the "comet type" nodule shown in Fig. 10.11, particle density appeared to be higher at the "comet head" compared to the "tail". This may arise through the fact that once the preferential growth begins (comet head), particle flow is not parallel to the cathode surface anymore, but particles hit the metal surface perpendicularly, as shown in Fig. 10.12. In such a situation the probability for particle incorporation is higher at the head rather than at the tail.

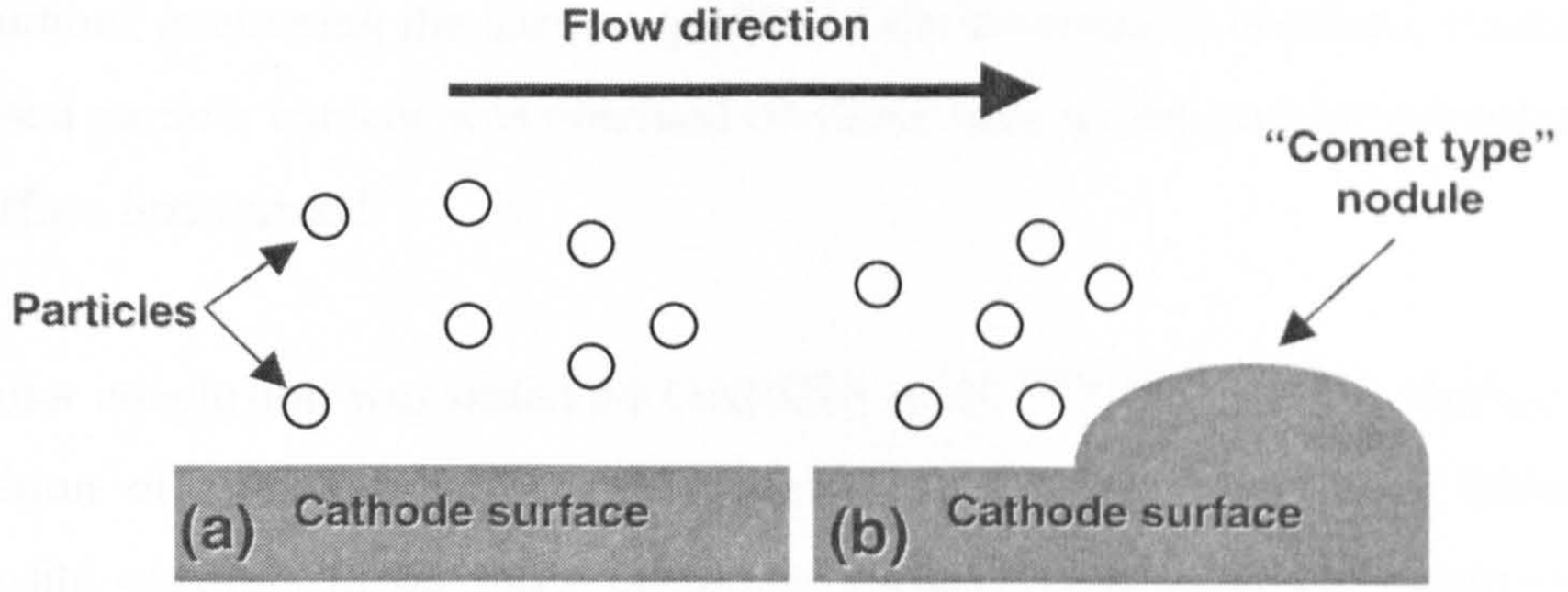

Figure 10.12 - Schematic of the particle incorporation process prior to and after formation of a "comet type" nodule. (a) No "comet type" nodules are present on the cathode surface. (b) "Comet type" nodule is present on the cathode surface.

"Nodular striped" structures seemed to be connected to the presence of particles in the electrolyte. In order to confirm this, copper coatings were produced without PS present. These coatings didn't show stripes on their surfaces at any cathode rotation speed values (see Fig. 10.13).

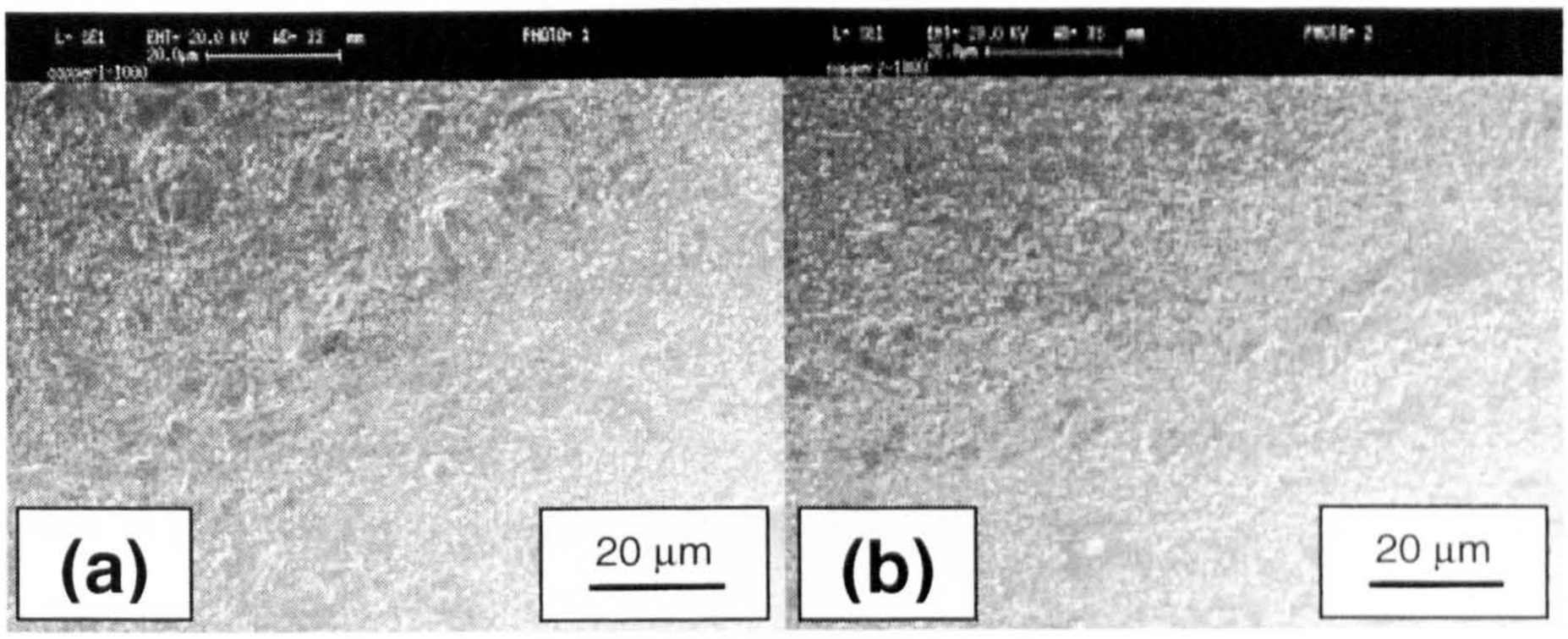

Figure 10.13 – SEM ,micrographs of: (a) Copper electrodeposit obtained at 620 rpm and 5 A dm^{-2} on 7.4 cm diameter mild steel cathode. (b) Copper electrodeposit obtained at 460 rpm and 5 A dm^{-2} on 7.4 cm diameter mild steel cathode. No particles in solution.

Since the reason for the formation of "comet-type" growths could therefore be attributed to the presence of particles in the electrolyte, it can be concluded that particle co-deposition does influence the final deposit morphology. Strong support for this hypothesis has been made by STANKOVIC AND GOJO [54] who studied the electroco-deposition of copper with inert, semi-conductive and conductive particles. The authors, evaluating the surface quality of the composites obtained, stated that an increased particle content was obtained on those sites where nodular irregularities on the surface had formed.

A similar conclusion was stated by GARCIA *et al.* [149]. The authors studied the co-deposition of silicon carbide with nickel from a Watts bath. They found these composite coatings to be more corrosion resistant than ordinary nickel coatings. They also found that the coating morphology was strongly influenced by the presence of the inert particles. The authors obtained pure nickel coating electrodeposited at 2 A dm^{-2}. They noted that the microstructure consisted of columnar grains perpendicular to the substrate surface. Cracks from 1 to 10 µm parallel to the substrate surface at different distances from the interface with the substrate were also visible. When the authors produced nickel/SiC composite coatings containing 5 µm SiC-particles, they noted that the microstructure was quite similar to the pure nickel coatings except that the co-deposition of SiC-particles caused some disorder of the columnar growth of the nickel matrix. The authors [149] also stated that incorporation of sub-micrometre SiC-particles has a large effect on

the microstructure. The voids between the SiC-particles and the nickel matrix seemed to result from the chemical etching used to reveal the microstructure during the metallographic preparation. Indeed the cross section of the same sample without any chemical etching showed a defect-free interface between the SiC-particles and the nickel matrix. Cracks were not noticed in these Ni–SiC composite coatings. In nickel–SiC coatings containing 0.3 μm SiC-particles, the columnar structure observed in particle-free coatings, is completely substituted by a very fine equiaxed grain structure.

In the present work on 1.27 cm diameter AISI 316 stainless steel cathodes, copper-PS composite coatings also showed nodular structures, but not in striped formations. These occurred at all rotation speed values, as shown in Fig. 10.14 for coatings produced at 0 and 1750 rpm. Also for these coatings, the "nodular" areas were richer in incorporated PS particles.

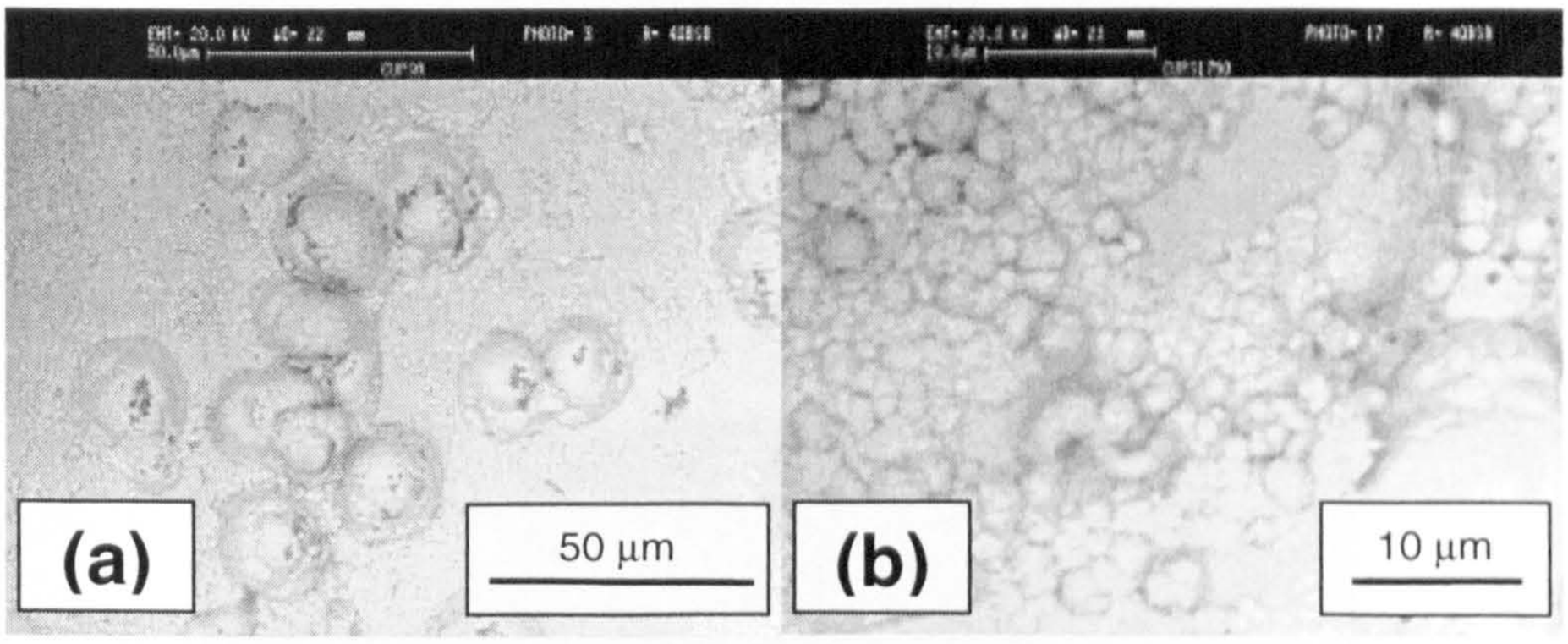

Figure 10.14 – (a) Backscattered electron image of a 2 μm copper-PS electrodeposit obtained at 0 rpm, 5 A dm^{-2} and 2 g l^{-1} PS particles loading on a 1.27 cm diameter AISI 316 stainless steel cathode. (b) Backscattered electron image of a 2 μm copper-PS electrodeposit obtained at 1750 rpm, 5 A dm^{-2} and 2 g l^{-1} PS particle loading on a 1.27 cm diameter AISI 316 stainless steel cathode.

Fig. 10.15 shows a sectioned copper-PS coating, produced at 700 rpm, 5 A/dm^2 and 2 g/l PS particle loading on a 7.4 cm diameter mild steel cathode, showing an area through one of the "nodular striped" structures. At high rotation speeds the copper coating did not seem to be compact and it was possible to see poorly coated substrate between each stripe. At low rotation speed values this did not occur, as shown in Figs. 10.16 and 10.17.

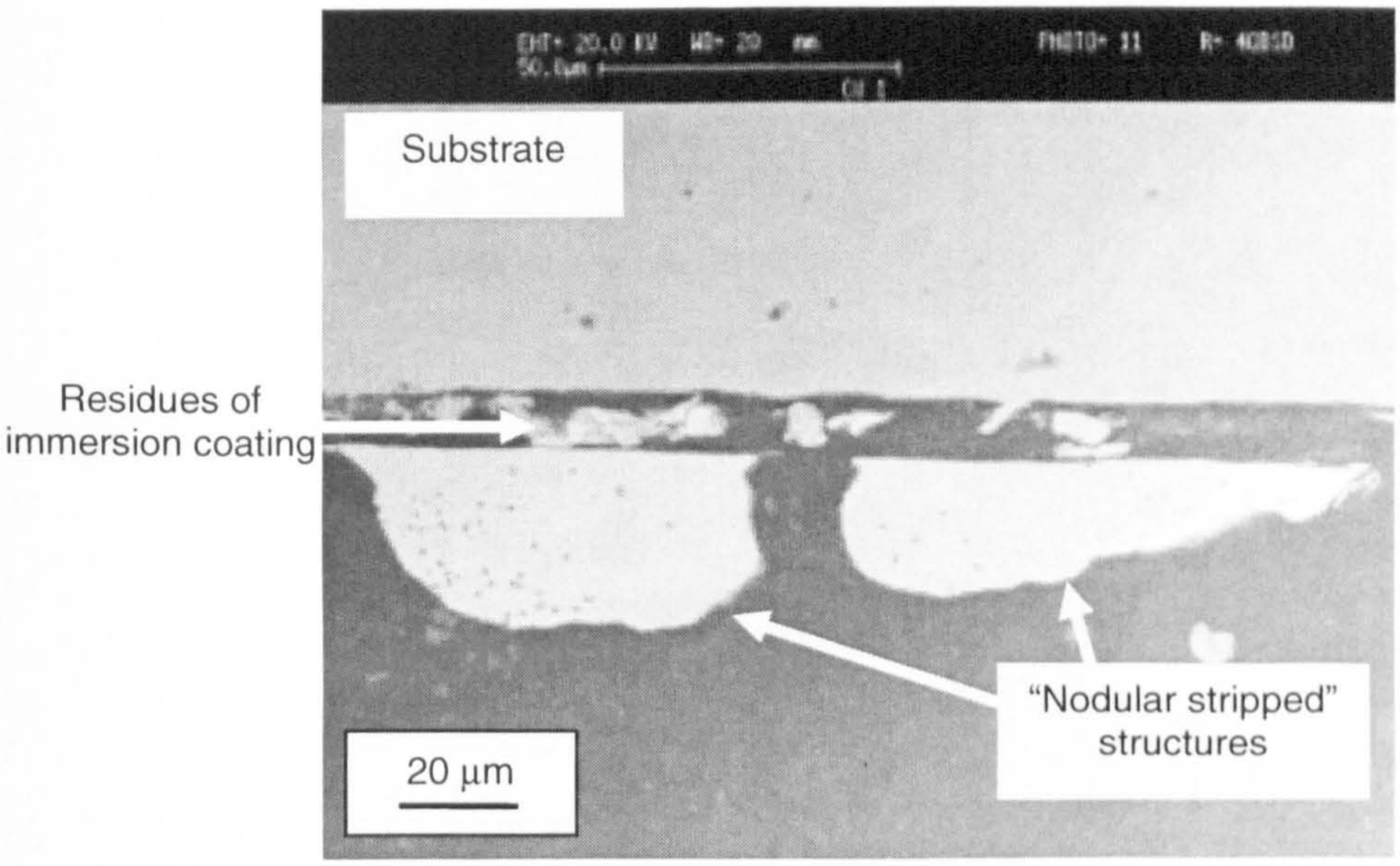

Figure 10.15 - Backscattered electron image of a copper-PS electrodeposit section (produced at 700 rpm, 5 A dm^{-2} and 2 g l^{-1} PS particle loading on a 7.4 cm diameter mild steel cathode) showing an area through one of the "nodular striped" structures.

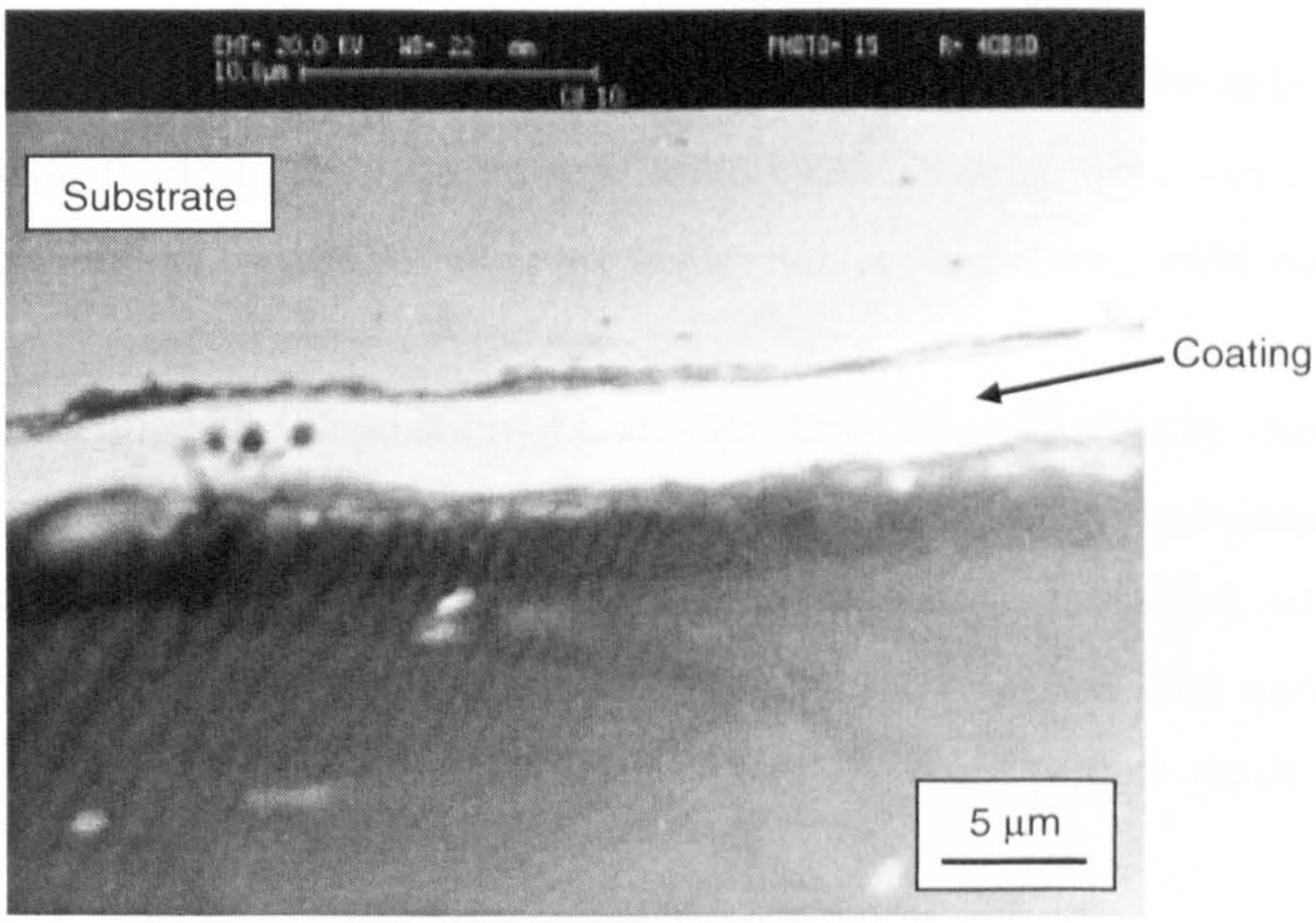

Figure 10.16 - Backscattered electron image of a copper-PS electrodeposit section produced at 30 rpm, 5 A dm^{-2} and 2 g l^{-1} PS particle loading on a 7.4 cm diameter mild steel cathode. No "nodular striped" structures were evident.

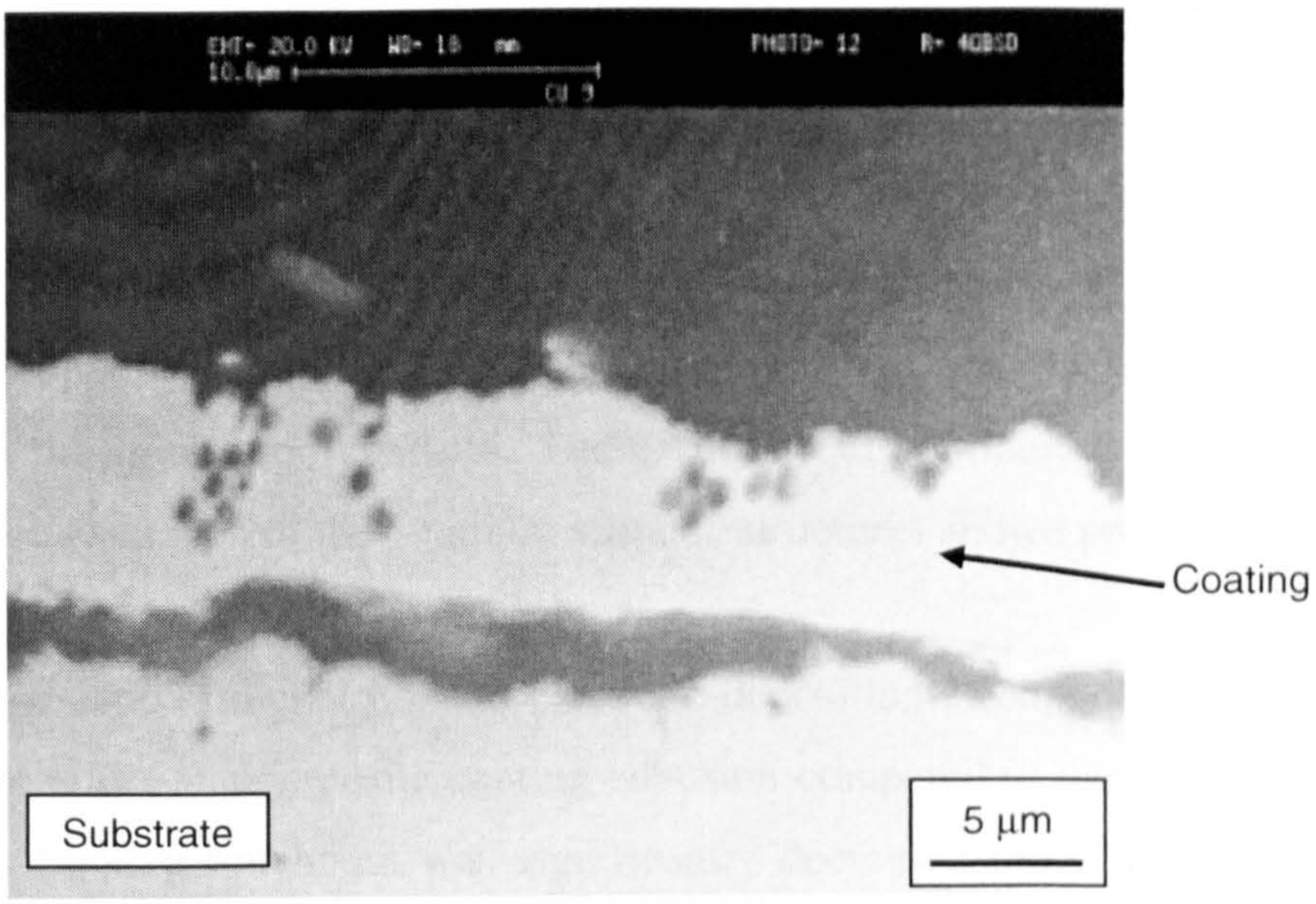

Figure 10.17 - Backscattered electron image of a copper-PS electrodeposit section produced at 60 rpm, 5 A dm^{-2} and 2 g l^{-1} PS particle loading on a 7.4 cm diameter mild steel cathode. No "nodular striped" structures were evident.

Copper-PS composite coatings were also obtained on 7.4 cm diameter mild steel cylinders previously electrodeposited with a 1 µm nickel coating. This was carried out in order to avoid the formation of copper immersion coatings on the mild steel.

An immersion coating is the deposition of a metallic layer on a substrate by chemical displacement from a solution of a salt of the coating metal [8]. In this case because, of its electropositive character, metals higher in the standard potentials series, such as iron (-0.44 V), easily precipitate copper (+0.34 V). A chemical reducing agent, as with electroless deposition, is not required because it is the substrate metal itself which undergoes oxidation, in this case:

$$Fe + Cu^{2+} \rightarrow Cu + Fe^{2+}$$

The coating obtained is usually about 1 µm thick and the adhesion with the substrate is very poor. This is why immersion methods are useful in many industrial processes (e.g. recovering the last traces of copper from leaching solutions, mill tailings, using "scrap" iron), but most are not concerned with the quality of the coating.

Immersion coating residues can be seen in Fig. 10.15 between the deposit and the substrate. They are formed before the electroco-deposition takes place and are usually approximately 1 µm thick. The gap (>1 µm) between substrate and coatings

could be a consequence of the bad adhesion properties exhibited by immersion coatings. Due to the weak adhesion and because of the stress due to the metallographic preparation of the samples (mechanical polishing, see Section 8.7) the gap was larger than 1 μm. In this way metal and second phase material were depositing on copper rather than mild steel. The cathode surface was not smooth but coarse due to the immersion coatings. These surface discontinuities could be the initiators for the formation of the "nodular striped" structures shown previously.

The electrodeposition of nickel prior to electroco-deposition of copper and PS has a very beneficial effect on composite coating adhesion compared to the ones obtained on mild steel. Coating roughness was significantly decreased too. This practice of "pre-plating" or deposition of "flash coatings" is quite well known and widely used in industrial applications concerning, amongst other systems, copper deposition [8]. However, despite the avoidance of immersion deposits, the formation of "nodular striped" structures at high rotation speed values was still evident, as shown in Fig. 10.18, but in this case the stripes were much smaller. This is probably because the decrease in roughness reduces localised stirring (agitation) effects that makes the stripes grow with a commensurate high concentration of PS particles.

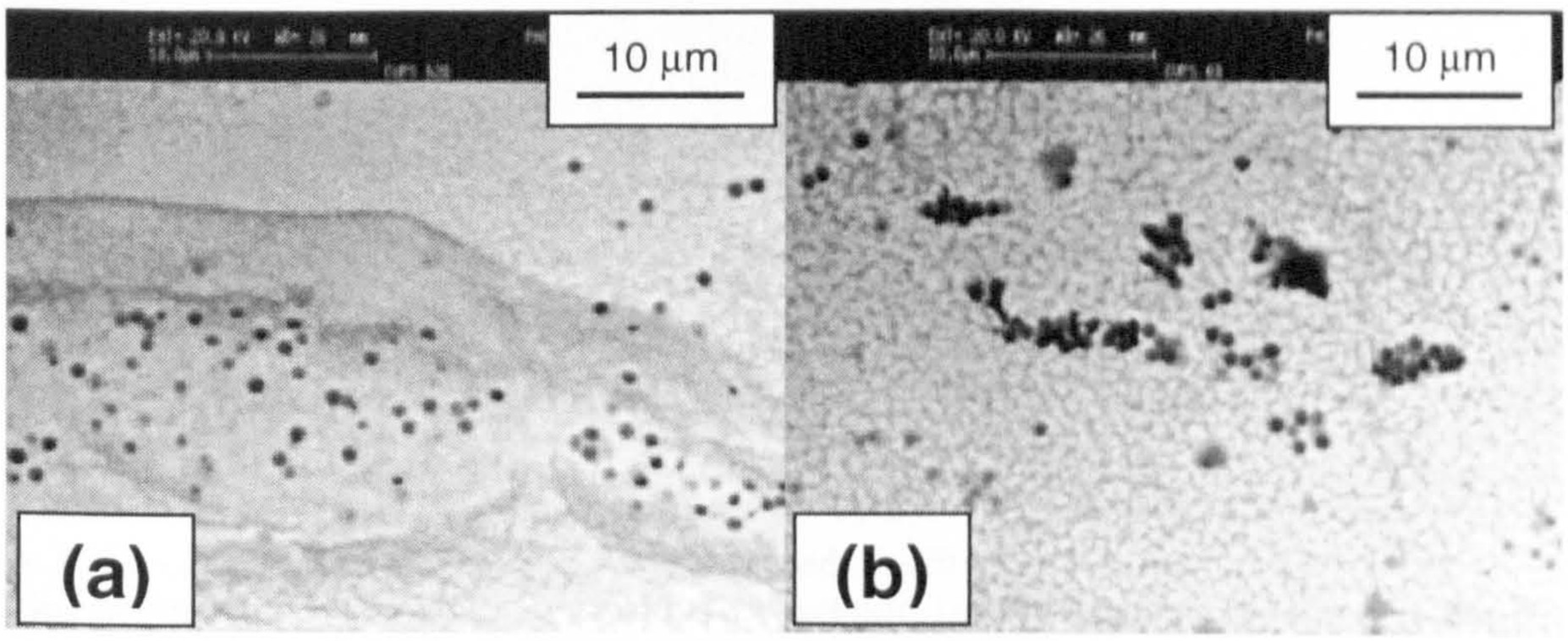

Figure 10.18 - Backscattered electron images of 2 μm copper-PS electrodeposits obtained at 5 A dm^{-2} and 2 g l^{-1} PS particle loading on 7.4 cm diameter cathode pre-plated with nickel. (a) 620 rpm. (b) 60 rpm.

10.3 Zinc-polystyrene composite coatings

Fig. 10.19 shows the surface morphology of a zinc-PS composite coating deposited at 620 rpm, 5 A/dm^2 and 2 g/l PS particle loading on a 7.4 cm diameter mild steel

cathode. It can be seen that in this case "nodular striped" structures were also obtained.

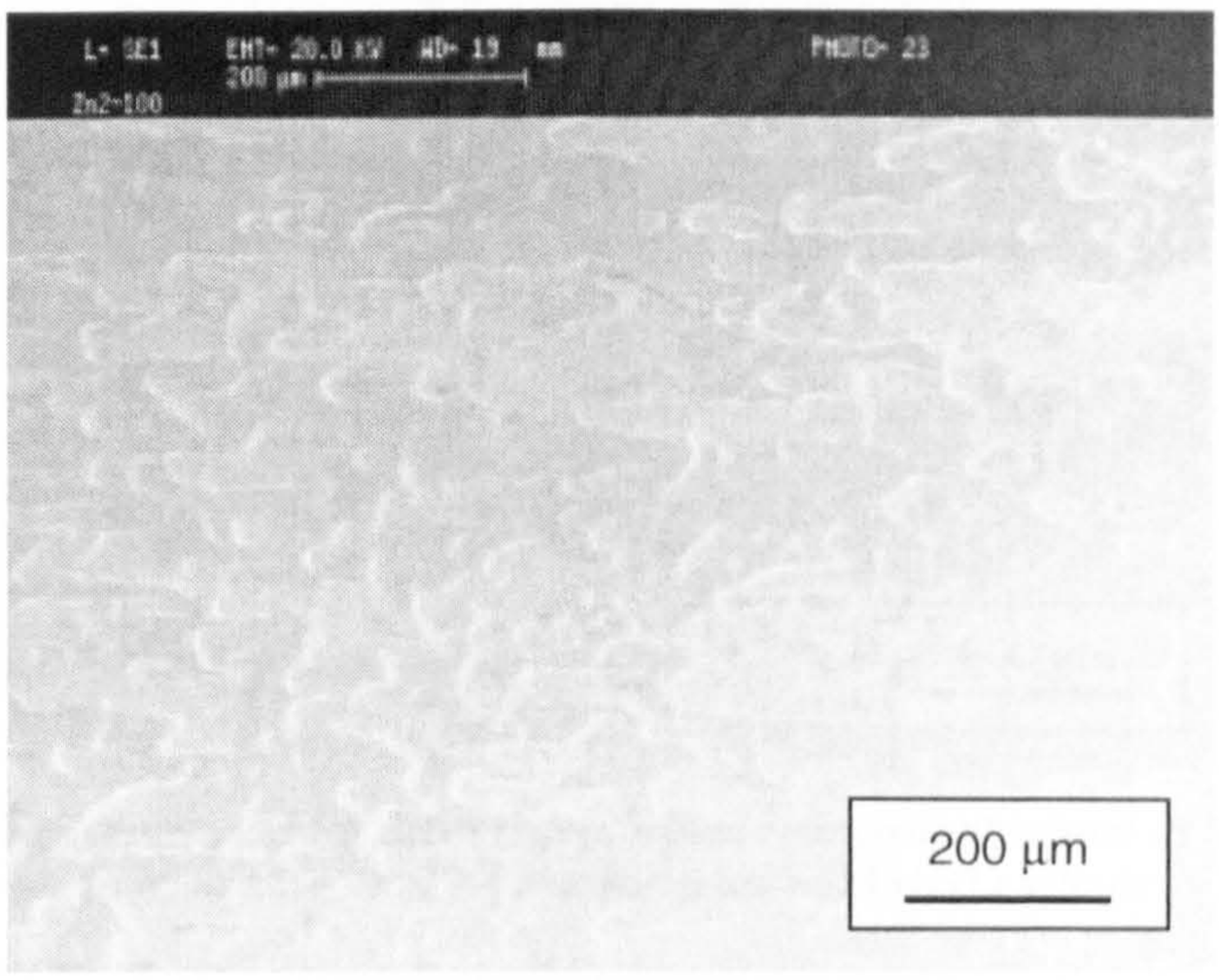

Figure 10.19 - SEM micrograph of a 2 µm zinc-PS electrodeposit obtained at 620 rpm, 5 A dm^{-2} and 2 g l^{-1} PS particle loading on a 7.4 cm diameter mild steel cathode.

In Fig. 10.20 the phenomenon is more evident as are the higher concentrations of PS particles with these features.

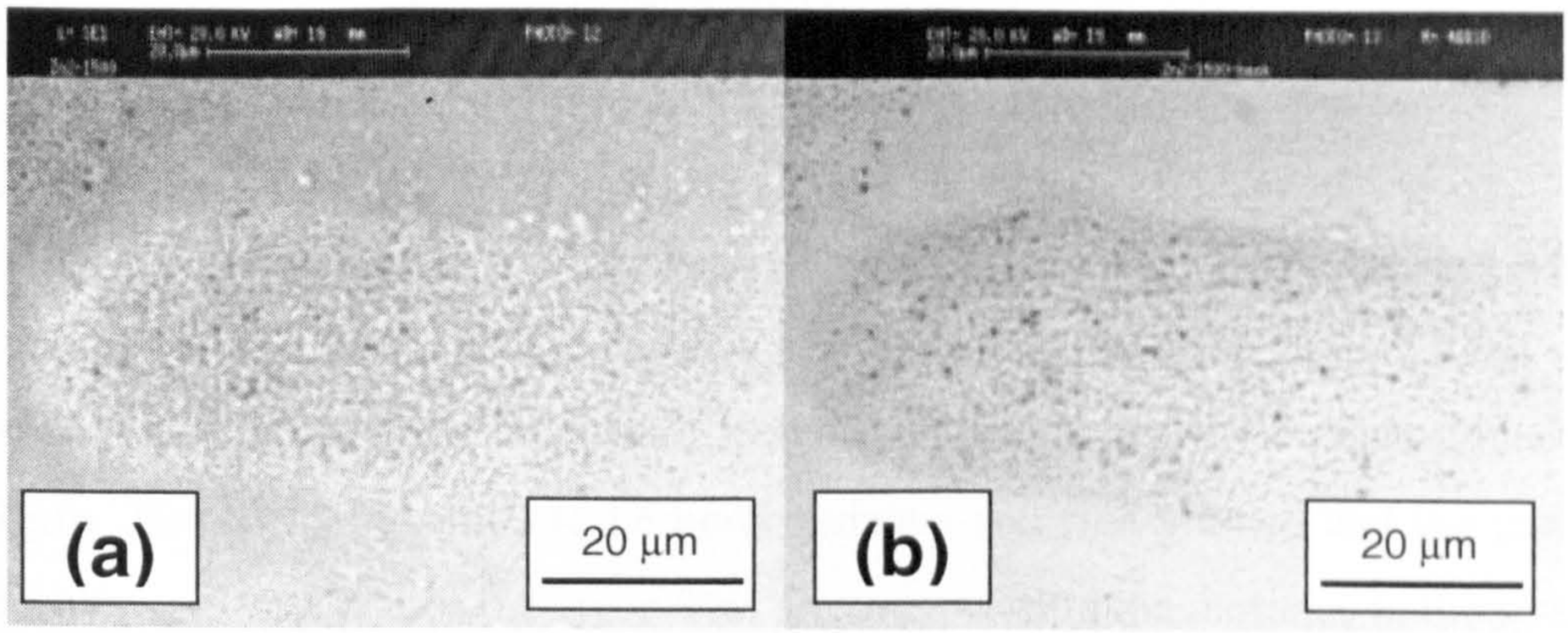

Figure 10.20 - 2 µm zinc-PS electrodeposit obtained at 620 rpm, 5 A dm^{-2} and 2 g l^{-1} PS particle loading on a 7.4 cm diameter mild steel cathode. (a) SEM image. (b) Backscattered image.

The "nodular striped" structures, observed previously, did not occur when the rotation speed was low, as shown in Fig. 10.21.

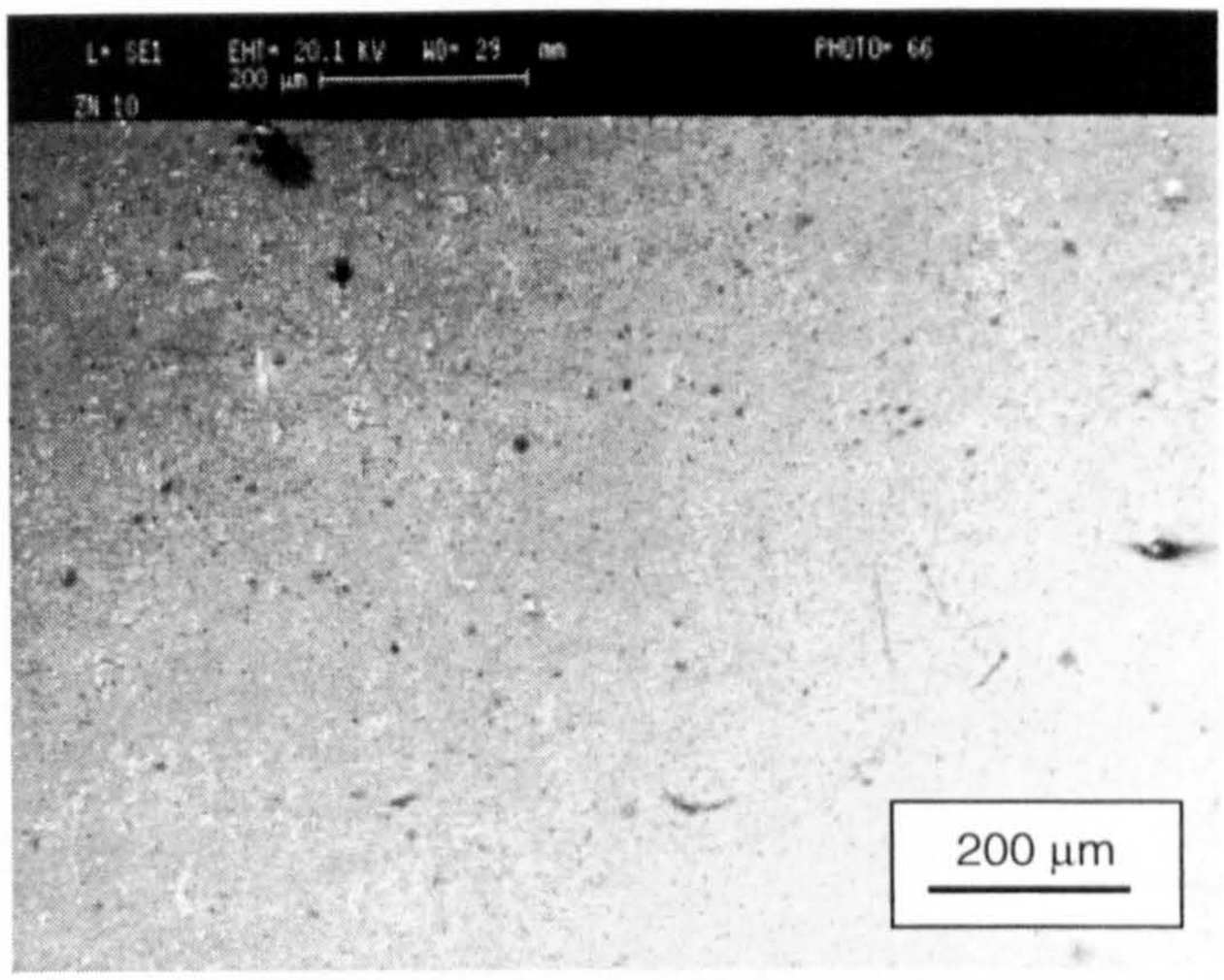

Figure 10.21 - SEM micrograph of a 2 µm zinc-PS electrodeposit obtained at 30 rpm, 5 A dm^{-2} and 2 g l^{-1} PS particle loading on a 7.4 cm diameter mild steel cathode.

Compared to copper-PS composite coatings shown previously (see Figs. 10.8 and 10.9), zinc-PS composite coatings exhibited smaller "nodular striped" structures. This confirms the hypothesis that the rougher the cathode surface the more pronounced is the phenomenon. Zinc does not form immersion coatings on mild steel, so the cathode surface is initially smoother than that for "unmodified" copper deposition (i.e. without nickel pre-plate).

10.4 Alumina composite coatings

Fig. 10.22 shows a copper-alumina composite coating obtained at 1000 rpm, 5 A/dm^2 and 39 g/l alumina particle loading on a 1.27 cm diameter AISI 316 stainless steel cathode. The alumina particles had an irregular geometry and an average dimension of 3 µm. The coating seemed to be homogeneous and fine-grained and the particle distribution uniform across the layer. The presence of alumina particles in the coating has been confirmed by EDAX analysis. Particles appeared to be fully/partially incorporated into the layer.

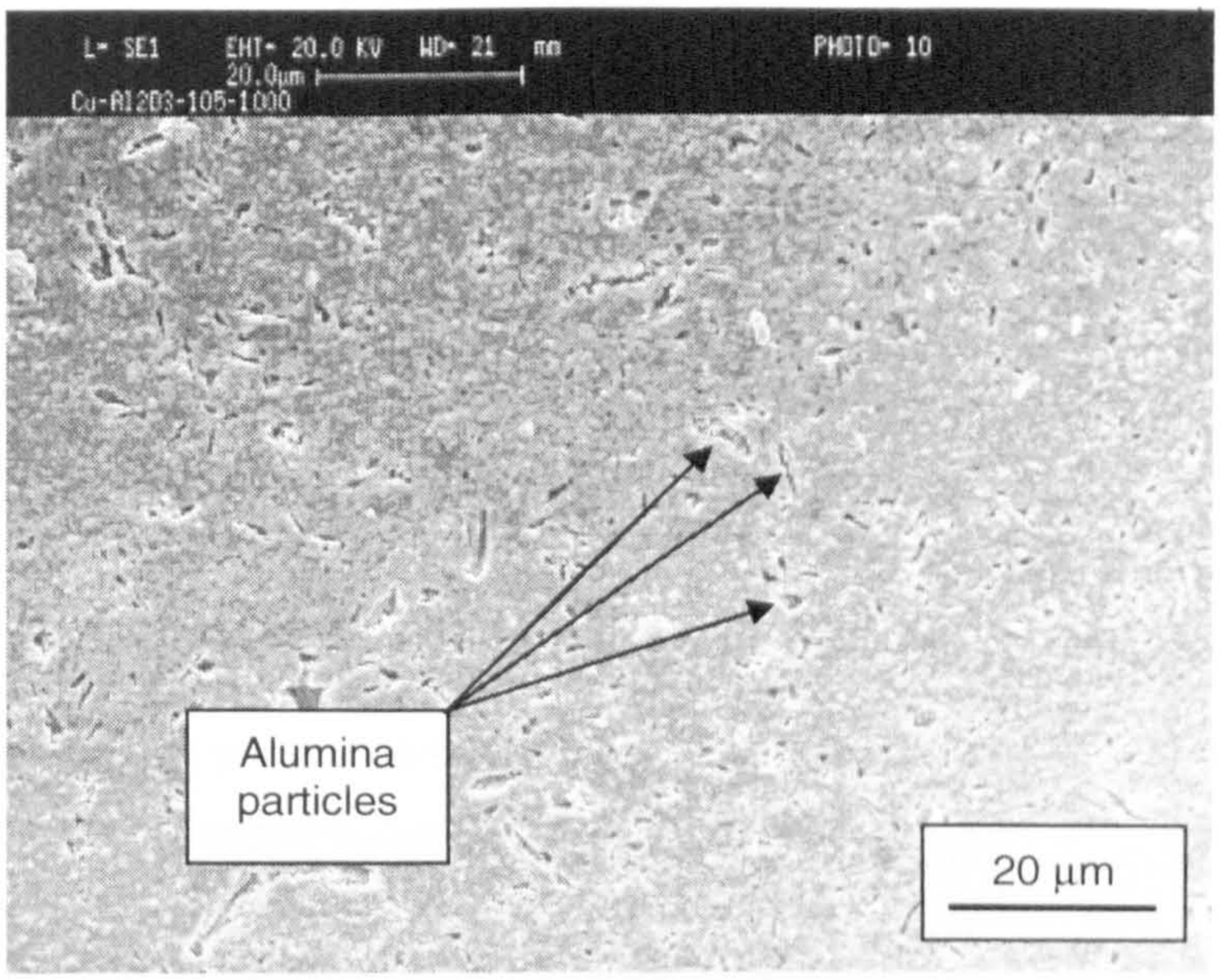

Figure 10.22 – SEM micrograph of a copper-alumina electrodeposit obtained at 1000 rpm, 5 A dm^{-2} and 39 g l^{-1} alumina particle loading on a 1.27 cm diameter AISI 316 stainless steel cathode.

Fig. 10.23 shows a sectioned copper-alumina coating, nominally 25 µm thick, produced at 220 rpm, 2 A/dm^2 and 158 g/l alumina particle loading on a 1.27 cm diameter AISI 316 stainless steel cathode. The coating seemed to be compact and the alumina distribution uniform through the layer.

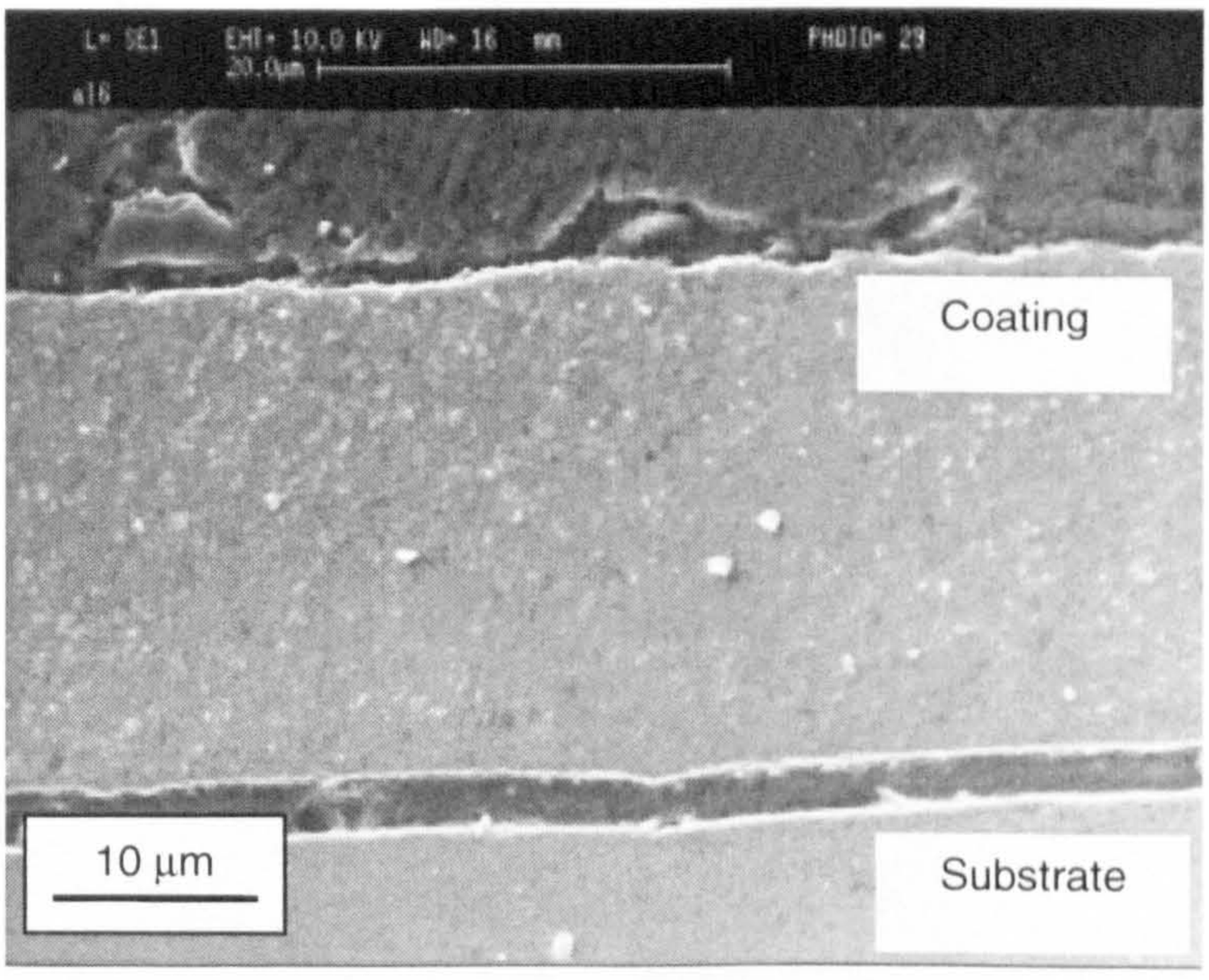

Figure 10.23 - SEM micrograph of a cross sectioned copper-alumina electrodeposit produced at 158 g l^{-1} alumina particle loading, 2 A dm^{-2} and 220 rpm on a 1.27 cm diameter AISI 316 stainless steel cathode.

Figs. 10.24 and 10.25 show the surface morphology of two zinc-alumina composite coatings produced at 5 A/dm^2 and 39 g/l alumina particle loading on 1.27 cm diameter AISI 316 stainless steel cathodes. The cathode rotation speeds were 1500 and 600 rpm respectively. The distribution of alumina particles across the layer seemed to be homogeneous. Coatings showed a typical morphology for zinc deposits from acid zinc sulphate electrolytes: stacks of hexagonal platelets orientated at random angles to the substrate [38].

Alumina particles were present in the coating (confirmed by EDAX analysis).

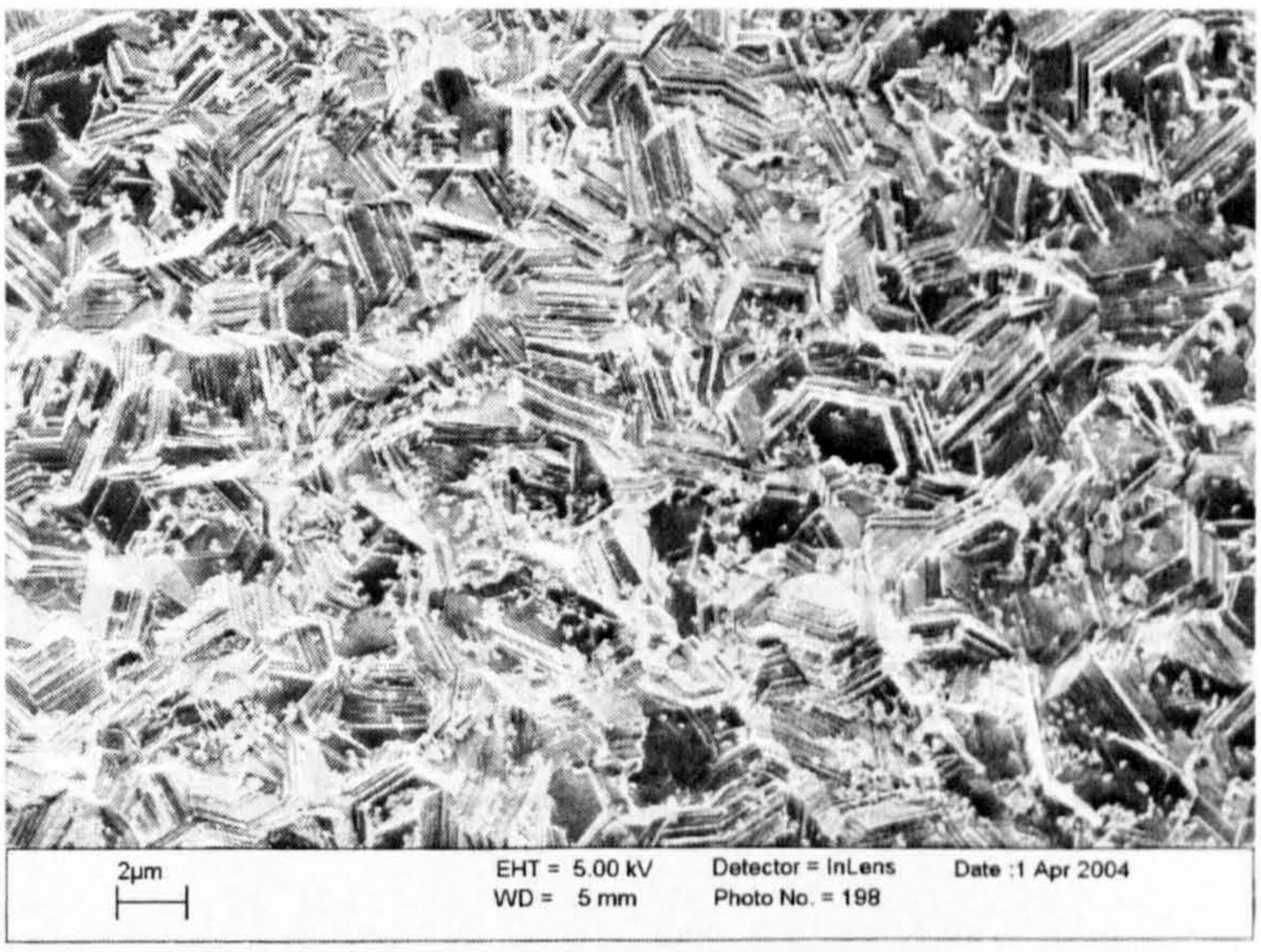

Figure 10.24 – FEGSEM micrograph of a zinc-alumina electrodeposit obtained at 5 A dm^{-2}, 39 g l^{-1} alumina particle loading and 1500 rpm on a 1.27 cm diameter AISI 316 stainless steel cathode.

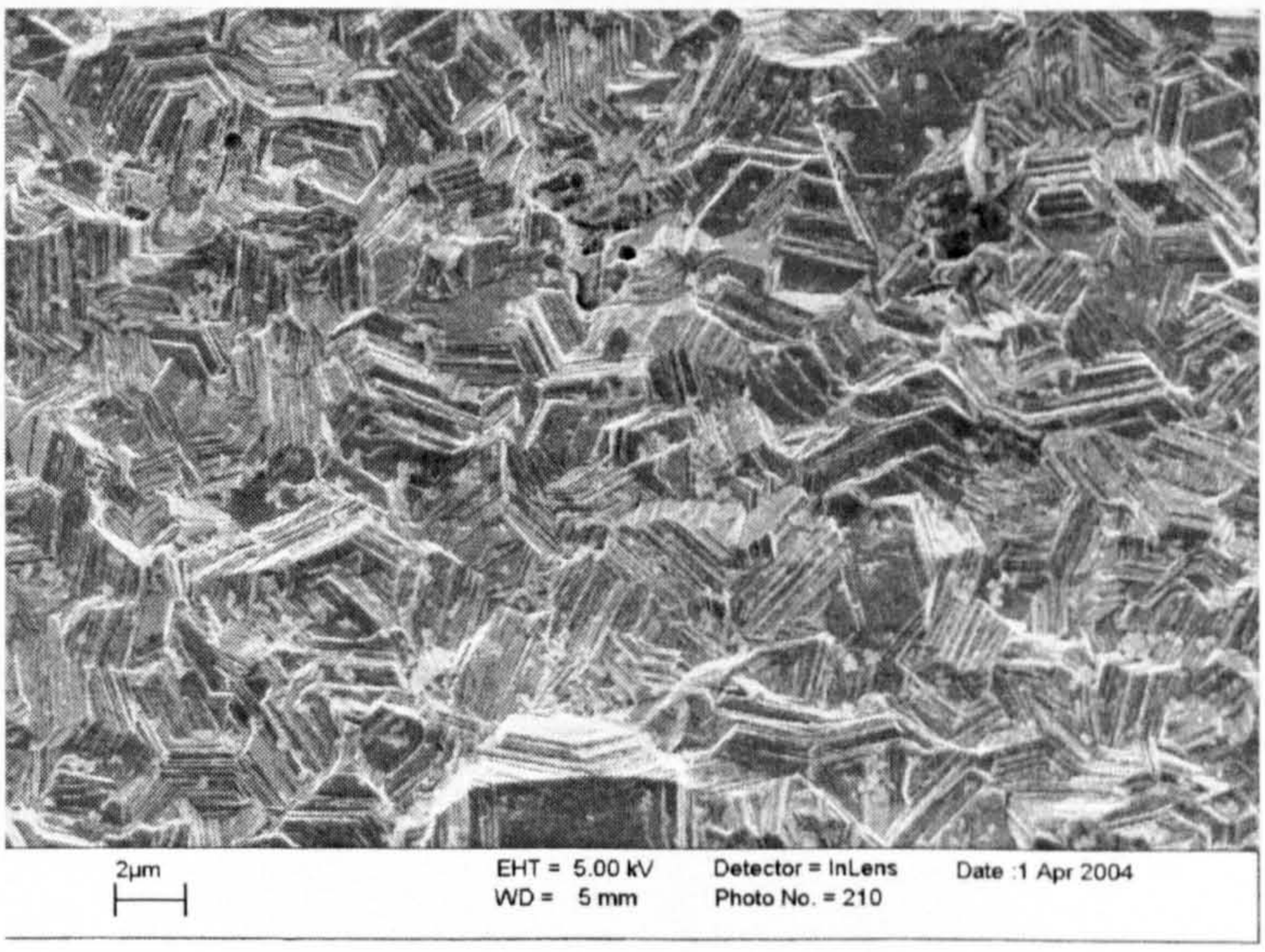

Figure 10.25 - FEGSEM micrograph of a zinc-alumina electrodeposit obtained at 5 A dm^{-2}, 39 g l^{-1} particle loading and 600 rpm on a 1.27 cm diameter AISI 316 stainless steel cathode.

It can be seen that particles seemed to lie on the surface of the electrodeposit as opposed to be partially entrapped, even if a cross section image analysis was not carried out and the assumption is limited to surface image analysis. HOVESTAD *et al.* obtained very similar morphologies [38] for the same co-deposition system, as will be discussed in Chapter 12.

Figs. 10.26 and 10.27 show the surface morphology of two nickel-alumina composite coatings produced at 5 A/dm^2 and 39 g/l alumina particle loading on 1.27 cm diameter AISI 316 stainless steel cathodes. The cathode rotation speeds were 1250 and 100 rpm respectively. The distribution of alumina particles across the layer seemed to be very homogeneous both at high and at low rotation speed values. The surface appearance seems to be similar to the ones obtained by BANOVIC *et al.* [148] for the same co-deposition system.

Alumina particles were present in the coating (confirmed by EDAX analysis) and they appeared to be fully/partially incorporated into the layer. Particle concentrations seemed higher at 1250 rpm rather than 100 rpm.

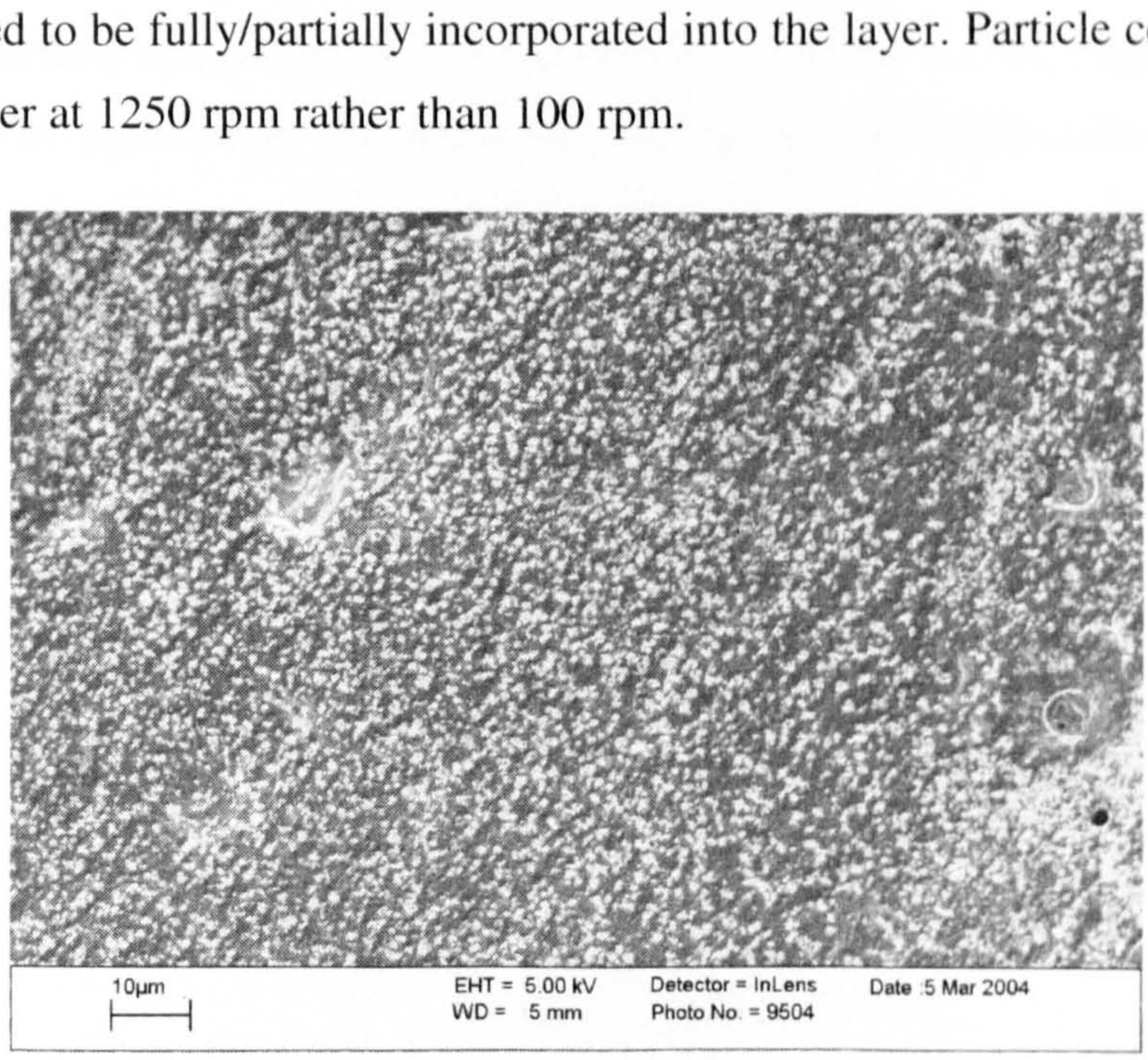

Figure 10.26 - FEGSEM micrograph of a nickel-alumina electrodeposit obtained at 5 A dm^{-2}, 39 g l^{-1} particle loading and 1250 rpm on a 1.27 cm diameter AISI 316 stainless steel cathode.

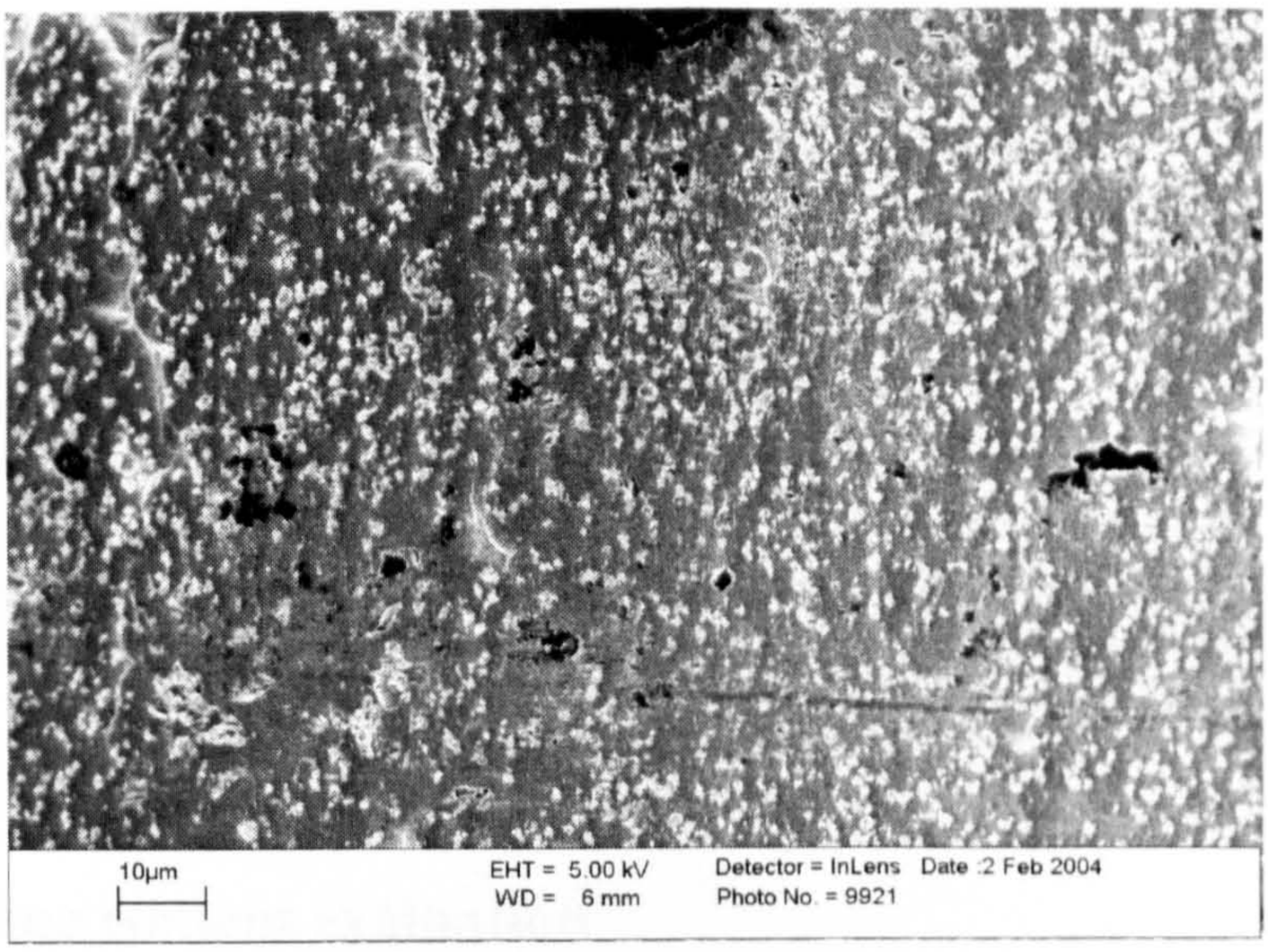

Figure 10.27 - FEGSEM micrograph of a nickel-alumina electrodeposit obtained at 5 A dm^{-2}, 39 g l^{-1} particle loading and 100 rpm on a 1.27 cm diameter AISI 316 stainless steel cathode.

In all the cases, the alumina coatings produced seemed to be relatively homogeneous in terms of particle distribution across the surface. Contrary to PS composite coatings the presence of particles in the electrolyte during the electrodeposition process did not significantly influence the coating morphology. The deposits with and without particles were very similar. No formation of striped structures was found.

11. Quantitative analysis of composite coatings produced

As shown in Chapter 7 an important matter in studying composite coatings is to produce a reliable method of qualitative and quantitative detection of second phase particles in the coating.

Different methods were excluded to perform this task as discussed in the following sections.

11.1 Alumina content evaluation

At first, the alumina content in the copper coatings was calculated by the weight gain of the samples, assuming 100% efficiency for the copper electrodeposition. This method represented the simplest way to calculate the particle concentration in the coatings produced, as a literature review suggests (see Chapter 7).

In order to give consistency to this technique, a study of cathode current efficiency was carried out. The assumption of 100% efficiency for the copper deposition is the main limitation of this method of analysis.

11.1.1 Cathode current efficiency studies

Electrodeposition of copper on stainless steel was carried out to evaluate the cathode current efficiency of this process.

Faraday's law (as described in Section 2.4) can predict, by measuring the quantity of electricity flowing in the cell, the amount of metal that will be deposited during the electrodeposition, assuming that copper deposition is the only reaction occurring at the cathode (which means having a 100% cathode current efficiency).

Faraday's law can be expressed by the formula (see Section 2.3):

$$\frac{W}{E} = \frac{Q}{F} \qquad \textbf{Eq. 2.9}$$

In Fig. 11.1 the mass of copper deposited is plotted against the current density (green curve), whilst the red curve represents the copper deposited calculated by Faraday's law (100% cathode current efficiency). At 1 A/dm^2 and 220 rpm the real efficiency is very low (67%), while for all the other current densities it ranges between 90% and 98% (blue curve). This suggests that another reaction is occurring at the same time as copper deposition, for example hydrogen evolution or oxygen reduction.

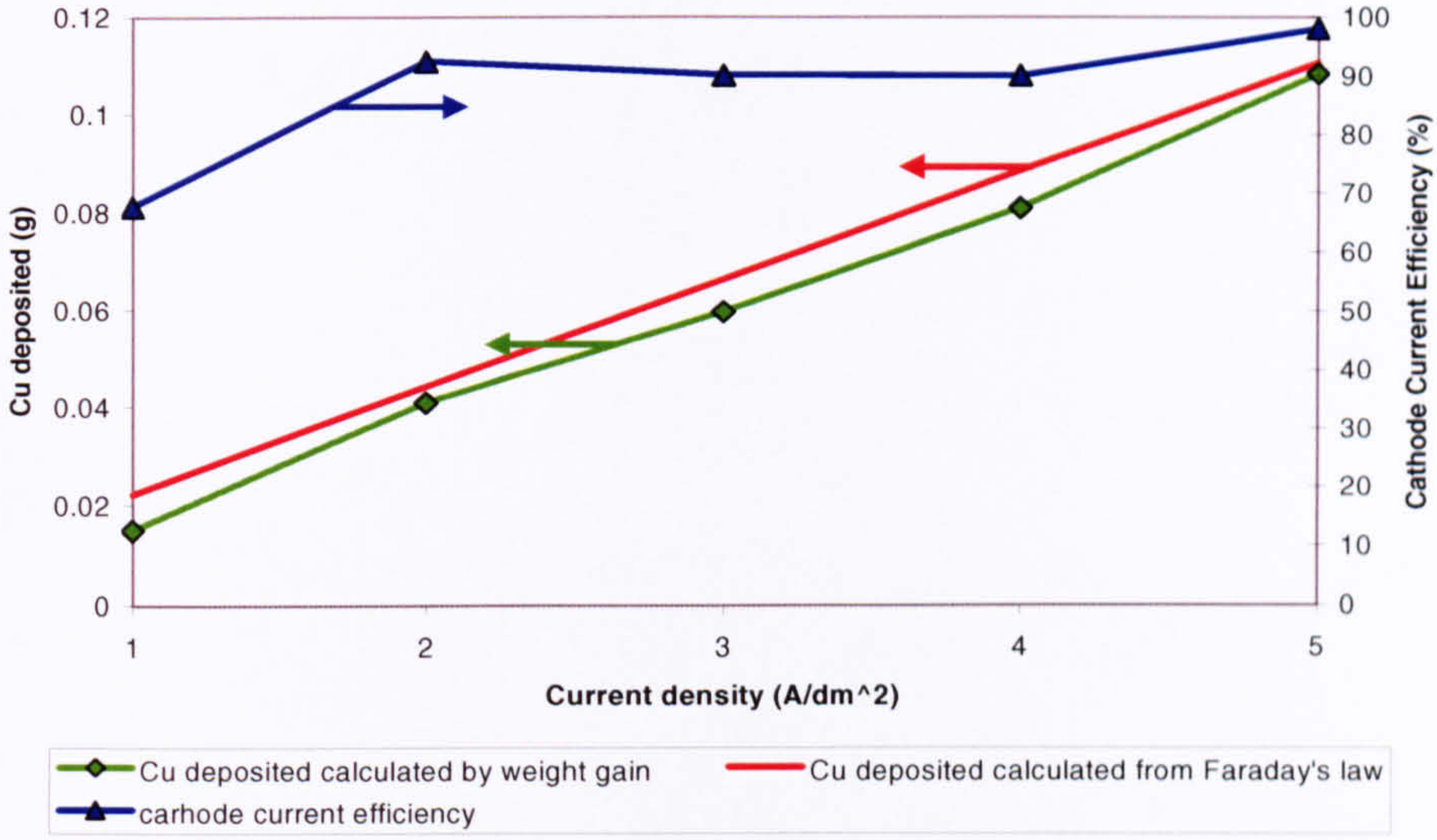

Figure 11.1 - Electrodeposition of copper on AISI 316 stainless steel. On the left hand side copper deposited *vs.* current density at 220 rpm compared with copper deposited calculated by Faraday's law (100% cathode current efficiency). On the right hand side cathode current efficiency *vs.* current density.

Fig. 11.2 shows the typical morphology of these coatings. Some surface "scars" (highlighted by arrows) can be seen and this might have been thought to be due to hydrogen evolution (hydrogen bubbles "masking" the surface). In order to establish what the concurrent reaction was, another trial was carried out. In this case, before copper deposition, nitrogen was used to purge the electrolyte for 1 hour, in order to remove all the oxygen present in the solution. Fig. 11.3 shows a coating obtained at 1 A/dm^2 using the second procedure; in this case the cathode current efficiency was 100% and there were no "scars" on the surface. The concurrent reaction with copper deposition was, therefore, most probably oxygen reduction.

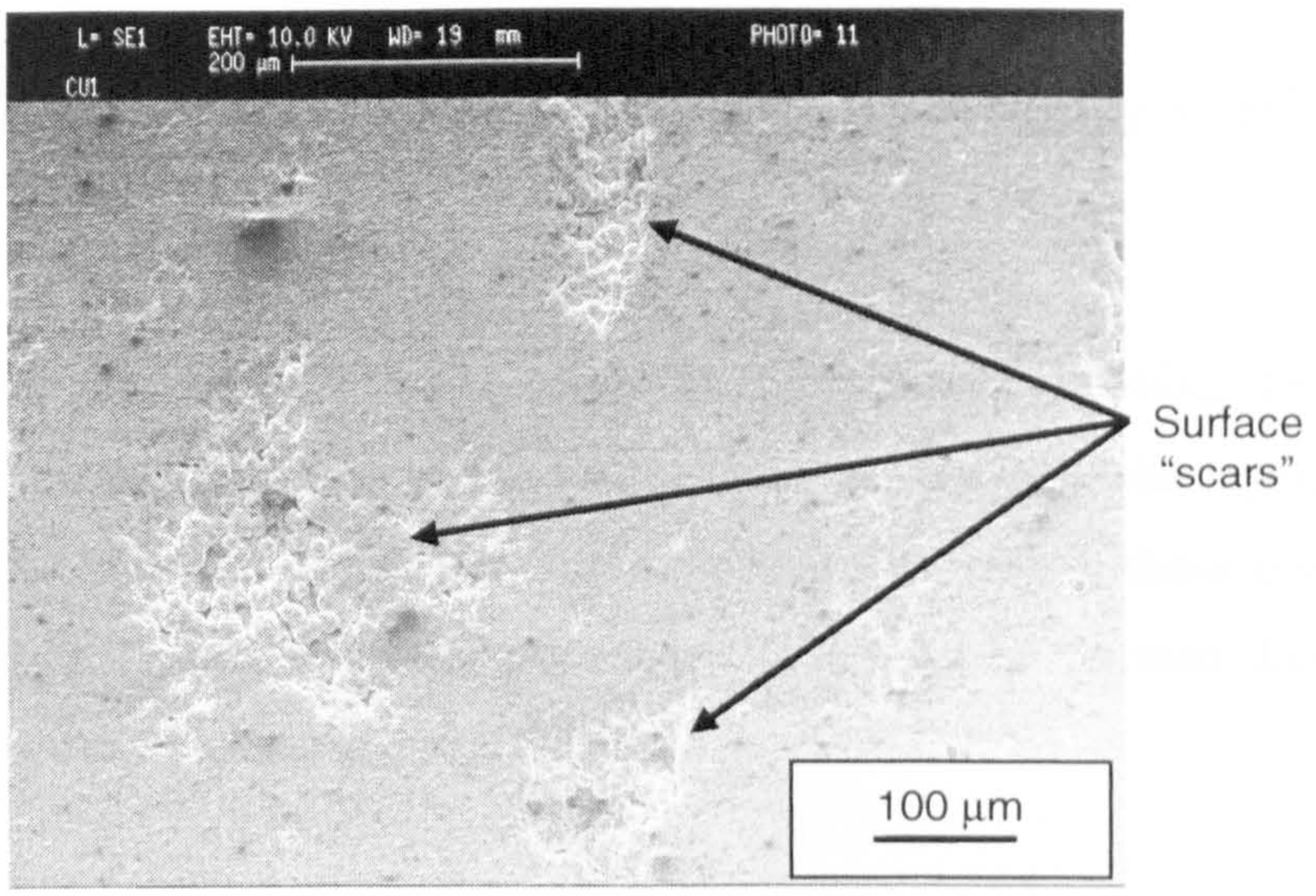

Figure 11.2 – SEM micrograph of a copper electrodeposit produced at 1 A dm^{-2} and 220 rpm on AISI 316 stainless steel. Arrows highlight surface "scars", present on the coating. These could be due to the presence of another reaction occurring at the same time copper deposition.

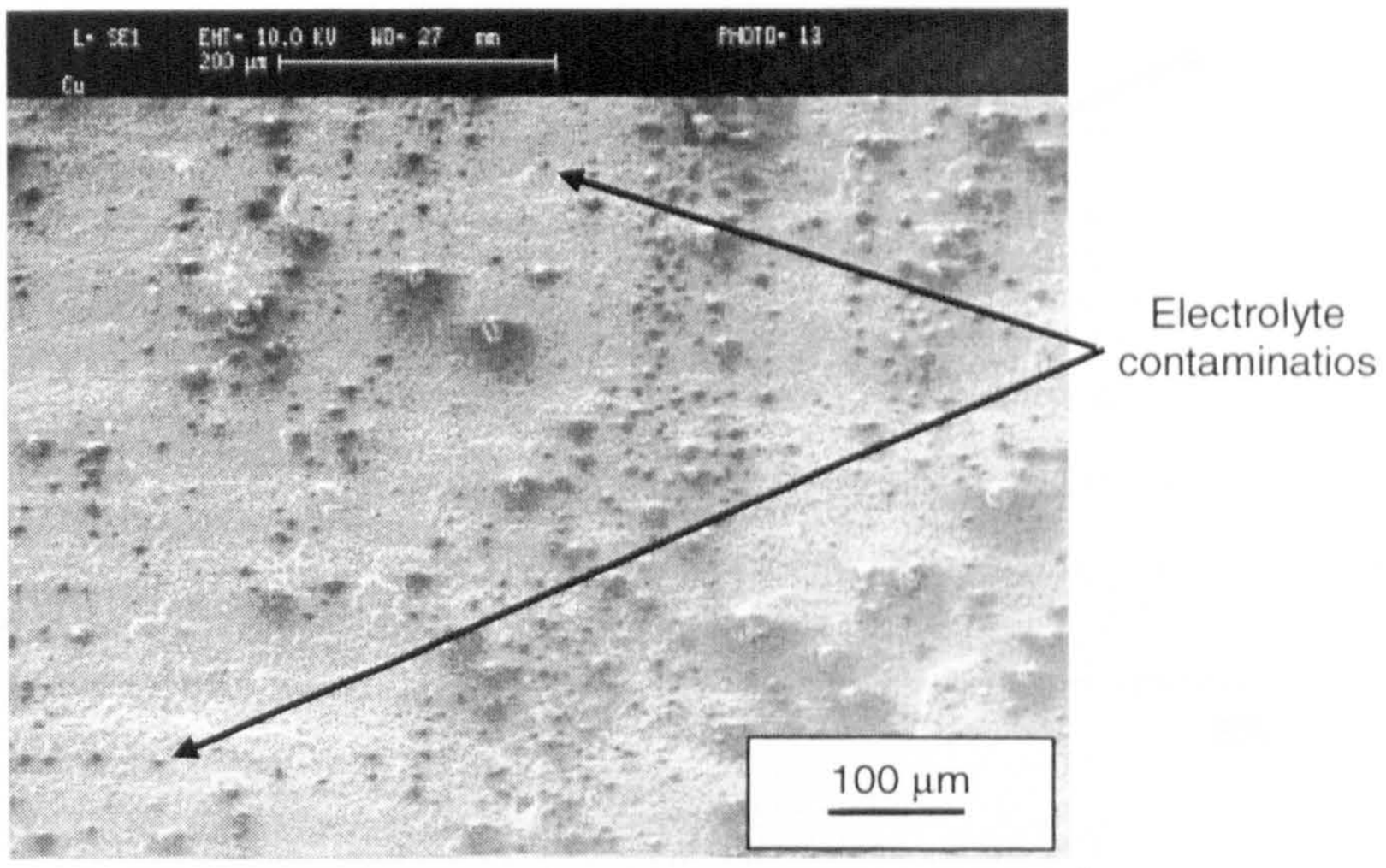

Figure 11.3 - SEM micrograph of a copper electrodeposit produced at 1 A dm^{-2} and 220 rpm on AISI 316 stainless steel (solution pre-treatment with nitrogen for 1 hour, prior to electrodeposition). No "scars" are present on the coating surface.

11.1.2 Alternative evaluation of the alumina content

A literature review suggests two alternative methods to estimate the alumina content in the coating:

- dissolution of the deposits in nitric acid, filtration of the slurry and weighing of the residue [57];
- dissolution of the deposits in nitric acid, fusing of the alumina with sodium carbonate, determination of the aluminium content by atomic absorption spectrophotometry [57]].

The first method has the disadvantage that the alumina is slightly soluble in the solutions used.

Alumina filters with holes of 0.02 μm (used to filter the slurry containing the deposit dissolved) were left in the solutions, used to produce and dissolve the layer, over a period of time in order to evaluate the alumina dissolution rate in these chemicals. Filters were weighed before and after immersion. The level of alumina dissolution was calculated by the weight loss of the filters.

Figs. 11.4 and 11.5 show the alumina filters' dissolution rate in the electrolyte (0.5 M $CuSO_4$ + 1.2 M H_2SO_4) and nitric acid (20% by weight).

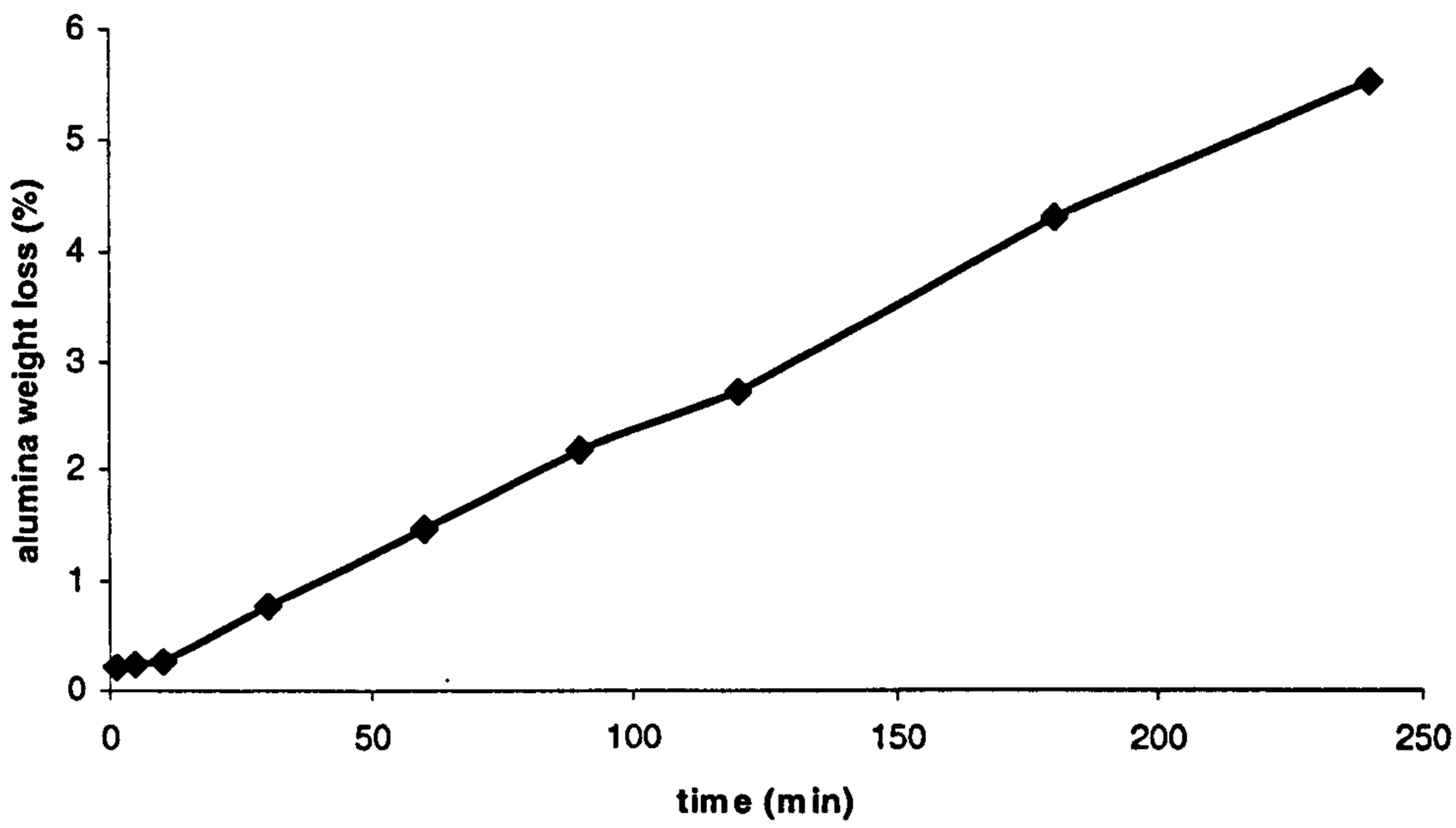

Figure 11.4 - Alumina filters dissolution rate in 0.5 M $CuSO_4$ + 1.2 M H_2SO_4.

The data indicated that the alumina has a significant solubility in the electrolyte. Filters lost up to 3% of their weight in the first hour in 20% w. nitric acid. As a consequence the holes of the filters could become bigger than 0.02 μm and could not be able to capture the alumina particles during the filtration process, especially the smaller ones (0.02 and 0.3 μm).

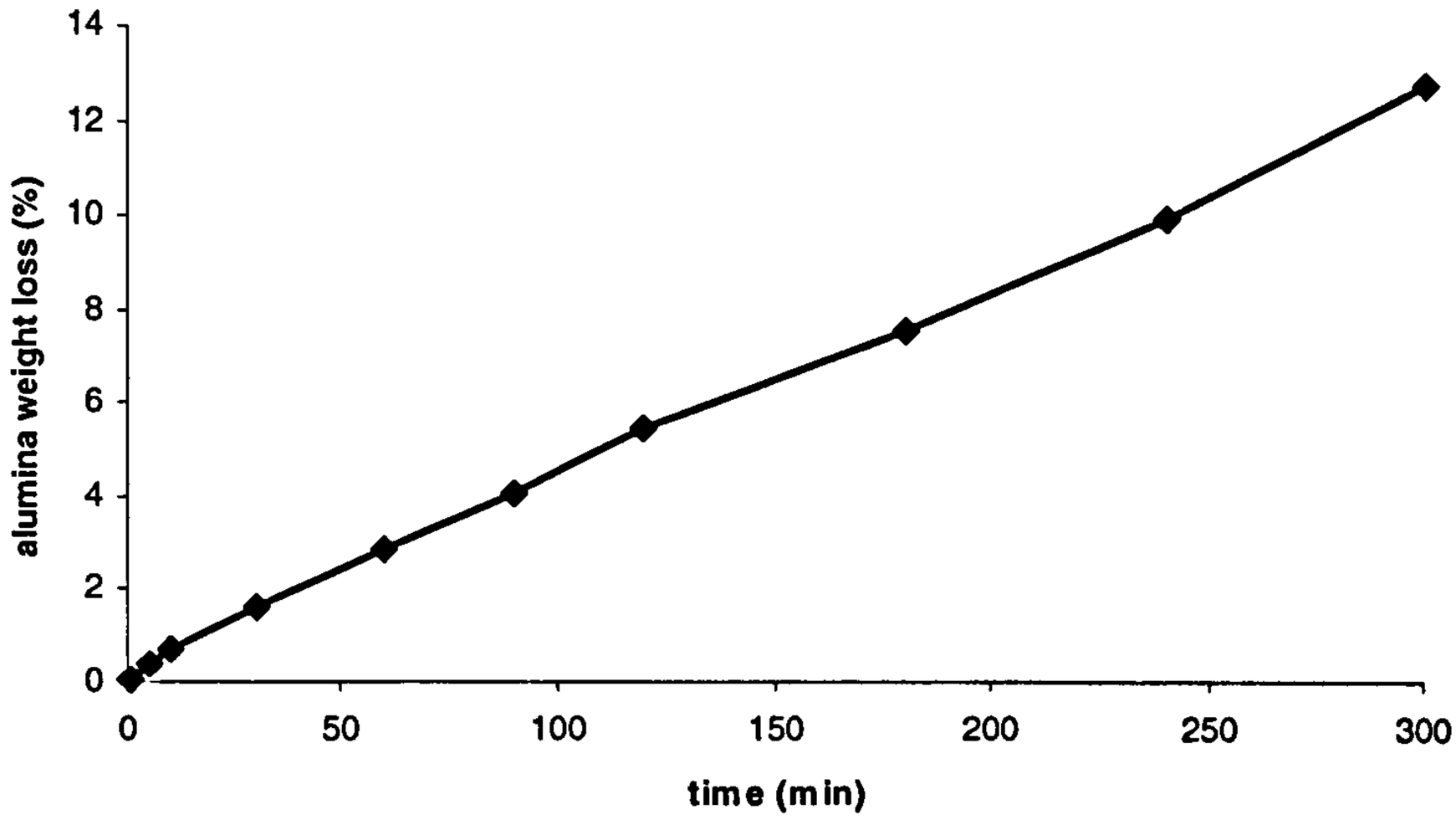

Figure 11.5 - Alumina filters dissolution rate in 20% w. nitric acid.

Figs. 11.6-11.7 show indeed the progressive dissolution of the alumina filters. It can be seen that the holes become larger because of the alumina dissolution. After 5 hours in nitric acid some holes have a diameter of more than 0.1 μm, compared to the initial diameter of 0.02 μm. In this situation the probability of loosing alumina particles during the filtration process is high, also due to the alumina dissolution in the reagents used that cause particles to become smaller. This suggests calculation of coating composition would not be accurate. This method could perhaps be used with other more inert particles (i.e. polystyrene).

The second method of calculating alumina content – atomic absorption spectrophotometry (AAS) - was independent of the particle size of the alumina, of its solubility in the reagents used and of the cathode efficiency for the copper deposition.

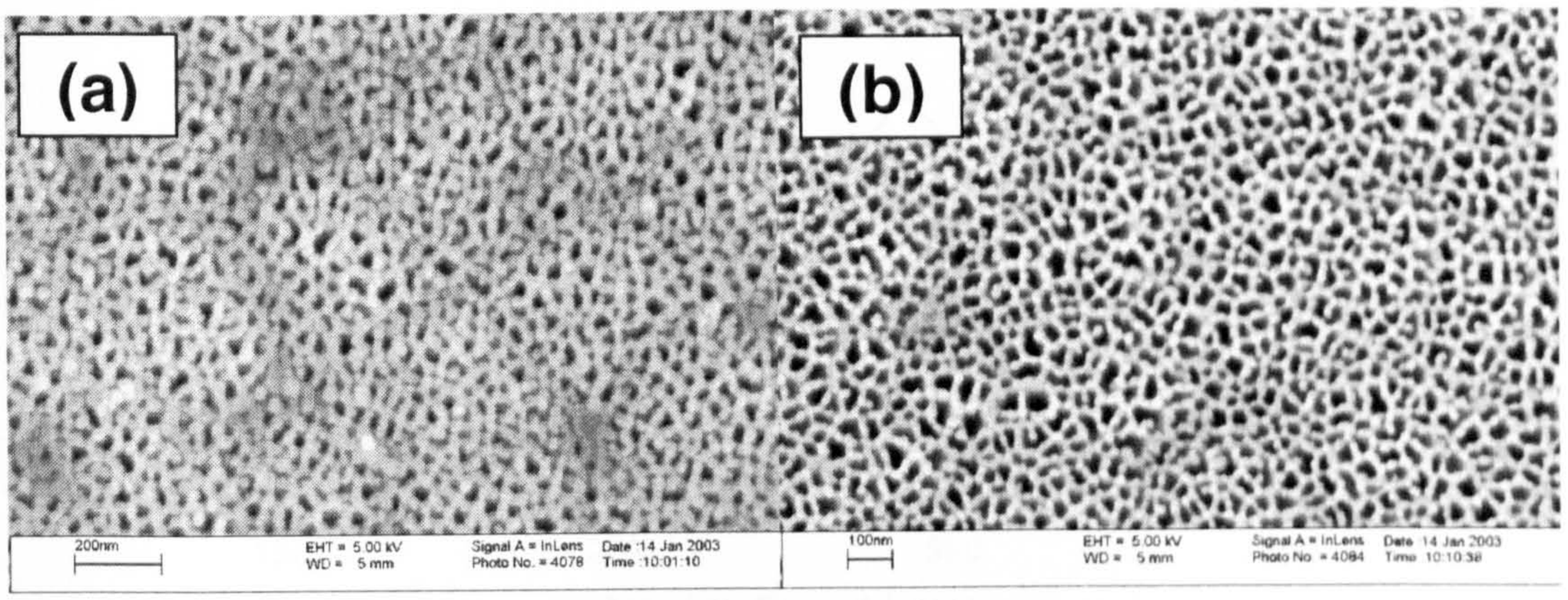

Figure 11.6 - Alumina filters after immersion in 0.5 M $CuSO_4$ + 1.2 M H_2SO_4 for: (a) 1 min. (b) 1 hour.

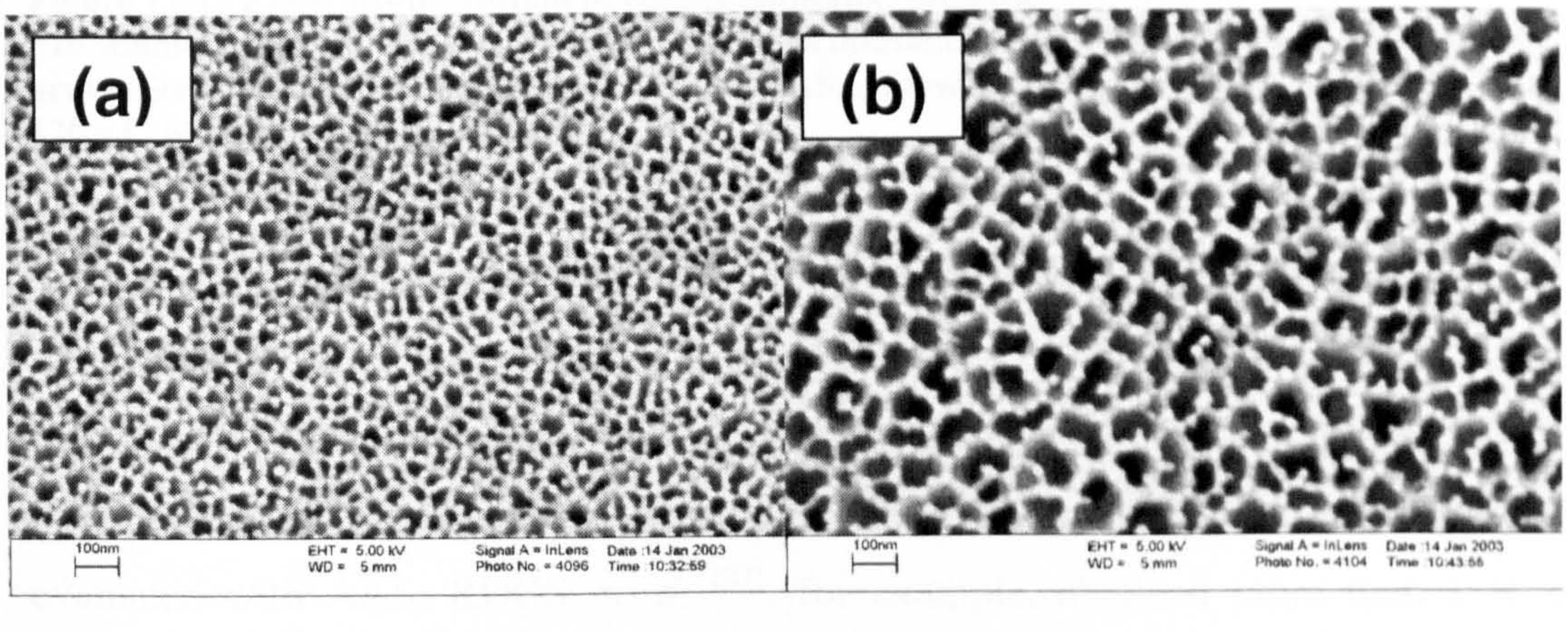

Figure 11.7 - Alumina filters after immersion in SG nitric acid 20% by weight for: (a) 30 min. (b) 5 hours.

Fig. 11.8 shows a comparison between the data obtained from this method and the initial gravimetric method. It can be seen that the alumina content in the coatings varied depending on the method of analysis employed. The gravimetric method gives higher alumina content values than AAS.

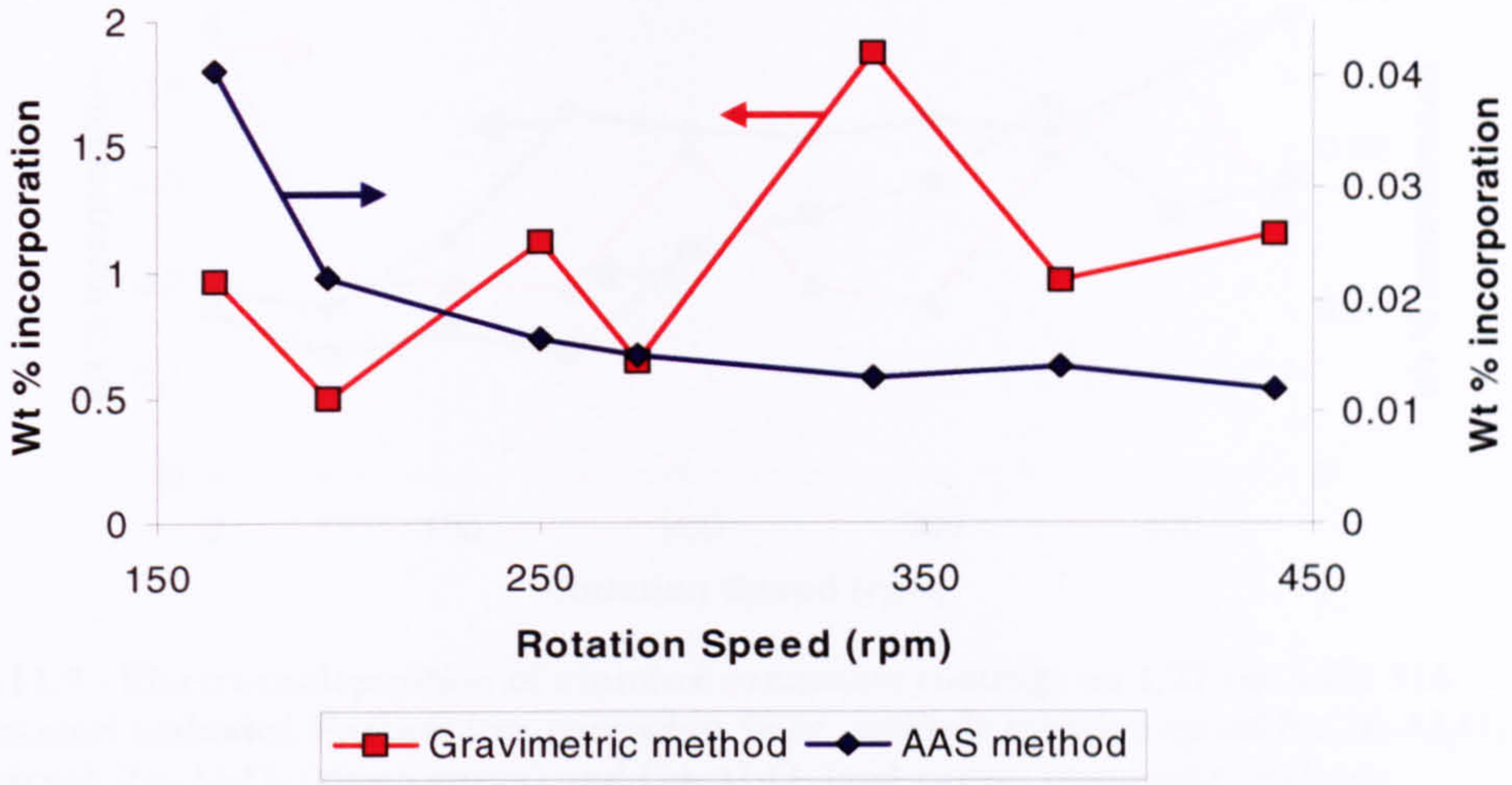

Figure 11.8 - Electroco-deposition of copper-alumina composite coatings on 1.27 cm AISI 316 stainless steel cathodes. Comparison between alumina content values obtained with the gravimetric method (red curve) and with the AAS analysis (blue curve) at 3 A dm^{-2} and 120 g l^{-1} alumina particle loading.

AAS was therefore employed to evaluate the alumina content in composite coatings with nickel, zinc and copper. Figs. 11.9-11.11 show the results. Alumina incorporation levels obtained with this method appear to be very small. Several investigators have produced coatings much richer in alumina content than those here evaluated with AAS. ROOS *et al.* [57], for example, obtained more than 1 % of alumina embedded in copper matrix with an alumina particle loading of 35 g/l; CELIS *et al.* [150] proved the validity of this method of analysis and obtained, even if they found a small systematic error when very small quantities of alumina were processed, alumina concentrations up to 1.1 wt.% for α-alumina co-deposition and up to 0.2 wt.% for γ-alumina. In all the cases data obtained in this work using AAS analysis were orders of magnitude lower then those by literature.

Due to this very low alumina levels obtained, this method of analysis was not continued, an image analysis of the coatings was preferred to obtain information on the coating surface compositions and was an analysis that could be made on both the alumina and the PS composite coatings.

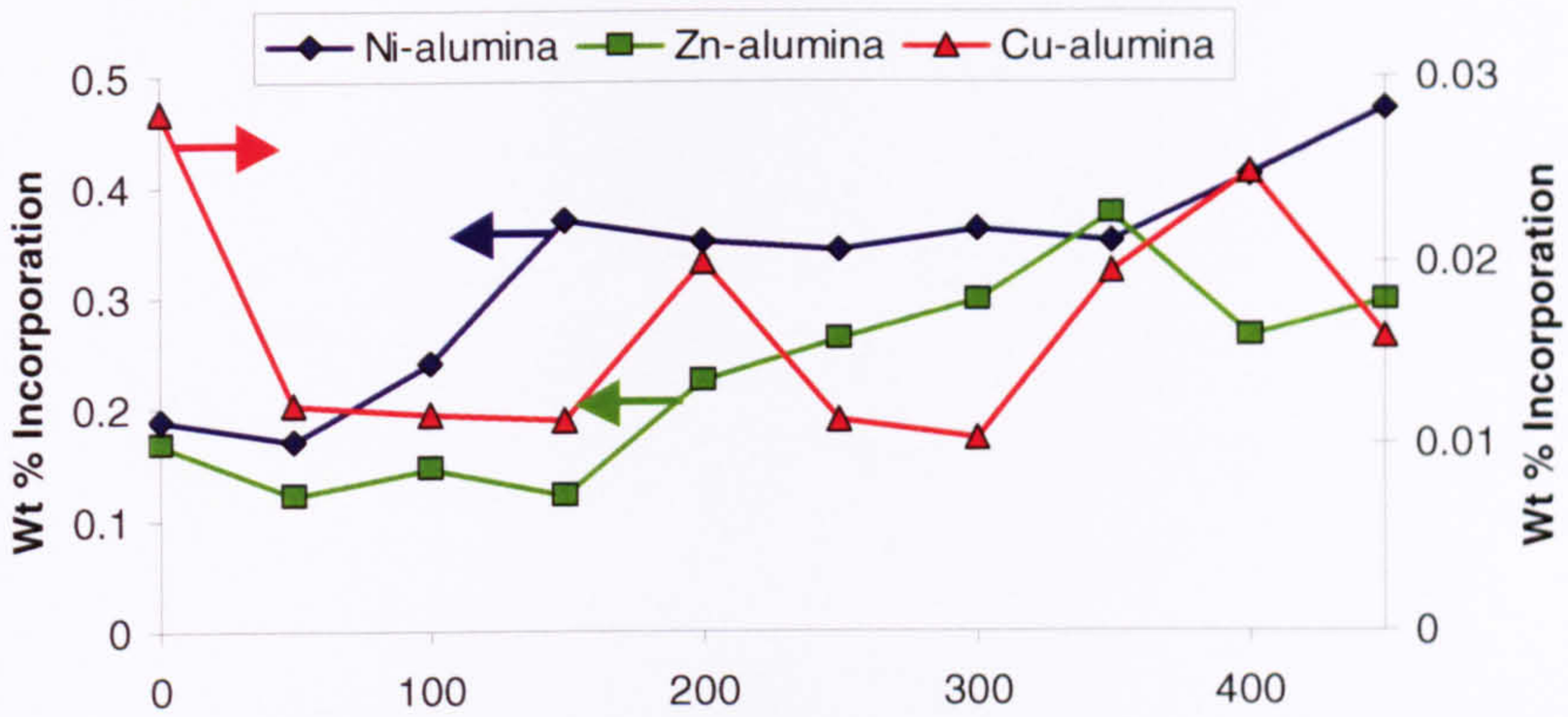

Figure 11.9 - Electroco-deposition of alumina composite coatings on 1.27 cm AISI 316 stainless steel cathodes. Particle incorporation % *vs.* cathode rotation speed for Ni-Al_2O_3 (blue curve), Zn-Al_2O_3 (green curve) and Cu-Al_2O_3 (red curve) composite coatings obtained at 3 A dm^{-2} and 39 g l^{-1} alumina particle loading. Alumina particle size 0.3 μm.

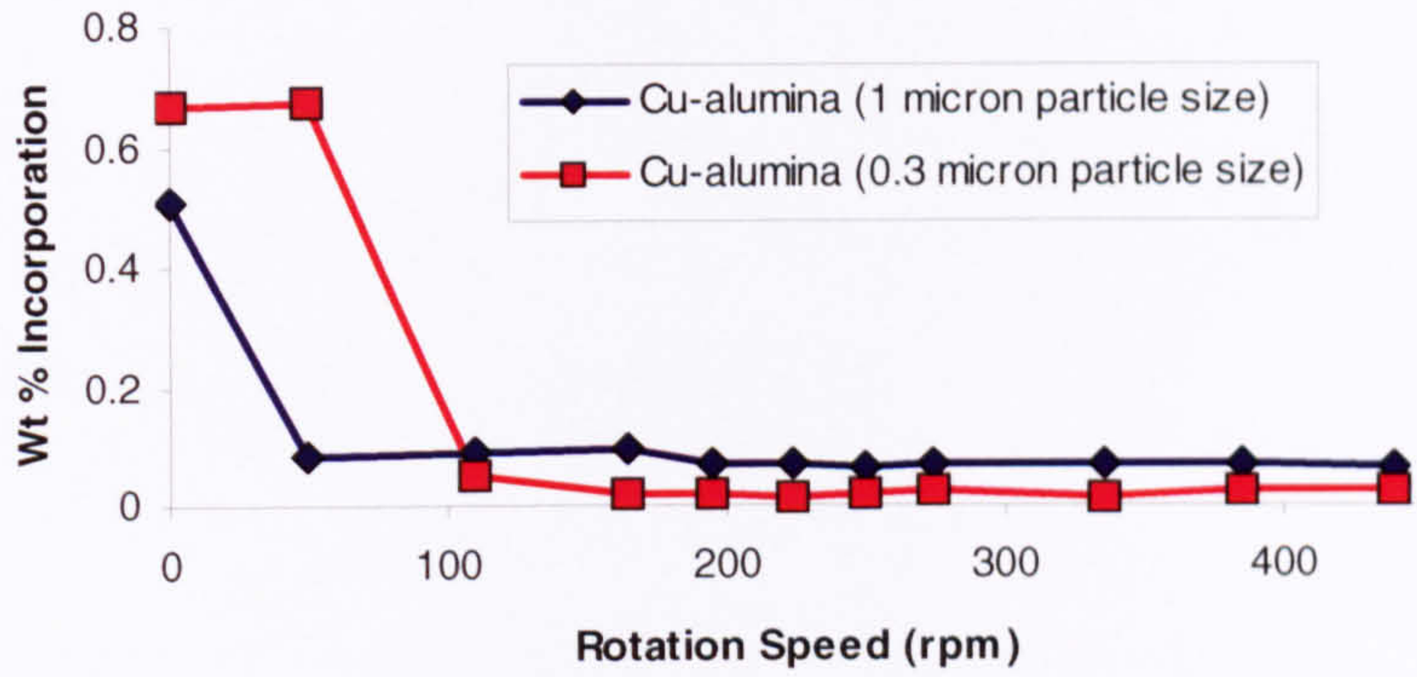

Figure 11.10 - Electroco-deposition of copper-alumina composite coatings on 1.27 cm AISI 316 stainless steel cathodes. Particle incorporation % *vs.* cathode rotation speed for Cu-Al_2O_3 composite coatings obtained at 3 A dm^{-2} and 39 g l^{-1} alumina particle loading. Blue curve: alumina particle size 0.3 μm; red curve: alumina particle size 1 μm.

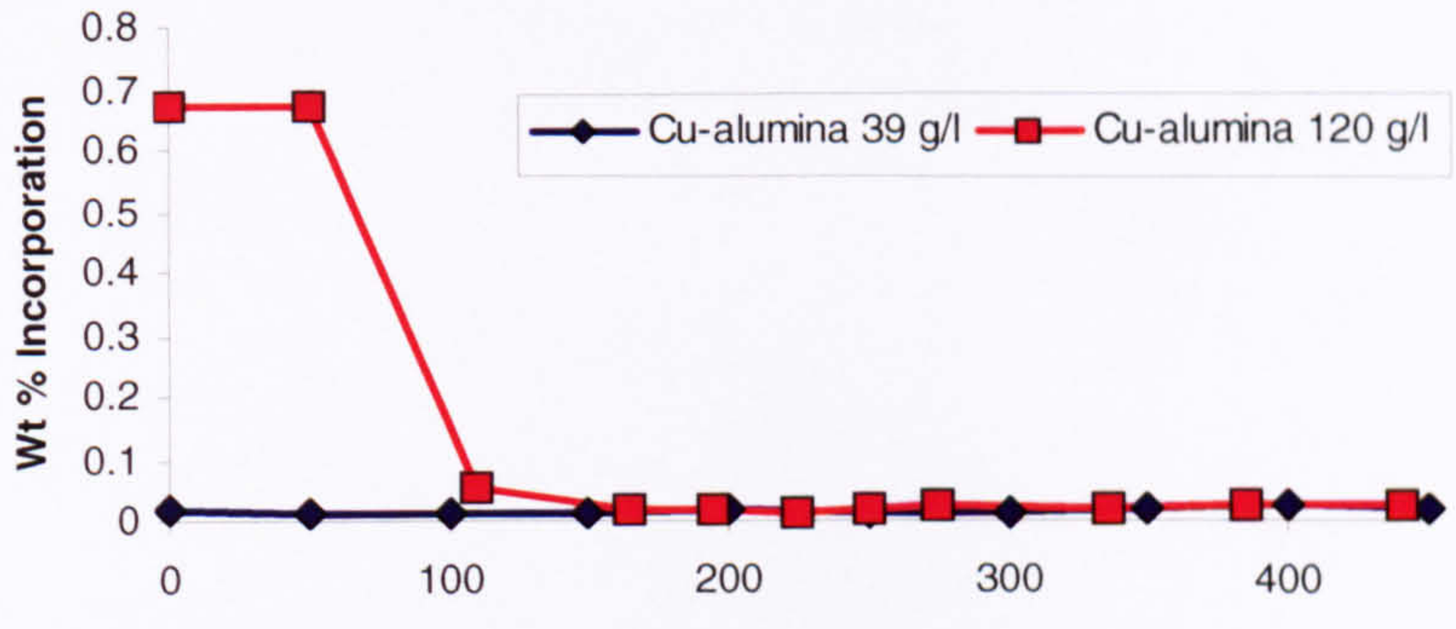

Figure 11.11 - Electroco-deposition of copper-alumina composite coatings on 1.27 cm AISI 316 stainless steel cathodes. Particle incorporation % *vs.* cathode rotation speed for Cu-Al_2O_3 composite coatings obtained at 3 A dm^{-2}. Alumina particle size 0.3 μm. Blue curve: alumina particle loading 39 g l^{-1}; red curve: alumina particle loading 120 g l^{-1}.

11.2 Scanning Electron Microscopy and image analysis

In order to evaluate the particle content in the coatings produced, Scanning Electron Microscopy in combination with image analysis was carried out. Backscattered electron images were taken for each sample (magnification 2500X). On these micrographs an image analysis was carried out, evaluating the particle percentage surface coverage.

Initially this was carried out manually. A grid was placed on every micrograph and the particles' surface coverage was calculated. Fig. 11.12 shows the amount of PS particle incorporation as a function of the cathode rotation speed for nickel-PS composite coatings obtained on 7.4 cm mild steel cathodes, evaluated with image analysis.

The alumina incorporation levels obtained with this method are higher than those obtained with the AAS analysis and a trend can be discerned. The only problem was that this procedure needed a large amount of time. For this reason the possibility of employing computer software was investigated.

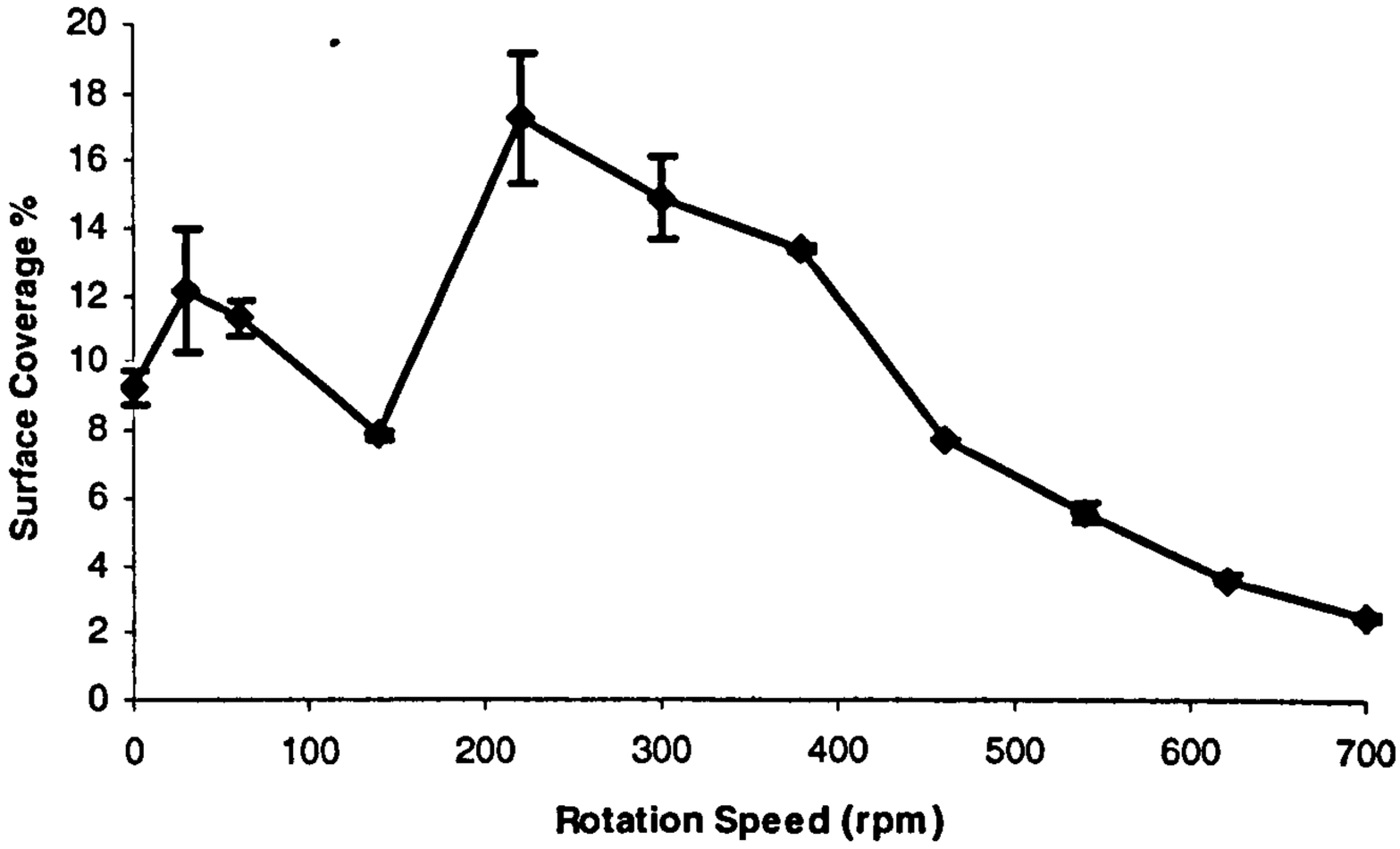

Figure 11.12 - Surface coverage *%* *vs.* cathode rotation speed for Ni-PS composite coatings produced at 5 A dm^{-2} and 2 g l^{-1} PS particle loading on 7.4 cm mild steel cathodes. Data obtained using "manual" image analysis technique.

11.2.1 Image analysis using Adobe Photoshop 7.0.1

Adobe Photoshop 7.0.1 has a subroutine that can calculate the number of white pixels present in a micrograph. Every micrograph was first divided in two different areas, the first containing the areas with particles and the second the metal background. On the first layer the number of pixels of the area containing particles was counted and their ratio in comparison with the rest of the micrograph calculated. Fig. 11.13 shows a comparison between this method and the manual method used earlier in the project for zinc-PS composite coatings obtained on 7.4 cm mild steel cathodes. It can be seen that the use of Adobe Photoshop 7.0.1 gives results closely comparable with the manual method.

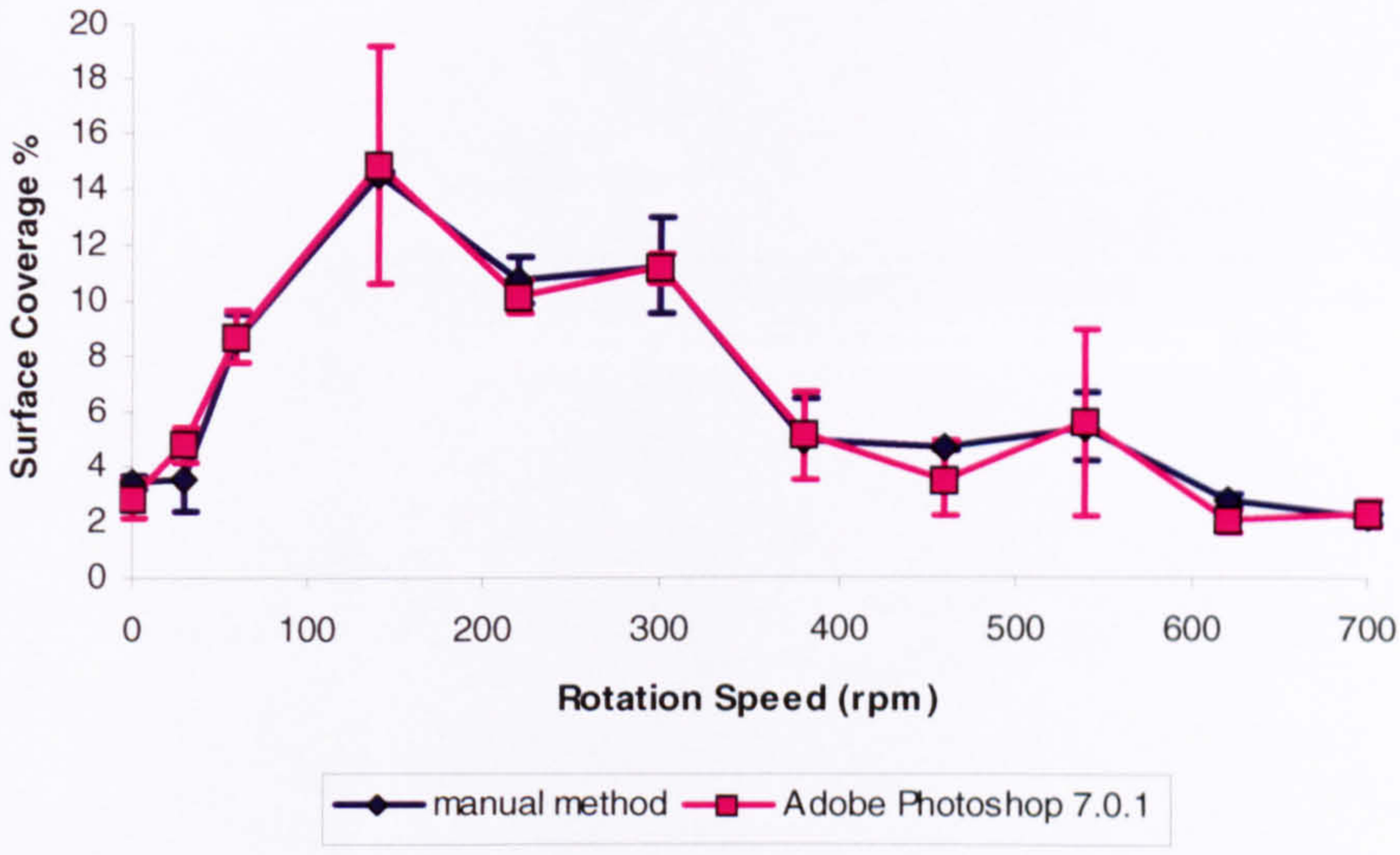

Figure 11.13 - Electroco-deposition of zinc-PS composite coatings on 7.4 cm mild steel cathodes. Comparison between particles content values obtained with the "manual" image analysis technique and with using the software Adobe Photoshop 7.0.1. Coatings produced at 5 A dm^{-2} and 2 g l^{-1} PS.

This method was used to analyse several composite coating systems. It was really useful to see how the surface coverage varied with the cathode rotation speed.

After a comparison with literature [25, 57-58], the method was found to suggest higher incorporation levels. This was probably because the software analysis was not really accurate: it took into account even the holes left by particles lost after coating post-treatments (ultrasonification) and not only the particles that were incorporated.

At this point another software called "white detector" able to analyse micrographs pixel per pixel in terms of grey scale was formulated.

11.2.2 Image analysis using the "white detector" software

This type of image analysis was based on software able to display and analyse the image in terms of grey scale, from total white (1) to total black (255). Once a range in the grey scale is stated to represent the inert particles on the coating surface, the software is able to count all of them, giving the surface coverage percentage of the inert particles as results. Fig. 11.14 shows the software interface.

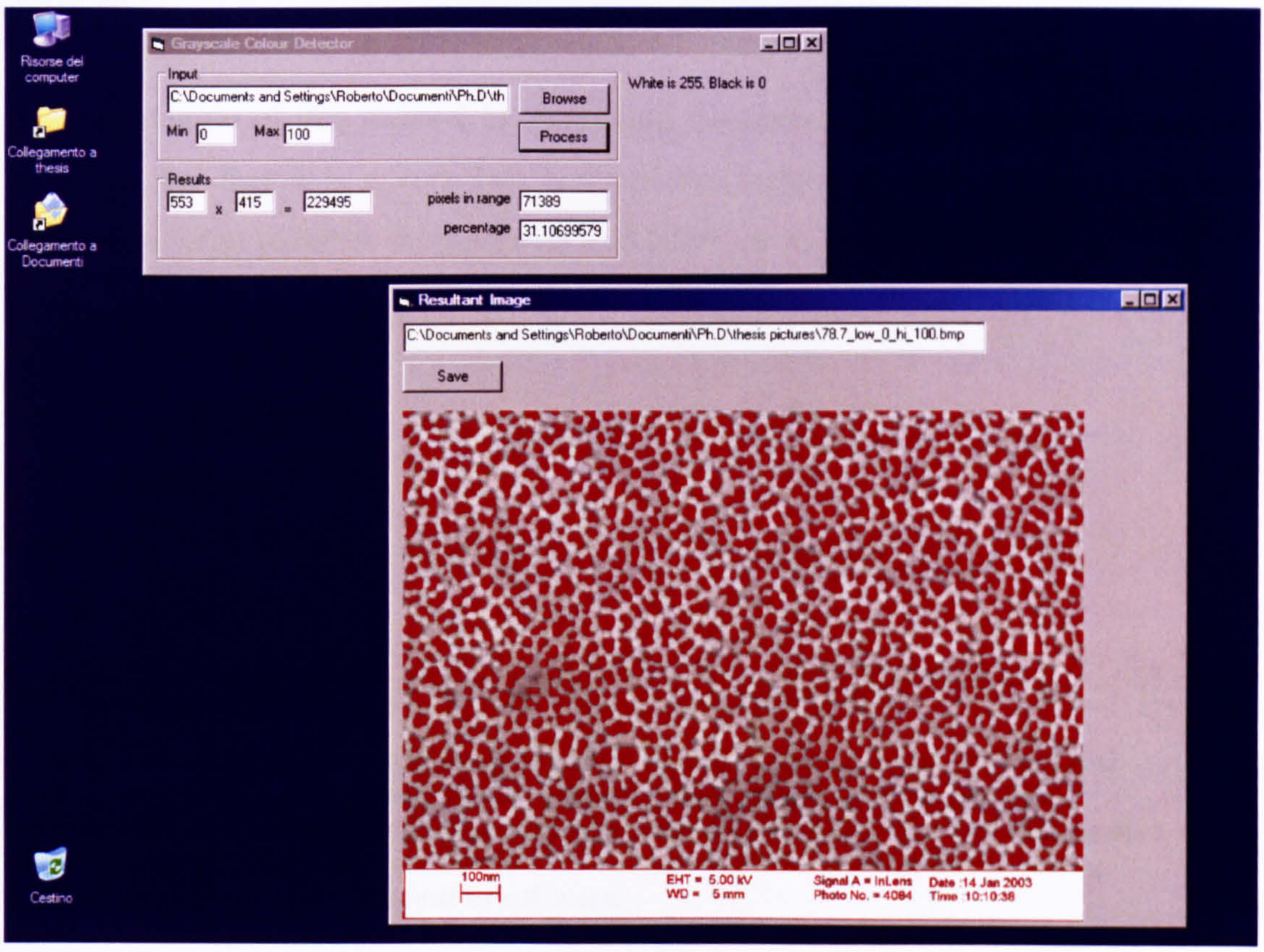

Figure 11.14 - The "white detector" software interface: an example of its application. In the micrograph all the pixels included in the range between 0 and 100 in terms of grey scale are red.

The "white detector" software is able to process micrographs pixel per pixel in terms of grey scale level. Micrographs can be loaded by means of the browse button. Once the micrographs is loaded, the operator decides which range of pixels in terms of grey scale levels they want to analyse by means of introducing a minimum (0 in Fig. 11.14) and a maximum value (100 in Fig. 11.14) in the specific windows. The

operator can now process the picture clicking on the "process" button and the software provides:

- the overall number of pixels in the micrograph;
- the number of pixels included in the range chosen;
- the percentage of pixels included in the range chosen with regard to the overall number of pixels;
- a modified micrograph where all the pixels included in the range chosen are red, in order to eye-detect the percentage of pixels included in the range chosen.

The new picture can then be saved and the percentage incorporation obtained recorded.

The advantages of this method in evaluating the percentage of inert particle surface coverage are that it is a very fast and reliable technique. The software is able to discern between particles incorporated and holes, as shown in Fig. 11.15.

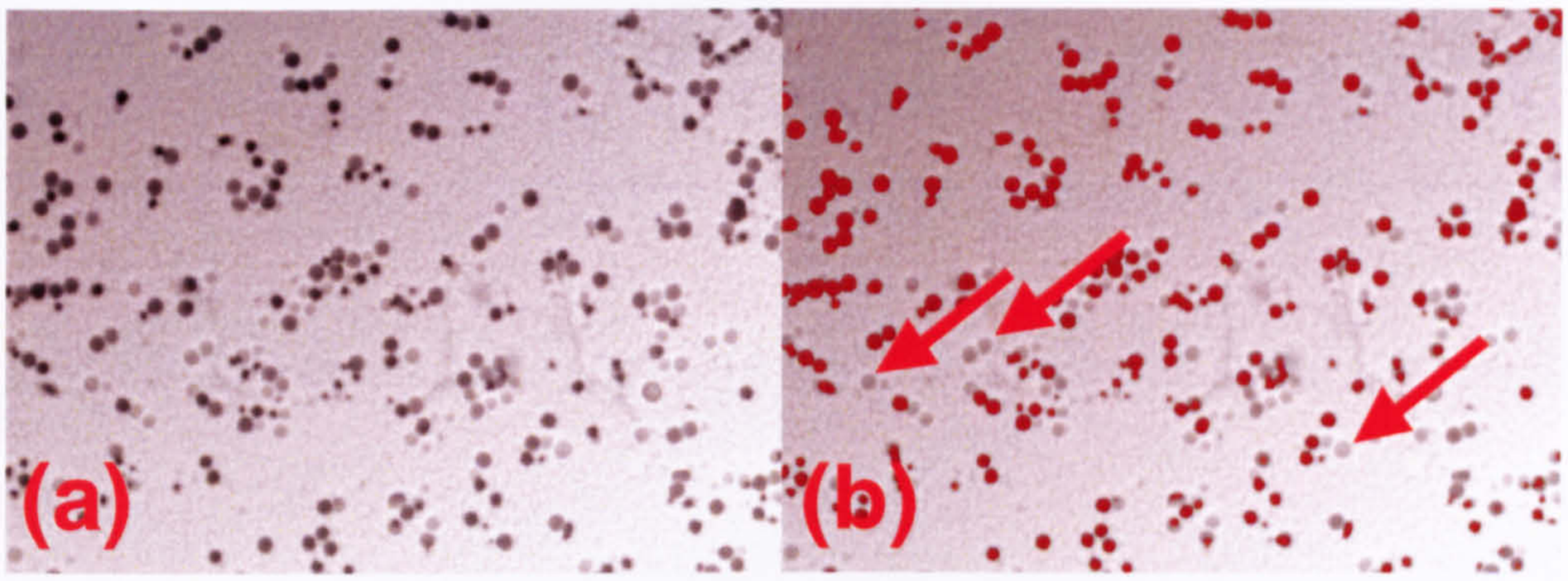

Figure 11.15 - (a) Backscattered image of a nickel-PS composite coating. (b) The same coatings processed with "white detector" software, black pixels in (a) (polystyrene particles) are now red and the surface percentage can be calculated. For this coating the surface coverage percentage was 6.3%. Arrows highlight holes present on the coating surface that are not taken in count by software.

All the data presented in this work were obtained with this method of analysis. The main disadvantage was that this was a "surface only" technique rather than a "total coating depth" analysis. As a consequence of this, the use of "image analysis" is reliable only for coatings of thickness comparable with the particle size used during co-deposition. This, as discussed in Section 13.3.1, made difficult the analysis of coatings containing very small particles.

12. Hydrodynamic influence

In order to investigate the hydrodynamic influence on the electrolytic co-deposition process all the composites coatings, obtained in this work, have been produced under several hydrodynamic conditions.

The amount of particles incorporated was calculated using microscopy and image analysis as discussed in chapter 11.

12.1 Nickel-polystyrene composite coatings

Fig. 12.1 shows the concentration of PS particles incorporated as a function of cathode rotation speed for nickel-PS composite coatings produced at 5 A/dm^2 and 2 g/l PS particle concentration on 7.4 cm diameter mild steel cathodes. The concentration of PS particles incorporated reached a maximum at 220 rpm and then decreased with increase in cathode rotation speed.

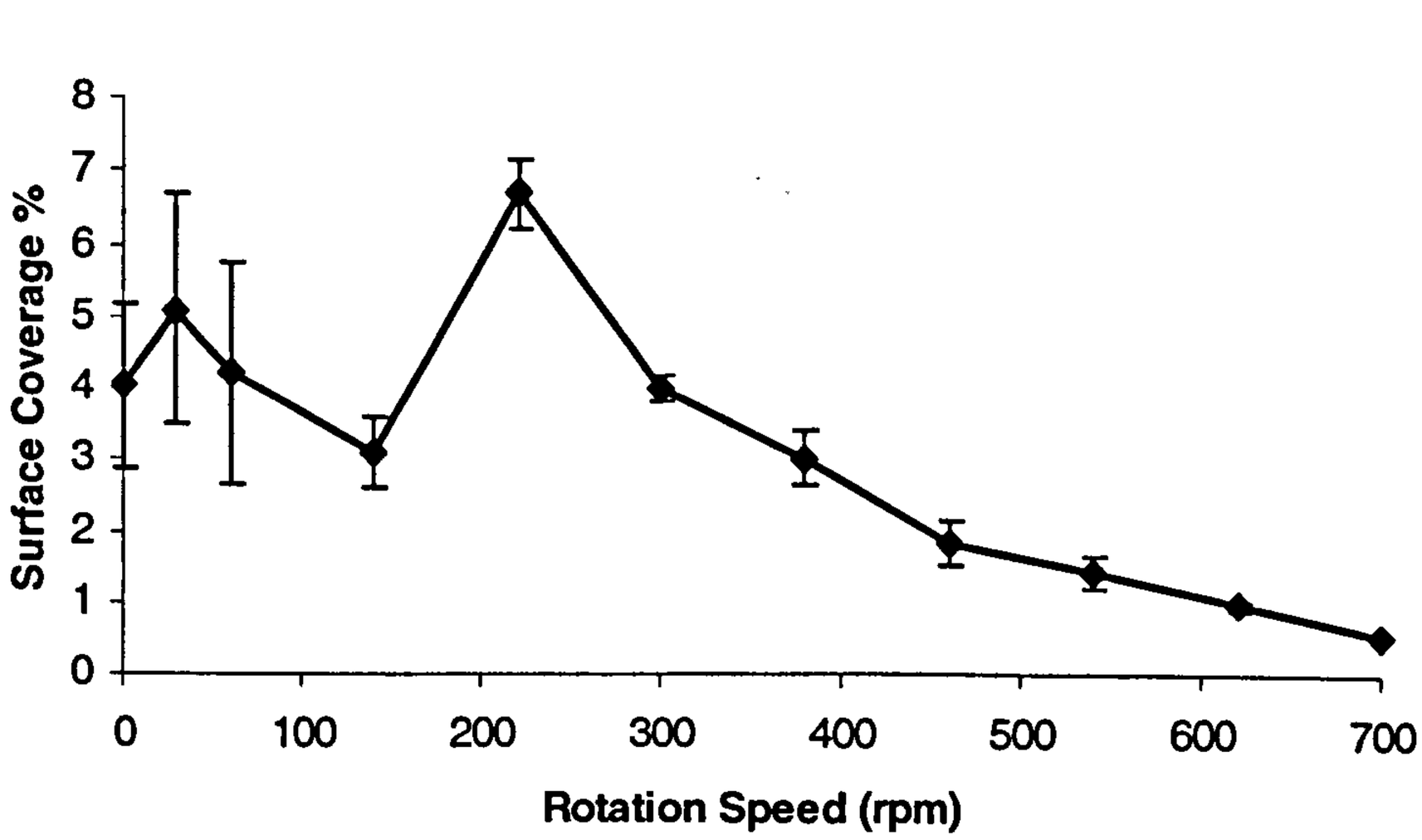

Figure 12.1 - Surface coverage *% vs.* cathode rotation speed for nickel-PS composite coatings produced at 5 A dm^{-2} and 2 g l^{-1} PS particle loading on 7.4 cm diameter mild steel cathodes.

Error bars appeared to be large at low rotation speed values (up to 220 rpm), while they became very small for higher rotation speed values (between 220 and 700 rpm). Essentially two ranges of rotation speeds were characterised:

- low rotation speeds: the trend was not clear and large error bars were observed;

- high rotation speeds: the trend was quite clear and small error bars were observed.

In Figs. 12.2 and 12.3 coatings with a similar PS surface coverage, but obtained at different rotation speed values, were compared in order to investigate the reasons for the different trends noted in Fig. 12.1.

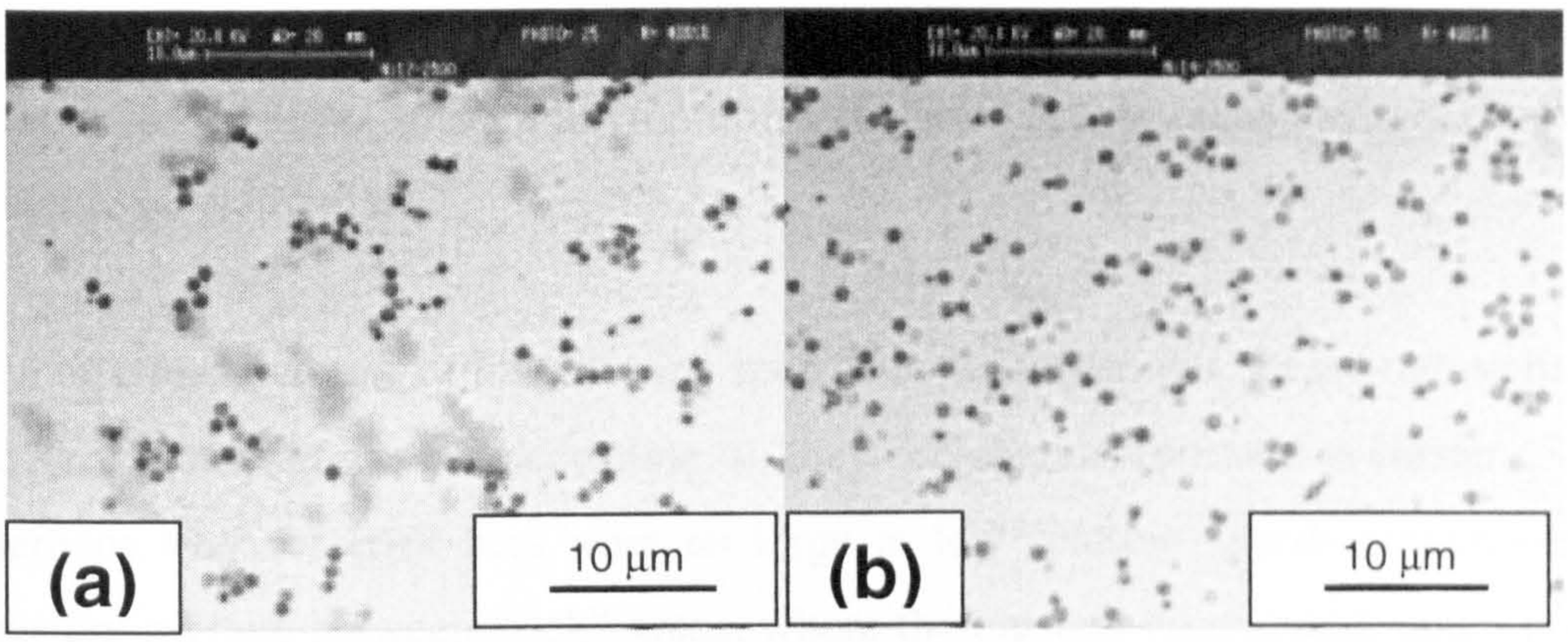

Figure 12.2 - Backscattered electron images of 2 µm nickel-PS electrodeposits obtained at 5 A dm^{-2} and 2 g l^{-1} PS particles loading on 7.4 cm diameter mild steel cathodes. (a) Rotation speed: 60 rpm, surface coverage: 4.5%. Particles tended to be agglomerated. (b) Rotation speed: 300 rpm, surface coverage: 4.3%. Particles distribution across the coating was more homogeneous and the number of holes was increased.

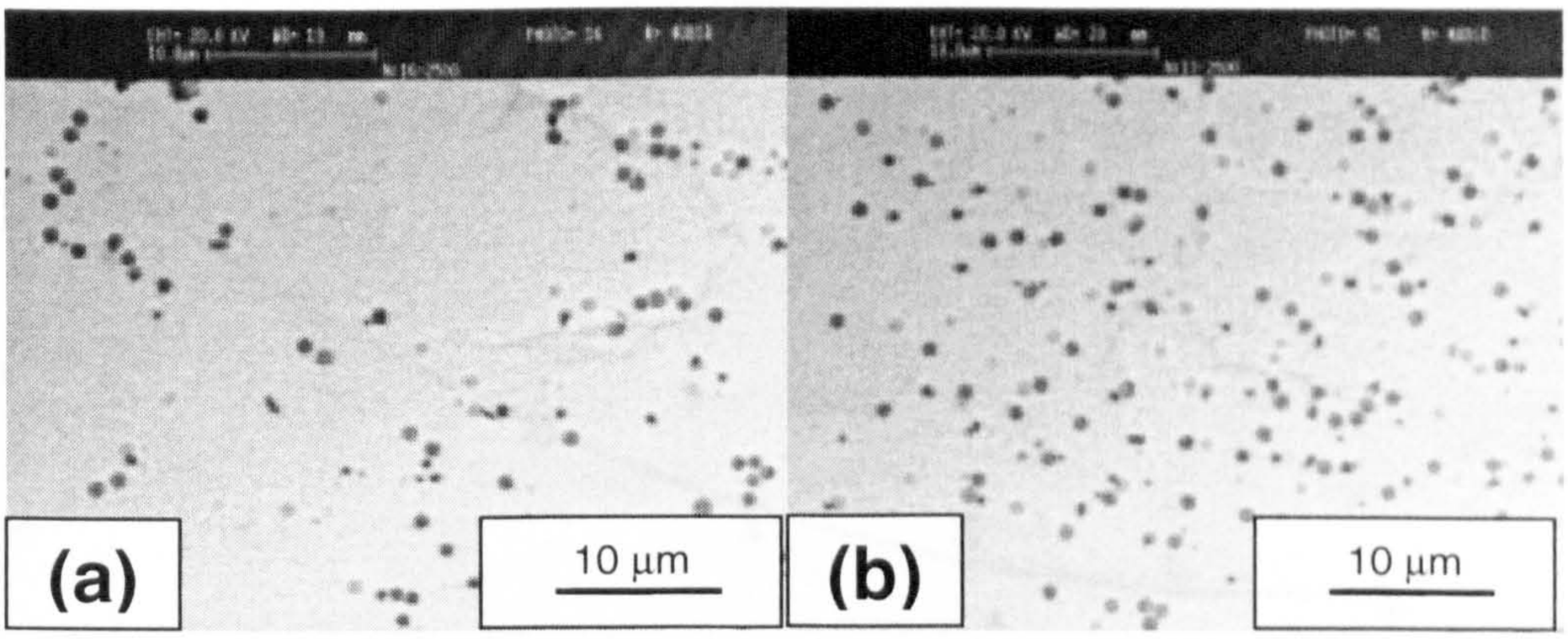

Figure 12.3 - Backscattered electron images of 2 µm nickel-PS electrodeposits obtained at 5 A dm^{-2} and 2 g l^{-1} PS particles loading on 7.4 cm diameter mild steel cathodes. (a) Rotation speed: 140 rpm, surface coverage: 2.75%. Particles tended to be agglomerated. (b) Rotation speed: 380 rpm, surface coverage: 2.75%. Particles distribution across the coating was more homogeneous and the number of holes was increased.

It can be seen that samples were quite similar in surface concentration (4.5 and 4.3 % for Fig. 12.2 (a) and (b) respectively; 2.75 % for both Fig. 12.3 (a) and (b)) but their morphology was very different. At low rotation speeds particles tended to be agglomerated in the coating. At high rotation speeds the distribution of particles

across the coatings was more homogeneous. On the other hand, the number of holes had increased as well. These holes are imprints of particles loosely attached to the surface and probably lost with following ultrasonic treatment after electrocodeposition. CELIS *et al.* [42, 72] stated that the incorporation of particles as agglomerates, rather than single particles, is the reason for the increase in particles incorporated in the transition zone, when the electrolyte flow, laminar at low rotation speeds, becomes turbulent. Once the electrolyte flow is completely turbulent, agglomerates were not present anymore in the electrolyte, because the agitation was enough to break them up.

It can be concluded that at low rotation speeds the agitation was not enough to break particle agglomerates in the electrolyte, so they became incorporated as clusters. This is perhaps why the error bars were so large at low rotation speeds (experimental points are average between "rich" areas, where the clusters were found, and "poor" areas, were low particle incorporations levels were found) and so small at high values. At high rotation speed values the trend for particle incorporation was quite clear (see Fig. 12.4).

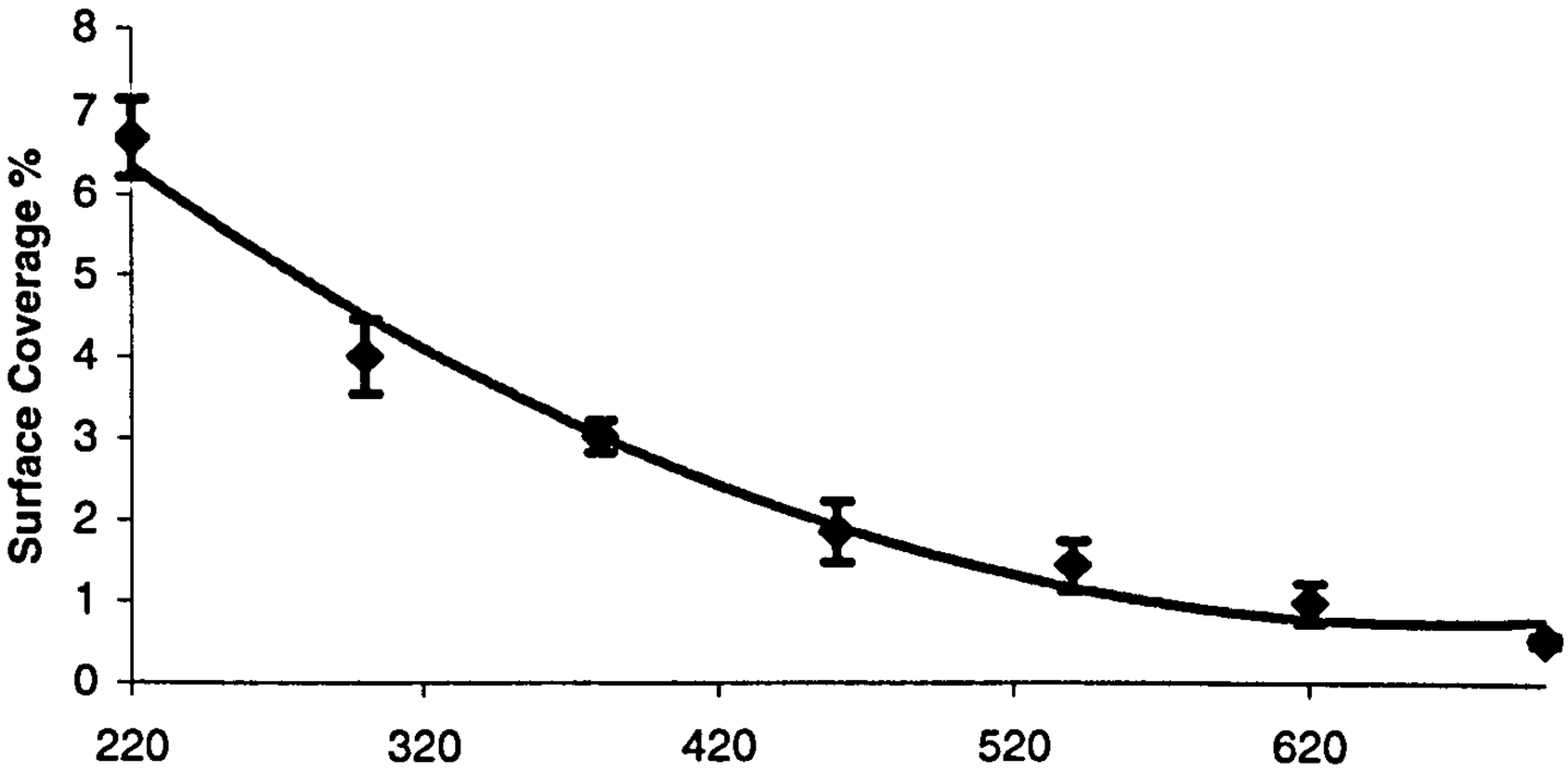

Figure 12.4 - Surface coverage % *vs.* cathode rotation speed for nickel-PS composite coatings produced at 5 A dm^{-2} and 2 g l^{-1} PS particle loading on 7.4 cm diameter mild steel cathodes. High rotation speed range.

Surface coverage decreased with increase in cathode rotation speed. This was probably due to the increasing centrifugal forces experienced by particles in the electrolyte. These forces tend to push particles away from the cathode surface. As a

consequence the particles' residence time on the cathode is decreased as well as the probability for them to be incorporated. Holes are present on the final coating surface as a consequence of particles being swept away. Such behaviour has also been encountered by CELIS *et al.* [42, 72].

The model proposed by CELIS, ROOS and BUELENS [19, 96] (see Section 4.4) is the one that better matches the findings of the present work. A particle is said to approach the cathode surface in several steps. First of all, when the particle is wetted by the electrolyte, its surface adsorbs metal ions. Now the particle can move, because of electrophoretic motion caused by the positive charged ions adsorbed on the surface, towards the cathode surface. Once the particles come in contact with the cathode, the ions present on the particle surface begin their reduction on the growing metal layer. If the contact time is long enough then the metal layer can grow and can incorporate the particle. This is what happens when the cathode rotation speed is low (up to 150 rpm, see Fig.12.1). The probability of particle incorporation at this stage is very high, because they have the time to be incorporated on the deposit surface. This is confirmed by the absence of holes on the final coating surface when the flow is laminar. If the contact time is too short then the particles are moved away from the surface before the ionic reduction is able to help capture them. Particles move away from the cathode surface and in some cases they leave an imprint on the final coating surface.

With regard to Fig. 12.1, three different zones with different hydrodynamics can be discerned as shown in Fig. 12.5: laminar, transition and turbulent. The data shown in the laminar zone, due to the presence of large error bars discussed previously, are not very clear and a constant trend can be discerned.

BUELENS *et al.* [42] in 1983 (see section 3.2), studying the co-deposition of both copper and gold with alumina using a rotating disc system (RDE) technique, found similar trends. Fig. 12.6 shows their results.

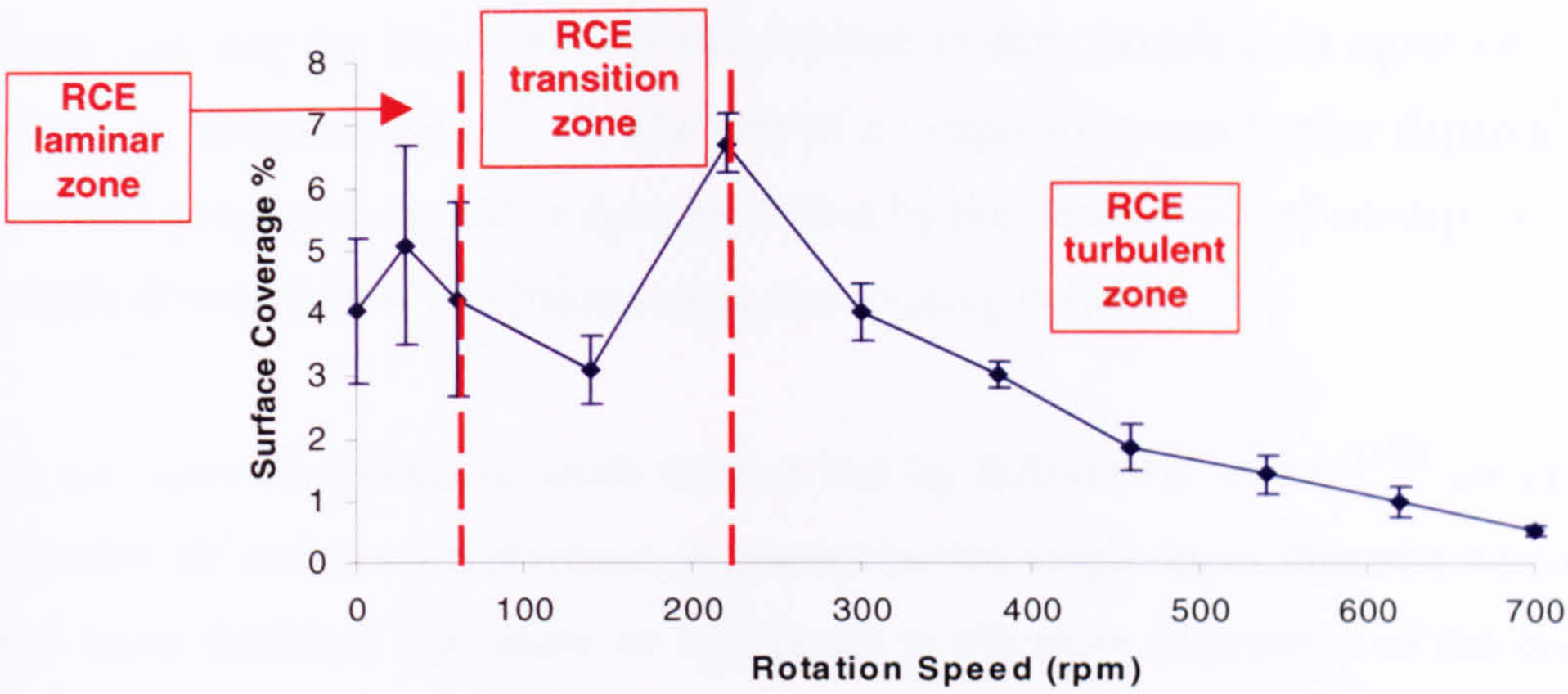

Figure 12.5 - Surface coverage *% vs.* cathode rotation speed for nickel-PS composite coatings produced at 5 A dm^{-2} and 2 g l^{-1} PS particle loading on 7.4 cm diameter mild steel cathodes. Dashed red lines highlight the three zones with different hydrodynamics.

The different electrode geometry is, furthermore, responsible for the shift of rotation speed at the change from laminar to transitional flow, and from transitional to turbulent. For the RCE system all the transition rotation speeds are much lower than those for RDE system. RDE cells are often used to investigate hydrodynamics behaviours related to laminar flow because the rotational speed transition laminar to turbulent is high. This is not true for RCE cells, which have a much lower transition rotational speed, so this kind of system is often used when a turbulent flow has to be investigated.

Comparison between Figs. 12.5 and 12.6 reveals that that the transition and the turbulent zones are very well matched in terms of their particle content trends. Incorporation levels are different of course, due to the different cell system used and to the different electrode type and dimensions.

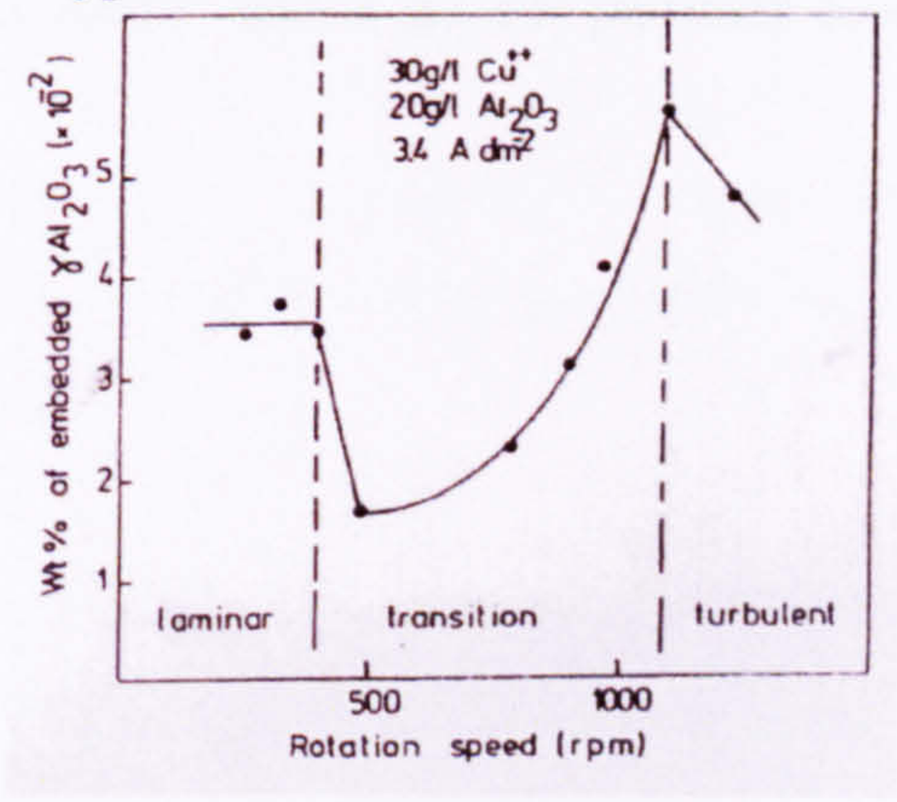

Figure 12.6 - Effects of disc rotation speed on percentage of alumina particles co-deposited with copper [42].

These results shows that the reduction of ions adsorbed on PS particles was the rate-determining step for the nickel-PS polystyrene system, which is in agreement with previously published data [42, 72]. The rate of co-deposition was further dependent on the mass transport to the electrolyte, as shown by the dependency of co-deposition on the hydrodynamic flow conditions along the rotating cylinder.

This can also be related to work carried out by BANOVIC *et al.* [148] on the co-deposition of nickel with alumina, in particular for single layer deposits where the metal layer thickness was more or less equal to the main dimension of the particle (see Section 3.2).

12.2 Copper-polystyrene composite coatings

Copper-polystyrene composite coatings were initially produced at 5 A/dm^2 and 2 g/l PS particles loading on 7.4 cm diameter mild steel cathodes at different rotation speed values. Fig. 12.7 (blue curve) shows the concentration of PS particles incorporated as a function of cathode rotation speed. Two maxima can be seen, at 60 and 540 rpm. Very poor data concerning the incorporation of PS particles in a copper matrix are present in literature.

As shown in section 8.4.1, when mild steel is placed in contact with a copper electrolyte, immersion coatings of copper are produced on the cathode surface. To avoid this problem the co-deposition of copper with polystyrene was carried out for a second time on cylinders pre-plated with a 1 µm nickel deposit. Fig. 12.7 shows the level of PS particles incorporated as a function of the cathode rotation speed for coatings produced at 5 A/dm^2 and 2 g/l PS particles loading on 7.4 cm diameter cathodes.

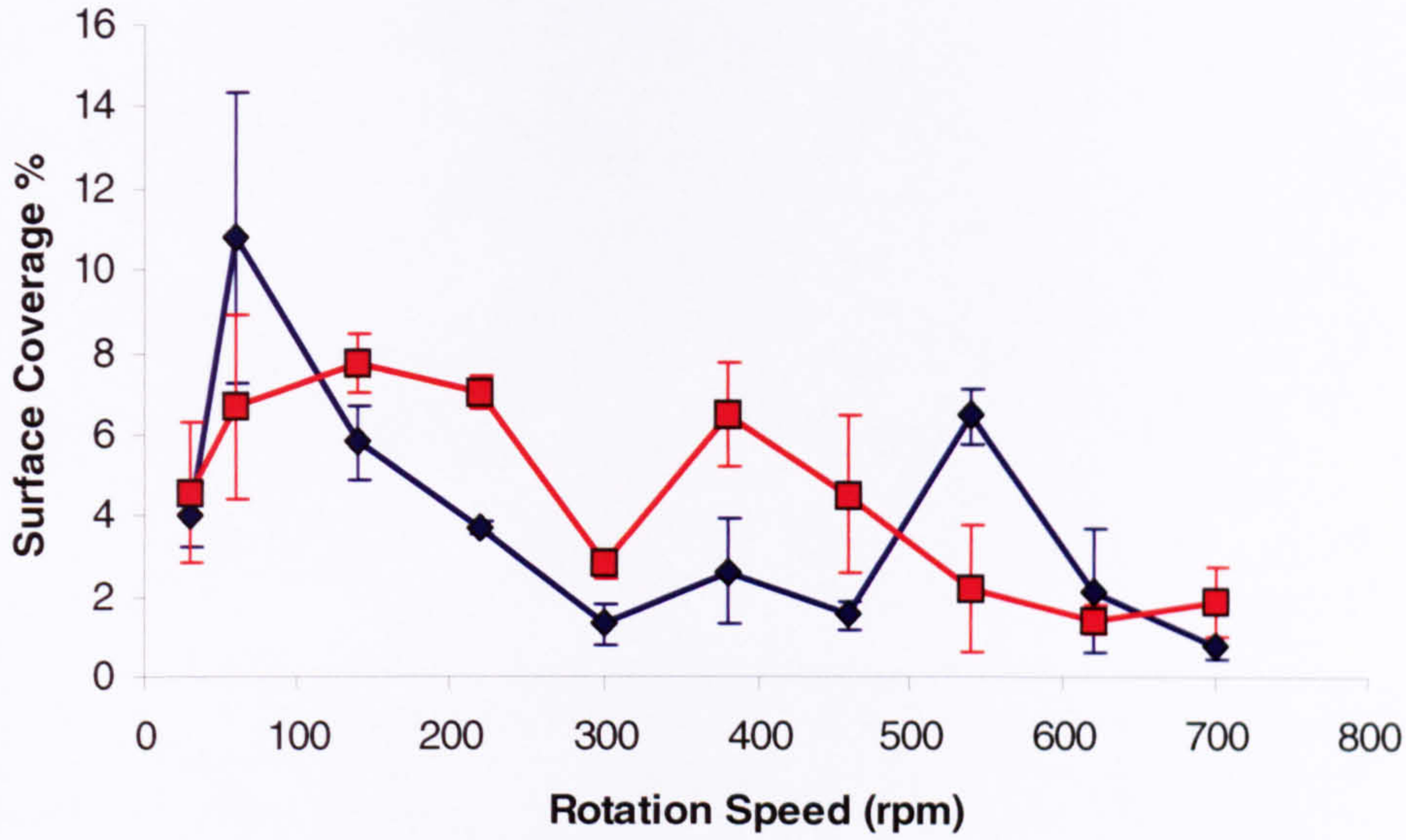

Figure 12.7 - Blue curve: surface coverage % *vs.* cathode rotation speed for copper-PS coatings produced at 5 A dm^{-2} and 2 g l^{-1} PS particle loading on 7.4 cm diameter mild steel cathodes. Red curve: surface coverage % *vs.* cathode rotation speed for Cu-PS composite coatings produced at 5 A dm^{-2} and 2 g l^{-1} PS particle loading on 7.4 cm cathodes pre-plated with nickel.

PS particle content initially increased with increasing rotation speed. The highest concentration of PS particles in the electrodeposit was achieved at 140 rpm (7.7 %). A decrease was then noted with increase in cathode rotation speed. Relatively large error bars were observed at most of the rotation speeds investigated.

It can be seen that, pre-electroplating the sample surfaces with nickel produced much clearer data, a trend can be seen and it is similar to the ones obtained for Ni-PS and Zn-PS systems, as discussed below. Without pre-plating, data were irregular and no distinct trend was evident. Hence the roughness present at the cathode surface before electroco-deposition may have well influenced the process: the local turbulence was increased because of roughness, and forces acting on the particles were too low to give them sufficient time to be incorporated in the growing metallic layer. This was why incorporation levels were lower when copper immersion coatings were initially produced on the unplated steel.

As for the nickel-PS system (see Figs. 12.2 and 12.3), in Fig. 12.8 coatings similar in surface coverage, but obtained at different rotation speed values were compared to obtain information about the data in Fig. 12.7 (red curve).

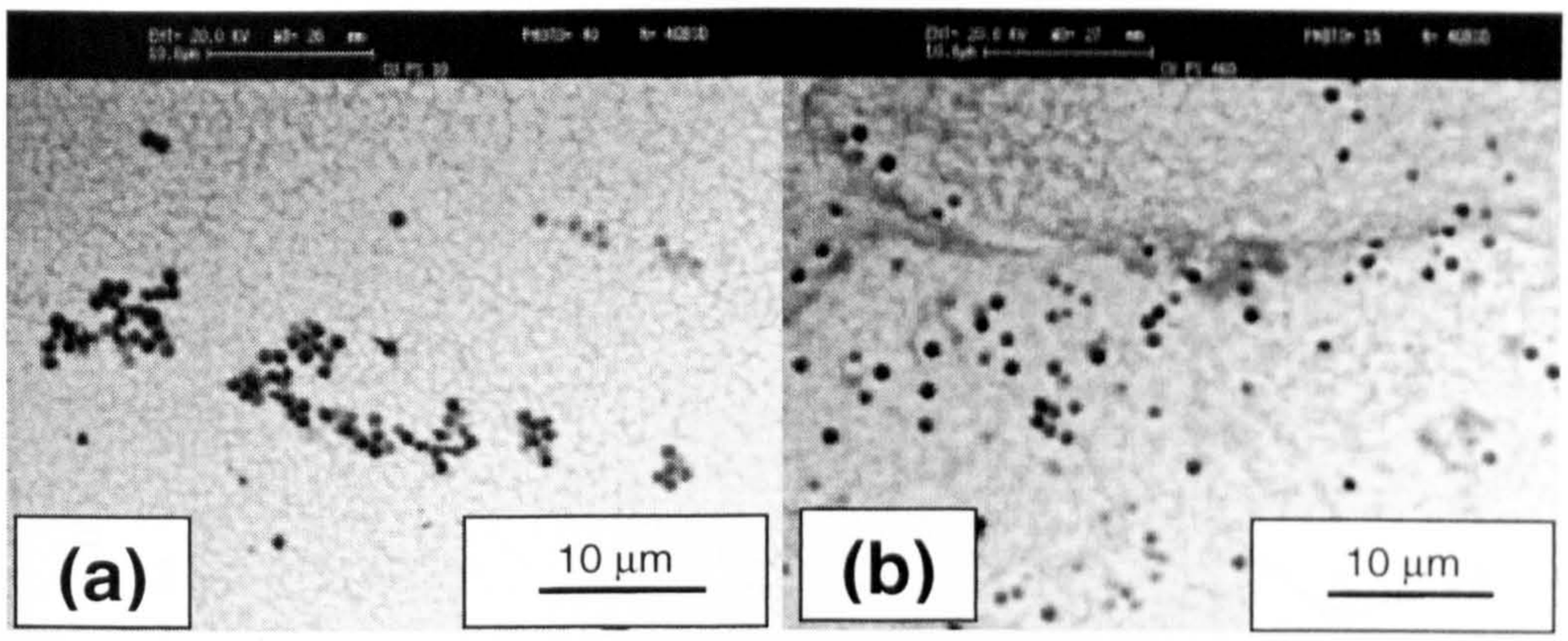

Figure 12.8 - Backscattered electron images of 2 µm copper-PS electrodeposits obtained at 5 A dm^{-2} and 2 g l^{-1} PS particles loading on 7.4 cm diameter mild steel cathodes pre-plated with nickel. (a) Rotation speed: 30 rpm, surface coverage: 3.4%. Particles tended to be agglomerated. (b) Rotation speed: 460 rpm, surface coverage: 3.5%. Particles distribution across the coating was more homogeneous and the number of holes was increased.

It can be seen that the samples were very similar in surface PS concentration (3.4 and 3.5 %) but their morphologies are very different. At low rotation speeds particles tended to be agglomerated in the coating. At high rotation speeds the distribution of particles across the coating was more homogeneous. Therefore the number of holes had increased as well. This confirms that as shown for the nickel-PS system, at low rotation speeds the agitation was insufficient to disrupt particle agglomerates in the electrolyte, so they became incorporated as clusters. Large error bars at low rotation speed values were also evident (Fig. 12.7, red curve).

Error bars were found to be large also at high rotation speed values (Fig. 12.7, red curve). This was probably a consequence of the formation of "nodular striped" structures (see Section 10.2) on copper-PS composite coatings obtained at high rotation speed values. "Nodular striped" structures were found to be richer in incorporated particles compared with the rest of the coating, so average experimental points contain large error bars.

12.3 Zinc-polystyrene composite coatings

Fig. 12.9 shows the concentration of PS particles incorporated as a function of cathode rotation speed for zinc-PS composite coatings produced at 5 A/dm^2 and 2 g/l PS particles concentration on 7.4 cm diameter mild steel cathodes.

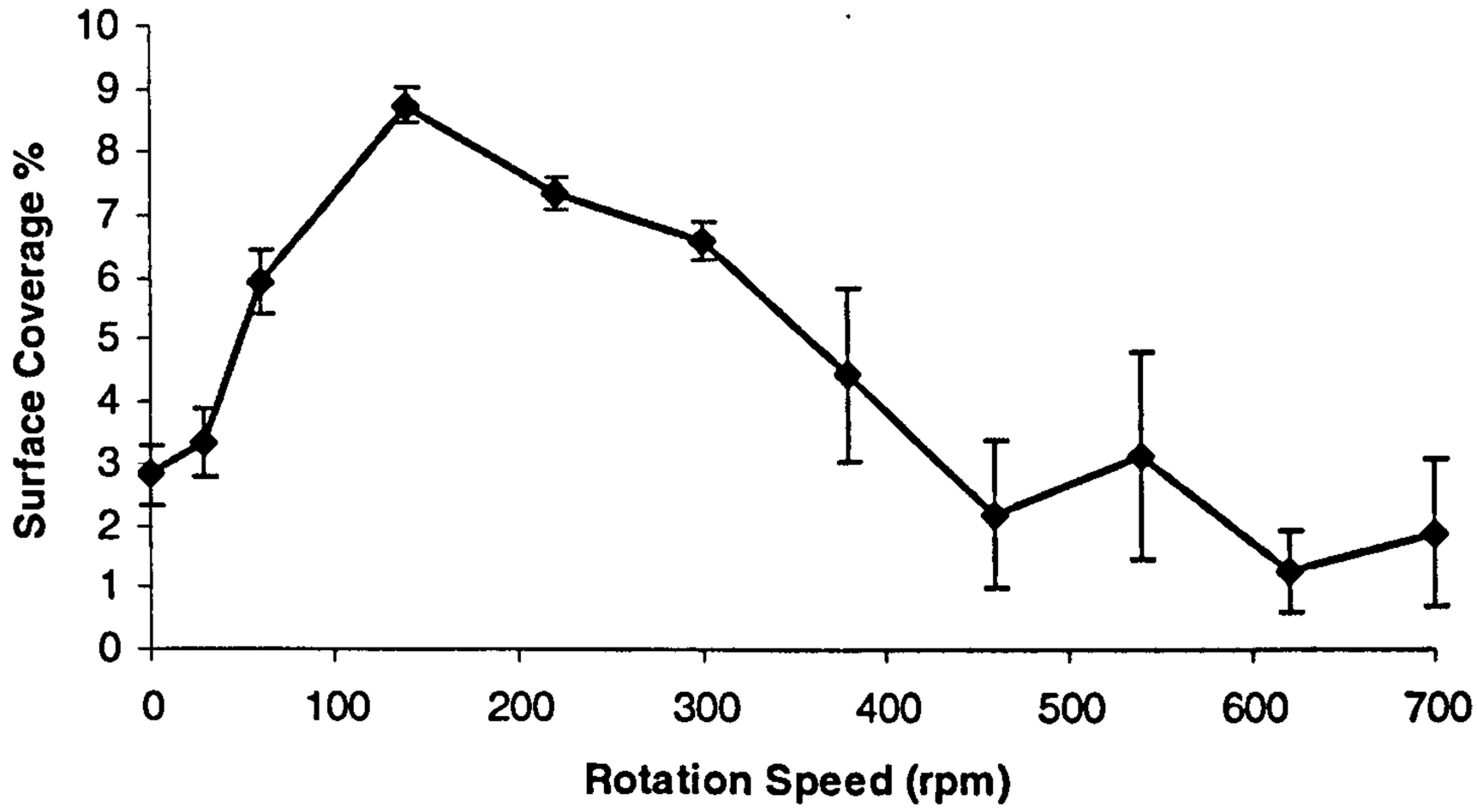

Figure 12.9 - Surface coverage % *vs.* cathode rotation speed for zinc-PS composite coatings produced at 5 A dm^{-2} and 2 g l^{-1} PS particle loading on 7.4 cm diameter mild steel cathodes.

The concentration of PS particles incorporated reaches a maximum at 140 rpm, and then decreased with increase in cathode rotation speed. For zinc-PS the error bars appear quite small up to 300 rpm and become larger for higher values of rotation speed. Fig. 12.10 shows two of the coatings produced. It can be seen from the micrographs that the coating surface morphology at low rotation speed values (Fig. 12.10 (a)) was quite flat and regular. When the rotation speed was increased (see Fig. 12.10 (b)) the morphology was rather irregular and dendritic structures were present. This could explain the presence of large error bars at high rotation speed values.

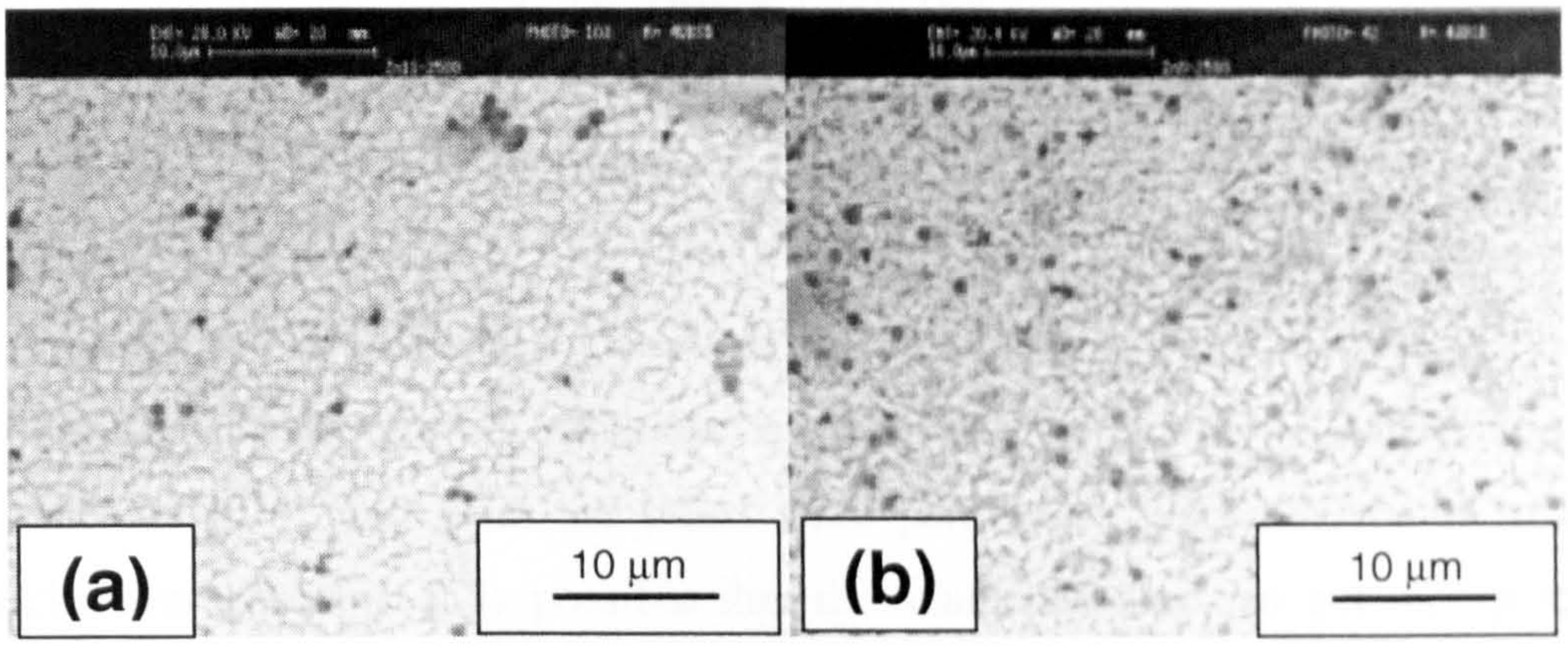

Figure 12.10 - Backscattered electron images of 2 µm zinc-PS electrodeposits obtained at 5 A dm^{-2} and 2 g l^{-1} PS particles loading on 7.4 cm diameter mild steel cathodes. (a) Rotation speed: 0 rpm, surface coverage: 2.6%. Coating surface morphology was flat and regular. (b) Rotation speed: 380 rpm, surface coverage: 4.2%. Coating surface morphology was irregular and dendritic structures can be seen.

As already seen in chapter 10, irregularities on the cathode surface promote local turbulence, increasing locally the amount of particles incorporated.

The same system, zinc-polystyrene, was studied by HOVESTAD *et al.* [32] in 1998 using a rotating cylinder electrode (see Section 3.4). They found out, in agreement with what has been discussed above, that the probability for a particle to be incorporated in a metal growing layer is strongly related to the cathode surface roughness.

In particular, when CTAC (cetyltrimethylammonium chloride, a surfactant with the similar chemical characteristic as the one used in the present work) was used in the electrolyte, the coating morphology obtained was very similar to the one shown in Fig. 12.10 (b).

12.4 Alumina composite coatings

Fig. 12.11 shows the level of alumina particles incorporated as a function of the cathode rotation speed for nickel-alumina composite coatings obtained at 5 A/dm^2 and 39 g/l alumina particles loading on 1.27 cm diameter AISI 316 stainless steel cathodes. The alumina particle size was 3 µm.

It can be seen that in this case the particle incorporation levels are not influenced by rotation speed: the alumina content in the coatings was more or less constant although large error bars were present.

It is important to reiterate the conclusions drawn after the particle characterisation in Section 9.1. It has been shown that the "as received" alumina particle distribution is not uniform at all, and, with the stated sized particles, a large amount of smaller particles were present. It is possible that the small particles can get incorporated more easily than the larger ones (bigger particles experience more centrifugal force in the electrolyte than the small ones). In this way, it is probable that the coating could have a high proportion of smaller alumina particles at all the rotation speeds because of the difficulty of incorporating larger ones, hence the constancy in particle incorporation versus rotation speed.

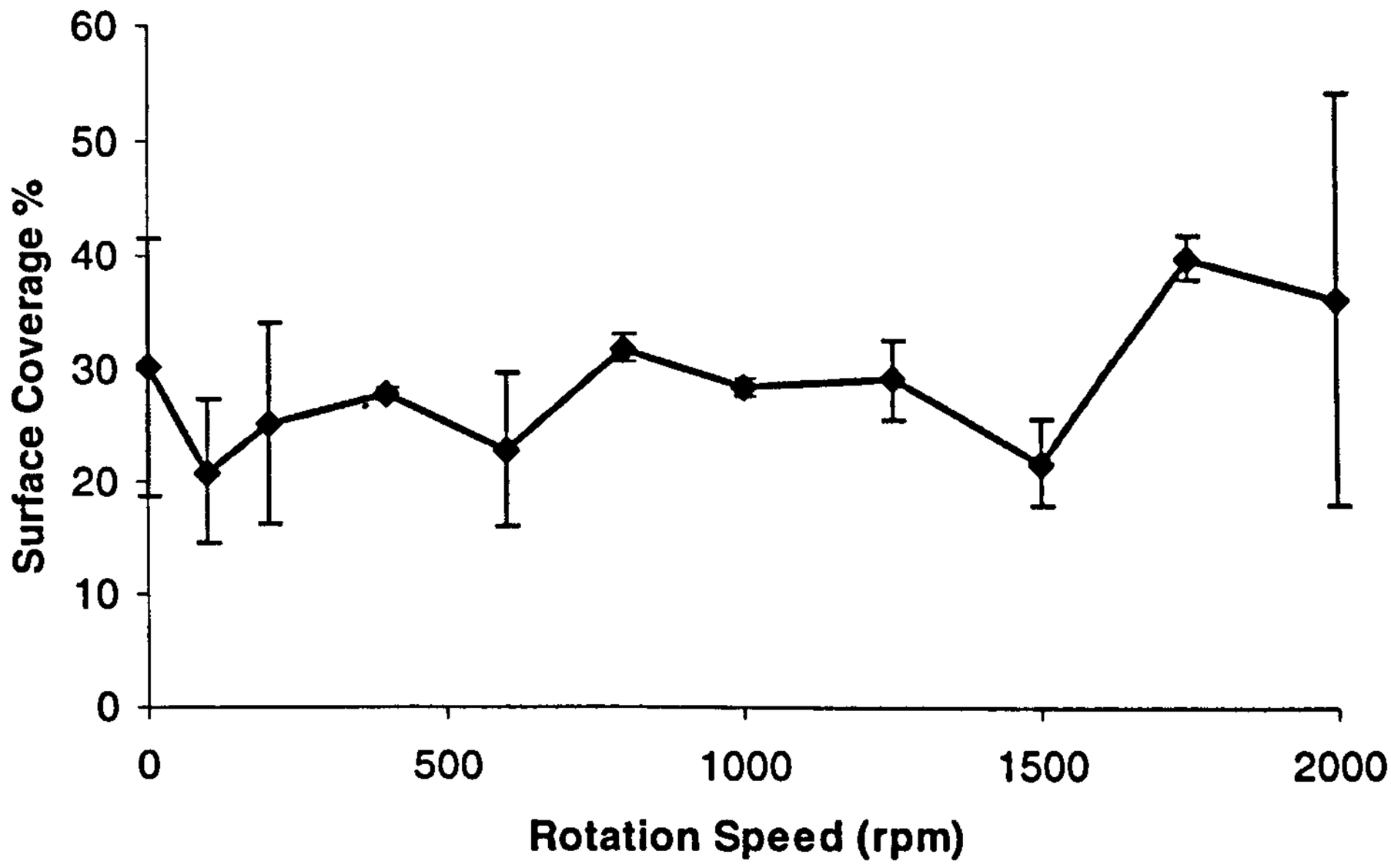

Figure 12.11 - Surface coverage % *vs.* cathode rotation speed for nickel-alumina composite coatings produced at 5 A dm^{-2} and 39 g l^{-1} alumina particle loading on 1.27 cm diameter AISI 316 stainless steel cathodes. Alumina particles of 3 μm with a coating thickness of 3μm.

Fig. 12.12 shows the level of alumina particles incorporated as a function of the cathode rotation speed for copper-alumina composite coatings obtained at 5 A/dm^2 and 39 g/l alumina particle loading on 1.27 cm diameter AISI 316 stainless steel cathodes. The alumina particle size was nominally 3 μm.

As for the nickel-alumina system, the same conclusions can be drawn. Even in this case the alumina content in the coatings was more or less constant with the rotation speed. Incorporation levels, between 1 and 6%, seem to be much lower when compared with nickel-alumina, that are between 15 and 40%. This is really important and suggests that particle shape plays a key role in incorporation, as will be discussed in Section 13.2.2.

The only data available in the literature about the influence of the hydrodynamic regime on the co-deposition process when alumina is used as second phase material was the work, carried out by STOJAK AND TALBOT [58] in 1999, on the electroco-deposition of copper with alumina on a rotating cylinder electrode (see Section 3.4).

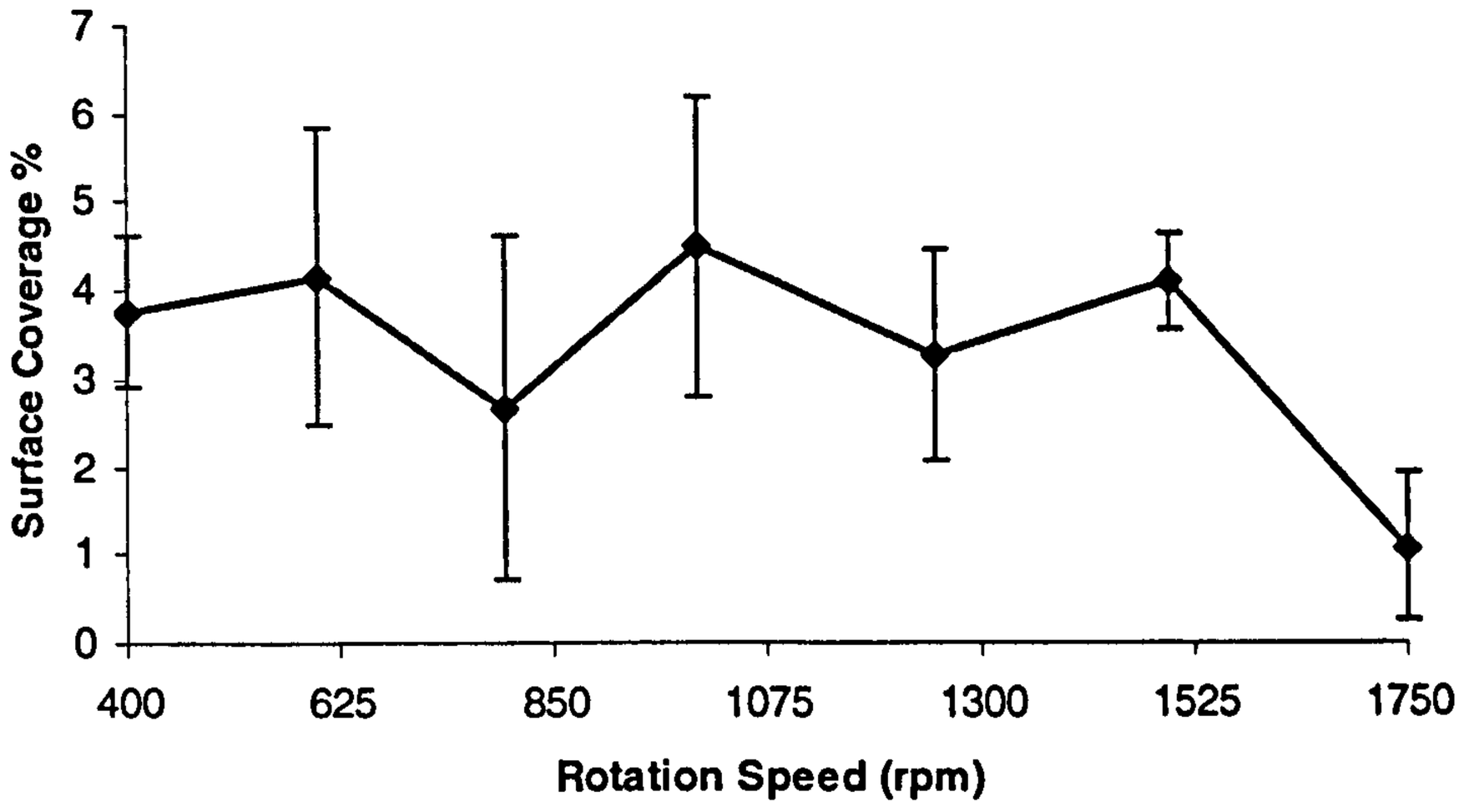

Figure 12.12 - Surface coverage *% vs.* cathode rotation speed for copper-alumina composite coatings produced at 5 A dm^{-2} and 39 g l^{-1} alumina particle loading on 1.27 cm diameter AISI 316 stainless steel cathodes. Alumina particles of 3 μm with a coating thickness of 3μm.

Comparison with data obtained by STOJAK AND TALBOT [58], shown in Fig. 3.9, shows that incorporation values are not comparable due to the difference in the method used to control the quality of the coating produced (in the present work a "surface coverage" was always evaluated, while STOJAK AND TALBOT [58] reported a mass percentage), but the dependence upon the cathode rotation speed is essentially the same: the amount of alumina particles incorporated is more or less the same under all the cathode rotation speeds investigated. The major scattering of the data produced in this work was, of course, due to the larger number of rotation speeds examined than those by STOJAK AND TALBOT [58].

This observation emphasises that as discussed in section 12.1, increasing the electrode rotational speed does increase the amount of particles that are in contact with it. However, in some cases, this does not result in a corresponding increase in co-deposition. This result supports the hypothesis that particle incorporation involves the reduction of adsorbed ions on the particle and that this becomes the rate-determining step of the process when the turbulence is increased [42, 58, 72, 96]. A particle in the electrolyte moves towards the cathode surface mainly because of the electrolyte agitation; once the particle is in contact with the surface, it has to remain in this situation for a sufficient time to be engulfed by the growing metal layer. Initially, increasing the rotation speed results in an increase in the number of collisions between particles and cathode surface per unit time which explains the initial increase in the number of particles incorporated. At the same time, increase in the cathode rotation speed increases the electrolyte agitation, with consequent decrease in the average contact time between cathode and particle. At this point the metal deposition rate becomes very important: if the reduction of adsorbed ions on the particle is fast enough, particles become incorporated, if not, they move away from the cathode surface leaving behind a hole, as shown schematically in Fig. 12.13. The hole can be either re-filled by depositing metal or present on the final coating if the current is switched off. A further increase in rotation speed brings about very low incorporation levels and when the agitation is over a critical value, co-deposition virtually ceases.

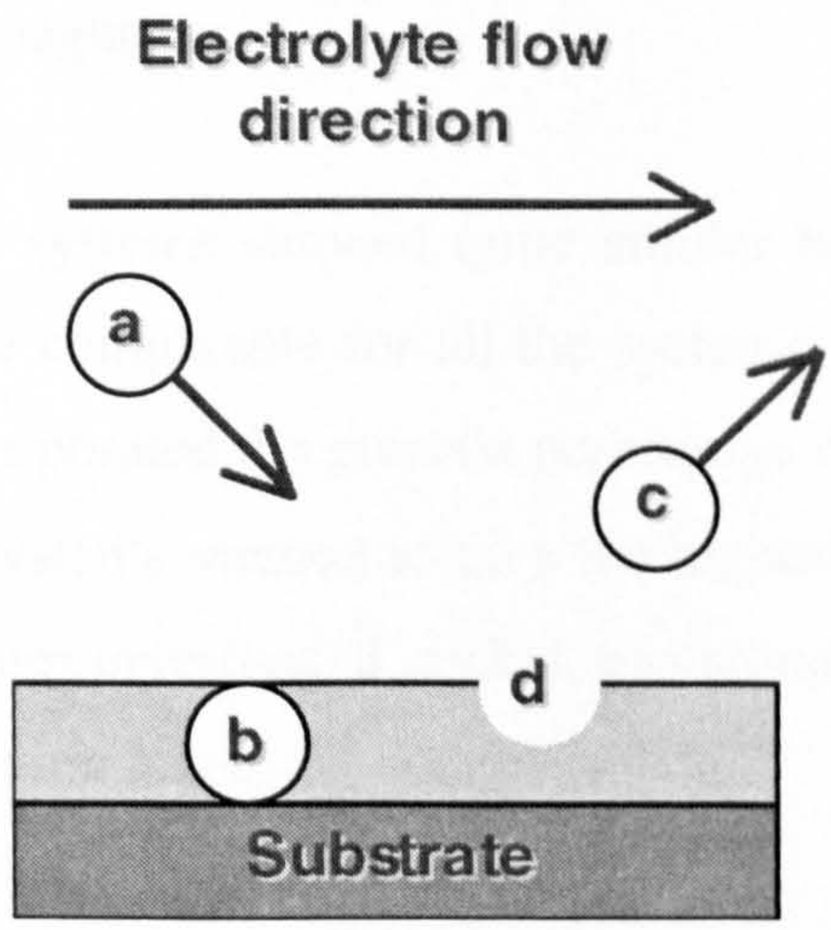

Figure 12.13 - Scheme for the particle incorporation process. (a) particle moving towards the cathode surface; (b) successful collision; (c) particle leaving the cathode surface after an unsuccessful collision; (d) hole left by the particle.

13. Metal matrix influence and second phase effects on co-deposition

Examination of the metal matrix type is a relatively uncommon approach to investigation of the co-deposition process. In most cases in the literature the parameter under study is the nature i.e. the shape, size and chemical nature of the material used as second phase.

In order to investigate the influence of the metal matrix on the electrolytic co-deposition process, nickel, zinc and copper were used to produce composite coatings with either polystyrene or alumina. The next section a comparison between all the systems investigated will be made together with an investigation of the second phase material influences in terms of particle size and particle shape on the co-deposition process.

13.1 Polystyrene composite coatings

Fig. 13.1 shows the concentration of PS particles incorporated as a function of cathode rotation speed for copper-PS, zinc-PS and nickel-PS composite coatings obtained at 5 A/dm^2 and 2 g/l PS particles loading on 7.4 cm diameter cathodes. Zinc and nickel were co-deposited with PS particles on mild steel cathodes, while copper was deposited with polystyrene on nickel pre-plated ones for reasons outlined in section 10.2 i.e. surface roughness.

It is clear that the three systems showed quite similar behaviour. Up to 220 rpm incorporation levels were comparable for all the systems, although zinc-PS seemed to be the system that incorporated the greatest percentage of particles. After 220 rpm zinc-PS and copper-PS systems seemed to give the highest incorporation levels. For all the rotation speed values investigated, nickel, excluding very low rotation speeds, gave the lowest incorporation levels.

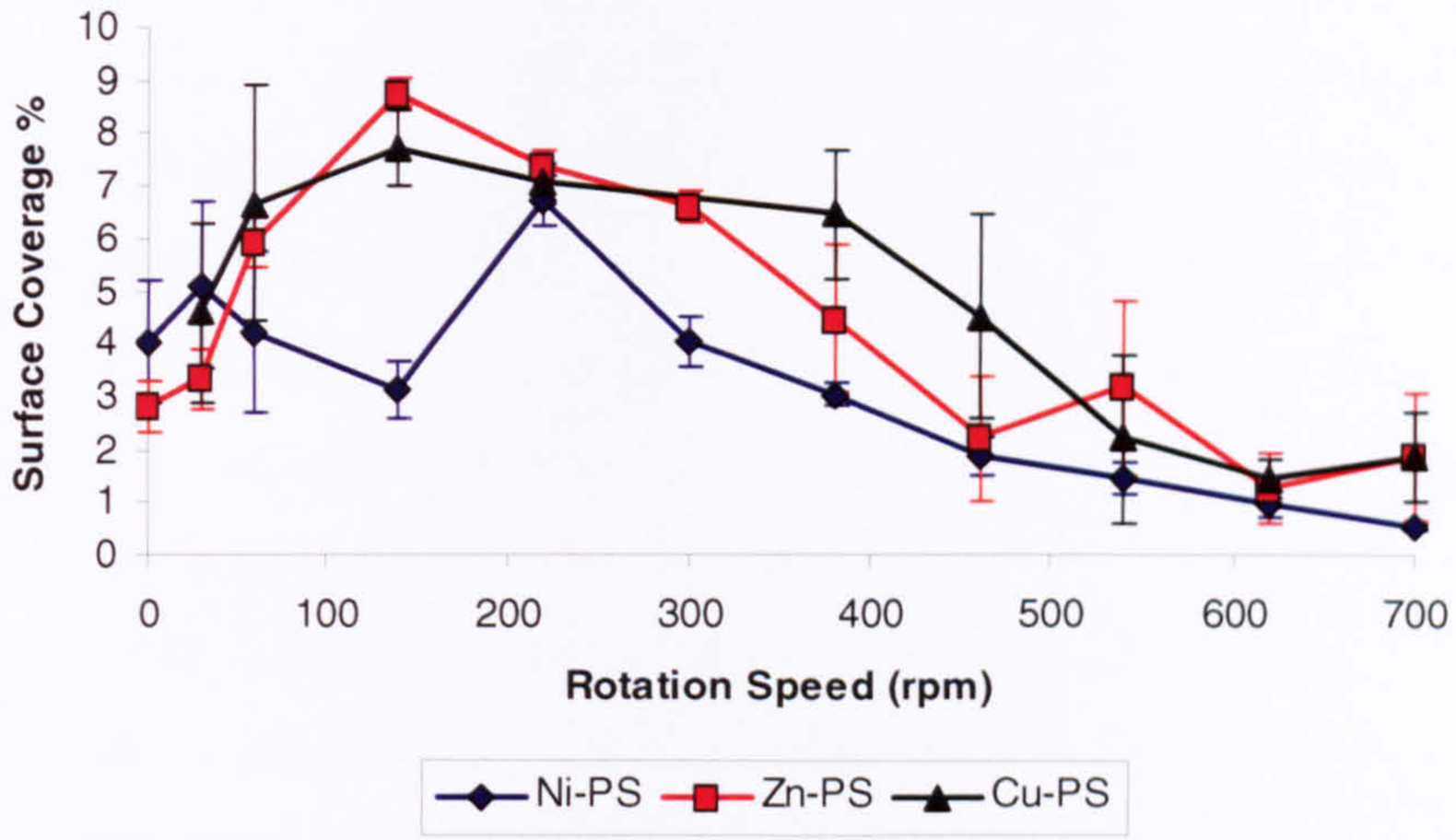

Figure 13.1 - Surface coverage *% vs.* cathode rotation speed for Cu-PS (black curve), Zn-PS (red curve) and Ni-PS (blue curve) composite coatings produced at 5 A dm^{-2} and 2 g l^{-1} PS particles loading on 7.4 cm cathodes. Zinc and nickel were co-deposited with PS particles on mild steel cathodes; copper was deposited with polystyrene on nickel pre-electroplated mild steel cathodes.

The same comparison can be made for zinc-PS and nickel-PS composite coatings obtained on 1.27 cm diameter AISI 316 stainless steel cathodes, as shown in Fig.13.2.

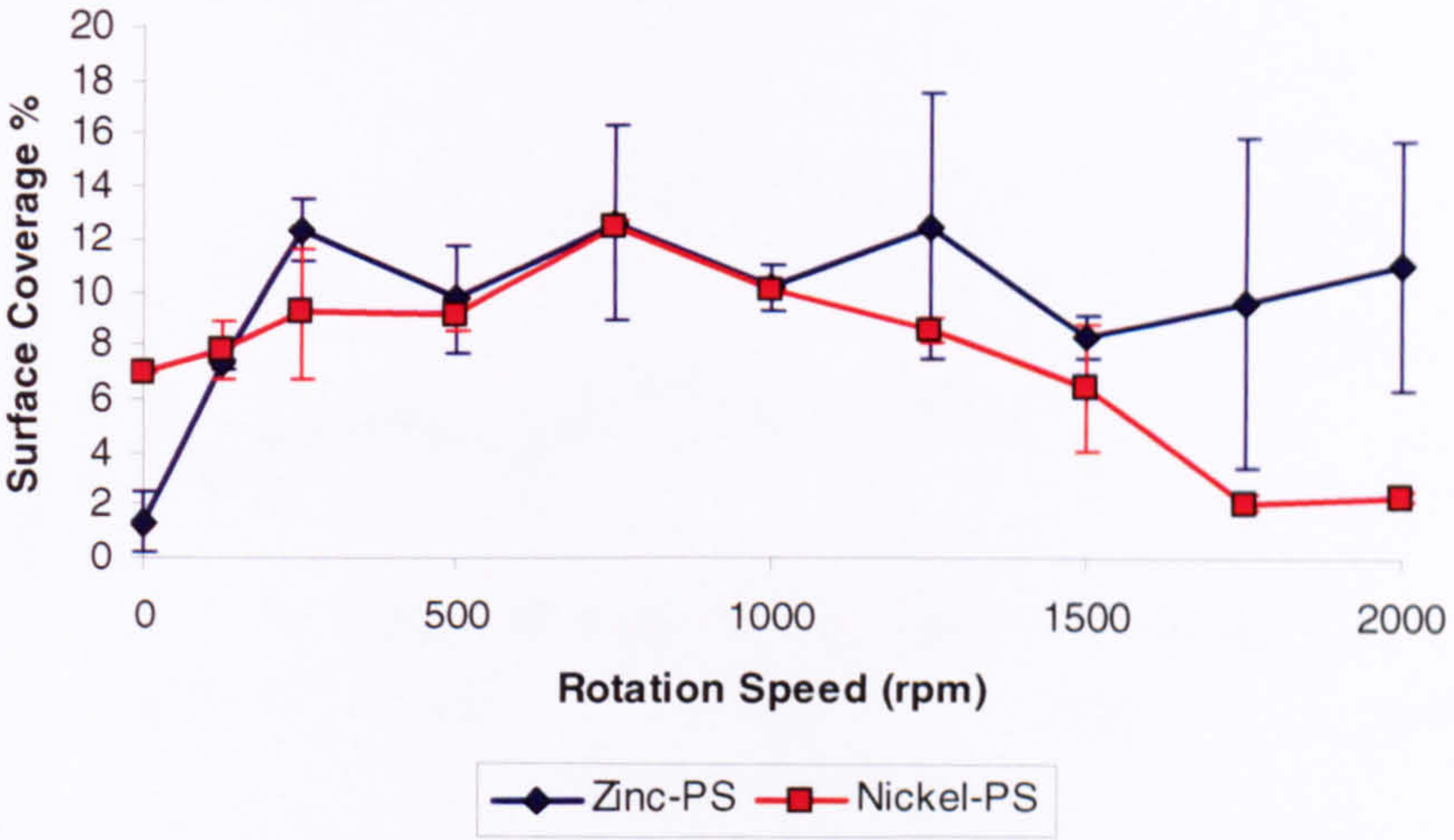

Figure 13.2 - Surface coverage *% vs.* cathode rotation speed for zinc-PS (red curve) and nickel-PS (blue curve) composite coatings produced at 5 A dm^{-2} and 2 g l^{-1} PS particles loading on 1.27 cm diameter AISI 316 stainless steel cathodes.

Also in this case, zinc-PS was the system that gave higher incorporation values for all the rotation speeds investigated. Only at very low rotation speed values did the nickel-PS system give higher incorporation percentages.

In all the cases, the concentration of PS particles incorporated reached a maximum usually at low cathode rotation speeds and then decreased with the increase of this parameter. Copper-PS and zinc-PS systems showed almost identical behaviour, while the nickel-PS showed lower levels of incorporation at all the rotation speeds. It is worth noting that the morphology of both copper and zinc, because of the "nodular striped" structures, was quite irregular (see Chapter 10), resulting in a heterogeneous distribution of particles in the coating. So the points on figures represent an average between very "rich" areas and very "poor" ones, in terms of particles incorporated. Nickel composite coatings were, on the contrary, flat and regular in terms of surface coating morphology (as shown in Section 10.1), and the distribution of particles incorporated was much more homogeneous at all rotation speed values.

13.2 Alumina composite coatings

Fig. 13.3 shows the concentration of 3 μm alumina particles incorporated as a function of cathode rotation speed for copper-alumina and nickel-alumina composite coatings obtained at 5 A/dm^2 and 29 g/l alumina particles loading on 1.27 cm diameter AISI 316 stainless steel cathodes.

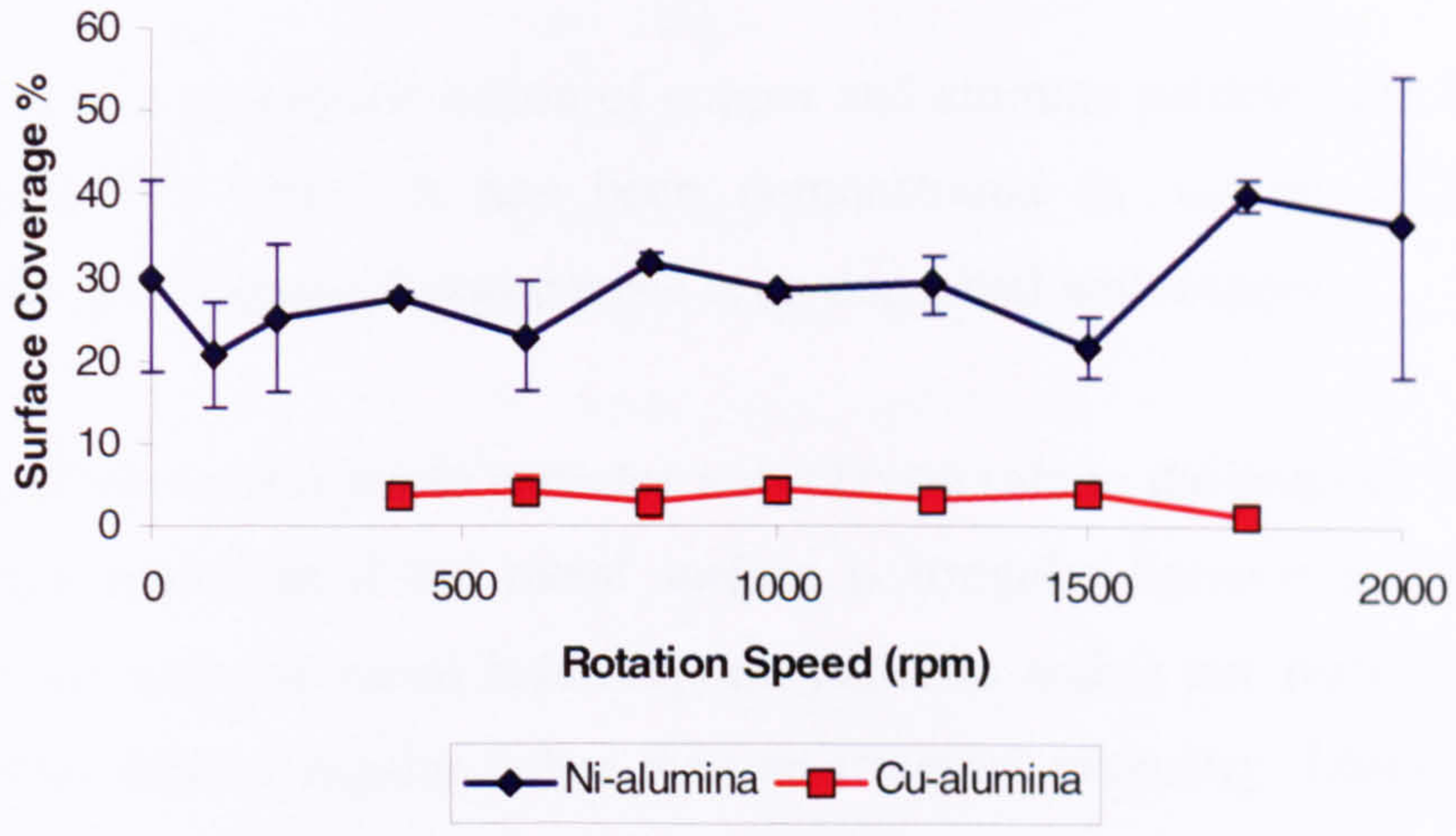

Figure 13.3 - Surface coverage *%* *vs.* cathode rotation speed for copper-alumina (red curve) and nickel-alumina (blue curve) composite coatings produced at 5 A dm^{-2} and 39 g l^{-1} alumina particle loading on 1.27 cm diameter AISI 316 stainless steel cathodes. Alumina particle size 3μm.

In this case the two systems showed very different behaviours, with the nickel-alumina system giving higher incorporation levels than the copper-alumina system.

Image analysis to evaluate the amount of particles incorporated was not possible on copper-alumina specimens obtained at very low rotation speeds (0, 100 and 200 rpm). This was because of dendrites growing at the coating surface making differentiation between deposit and particles very difficult.

The data shows clearly that the metal matrix had an influence on the incorporation process. This has also been confirmed by BANOVIC *et al.* [148]. They studied the nickel-alumina system as well, outlining interesting conclusions about the synergistic action of both metal matrix and alumina particles. The incorporation of alumina into the electrodeposited nickel was observed to affect the as-plated surface structure of the coating. They also found the "electrocomposite" surfaces observed were relatively flat and they demonstrated that this was due to the presence of particles in the electrolyte. Nickel electrodeposits are, in fact, reported to be liable to the formation of pyramidal structures that are not present if nickel is co-deposited with alumina. This results in a finer nickel grain size and a larger amount of grain boundaries capable of incorporating more particles. The smaller the grains, the higher the amount of particles incorporated. This is because particles usually deposit at grain boundaries, helped by vacancies, imperfections and discontinuities.

No evidence of a synergistic action of copper and alumina particles can be found in the literature [34], whilst it has been demonstrated in section 10.2 that this circumstance does happen if polystyrene is co-deposited with copper.

The shape of the second phase particles also plays a role in the process. The particle shape is less important if the metal surface is irregular because in this case the cavities of the growing metal layer capture particles and is not really important if these particles have a regular rather than an irregular geometry. Little evidence is present in the literature about this matter.

13.3 Second phase particle influences

As discussed in Section 3.1.3, composite coatings can achieve very different properties depending on the second phase material used. It has been shown that it is

possible to obtain smooth deposits rather than irregular ones simply by employing non-conducting particles rather than conductive ones [23].

In this work the choice of materials used as the second phase in the coatings produced was motivated essentially by two reasons:

- to gain information about the particle size influence on the process e.g. different alumina particle sizes, and
- to gain information about the material shape influence on the process, spherical vs. irregular and different particle sizes.

13.3.1 Electrodeposition of nickel with alumina, the influence of second phase particle size

Fig. 13.5 shows the level of alumina particles incorporated as a function of the cathode rotation speed for nickel-alumina composite coatings obtained at 5 A/dm^2 and 39 g/l alumina particles loading on 1.27 cm diameter AISI 316 stainless steel cathodes. Three sizes of alumina were used, particles of 0.3, 1 and 3 μm.

Due to difficulty in obtaining very thin electrodeposited layers, composite coatings with 0.3 μm particles were produced with a coating thickness of 1 μm. This has to be taken into account in the image analysis. In fact particles could be "buried" (see Fig.13.4) by the metal layer and their detection made impossible. This was already shown in Figs. 9.6 and 9.7 where very thick nickel coatings were produced: The presence of particles deep in the metal layer was documented by a cross sectional analysis of the specimen.

As a result, data obtained for 0.3 μm alumina particles were extremely variable, especially at high rotation speeds (see Fig. 13.5) with large error bars at all the rotation speeds. Data obtained for 1 μm alumina particles were coherent with that shown in Section 12.1 for nickel-PS composite coatings. Two ranges of rotation speeds were characterised:

- low rotation speeds: the trend was not true and large error bars were observed;
- high rotation speeds: the trend was quite clear and small error bars were observed.

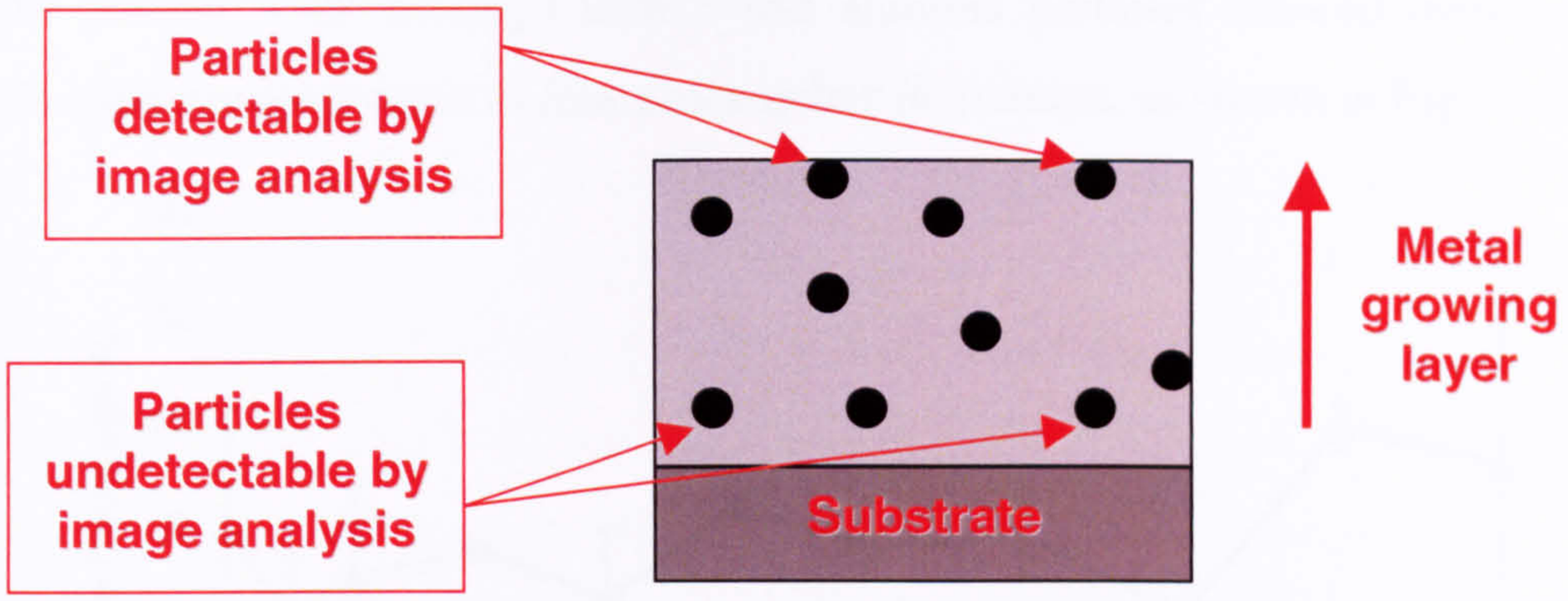

Figure 13.4 - Schematic of a composite coating where the coating thickness is greater than the particle size.

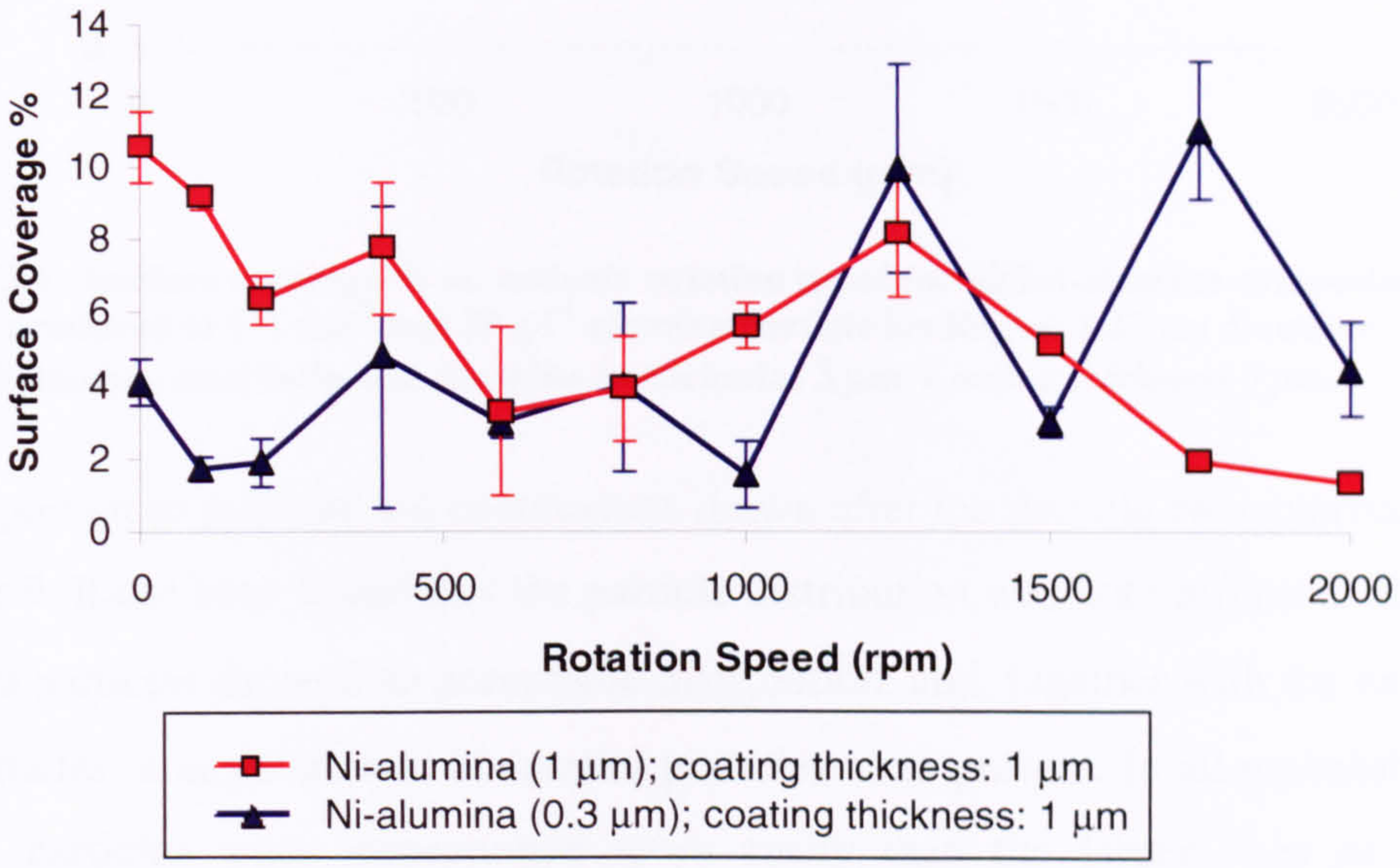

Figure 13.5 - Surface coverage *% vs.* cathode rotation speed for nickel-alumina composite coatings produced at 5 A dm^{-2} and 39 g l^{-1} alumina particle loading on 1.27 cm diameter AISI 316 stainless steel cathodes.

Up to 400 rpm, coatings with 1 μm particles seemed to be richer in alumina than those produced with 0.3 μm particles. This can cause confusion, in Ni-alumina coatings with 0.3 μm particles were probably richer in alumina, but the difficulty in detecting them (see Fig.13.4) made them seem poorer in particle content when compared with Ni-alumina coatings with 1 μm particles. Therefore, it is not easy to draw a conclusion about these influences. A further cross sectional morphology analysis should be carried out in order to find precisely how particles are distributed along the coating thickness for fine particle-containing deposits.

However, literature reviews suggest a poor influence of particle size on the codeposition process.

In the present work coatings with 3 μm alumina particles showed incorporation levels approximately three to four times richer in alumina, as shown in Fig. 13.6.

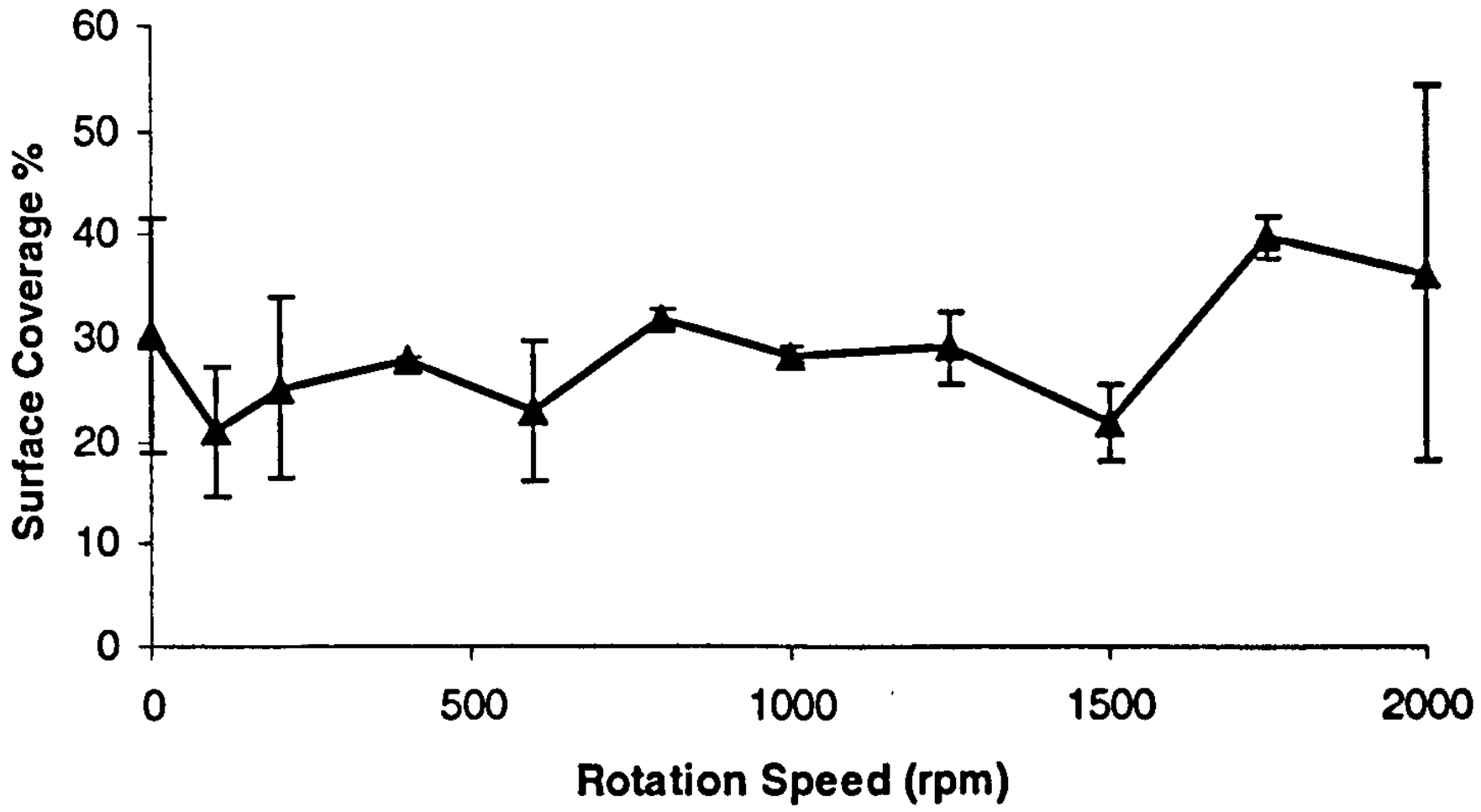

Figure 13.6 - Surface coverage % *vs.* cathode rotation speed for nickel-alumina composite coatings produced at 5 A dm^{-2} and 39 g l^{-1} alumina particle loading on 1.27 cm diameter AISI 316 stainless steel cathodes. Alumina particle size 3 μm. Coating thickness 3 μm.

It is important to reiterate the conclusions drawn after the particle characterisation in Chapter 9. It has been found that the particle distribution was not uniform at all, only 0.02 μm particles showed an acceptable distribution, and, together with the expected size particles, a large amount of smaller particles were present. In all probability the smaller particles were incorporated more easily than the larger ones as bigger particles experience greater centrifugal force in the electrolyte than the small ones. This could mask the results for the 3 μm alumina particle system resulting in smaller particles incorporated rather than single 3 μm ones.

13.2.2 Second phase material shape influences

Little evidence on particle shape influence has been reported in the literature. A 15 years old investigation, carried out by GRECO [65] studied the incorporation of fibres compared to particulate composites. The author noted that it was more difficult to produce composites containing fibres (regular shape) than particulate composites (irregular shape).

If the PS incorporation levels are compared with alumina incorporation levels in nickel coatings it can be seen that it was much easier to incorporate alumina than PS, the richest nickel-PS coating in PS had a surface coverage of 13.5 %, while that of

nickel-alumina was 39.8 %. This can be related to the particle shape of the second phase. Having irregular structures incorporated (alumina) is easier than having regular ones (the "spherical" PS), because an irregular structure, with cavities and peaks, can get "trapped" more easily on the growing metal layer. The metal growing layer can, for example, incorporate part of it and once the particle is attached to the surface, it can be totally incorporated afterward. In the PS case, because of the spherical shape of the particles, this is much more difficult so the particle needs to stay in contact with the cathode surface longer to get incorporated, and the probability of incorporation is lower. A possible schematic of this is shown in Fig. 13.7.

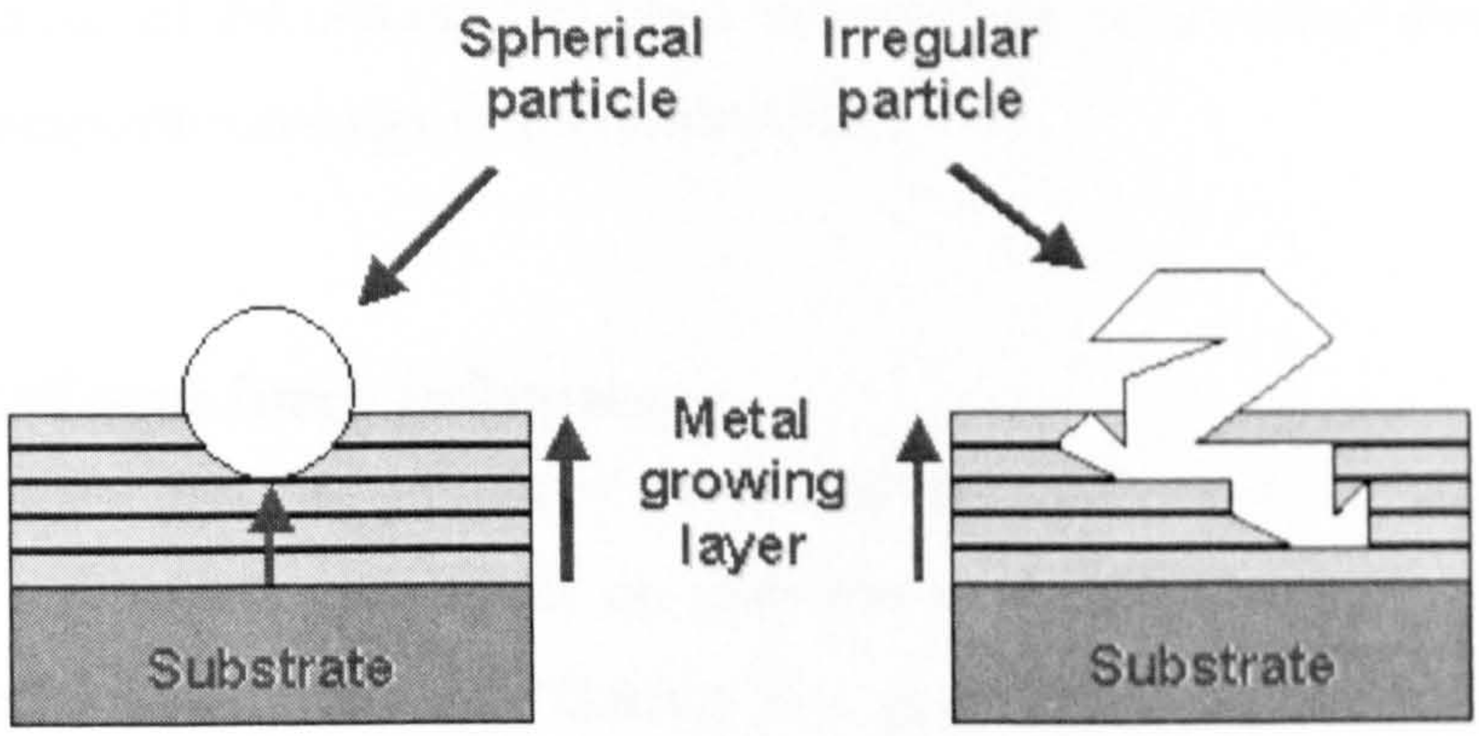

Figure 13.7 - Possible schematic for the incorporation of a regular and of an irregular particle in the metal growing layer.

This could be an explanation for the higher incorporation levels reported for nickel-alumina composites when compared to nickel-PS ones.

14. Flow behaviour and electrodeposition time influences

So far the process of electroco-deposition of composite coatings has been investigated focusing the attention on the cathode surface, looking at incorporation processes, coating morphology and hydrodynamics. This section aims to analyse how the particles are influenced when they are approaching the cathode surface. With regard to the cell design chosen, a rotating cylinder electrode cell, a study of the influence of centrifugal forces influence on particles is made.

An investigation of the coating thickness influence on the co-deposition process for nickel-PS composite coatings is also undertaken.

14.1 Centrifugal force influence

In order to find out the influence of centrifugal forces on the particles in the electrolyte, electrodeposition trials on cathodes with different diameters (1.27, 3.8 and 7.4 cm) were carried out. During this process, particles should experience different radial pressures due to the increasing centrifugal force as the distance from the axis is increased, see Fig. 14.1. This is true especially at low rotation speed, when the flow is laminar or in the transition phase (see Section 6).

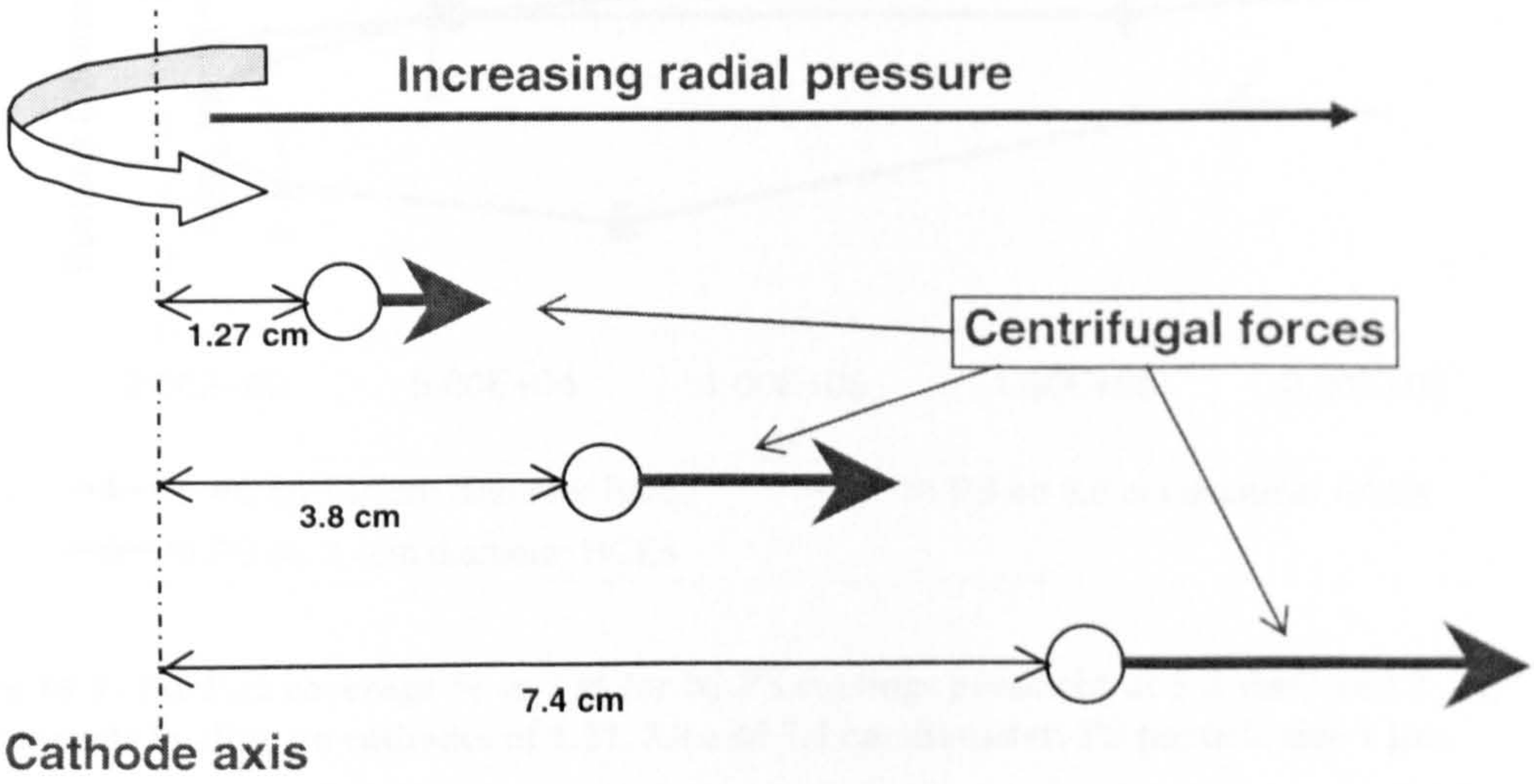

Figure 14.1 - Schematic of centrifugal forces on co-depositing particles as a result of the three diameters of RCE.

Fig. 14.2 shows PS particle incorporation plotted against $r\omega^2$ for nickel-PS composite coatings on 1.27, 3.8 and 7.4 cm diameter RCEs when $0< r\omega^2<2.00E+05$. In this way all the data are normalized with respect to centrifugal forces because the quantity $r\omega^2$ is directly proportional to the centrifugal force.

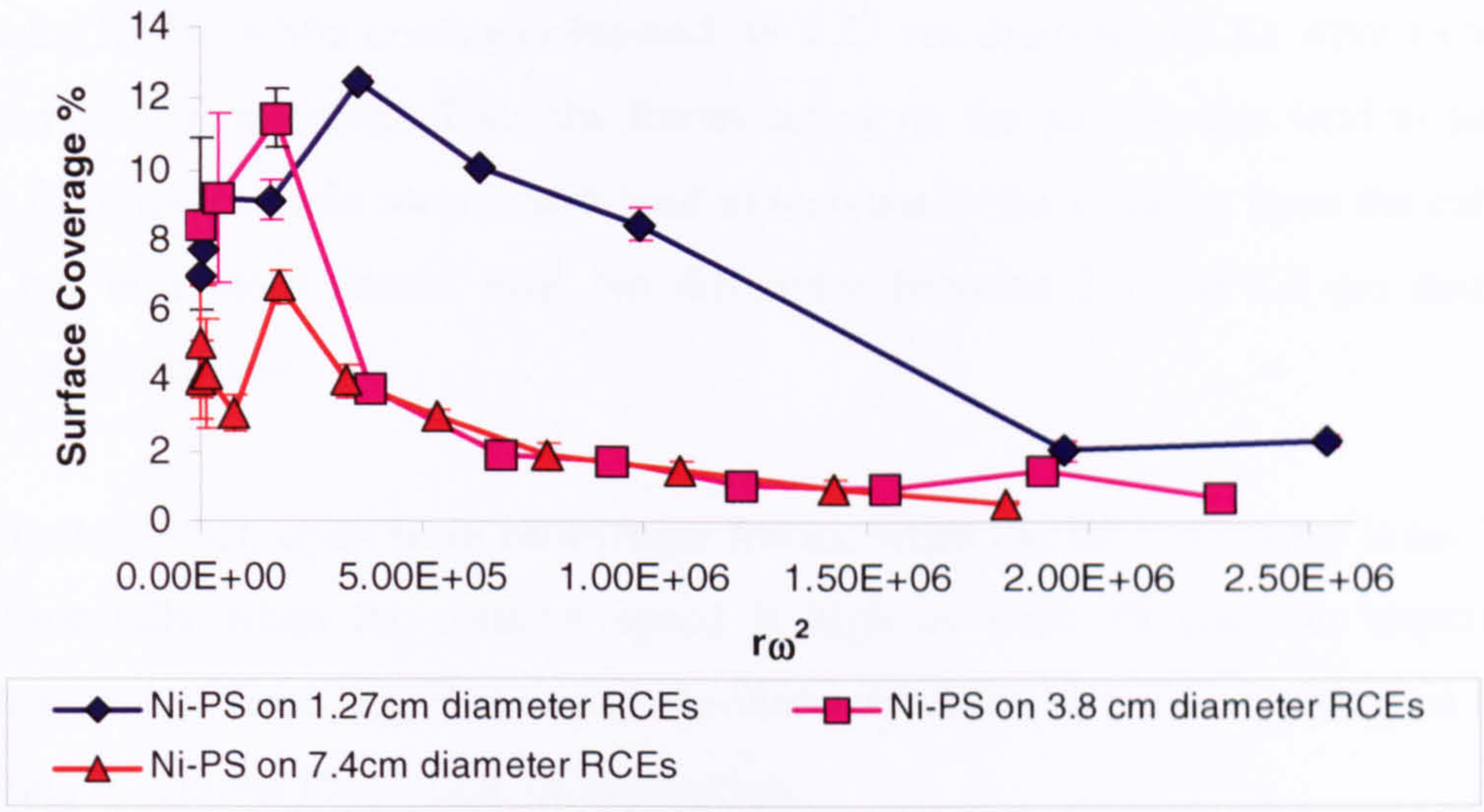

Figure 14.2 - Surface coverage *% vs.* $r\omega^2$ for Ni-PS coatings produced at 5 A dm^{-2} and 2 g l^{-1} PS particle loading on cathodes of 1.27, 3.8 and 7.4 cm diameter. PS particle size 1 μm.

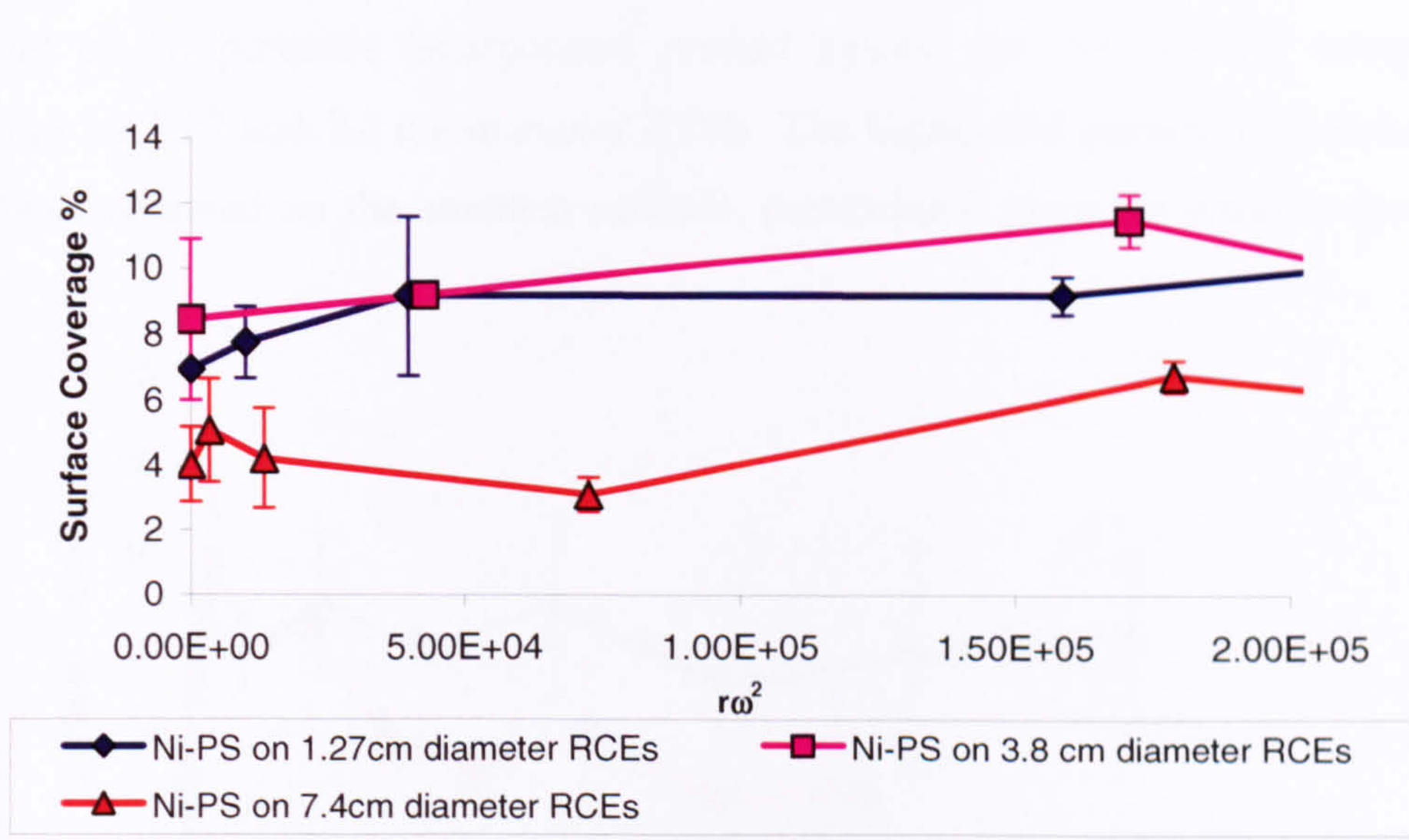

Figure 14.3 - Surface coverage *% vs.* $r\omega^2$ for Ni-PS coatings produced at 5 A dm^{-2} and 2 g l^{-1} PS particle loading on cathodes of 1.27, 3.8 and 7.4 cm diameter. PS particle size 1 μm.

At low $r\omega^2$ values (see Fig.14.3) the coatings obtained on 3.8 cm diameter cathodes gave PS incorporation levels comparable to those obtained on 1.27 cm diameter cathodes, while 7.4 cm diameter RCEs were the poorest in terms of particle

incorporated. Then when the flow can be assumed laminar, the forces acting on the particle that tend to push it away from the cathode surface tend to increase in a moderate fashion as the distance from the cathode axis is increased. At high values of the cathode diameter (see Fig. 14.2), composite coatings obtained on 3.8 cm diameter RCEs showed similar incorporation levels to the coatings obtained on 7.4 cm diameter RCEs, while coatings obtained on 1.27 cm diameter RCEs were richer in PS particles incorporated. Then the forces acting on the particle that tend to push it away from the cathode surface still tend to increase as the distance from the cathode axis, but in a more drastic way. No difference between 3.8 and 7.4 cm diameter RCEs was achieved.

This indicate that, apart from centrifugal forces, when the RCE diameter is too large and especially when the rotation speed is high as well, PS particles experience another kind of force, e.g. that due to the viscosity of the electrolyte, acting on them, resulting in a lower PS particle incorporation.

Similar conclusions can be drawn from the zinc-PS system. Fig 14.4 shows the amount of PS particles incorporated plotted against $r\omega^2$ for zinc-PS composite coatings on 1.27 and 7.4 cm diameter RCEs. The highest PS particle incorporations are those obtained on the smallest cathode, particularly when the rotation speed is high.

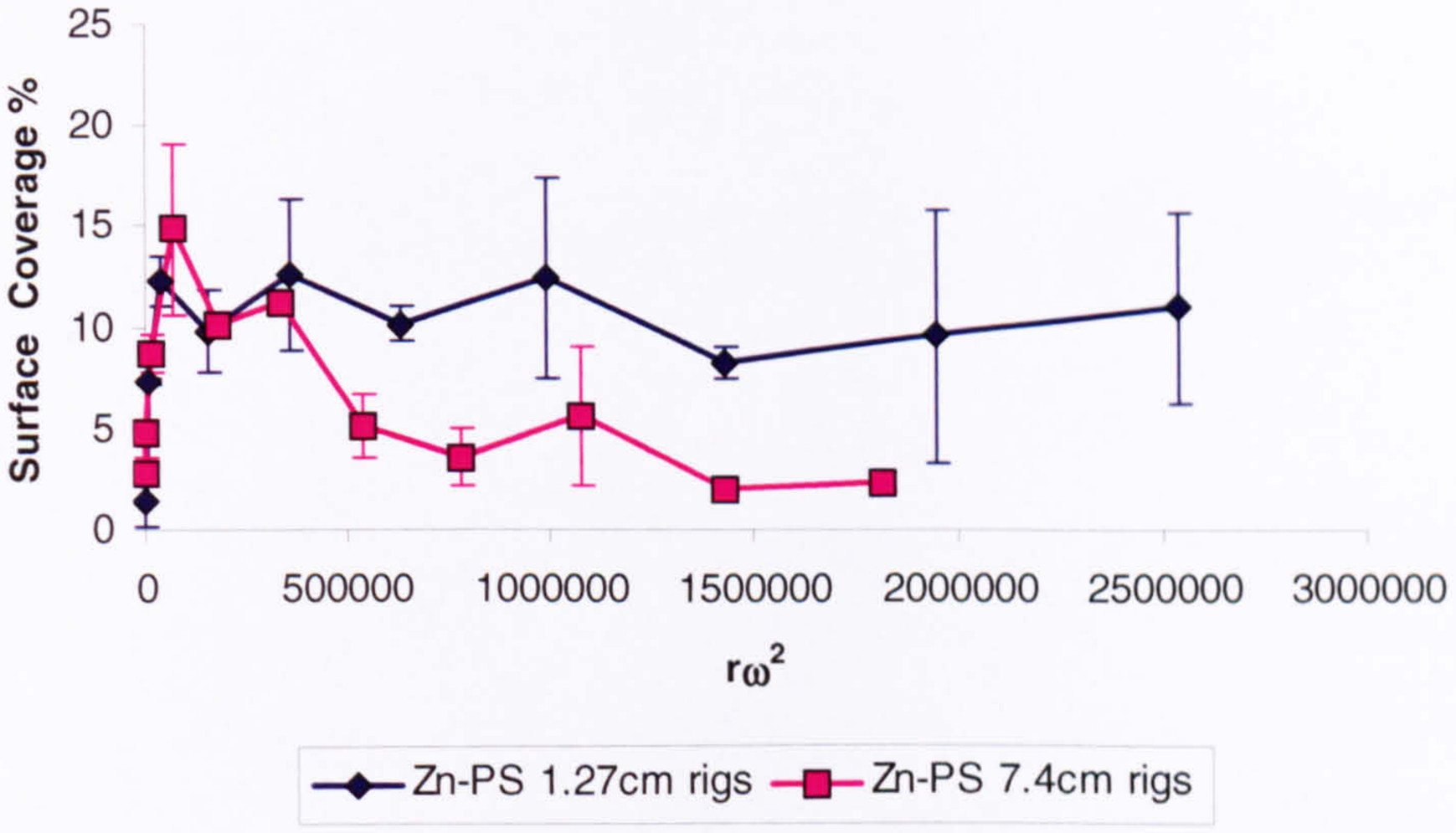

Figure 14.4 - Surface coverage *% vs.* $r\omega^2$ for Zn-PS coatings produced at 5 A dm^{-2} and 2 g l^{-1} PS particle loading on cathodes of 1.27 and 7.4 cm diameter. PS particle size 1 µm.

It is interesting to note that in the literature few studies consider the influence of centrifugal forces. This probably because the majority of mechanisms proposed has been formulated considering different agitation systems rather than the "rotating cylinder electrode" technique.

In Section 4.7 it was shown that FRANSAER, CELIS AND ROOS [98] proposed a model for the electrolytic co-deposition of spherical particles with metals on a rotating cylinder electrode based on a trajectory analysis of the particle deposition. But, in their theory, they chose a criterion of particle attachment once in contact with the electrode in which they assumed that all particles stick to the electrode upon contact. This assumption does not take in account the influence of centrifugal forces. Their balance of forces acting on the particle once in contact with the cathode surface should be changed in order to take in account centrifugal forces, see Fig. 14.5.

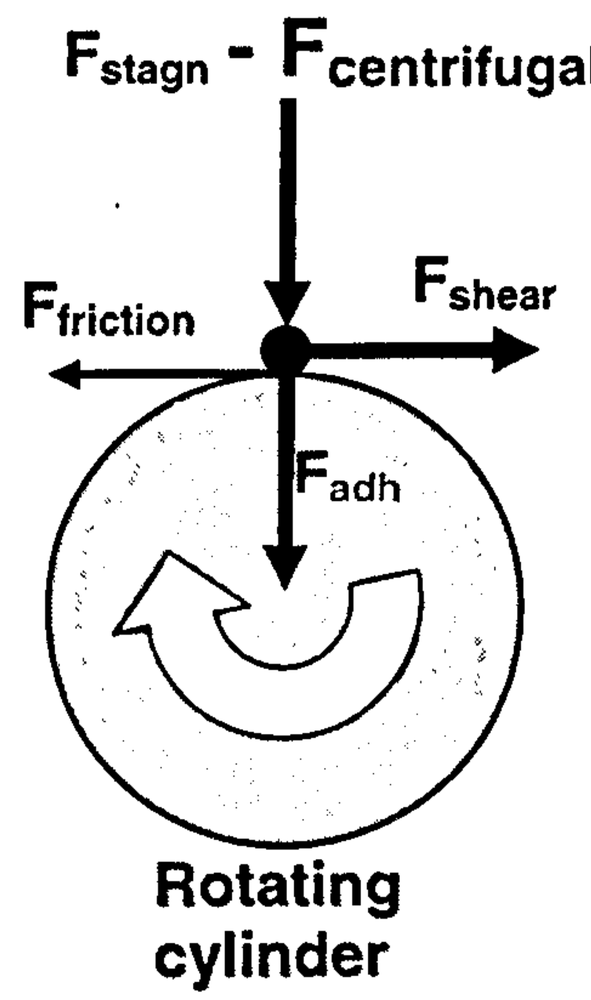

Figure 14.5 - Schematic of the various forces acting on a particle near a plane surface [98] modified to take into account the centrifugal force proposed in the present work.

14.2 Coating thickness influence

In order to evaluate the coating thickness influence on particle incorporation process, a set of trials was carried out using different electrodeposition times (25, 50, 75, 100, 116 s). In this manner coatings of different thickness ranging between 0.4 and 2 μm were obtained. In all cases the current density was 5 A/dm^2 and the rotation speed 750 rpm. Fig. 14.6 shows SEM images of the surfaces of these electrodeposits.

Between 25 (0.4 μm of thickness) and 75 (1.3 μm of thickness) seconds particle prints are clearly evident in the micrographs. This suggests that immediately after the initiation of electroco-deposition, particles are in contact with the cathode surface, hence the presence of their imprints, but they cannot be incorporated. The real incorporation seems to take place in the last seconds of the deposition.

After 75 seconds the layer thickness is 30% larger than the particle diameter, but this did not enhance the co-deposition of particles.

Only after 100 seconds (1.7 μm of thickness), when the metal layer thickness is 70% larger than the particle diameter, co-deposition took place with a large number of particles. Figs. 14.10 (d) and 14.10 (e), in fact, show far more particles incorporated than the previous three micrographs.

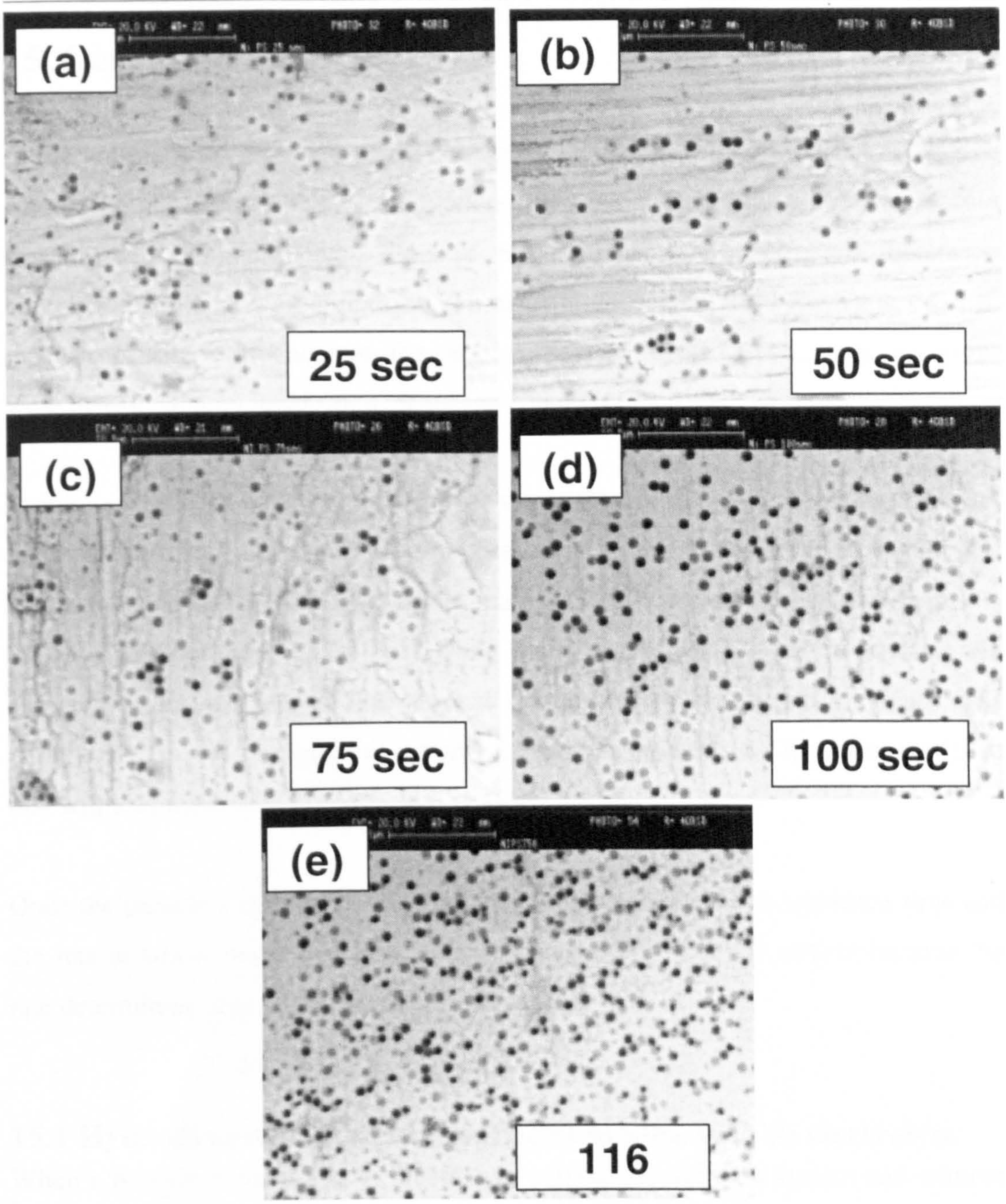

Figure 14.6 – SEM micrographs of nickel-PS electrodeposits obtained at 5 A dm^{-2}, 750 rpm and 2 g l^{-1} PS particle loading after: (a) 25 sec, (b) 50 sec, (c) 75 sec, (d) 100 sec, (e) 116 sec. PS particle size 1 μm.

15. General discussion

In the present work the electrolytic co-deposition of a metal with inert particles was studied. In particular, different electrodeposition parameters influencing the process were investigated and different kinds of inert particles in terms of shape, dimension and chemical nature were employed. Three different metals were chosen in order to evaluate possible influences on the process. Several levels of electrolyte agitations were investigated by means of a "Rotating Cylinder Electrode" cell.

In this section a possible mechanism for the co-deposition of a metal together with inert particles is proposed. The co-deposition is a process resulting from different mechanistic steps. Initially the particle mass transfer towards the cathode surface is the rate determining step. In fact, while metal ions present in the electrolyte are attracted by the cathode surface because of the presence of an electric field, inert particle are, initially at least, not charged, resulting in the need for a driving force that will lead them to be co-deposited with the metal.

Once the particle comes in contact with the cathode surface, the residence time and the rate at which metal ions reduce themselves on the cathode surface became the rate determining step of the entire process.

15.1 Hydrodynamic influence, particles motion into an electrolyte

When a particle is placed in an electrolyte without an agitation system and without an electric field, the only force acting on it, apart from possible natural convection, is the gravitational force that tends to bring the particle to the bottom of the cell. Metal ions are present in the solution at this stage, and particles in the bulk of the electrolyte can obtain an ionic cloud by adsorbing ions from the solution. At this stage of the process the chemical nature of the second phase material, together with its shape, play a key role on the ions' rate of adsorption. The metal under consideration is also important: different metals, in fact, produce ions with different diameters, therefore influencing the adsorption from a steric point of view. Particles with a net positive charge on the surface are easer to incorporate than those either negatively charged or neutral. In order to enhance incorporation, additives can be

added to the electrolyte solution with the purpose of increasing the level of adsorbed metal ions. Sometimes the use of cationic surfactants [1] avoids particle agglomeration by conferring a net positive charge on the particles with the additional benefit of increasing particle attraction to the cathode. The disadvantages are that surfactants and additives can also be incorporated in the deposit with detrimental effects and that they are competitors to metal ions in become adsorbed on the particle surface.

The cell system utilised in the present work, a RCE, is able to introduce different levels of agitation (see Section 8.3). If the solution is agitated, then particles can randomly move within the electrolyte. In their motion they can contact the electrode surface and this can represent the first driving force able to propel particles towards the electrode surfaces both cathode and anode as the particle motion is purely random without the presence of an electric field.

With the aid of an external current source, a potential difference can be applied across the electrodes and therefore an electric field is created within the electrolyte. This electric field makes possible the motion of metallic ions towards the cathode surface, where they can be reduced becoming electrodeposited metal. The electric field does have an effect also on inert particles that are neutral, but their surface is saturated with adsorbed metal ions, therefore a net positive charge is created on their surface. An electrophoretic motion arises and this represent the second driving force able to propel particles towards the electrode surface which in this case will be towards the cathode, see Fig. 15.1.

In the present work several electrode rotation speeds were investigated (see chapter 12) and these produced coatings with different levels of particle incorporation, proving that the electrolyte agitation is a parameter that does influence the co-deposition process. Different agitation levels result in different numbers of particles coming into contact with the cathode surface per unit time. As a consequence of this, an increasing particle content in the coating would be expected as the electrode rotation speed is increased. This does not occur and different effects can be encountered if the agitation level is increased (see Section 12.1). Three different

hydrodynamic regimes can be discerned: pure laminar, a "transition regime" and turbulent existed.

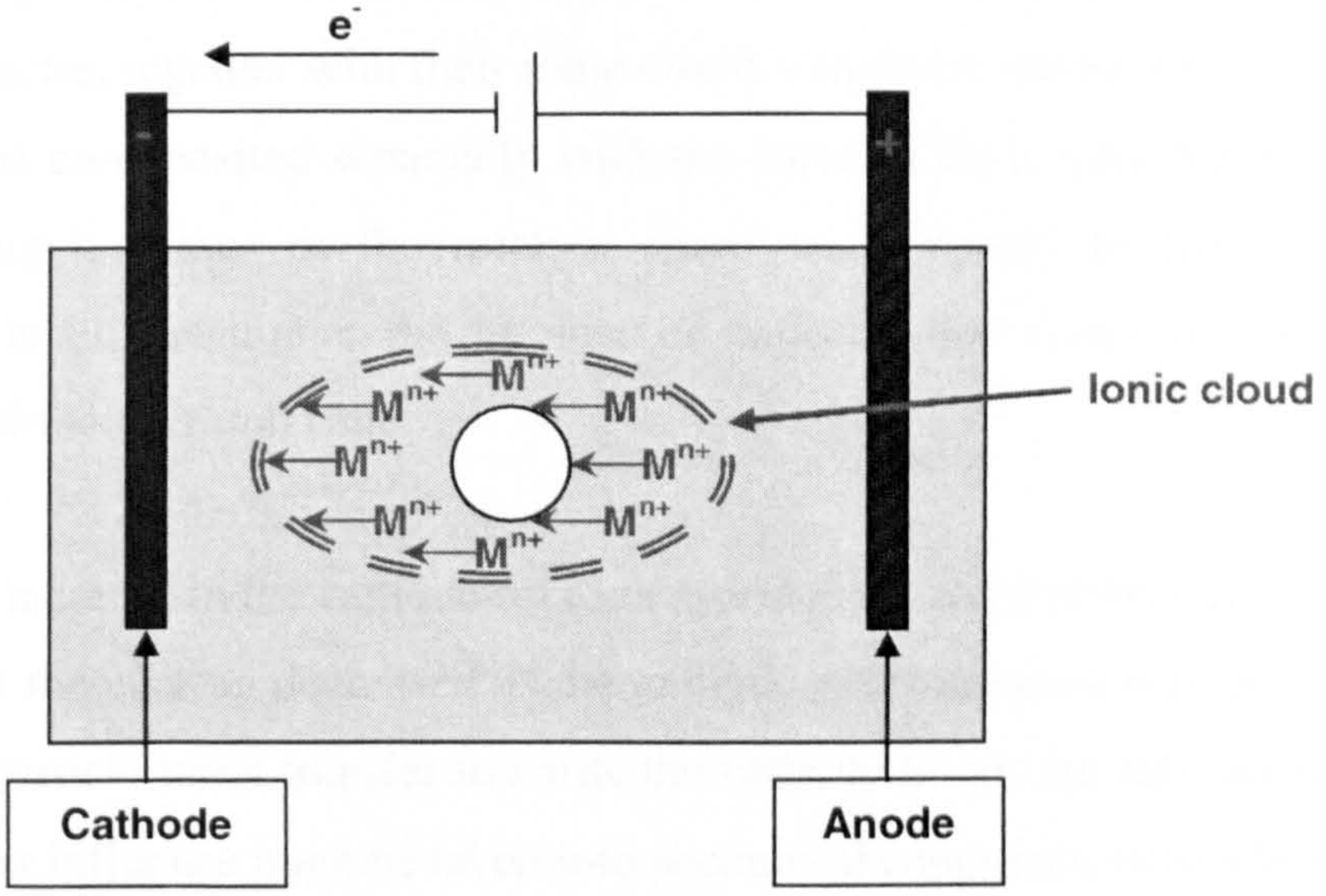

Figure 15.1 - Schematic for electrophoretic motion of inert particles within an electrolyte under an electric field.

When the electrolyte flow along the cathode surface was purely laminar, an unstable trend in terms of particle content in the coatings was obtained. In effect there was no influence created by the rotation speed and coatings were produced with a heterogeneous distribution of particles in the electrodeposit. This has been proved by the presence of large error bars for coatings obtained in this range of rotational speeds, by the absence of a clear trend and by morphological studies. This happened because particles were incorporated as "agglomerates" rather than individuals (see Figs 12.2 and 12.3). The technique chosen to evaluate the particle level in the coating, the image analysis, produces not accurate data in this hydrodynamic regime. All the experimental points reported were averages between different locations on the coating surface. At low cathode rotation speed, because of the presence of agglomerates, coatings were heterogeneous in terms of particle distribution, resulting in averages between "rich" and "poor" areas in terms of particle levels (see Section 12.1). The incorporation of particles as agglomerated structures has been widely reported in the past [47, 58, 72, 117].

As the cathode rotation speed was further increased, a "transition regime" was encountered. In this case the particle level in the coating initially decreased reaching

a minimum value, it then increased until a maximum was obtained (see Figs. 12.1 and 12.9). It is reasonable to postulate that in this case the agitation level is able to bring the particles to the cathode surface and break the agglomerates at the same time. Particles, together with their ionic cloud, can move towards the cathode surface and can be co-deposited separately with the metal. This is why the particle level in the coating increases as the rotation speed is increased. In fact the higher the agitation level, the higher the number of particles that come in contact with the cathode surface per unit time.

A further increase in the cathode rotation speed produced a reverse trend: the particle content of the coating decreased as the cathode rotation speed was increased. In this case the particle mass transfer towards the cathode is not the rate-determining step, but another influence must be taken into account: the presence of an electric field and the reduction of metal ions onto the cathode surface. Fig.15.2 shows particles in the electrolyte when the flow along the cathode surface is laminar and in the "transition zone".

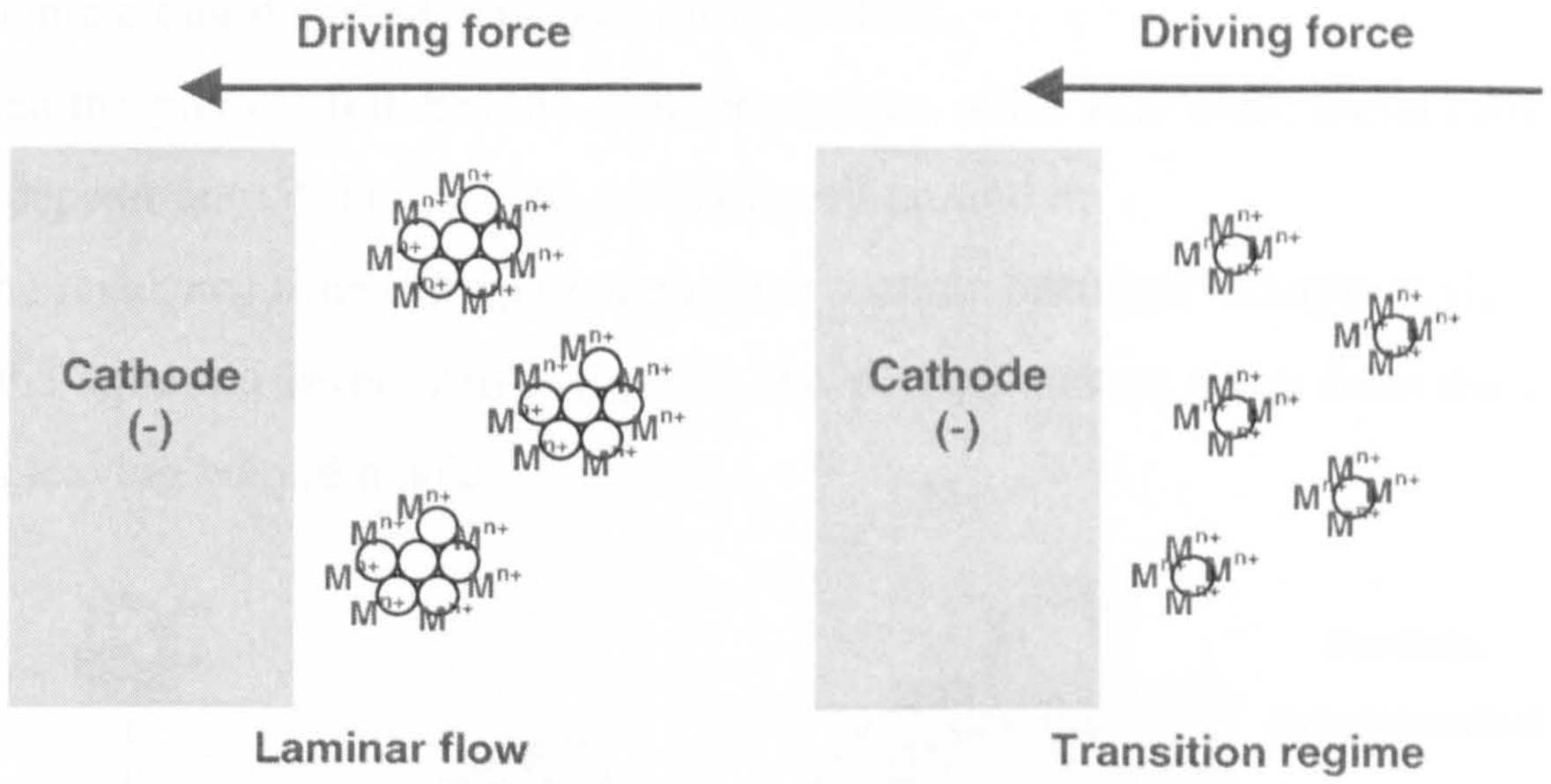

Figure 15.2 - Particles in the electrolyte under different hydrodynamic conditions.

15.2 Electrodeposition of metal: the influence of the metal ions' reduction rate

When the electrode rotation speed produces a turbulent flow along the cathode surface a reverse trend was obtained. This suggests that a different rate-determining step is acting.

The key point at this stage of the process is how fast the metal layer is growing on the substrate. In particular, the rate at which the metals ions, adsorbed on the inert particle surface, are able to reduce. The agitation of the electrolyte is very high in this regime, so it is reasonable to imagine that there is not inert particle mass transfer control. A large number of particles can reach the cathode surface, but they must stay in contact for sufficient time to allow the growing metal layer to incorporate them. The ions adsorbed on the inert particle surface are reducing on the cathode creating, because of conduction, a sort of "anchor" that tends to keep the particles attached to the cathode surface. The process is now under charge transfer control. Therefore, depending on the cathode rotation speeds, an equilibrium is created: a certain number of particles will be anchored and eventually be incorporated, whilst other particles will be removed prior to being eventually incorporated. This was proved by the presence of holes on the coating surface when the cathode rotational speed was high, see Figs. 10.1 and 10.2, and their absence when the speed was low. Fig. 15.3 shows a schematic for this mechanism:

(a) particle is moving towards the cathode surface because of agitation and because of the ionic cloud positively charged on its surface;

(b) when the particle touches the cathode surface, since it is inert, metal ions cannot electrodeposit onto it, but instead, must deposit around it;

(c) if the residence time is long enough, then particle becomes incorporated;

(d) if the agitation level is to high, then the particle moves away from the cathode surface leaving behind a hole.

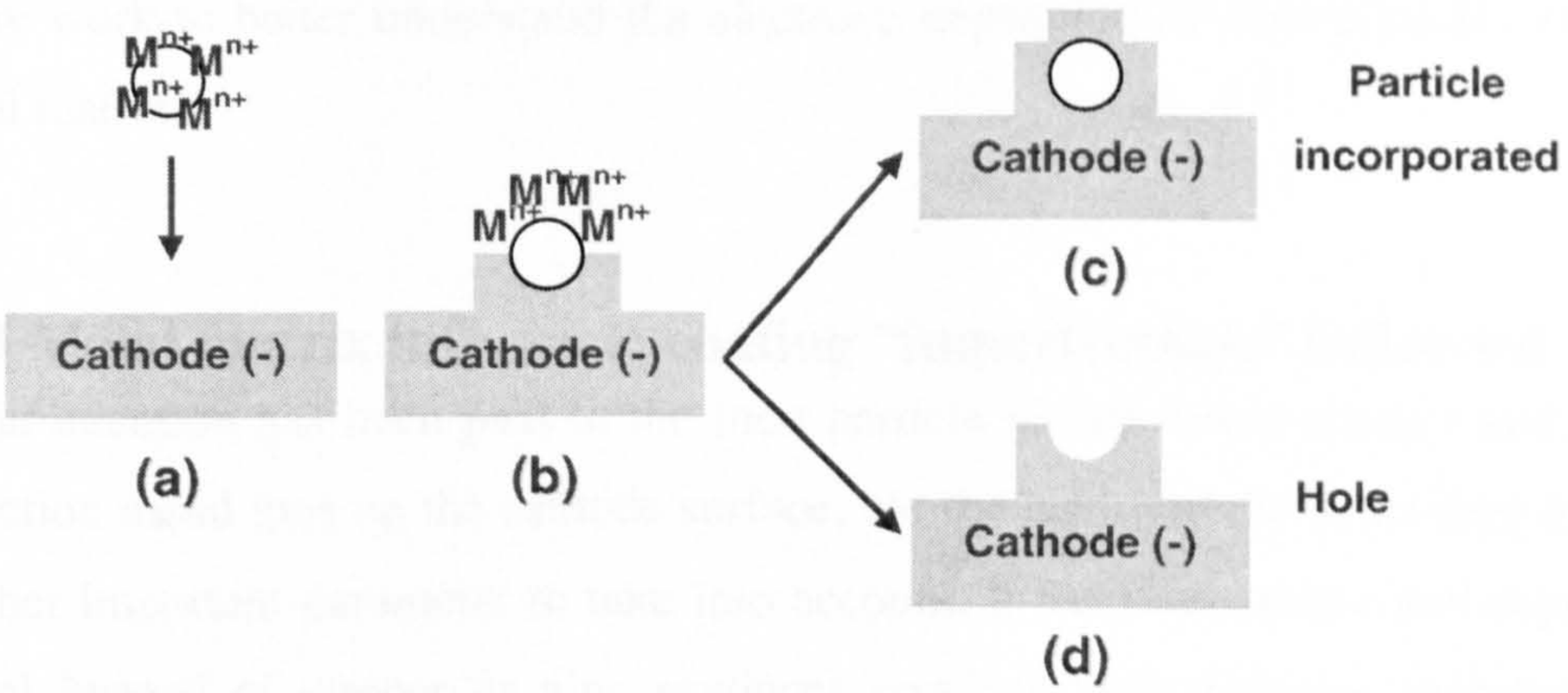

Figure 15.3 - Schematic for particle incorporation when the electrolyte flow along the cathode surface is turbulent:

Another parameter that is also very important is the particle geometry. It has been shown in Section 13.2.2 that if nickel-PS and nickel-alumina composite coatings obtained at the same experimental conditions are compared, it was much easier to incorporate alumina than PS. This was attributed to irregular shape of alumina, with cavities and peaks. The nickel ions adsorbed on the alumina surface can reduce on the cathode entrapping part of the particle. The growing metal layer can incorporate the rest of the particle afterwards, see Fig. 13.7. This is not possible for the spherical PS particles: to have a successful contact between particle and metal layer, nickel ions adsorbed on the PS particle must reduce on the cathode surface fast enough to be able to incorporate most of the particle, not a small part of it as for alumina. If this does not occur, the PS particle is removed from the growing metal layer because of the electrolyte agitation.

The studies carried out to investigate the coating thickness influence on particle incorporation process provide support to this theory, see Section 14.2). A significant amount of PS particles incorporated were obtained only when the coating thickness was much larger than the particle diameter, about 1 μm. An absence of particle incorporation was noted when the coating thickness was less than 1.3 μm, but high levels of incorporation were reported when the coating thickness was between 1.7 and 2 μm. In all probability, if alumina would be co-deposited with nickel, it would be possible to obtain higher incorporation levels at lower coating thickness, just because of the irregular shape of the particles. This could be the subject of possible future work to better understand the electroco-deposition of inert particles within a metal matrix.

15.3 Metal matrix influence: coating "imperfections" influence

So far attention has been paid to the inert particle incorporation process and on the reduction metal ions on the cathode surface, but the nature of the depositing metal is another important parameter to take into account. It has been shown that depositing nickel instead of copper or zinc produces coatings with different morphological characteristics. This causes a further influence on the process and the coating morphology itself, in fact, does influence the co-deposition process. For nickel-PS

composite coatings, it has been shown that incorporated particle concentration is higher in the vicinity of a surface imperfection, see Figs. 10.3 and 10.4.

When copper was deposited together with PS particles, "nodular striped" structures were present on the final coating surface. These nodular stripes that were attributed to localised accelerated growth orientation, typical of copper deposition, showed a very high concentration of particles incorporated when compared to the rest of the coating. Such structures proved to result from the presence of inert particles in the electrolyte.

The same result was found for zinc-PS composite coatings. Furthermore these composite coatings showed a significant level of particles incorporated at high cathode rotation speeds compared to nickel-PS and copper-PS. Fig. 12.9 shows that at high cathode rotation speeds large error bars are present, with surface coverage levels up to 5% at 540 rpm. This was related to the coarse morphology the zinc deposits exhibited at high cathode rotation speeds.

All this evidence suggests a possible mechanism to take into account the influence of the metal coating morphology. Small imperfections on the coating surface influence the particle incorporation process possibly with the following mechanism.
Near the imperfection the hydrodynamic regime is locally altered reaching a higher turbulence, which allows the particles to have a higher number of contacts with the surface. This also allows the creation of stagnant zones where particles are immobilised and become incorporated into the growing metal layer (see Fig. 10.5). The higher turbulence also permits a higher local limiting current density, so the coating can grow faster locally. Therefore, the particles have a higher probability of being incorporated in these regions because of the locally higher current density, locally higher turbulence (increasing number of particles in contact with the surface) and creation of stagnant areas (capable of holding particles prior to their incorporation).

Of course, different electrodeposited metals show different kinds of imperfections: surface cracks when nickel is deposited, dendritic growths for copper and coarse surfaces at high cathode rotation speeds for the zinc system. In all cases these areas

were found to be significantly richer in incorporated particles than the rest of the coating.

Another aspect of the co-deposition of copper with PS particles to be analysed is the formation of "comet type" structures with high concentration of particles incorporated. A similar phenomenon was also found, but on a minor scale, for zinc-PS composite coatings. The formation of a structure perpendicular to the coating surface, the "comet type" nodules, see Fig. 10.11, causes two consequences:

1. a local mixing of the electrolyte;
2. a flow that is not parallel to the cathode surface. Particles can hit the metal surface perpendicularly, as shown in Fig. 10.12. In such a situation the probability for particle incorporation is higher at the head rather than at the tail of the "comet".

Other evidence that supports the proposed mechanism was the fact that when cathodes were electrodeposited with a 1 μm nickel coating prior to co-deposition with copper and polystyrene thus avoiding the formation of immersion coatings prior to electroco-deposition and hence a smoother surface to deposit on the phenomenon of "nodular striped" structures still occurred, but in this case the stripes were much smaller. Therefore it is reasonable to state that the initial roughness of a substrate prior to deposition does enhance local re-mixing of the electrolyte promoting the formation of structures with higher incorporated particle levels.

What has been discussed in this section is in agreement with what was found when studying the hydrodynamic influence (see sections 15.1 and 15.2). The two phenomena act simultaneously on a different scale: micro scale for particles incorporation and metal ion reduction reactions, while it is a macro scale when the substrate roughness influences the process.

15.4 The synergistic action of metal and inert particles

It was shown how the presence of particles in the electrolyte promotes the formation of composite coatings with a different morphology compared to that obtained when only the metal is deposited. This was attributed to the presence of particles in the

electrolyte, but it is interesting to note that the same kinds of particle produce different final coating morphologies depending on the co-deposited metal. This is because there is a synergistic action between the metal and particles. "Nodular striped" structures found on copper-PS composite coatings, were also present, to a smaller extent, on zinc-PS composite coatings, but not found at all on nickel-PS composites. It is clear that the phenomenon is enhanced by the presence of particles in the electrolyte and this was verified by the absence of such structures when copper alone was deposited.

When copper is deposited, the tendency of this metal to grow dendritically strongly emphasises the formation of nodular structures with rich particle contents. A dendritic growth, in fact, can be considered as the first step of the formation of "nodular striped" structures, being a sort of surface imperfection that can grow and incorporate particles following the mechanism proposed in Section 10.2. Even avoiding the formation of copper immersion coatings, the stripes obtained were significantly larger than those found on zinc composites. Totally different behaviour was found for the nickel-PS composites coatings, where only flat and regular morphology and no nodular structures were detected. This therefore strong illustrates the relationship to the metal employed.

At this point another parameter should be investigated as well: it is reasonable to imagine that current density plays a key role in this matter. Most coatings produced in the present work were obtained at 5 A/dm^2. At this current density, "nodular striped" structures were found for copper and zinc when co-deposited with PS. They were not found on nickel-PS composites, but probably, if the current density was further increased, such structures would also appear for this system. A literature review suggests [148], in fact, that at high current densities the nickel particles are being incorporated faster than they can diffuse across the surface. This results in the growth of nickel around the particle becoming rough and the formation of a ridge. This, as shown for copper and zinc systems, could be the promoter for the formation of structures with higher incorporated particle concentrations, following the mechanism proposed in section 15.3. This could be the subject of possible future work to better understand the electroco-deposition of inert particles within a metal matrix.

15.5 The influence of a cylindrical cell design

So far the process of electroco-deposition of composite coatings has been investigated focusing attention close to the cathode surface, but the effect of RCE on particles in the bulk of the solution also needs to be considered. These particles will be subject to different kinds of forces.

In order to investigate which kind of forces are involved in the process, a study on the influences of centrifugal forces was carried out. The starting point was that if inert particles within the electrolyte experience centrifugal forces they would be different for composite coating processes on rotating cylinder cathodes with different diameters (see Fig. 14.1). This is because particles, during the process, should experience different radial pressures due to the increasing centrifugal force as the distance from the vertical rotational axis is increased. In theory, if data are plotted against $r\omega^2$, a quantity proportional to the centrifugal force, then they are normalised with respect to centrifugal forces. If centrifugal forces are the only ones acting, the plots obtained for different cathode diameters must overlap.

Data did not overlap and incorporation levels decreased when the cathode rotation axis distance was increased. This means that apart from centrifugal forces, other forces are acting on the particles in the electrolyte. Forces that tend to push particles away from the cathode surface and that increase their influence as the distance from the cathode rotation axis is increased, strongly experienced when the flow can be assumed to be laminar.

Such forces, for instance, could be due to the viscosity of the electrolyte and this could be the subject of possible future work to better understand the electroco-deposition of inert particles within a metal matrix. Co-deposition of composite coatings is a process that has been widely studied mainly using RDE cells. Very little work has been carried out using a RCE cell.

16. Conclusions

In the present work the electroco-deposition of inert particles within a metal matrix was investigated using a rotating cylinder electrode system.

- A SEM characterisation of the inert particles used was carried out.
- A reliable method for a qualitative and quantitative detection of second phase particles in the coating was produced.
- Nickel-polystyrene composite coatings were obtained with a maximum of 12.5 % of PS particles surface coverage.
- Copper-polystyrene composite coatings were obtained with a maximum of 7.7 % of PS particles surface coverage.
- Zinc-polystyrene composite coatings were obtained with a maximum of 15 % of PS particles surface coverage.
- Nickel-alumina composite coatings were obtained with a maximum of 30 % of alumina particles surface coverage.

A morphological study of the coatings produced was performed.

- Two different kinds of particle-related features were characterised: particles totally incorporated into the electrodeposit and holes (imprints of particles loosely attached to the surface and lost with the ultrasonic treatment after electroco-deposition).
- Small imperfections on the coating surface and the initial substrate finishing did influence the particle incorporation and a possible mechanism was proposed.
- The presence of particles in the electrolyte influenced the final coating morphology. Differences between metal-only and composite coatings in terms of surface morphology were shown.

The rotating cylinder electrode system was used to investigate the influence of different level of agitations on the electroco-deposition of composite coatings process.

- A correlation between surface morphology and particle incorporation levels was proposed. In particular the two different kinds of particle-related features found were related to the electrolyte agitation level.
- The incorporation of particles agglomerates at low agitation levels was proved.
- The presence of three different zones in terms of agitation levels with different hydrodynamics (laminar, a transition zone and turbulent) was found.
- Different process rate-determining steps were proposed with regard to the three different zones in terms of agitation levels:
    - *in the laminar zone the process was under agglomerated particle transfer control*: the SEM analysis that was carried out clearly proved the presence of agglomerates of particles incorporated in the coating produced. As a consequence, the evaluation of the incorporated particles density gave very scattered data.
    - *In the transition zone the process was under particle transfer contro*l: this was evident by the fact that an increase in cathode rotation speed provoked an increase in the density of incorporated particles. Agglomerates of particles were not detected by means of SEM analysis.
    - *The reduction of ions adsorbed on inert particles was the rate-determining step in the turbulent zone*. In this case the particle residence time on the cathode surface was important and this was proved by the presence of a maximum in incorporated particles density *vs.* cathode rotation speed.
- The particle size distribution played a key role in alumina composite systems, not allowing a reliable analysis of the particle size influence on the co-deposition process. The particle distribution of the alumina powders used in this work was very poor. It was proved that particles suspended in the electrolyte experienced different forces. In particular, the centrifugal force is proportional to the particle mass. Therefore in all probably particles with large mass are more difficult to incorporate than smaller particles, thus the instability of the plots produced for this system due to different particles sizes being incorporated rather than the suggested nominal one.

Nickel, zinc and copper were successfully used to produce composite coatings with either polystyrene or alumina in order to investigate the influence of both the metal matrix and second phase material on the electrolytic co-deposition process.

- A relationship between metal and particle was shown. The same kind of particle produced different final coating morphologies depending on the co-deposited metal.
- When copper was deposited with PS on mild steel, the coating obtained showed very poor adhesion. Adhesion was improved by flash-plating mild steel with 1 μm nickel deposit prior to electroco-deposition.
- The strong influence of particle shape was highlighted and related to the reduction of ions adsorbed on the particle surface. In particular it was easier to incorporate irregular rather than regular particle geometries.

An investigation into the forces acting on a particle in the bulk of an electrolyte while a cylindrical cathode is rotating was carried out. In particular forces depending on the distance from the cathode axis were analysed utilizing rotating cathodes with different diameters.

- When the flow is assumed to be laminar, the forces acting on the particle that push it away from the cathode surface tended to increase, as the distance from the cathode axis is increased. This results in poorer incorporation levels as the distance from the cathode axis was increased.
- At high agitation levels the forces acting on the particle that tend to push it away from the cathode surface still tended to increase as the distance from the cathode axis is increased. Under this hydrodynamic regime the influence of the distance from the cathode axis was more pronounced than that under the laminar regime, the particle incorporation levels, in fact, were found to be very different (an increase of 8-10% when the cathode diameter was increased from 1.27 to 7.8 cm).
- Centrifugal forces are not the only forces acting on the particle when the rotation speed is high. This was proved by the fact that if the incorporated particle density was normalized with respect of cathode diameters (incorporated particles density plotted *vs.* $r\omega^2$) different trends were obtained. A possible force acting at this stage could be due to the electrolyte dynamic viscosity: the higher this viscosity,

which is a function of the electrolyte hydrodynamic regime, the lower the particle mobility.

In order to evaluate the coating thickness influence on particle incorporation processes, a set of trials was carried out using different electrodeposition times.

- Immediately after the initiation of electroco-deposition, particles were in contact with the cathode surface verified by the presence of imprints on the coating surface, but the real incorporation took place in the last seconds of the deposition, when the coating thickness was 70 % larger than the particle diameter.
- This behaviour was related to the reduction of ions adsorbed on the particle surface, suggesting that the higher the adsorbed ions reduction rate the smaller the minimum coating thickness able to incorporate the particles.

17. Future work

Some aspects that were overlooked in the present work and that could be the subject of possible future work to better understand the electroco-deposition of inert particles within a metal matrix are as follows:

- In order to further investigate the coating thickness influence on the particle incorporation process, the experiments carried out in the present work could be repeated using alumina (irregular geometry) instead of PS (spherical geometries) as the second phase material for co-deposition with nickel. The coatings produced in this way should be richer in particle incorporation levels following the assumption that it is easier to incorporate irregular particle geometries rather then regular.
- An in-depth investigation into the production of composite electrodeposits at different current densities in order to investigate the influence of this key parameter on the process. In particular this process variable was found to play a key role when the electrolyte agitation was turbulent. Under this hydrodynamic regime, in fact, the rate determining step was the rate of reduction of the particles adsorbed on the particle surface.
- Investigation of the influence of initial surface roughness on the electroco-deposition process, producing coatings on substrates with different initial roughness. Roughness levels should be quantified.
- Analysis of alumina particles distribution employing other techniques rather than SEM. SEM provides a qualitative analysis, while a quantitative technique should be employed.
- Production of composite electrodeposits using a pulse current. It has been reported that it is possible, by means of pulse current, to obtain more uniform particle distributions than those obtained under DC conditions.
- Investigation of the forces acting on particles in the electrolyte prior to incorporation and their relations with cell geometry (RDE *vs.* RCE) and electrolyte characteristics i.e. conductivity, viscosity.
- Evaluation of the performances of the composite coatings produced. The present work was, in fact, mainly focused on the mechanism of the electrolytic co-deposition, but composite coatings are produced in order to achieve a certain

feature that the metal only coatings cannot provide. Literature suggests, for example, that the co-deposition of alumina with copper improve the wear resistance of the coating. It would be interesting to investigate the appropriate operating conditions such as current density, particle loading, hydrodynamic regime in order to achieve the optimum performance for this characteristic. Other coating properties such as lubricity, coefficient of friction and corrosion resistance are other possible parameters worthy of investigation.

- Production of composite electrodeposits using different metal/second phase material combinations in order to confirm and validate the findings of the present work. A large range of composites can be found in literature. In the present work the investigations were limited to matrix metals of copper, zinc and nickel, but other metals used to produce composites are, for instance, cobalt, silver, gold and metal alloys. Alumina and polystyrene were used as second phase materials, but other possible candidates are graphite, silicon carbide, tungsten carbide, diamond, zirconia, glass, synthetic materials (i.e. PTFE, oil containing capsules) and metallic powders like chromium particles.

18. References

1. C.G. FINK AND J.D. PRINCE, "The Co-deposition of Copper and Graphite", *Transactions of The American Electrochemical Society*, **54**, pge.315 (1928)

2. G.H.L. AQUESSE, Belgian Patent 2571772, (Oct 1951)

3. W. METZGER, *Galvanotechnik*, **63** (8), pge.722 (1972)

4. U. LANDAU, E. YEAGER AND D. KORTAN, "*Plating-New Prospect for an Old Art*", Electrochemistry in Industry, New Directions, Editors, Plenum Press, New York (1982)

5. V.A. ETTEL AND I.H. WARREN, "*Fundamentals, Practice and Control in Electrodeposition - An 'Overview*", Application of Polarization Measurements in the Control of Metal Deposition, Editor, Elsevier, Amsterdam (1984)

6. J.W. DINI, "*Electrodeposition-The Materials Science of Coatings and Substrates*", Editor, Noyes Publications, New Jersey (1993)

7. D. LANDOLT, "Electrodeposition Science and Technology in the Last Quarter of the Twentieth Century", *Journal of the Electrochemical Society*, **149** (3), S9-S20 (2002)

8. F.A. LOWENHAIM, "*Electroplating*", Editor, Mc Graw-Hill, Inc. (1978)

9. W.H. SAFRANEK, "*The Properties of Electrodeposited Metals and Alloys*", 2nd ed., pge. 1, AESF, Orlando, FL (1986)

10. J.H. LINDSAY AND D.D.SNYDER, "*Electrodeposition Technology, Theory and Practice*", L.T. Romankiv and D.R. Turner Editors, PV 87-17, pge.43, The Electrochemical Society Pennington, NJ (1987)

11. K. SHEPPARD, "Something Old, Something New", *The Electrochemical Society Interface*, **4** (2), 25 (1995)

12. L.T. ROMANKIV, "A path: from electroplating through lithographic masks in electronics to LIGA in MEMS", *Electrochimimica Acta*, **42**, pge.2985 (1997)

13. J.M. WEST, "*Electrodeposition and Corrosion Processes*", Editor, Van Nostrand Reinhold Company, London (1965)

14. C.W. DAVIES, "Electrochemistry", *Newnes International Monographs On Corrosion Science And Technology*, General Editor, L. L. Shreir, Ph. D. (Lond.), F.R.I.C., F.I.M.

15. J.P. CELIS AND J.R. ROOS, "Electrolytic and Electroless Composite Coatings", *Reviews in Coatings and Corrosion*, **5**(1-4), pge.1 (1982)

16. C. FAURE, S. RAVAINE AND F. ARGOUL, "Electrochemical Co-deposition of Multilamellar Vescicles in an Inorganic Matrix", *Journal of the Electrochemical Society*, **147** (2), pge.575 (2000)

17. J. EHRHARDT, "Composite Electroplating Using the Brush Technique", *Industrial and Engineering Chemistry – Product Research and Development*, **24** (4), pge.575 (1985)

18. J. O'M. BOCKRIS, A.K.N. REDDY, "*Modern Electrochemistry - An Introduction to an Interdisciplinary Area*", Editors, Plenum/Rosetta.

19. J.P. CELIS, J.R. ROOS, C. BUELENS AND J. FRANSAER, "Mechanism of Electrolytic Composite Plating: Survey and Trends", *Transactions of the Institute of Metal Finishing*, **69** (4), pge.133 (1991)

20. E.A. BRANDES AND D. GOLDTHORPE, "Electroco-deposition of Cermets", *Metallurgica*, **76**, pge.195 (1967)

21. J.E. HOFFMANN AND R.C. ERNST, *INCRA-project No.31*, (1964)

22. R.V. WILLIAMS AND P.W. MARTIN, "Electrodeposited Composite Coatings", *Proceeding Of The 6th International Conference on Electrodeposition and Metal Finishing – Transactions of the Institute of Metal Finishing*, **42**, pge.182 (1964)

23. R. BAZZARD AND P.J. BODEN, "Nickel-Chromium Alloys by Co-deposition: Part 1 – Co-deposition of Chromium Particles in a Nickel Matrix", *Transactions of the Institute of Metal Finishing*, **50**, pge.63 (1972)

24. T. HIRATO, J. FRANSAER AND J.P. CELIS, "Electrolytic Co-deposition of Silica Particles with Alumina from $AlCl_3$-Dimehylsulfone Electrolytes", *Journal of the Electrochemical Society*, **148** (4), C280 (2001)

25. V. TERZIEVA, J. FRANSAER AND J.P. CELIS, "Co-deposition of Hydrophilic and Hydrophobic Silica with Copper from Acid Copper Sulphate Baths", *Journal of the Electrochemical Society*, **147** (1), pge.198 (2000)

26. F.K. SAUTTER, "Electrodeposition of Dispersion-Hardened Nickel-Al_2O_3 Alloys", *Journal of the Electrochemical Society*, **110**(6), pge.557 (1963)

27. F. MATHIS, B. PIERRAGI, B. LAVELLE AND B. CRIQUI, "Deposition Processes and Characterisation of Ni-SiC Composite Coatings", *Automotive Technology and Automation – Proceedings of the 24th ISATA, Florence, Italy*, pge.171 (May 1991)

28. S.H. YEH AND C.C. WAN, "Co-deposition of SiC Powders with Nickel in a Watts Bath", *Journal of Applied Electrochemistry*, **24**(10), pge.993 (1994)

29. H. HAYASHI, S. IZUMI AND I. TARI, "Co-deposition of α-Alumina Particles from Acid Copper Sulfate Bath", *Journal of the Electrochemical Society*, **140**(2), pge.362 (1993)

30. J.P. BONINO, S. LOUBIERE AND A. ROUSSET, "Reactivity and Co-deposition of Co_3O_4 Powders with Nickel in a Watts Bath", *Journal of Applied Electrochemistry*, **28**, pge.1277 (1998)

31. O. BERKH, S. ESKIN, A. BERNER AND J. ZAHAVI, "Electrochemical Cr-Ni-Al_2O_3 Composite Coatings Part I: Some Aspects of the Co-deposition Process", *Plating and Surface Finishing*, **82**(1), pge.54 (1995)

32. A. HOVESTAD AND L.J.J. JANSSEN, "Electrochemical Co-deposition of Inert Particles in a Metallic Matrix", *Journal of Applied Electrochemistry – Reviews in Applied Electrochemistry 40*, **25**(6), pge.519 (1995)

33. A.M.J. KARIAPPER AND J. FOSTER, "Further Studies on the Mechanism of Formation of Electrodeposited Composite Coatings", *Transactions of the Institute of Metal Finishing*, **52**, pge.87 (1974)

34. J.P. CELIS AND J.R. ROOS, " Kinetics of the Deposition of Alumina Particles from Copper Sulfate Plating Baths", *Journal of the Electrochemical Society*, **124**(10), pge.1508 (1977)

35. G.N.K. RAMESH BAPU AND M. MOHAMMED YASUF, "Electrodeposition of Nickel-Vanadium Pentoxide Composite and its Corrosion Behaviour", *Materials Chemistry and Physics*, **36**, pge.134 (1993)

36. E.V. SAKSIN, A.A. SHEVYREV, A.V. SHKURANKOV, L.K. BOBROVSKII AND A.V. ROMANYUK, "Properties and Structure of Metal-Fluoroplastic Composite Coatings", *Russian Journal of Applied Chemistry*, **68**(11), *pt.1*, pge.1596 (1995)

37. R. NARAYAN AND B.H. NARAYANA, "Electrodeposited Chromium-Graphite Composite Coatings", *Journal of the Electrochemical Society*, **128**(8), pge.1704 (1981)

38. A. HOVESTAD, R.J.C.H.L. HEESEN AND L.J.J. JANSSEN, "Electrochemical Deposition of Zinc-Polystyrene Composites in the Presence of Surfactants", *Journal of Applied Electrochemistry*, **29**(3), pge.331 (1999)

39. C. KERR, D. BARKER, F. WALSH AND J. ARCHER, "The Electrodeposition of Composite Coatings Based on Metal Matrix-Included Particle Deposits", *Transactions of the Institute of Metal Finishing*, **78**(5), pge.171 (2000)

40. M. SIMMONS, PhD Thesis, Loughborough University, Loughborough (2002)

41. P. GYFTOU, M. STROUMBOULI, E.A. PAVLATOU AND N. SPYRELLIS, "Electrodeposition of Ni/SiC Composites by Pulse Electrolysis", *Transactions of the Institute of Metal Finishing*, **80**(3), pge.88 (2002)

42. C. BUELENS, J.P. CELIS AND J.R. ROOS, "Electrochemical Aspects of the Co-deposition of Gold and Copper with Inert Particles", *Journal of Applied Electrochemistry*, **13**(4), pge.541 (1983)

43. P.J. SONNEVELD, W. VISSCHER AND E. BARENDRECHT, "The Influence of Suspended particles on the Mass Transfer at a Rotating Disc Electrode. Non-Conducting Particles", *Journal of Applied Electrochemistry*, **20**, pge.563 (1990)

44. D.W. GIBBONS, R.H. MULLER AND C.W. TOBIAS, "Mass transport to Cylindrical Electrodes Rotating in Suspensions of Inert Particles", *Journal of the Electrochemical Society*, **138**(11), pge.3255 (1991)

45. Y. SUZUKI, M. WAJIMA AND O. ASAI, "Cathodic Polarisation Behaviour of Ag-Al2O3 Particles", *Journal of the Electrochemical Society*, **133**(2), pge.259 (1986)

46. S.W. WATSON AND R.P. WALTERS, "The Effect of Chromium Particles on Nickel Electrodeposition", *Journal of the Electrochemical Society*, **138**(12), (1991)

47. S.W. WATSON, "Electrochemical Study of SiC Particle Occlusion During Nickel Electrodeposition", *Journal of the Electrochemical Society*, **140**(8), pge.2235 (1993)

48. B.J.HWANG AND C.S. HWANG, "Mechanism of Co-deposition of Silicon Carbide with Electrolytic Cobalt", *Journal of the Electrochemical Society*, **140** (4), pge.979 (1993)

49. M. VERELEST, J.P. BONINO AND A. ROUSSET, "Electroforming of Metal Matrix Composite: Dispersoid Grain Size Dependence of Thermostructural and Mechanical Properties", *Materials Science and Engineering*, **A135**, pge.51 (1991)

50. R. NARAYAN AND S. CHATTOPADHY, "Electrodeposited Cr-Al_2O_3 Composite Coatings", *Surface Technology*, **16**(3), pge.227 (1982)

51. V.P. GRECO AND W. BALDAUF, "Electrodeposition of Ni-Al_2O_3, Ni-TiO_2 and Cr-TiO_2 Dispersion Hardened Alloys", *Plating*, **55**, pge.250 (1968)

52. J. FOSTER AND B. CAMERON, "The Effect of Current Density and Agitation on the Formation of Electrodeposited Composite Coatings", *Transactions of the Institute of Metal Finishing*, **54**, pge.178 (1976)

53. J. ZAHAVI AND H. KERBEL, "Properties of Electrodeposited Composite Coatings", *Plating and Surface Finishing*, **69**(1), pge.76 (1982)

54. V.D. STANKOVIC AND M. GOJO, "Electrodeposited Composite Coatings of Copper with Inert, Semiconductive and Conductive Particles", *Surface and Coatings Technology*, **81**(2-3), pge.225 (1996)

55. V. SOVA, "Electrodeposited Composite Coatings for Protection from High Temperature Corrosion", *Transactions of the Institute of Metal Finishing*, **65**, pge.21 (1987)

56. E.S. CHEN, G.R. LAKSHMINARAYANAN AND F.K. SAUTTER, "The Co-deposition of Alumina and Titania with Copper", *Metallurgical Transactions*, **2**, pge.937 (1971)

57. J.R. ROOS, J.P. CELIS AND J.S. JELSEN, "Co-deposition of Alpha- and Gamma-Alumina with Copper from Copper Sulphate Baths", *Transactions of the Institute of Metal Finishing*, **55**, pge.113 (1977)

58. J.L. STOJAK AND J.B. TALBOT, "Investigation of Electroco-deposition Using a Rotating Cylinder Electrode", *Journal of the Electrochemical Society*, **146** (12), pge.4504 (1999)

59. P. NOWAK, R.P. SOCHA, M. KAISHEVA, J.P. CELIS AND Z. STOINOV, "Electrochemical Investigation of the Co-deposition of SiC and SiO_2 Particles with Nickel", *Journal of Applied Electrochemistry*, **30**, pge.429 (2000)

60. L. BENEA, P.L. BONORA, A. BORELLO, S. MARTELLI, F. WENGER, P. POINTHIAUX AND J. GALLAND, "Composite Electrodeposition to Obtain Nanostructured Coatings", *Journal of the Electrochemical Society*, **148** (7), C461 (2001)

61. J. MASALKI, B. SZCZYGIEL, J. GLUZEK, "EIS Study of the Co-deposition of SiC Powder with Nickel in a Watts Bath", *Transactions of the Institute of Metal Finishing*, **80**(3), pge.101 (2002)

62. K. KONDO, A. OHGISHI AND Z. TANAKA, "Electrodeposition of Zinc-SiO2 Composite", *Journal of the Electrochemical Society*, **147** (7), pge.2611 (2000)

63. B. BOZZINI, B. BREVAGLIERI, P.L. CAVALLOTTI, G. GIOVANNELLI AND S. NATALI, "Hydrodynamic Problems Related to the Electrodeposition of AuCu/B_4C Composites", *Electrochimica Acta*, **45**, pge.3431 (2000)

64. S. SURVILIENE, L. ORLOVSKAJA, G. BIKULCIUS AND S. BIALLOZOR, "Effect of MoO_2 and TiO_2 on Electrodeposition and Properties of Chromium Coating", *Surface and Coating Technology*, **137**, pge.230 (2001)

65. V.P. GRECO, "A Review of Fabrication and Properties of Electrocomposites", *Plating and Surface Finishing*, **76**(10), pge.68 (1989)

66. Y. SUZUKI AND O. ASAI, "Adsorption Co-deposition Process of Al_2O_3 Particles onto Ag-Al_2O_3 Dispersion Films", *Journal of the Electrochemical Society*, **134**(8), pge.1905 (1987)

67. I. GARCIA, F. FRANSAER, J.P. CELIS, "Electrodeposition and Sliding Wear Resistance of Nickel Composite Coatings Containing Micron and Submicron SiC Particles", *Surface and Coating Technology*, **148**, pge.171 (2001)

68. M.R. KALANTARY AND D.R. GABE, "Vibratory Agitation for Electrodeposition: II Enhancement of Deposition Rate", *Transactions of the Institute of Metal Finishing*, **67**, pge.28 (1989)

69. C.P.S. JOHAL, M.R. KALANTARY AND D.R. GABE, "Vibratory Agitation for Electrodeposition: III Electrodeposition of Composites", *Transactions of the Institute of Metal Finishing*, **67**, pge.31 (1989)

70. N. MASUKO AND K. MUSHIAKE, "Electrodeposition of Ni-Al2O3 Composites on Rotating Cylinder Electrodes", *Journal of the Metal Finishing Society of Japan*, **28**(10), pge.534 (1977)

71. N. MASUKO AND K. MUSHIAKE, "Effect of Rotation of Substrate on Alumina Content of Electrodeposited Nickel-Alumina Composites", *Journal of the Metal Finishing Society of Japan*, **29**(12), pge.646 (1978)

72. J.R. ROOS, J.P. CELIS, H. KELCHTERMANS, M. VAN CAMP AND C. BUELENS, "Kinetics of Electrolytic Co-deposition of Cu-Al_2O_3: Rotating Disc Electrode Experiments", *Proceeding of INTERFINISH '80 – 10th International Congress on Metal Finishing*, pge.203 (1980)

73. N. SOMBATSOMPOP, K. SUKEEMITH, T. MARKPIN AND N.TAREELAP, "A New Experimental Apparatus of Electro-Co-deposited System for Ni-WC Composite Coatings", *Materials Science and Engineering A*, **381**(1-2), pge.175 (2004)

74. J.L. STOJACK AND B. TALBOT, "Effect of Particles on Polarization During Electroco-deposition Using a Rotating Cylinder Electrode" *Journal of Applied Electrochemistry*, **31**, pge.559 (2001)

75. B. BOZZINI, M. SERRA AND A. FANIGLIULO, "Electrochemical Behaviour of Baths for the Co-deposition of Au/B_4C Composites", *Transactions of the Institute of Metal Finishing*, **79**(4), pge.133 (2001)

76. B. BOZZINI AND A. FANIGLIULO, "Raman Spectroscopy of Organic Species Incorporated into Electrodeposited Gold Layer", *Transactions of the Institute of Metal Finishing*, **80**(1), pge.25 (2002)

77. K. HELLE AND A. OPSHOOR, "Electroplating with Fluoropolymer Inclusions", *Proceeding of INTERFINISH '80 – 10th International Congress on Metal Finishing*, pge.234 (1980)

78. K. HELLE AND F. WALSH, "Electrodeposition of Composite Layers Consisting of Inert Inclusions in a Metal Matrix", *Transactions of the Institute of Metal Finishing*, **75**(2), pge.53 (1997)

79. K. HELLE, "Electroplating with Inclusions", *Proceedings 4th International Conference in Organic Coating Science and Technology*, Athens, pge.241 (July 1978)

80. K. HELLE, R.C. GROOT AND A. KAMP, "Co-deposition of a Metal and Fluorocarbon Resin Particles", US Patent 4098654, (1978)

81. Y.S. CHANG AND J.Y. LEE, "Wear Resistant Nickel Composite Coating from Bright Nickel Baths with Suspended Very Low Concentration Alumina", *Materials Chemistry and Physics*, **20**, pge.309 (1998)

82. K. MEGURO, T. USHIDA, T. HIRAOKA AND K. ESUMI, "effect of Surfactants and Surface Treatment on Aqueous Dispersions of Silicon Carbide", *Bulletin of the Chemical Society of Japan*, pge.89 (1987)

83. N.K. SHRESTHA, I. MIWA AND T. SAJI, "Composite Plating of Ni/SiC Using a Cationic Surfactant with Azobenzene Group", *Journal of the Electrochemical Society*, **148**(2), C106 (2001)

84. T.W. TOMASZEWSKI, L.C. TOMASZEWSKI AND H. BROWN, "Satin Nickel by Co-deposition of Finely Dispersed Solids", *Proceeding of the American Electroplaters Society*, **50**, pge.169 (1963)

85. T.W. TOMASZEWSKI, L.C. TOMASZEWSKI AND H. BROWN, "Co-deposition of Finely Dispersed Particles with Metals", Plating, **56**, pge.51 (1991)

86. C.C. LEE AND C.C. WAN, "A Study of the Composite Electrodeposition of Copper with Alumina Powder", *Journal of the Electrochemical Society*, **135**(8), pge.1930 (1988)

87. G.R. LAKSHMINARAYANAN, E.S. CHEN AND F.K. SAUTTER, "The Effects of Chloride Ion on the Co-deposition of Alumina with Copper", *Plating and Surface Finishing*, **63**(4), pge.38 (1976)

88. J.R. ROOS AND J.P. CELIS, "Is the Electrolytic Co-deposition of Solid Particles a Reliable Coating Technology?", *Proceedings 71st American Electroplaters and Surface Finishers Conference, AESF'84, New York*, pge.1 (1984)

89. S. ALEXANDRIDOU, C. KIPARISSIDES, J. FRANSAER AND J.P. CELIS, "On the Synthesis of Oil-Containing Microcapsules and their Electrolytic Co-deposition", *Surface and Coatings Technology*, **71**(3), pge.267 (1995)

90. R.A. TACKEN, P. JISKOOT AND J.J. JANSSEN, "Effect of Magnetic Charging of Ni on Electrolytic Co-deposition of Zn with Ni Particles", *Journal of Applied Electrochemistry*, **26**(2), pge.129 (1996)

91. J.C. WHITTHERS, "Electrodepositing Cermets", *Product Finishing*, **26**, pge.62 (1962)

92. J.M. SYKES AND D.J.ALNER, "The Use of Surface-Active Agents in Promoting Co-deposition of Polymer Particles with Electroplated Metal", *Transaction of the Institute of Metal Finishing*, 51, pge.171 (1972)

93. J.M. SYKES AND D.J.ALNER, "Mechanism for the Formation of Electrodeposited Composite Coatings", *Transaction of the Institute of Metal Finishing*, **52**, pge.28 (1974)

94. T.W. TOMASZEWSKI, "Effects of Anions on the Formation of Electrodeposited Composite Coatings: Some Experimental evidence", *Transaction of the Institute of Metal Finishing*, **54**, pge.45 (1976)

95. N. GUGLIELMI, "Kinetics of the Deposition of Inert Particles from Electrolytic Baths", *Journal of the Electrochemical Society*, **119**(8), pge.1009 (1972)

96. J.P. CELIS, J.R. ROOS AND C. BUELENS, "A Mathematical Model for the Electrolytic Co-deposition of Particles with a Metallic Matrix", *Journal of the Electrochemical Society*, **134**(6), pge.1402 (1987)

97. J.L. VALDES, "Electrodeposition of Colloidal Particles", *Journal of the Electrochemical Society*, **133**(4), pge.223C (1987)

98. J. FRANSAER, J.P. CELIS AND J.R. ROOS, "Analysis of the Electrolytic Co-deposition of Non-Brownian Particles with Metals", *Journal of the Electrochemical Society*, **139**(2), pge.413 (1992)

99. J.VISSER, *J.Coll. Int. Sci.*, **34**, 26 (1970)

100. P.M. VEREECKEN, I. SHAO AND P.C. SEARSON, "Particle Co-deposition in Nanocomposite Films", *Journal of the Electrochemical Society*, **147**(7), pge.2572 (2000)

101. I. SHAO, P.M. VEREECKEN, R.C. CAMMARATA AND P.C. SEARSON, "Kinetics of Particle Co-deposition of Nanocomposites", *Journal of the Electrochemical Society*, **149**(11), pge.C610 (2002)

102. E.L. CUSSLER, "*Diffusion: Mass Transfer in Fluid Systems*", Cambridge University Press, New York (1997)

103. J.S.NEWMAN, "*Electrochemical Systems*", 2nd ed., Prentice Hall, Englewood Cliffs, NJ (1991)

104. V.G. LEVICH, "*Physicochemical Hydrodynamics*", Prentice Hall, Englewood Cliffs, NJ (1962)

105. R. NARAYAN AND B.H. NARAYAN, "Electrodeposited Composite Coatings", *Reviews in Coatings and Corrosion*, **4**(2), pge.113 (1981)

106. W.A. DONAKOWSKI AND J.R. MORGAN, "Zinc/Graphite – A Potential Substitute for Anti-Galling Cadmium", *Plating and Surface Finishing*, pge.315 (1928)

107. E.C. KEDWARD, "Engineering Applications of Electrodeposited Composite Coatings", *Metallurgica*, **55**(8), pge.393 (1988)

108. A. SACHIAN, M. BLIDARIU, E. ROMAN AND C. RADUCANU, " Functional Composite Zinc Electrodeposition", *Transactions of the Institute of Metal Finishing*, **75**(6), pge.213 (1997)

109. J. ZAHAVI AND J. HAZAN, "Electrodeposited Nickel Composite Containing Diamond Particles", *Plating and Surface Finishing*, pge.57 (Feb. 1983)

110. Y.Z. WANG, J.L. WANG, H.M. TAO, G.X. CHENG AND Z.H. DONG, "Preparation and Characterisation of Cu-$MoSi_2$ Composite Coatings", *Transactions of the Institute of Metal Finishing*, **77**(1), pge.52 (1999)

111. G. AKDOGAN, T.A. STOLARSKI AND S. TOBE, "Wear of metal/PTFE coatings in rolling line contact", *Journal of Materials Science*, **37**, pge.5013 (2002)

112. Z. GUO AND X. ZHU, "Studies on Properties and Structure of Electrodeposited RE-Ni-W-B-SiC Composite Coatings", *Materials Science and Engineering*, **A363**, pge.325 (2003)

113. F. FONTENAY, P. MOLLER AND L.B. ANDERSEN, "Corrosion Resistance and Microstructure of Electrolytic Zinc Composite Coatings", *Proceedings of American Electroplaters and Surface Finishers Conference, Surfin 2000, Chicago, USA*, (2000)

114. F. ERLER, C. JAKOB, H. ROMANUS, L. SPIESS, B. WIELAGE, T. LAMPKE AND S. STEINHÄUSER, "Interface Behaviour in Nickel Composite Coatings with Nano-Particles of Oxidic Ceramic", *Electrochimica Acta*, **48**, pge.3063 (2003)

115. M.HIRAMATSU, H. KAWASAKI, Y. NAKAYAMA AND T. OMI, "Surface Morphology and Polymer Adhesion of an Electroplated Zinc/Silica Composite", *Plating and Surface Finishing*, **74**(7), pge.48 (1987)

116. I. MANNA, P.P. CHATTOPADHYAY, B. CHATTERJEE AND S.K. PABI, "Co-deposition of Nanocrystalline Aluminides on a Copper Substrate", *Journal of Materials Science*, **36**, pge.1419 (2001)

117. A.F. ZIMMEMAN, G. PALUMBO, K.T. AUST AND U. ERB, "Mechanical Properties of Nickel Silicon Carbide Nanocomposites", *Materials Science and Engineering*, **A328**, pge.137 (2002)

118. A. KENTEPOZIDOU, C. KIPARISSIDES, F. KOTZIA, C. KOLLIA AND N. SPYRELLIS, "Nickel/Microcapsules Composite Electrocoatings; The Synthesis of Water Containing Microcapsules and Preparation of the Coatings", *Journal of Materials Science*, **31**(5), pge.1175 (1996)

119. Y. KUNUGI, T. NONAKA, Y.B. CHONG AND N. WATANABE, "Preparation of Hydrophobic Zinc and Lead Electrodes and Their Application to Electroreduction of Organic Compounds Electro-Organic reactions on

Organic Electrodes. Part 20: Electrolysis Using Composite-Plated Electrodes. Part IX", *Journal of the Electroanalytical Chemistry Society*, **356**(1-2), pge.163 (1993)

120. Y. ONO AND T. NONAKA, "Electrolysis Using Composite-Plated Electrodes X. Preparation of Hydrophobic Nickel and Zinc Electrodes Composite-Plated Pitch and Their Application in Electroreduction of Organic Compounds", *Denki Kagaku*, **62**(11), pge.1048 (1994)

121. C. IWAKURA, N. FURUKAWA AND M. TANAKA, "Electrochemical Preparation and Characterization of Ni/(Ni + RuO_2) Composite Coatings as an Active cathode for Hydrogen Evolution", *Electrochimica Acta*, **37**(4), pge.757 (1992)

122. H. DASARATHY, C. RILEY, H.D. COBLE, W.R. LACEFIELD AND G. MAYBEE, "Hydroxyapatite/Metal Composite Coatings Formed by Electrodeposition", *Journal of Biomedical Materials Research*, **31**, pge.81 (1996)

123. P. GYFTOU, E.A. PAVLATOU, N. SPYRELLIS AND K.S. HATZILYBERIS, "Nickel Matrix Composite Coatings: Application in Textile Machinery and Evaluation of Cotton Products Quality", *Transactions of the Institute of Metal Finishing*, **78**(6), pge.223 (2000)

124. W. METZGER, *German Patent* DAS 1621206

125. W. METZGER, R. OTT, G. PAPPE AND H. SCHMIDT, "Process for Electroless Metallizing Incorporating Wear-Resisting Particles", *US Patent* 3617363 (1967)

126. N. FELDSTEIN, "Composite Electroless Nickel Coatings for the Aerospace & Airline Industries", *Plating and Surface Finishing*, **85**(11), pge.248 (1998)

127. A. GROSJEAN, M. REZRAZI AND P. BERCOT, "Some Morphological Characteristics of the Incorporation of Silicon Carbide (SiC) Particles into Electroless Nickel Deposits", *Surface and Coatings Technology*, **130**, pge.252 (2000)

128. A. GROSJEAN, M. REZRAZI, J. TAKADOUM AND P. BERCOT, "Hardness, Friction and Wear Characteristics of Nickel-SiC Electroless Composite Deposits", *Surface and Coatings Technology*, **137**, pge.92 (2001)

129. C.M. DAS, A.K. GROVER AND A.K. SURI, "Co-Deposition of Luminescent Particles with Electroless Nickel", *Transaction of the Institute of Metal Finishing*, **80**(4), pge.128 (2002)

130. R.B. BIRD, W.E. STEWART, E.N. LIGHTFOOT, "*Transport Phenomena*", 2nd Edition, Editors, John Wiley & Sons, Inc., New York (2002)

131. R.B. BIRD, C.F. CURTISS, "Tangential Newtonian Flow in Annuli – I – Unsteady State Velocity Profiles", *Chemical Engineering Science*, **11**, pge.108 (1959)

132. R.B. BIRD, C.F. CURTISS, "Tangential Newtonian Flow in Annuli – II – Steady State Pressure Profiles", *Chemical Engineering Science*, **11**, pge.114 (1959)

133. Z. SERHAL, J. MORVAN, P. BERÇOT, M. REZRAZI AND J. PAGETTI, "Determination of the Incorporation Rate of PTFE Particles in Au-Co-PTFE Composite Coatings by InfraRed Reflection Absorption Spectroscopy", *Surface and Coatings Technology*, **145**, pge.233 (2001)

134. Z. SERHAL, J. MORVAN, P. BERÇOT AND M. REZRAZI, "Fast Method of Qualitative Analysis of PTFE Particles in the Au-Co-PTFE Composite Coatings by InfraRed Spectroscopy"", *Surface and Coatings Technology*, **140**, pge.166 (2001)

135. J.E. HOFFMANN AND C.L. MANTEL, "Mechanism of the Co-deposition of Alumina with Electrolytic Copper", *Transactions of the Metallurgical Society of AIME*, **236**, pge.1015 (1966)

136. G.N.K. RAMESH BAPU AND S. MOHAN, "Electrodeposition of Nickel-PTFE Polymer Composites", *Plating and Surface Finishing*, **82**(4), pge.86, (1995)

137. R.N. DUNCAN, *Metal Finishing*, **9**, pge. 33 (1989)

138. B. BOZZINI, *Praktische Metallographie*, **33**, pge. 130 (1996)

139. B. BOZZINI, P.L. CAVALLOTTI AND G. GIOVANNELLI, *AIFM galvanotacnica e Nuove Forniture*, **5**, pge. 92 (1995)

140. F. EBA, Thesis, Université de Franche-Comté, Besançon (1996)

141. E. PENA MUNOZ, Thesis, Université de Franche-Comté, Besançon (1997)

142. E. PENA MUNOZ, P. BERÇOT AND J. PAGETTI, Matériaux et Techniques, **11-12**, pge.19 (1996)

143. E. PENA MUNOZ, P. BERÇOT, A. GROSJEAN, M. REZRAZI AND J. PAGETTI, " Electrolytic and Electroless Coatings of Ni-PTFE Composites. Study of Some Characteristics", *Surface and Coatings Technology*, **107**, pge.85 (1998)

144. ŁOSIEWICZ, A. STEPIEŃ, D. GIERLOTKA AND A. BUDNIOK, "Composite Layers in Ni-P System Containing TiO_2 and PTFE", *Thin Solid Films*, **349**, pge.43 (1999)

145. Z. SERHAL, P. BERÇOT, J. MORVAN, M. REZRAZI AND J. PAGETTI, "Quantitative Characterization of Au-Co-PTFE Composite Coatings by Differential Enthalpic Analysis", *Surface and Coatings Technology*, **150**, pge.290 (2002)

146. M. A. BRIMI and J. R. LUCK, *Electrofinishing*, American Elsevier Publishing Company Inc., New York (1965)

147. K. BARMAK, S.W.BANOVIC, C.M. PETRONIS, D.F. SUSAN AND A.R. MARDER, "Structure of Electrodeposited Graded Composite Coatings of Ni-Al-Al_2O_3", *Journal of Microscopy*, **185**, pge.265 (1997)

148. S.W.BANOVIC, K. BARMAK AND A.R. MARDER, "Characterization of Single and Discretely-Stepped Electro-Composite Coatings of Nickel-Alumina", *Journal of Materials Science*, **34**, pge.3203 (1999)

149. I. GARCIA, A. CONDE, G. LANGEELAN, J. FRANSAER AND J.P. CELIS, "Improved Corrosion Resistance Through Microstructural Modifications Induced by SiC-Particles with Electrolytic Nickel", *Corrosion Science*, **45**, 1173 (2003)

150. J.P. CELIS, J.A. HELSEN, P. HERMANS AND J.R. ROOS, "The Determination of Alumina in a Copper Matrix by Atomic Absorption Spectrometry", *Analytica Chimica Acta*, **92**, pge.413 (1977)

151. L.VELEVA, L. DIAZ-BALLOTTE AND D.O. WIPF, "An In Situ Electrochemical Study of Electrodeposited Nickel-Yttrium Oxide Composite Using Scanning Electrochemical Microscopy", *Journal of the Electrochemical Society*, **150**(1), pge.C1 (2003)

152. L.G. YU AND X.S. ZHANG, "The Friction and Wear Properties of Electroless Ni-Polytetrafluoroethylene Composite Coating", *Thin Solid Films*, **245**(1-2), pge.98 (1994)

153. M. MUSIANI, "Electrodeposition of Composites: an Expanding Subject in Electrochemical Materials Science", *Electrochimica Acta*, **45**, pge.3397 (2000)

19. Further reading

1. D.L. WANG, J. LI, C.S. DAI AND X.G. HU, "An Adsorption Strength Model for the Electrochemical Co-deposition of α-Al_2O_3 Particles and a Fe-P Alloy", *Journal of Applied Electrochemistry*, **29**, pge.437 (1999)

2. L. ORLOVSKAJA, N. PERIÉNNE, M. KURTINAITIENE AND S. SURVILIÉNE, "Ni-SiC Composite Plated Under a Modulated Current", *Surface and Coatings Technology*, **111**, pge.2340 (1999)

3. J.M. MACIEL AND S.M.L. AGOSTINHO, "Construction and Characterisation of a Rotating Cylinder Electrode for Different Technological Applications", *Journal of Applied Electrochemistry*, **29**, pge.741 (1999)

4. A. GROSJEAN, M. REZRAZI, P. BERCOT AND M. TACHEZ, "Adaptation of a Mathematical Model to the Incorporation of Silicon Carbide Particles in an Electroless Nickel Deposit", *Metal Finishing*, pge.14 (April 1988)

5. J. TANG, L. HUANG, S. YAO AND S. ZHOU, "Research on Coatings of Metals and PTFE", *Plating and Surface Finishing*, **85**(9), pge.84 (1998)

6. J.P. CELIS AND J. FRANSAER, "Composite Coatings – New Insight Leading to Improved Process Control", *Transaction of the Institute of Metal Finishing*, **75**(3), pge.118 (1997)

7. D.F. SUSAN, K. BARMAK AND A.R. MARDER, "Electrodeposited Ni-Al Particle Composite Coatings", *Thin Solid Films*, **307**, pge.133 (1997)

8. J. FRANSAER, .P. CELIS AND J.R. ROOS, "Variations in the Flow of Current to Disk Electrodes Cause by Particles", *Journal of Electroanalytical Chemistry*, **391**, pge.11 (1995)

9. P.R.WEBB AND N.L. ROBERTSON, "Electrolytic Co-deposition of Ni-γ–Al_2O_3 Thin Films", *Journal of the Electrochemical Society*, **141**(3), pge.669 (1994)

10. G.N.K. RAMESH BAPU, "Electroco-deposition and Characterization of Nickel-Titanium Carbide Composites", *Surface and Coatings Technology*, **67**, pge.105 (1994)

11. A. TAKAHASHI, Y. MIYOSHI AND T. HADA, "Effect of SiO_2 Colloid on the Electrodeposition of Zinc-Iron Group Metal Alloy Composites", *Journal of the Electrochemical Society*, **141**(4), pge.954 (1994)

12. Y. SOFER, Y. YARNITZKY AND S.F. DIRNFELD, "Evaluation and Uses of Composite Ni-Co Matrix Coatings with Diamond on Steel Applied by Electrodeposition", *Surface and Coatings Technology*, **42**(3), pge.227 (1990)

13. C. WHITE AND J. FOSTER, "Factors Affecting the Entrapment of Alumina Particles During the Electrodeposition of Copper", *Transaction of the Institute of Metal Finishing*, **59**, pge.8 (1980)

14. J.P. CELIS, H. KELCHTERMANS AND J.R. ROOS, "Properties of Electrodeposited Copper-Alumina Coatings", *Transaction of the Institute of Metal Finishing*, **56**, pge.41 (1978)

15. J. FOSTER AND A.M. KARIAPPER, "A Study of the Mechanism of Formation of Electrodeposited Composite Coatings", *Transaction of the Institute of Metal Finishing*, **51**, pge.27 (1972)

16. D.W. SNAITH AND P.D. GROVES, "A Study of the Mechanism of Cermet Electrodeposition", *Transaction of the Institute of Metal Finishing*, **50**, pge.95 (1971)

17. D.W. SNAITH AND P.D. GROVES, "Some Further Studies of the Mechanism of Cermet Electrodeposition: Part 2 – Variable Factors in the Process of Electrodeposition of Metal-Matrix Composites", *Transaction of the Institute of Metal Finishing*, **56**, pge.9 (1977)

18. M. EISENBERG, C.W. TOBIAS AND C.R. WILKE, "Ionic Mass Transfer and Concentration Polarization at Rotating Electrodes", *Journal of the Electrochemical Society*, **101**(6), pge.306 (1954)

19. A.G. McCORMAK, M.J. POMEROY AND V.J. CUNNANE, "Microstructural development and Surface Characterization of Electrodeposited Nickel-Yttria Composite Coatings", *Journal of the Electrochemical Society*, **150**(5), pge.C356 (2003)

20. P. BERCOT, E. PENA MUNOZ AND J. PAGETTI, "Electrolytic Composite Ni-PTFE Coatings: an Adaptation of Guglielmi's Model for the Phenomena of Incorporation", *Surface and Coatings Technology*, **157**, pge.282 (2002)

21. X.H. CHEN, F.Q. CHENG, S.L.LI, L.P. ZHOU AND D.Y. LI, "Electrodeposited Nickel Composites Containing Carbon Nanotubes", *Surface and Coatings Technology*, **155**, pge.274 (2002)

22. C. MÜLLER, M. SARRET AND M. BENBALLA, "ZnNi/SiC Composites Obtained from an Alkaline Bath", *Surface and Coatings Technology*, **162**, pge.49 (2002)

23. V. MEDELIENE, "The Influence of B_4C and SiC Additions on the Morphological, Physical, Chemical and Corrosion Properties of Ni Coatings", *Surface and Coatings Technology*, **154**, pge.104 (2002)

24. P.A. GAY, P. BERCOT AND J. PAGETTI, "Electrodeposition and Characterisation of Ag-ZrO_2 Electroplated Coatings", *Surface and Coatings Technology*, **140**, pge.147 (2001)

25. Y. WANG, E.R. FACHINI, G. CRUZ, Y. ZHU, Y. ISHIKAWA. J.A. COLUCCI AND C.R. CABRERA, "Effect of Surface Composition of Electrochemically Co-deposited Platinum/Molybdenum Oxide on Methanol Oxidation", *Journal of the Electrochemical Society*, **148**(3), pge.C222 (2001)

26. X. PENG, D. PING, T.LI AND W. WU, "Oxidation Behaviour of a Ni-La_2O_3 Co-deposited Film on Nickel", *Journal of the Electrochemical Society*, **145**(2), pge.389 (1998)

27. M. MUSIANI AND P. GUERRIERO, "Electrodeposited Tl_2O_3-Matrix Composites: I. Effect of the Dispersed Phase on Nucleation and Growth of the Matrix", *Journal of the Electrochemical Society*, **145**(2), pge.549 (1998)

28. A.F. KARAN, J.M. KRAFTT AND G. STREMSDOERFER, "An Investigation of Activation of PTFE and Graphite Fine Particles Prior to Electroless Plating", *Transaction of the Institute of Metal Finishing*, **76**(2), pge.69 (1998)

29. Y.L. WANG, Y.Z. WAN, S.M. ZHAO, H.M. TAO AND X.H. DONG, "Electrodeposition and Characterization of Al_2O_3-Cu(Sn), CaF_2-Cu(Sn) and Talc-Cu(Sn) Electrocomposite Coatings", *Surface and Coatings Technology*, **106**, pge.162 (1998)

30. S.H. YEH AND C.C. WAN, "A Study of SiC/Ni Composite Plating in the Watts Bath", *Plating and Surface Finishing*, **84**(3), pge.54 (1997)

31. R.R. OBERLE, M.R. SCANLON, R.C. CAMMARATA AND P.C. SEARSON, "Processing and Hardness of Electrodeposited Ni/Al_2O_3 Nanocomposites", *Applied Physics Letters*, **66**(1), pge.19 (1995)

32. V. BHALLA, C. RAMASAMY, N. SINGH AND M. PUSHPAVANAM, "Friction and Wear Characteristics of Electrodeposited Copper Composites", *Plating and Surface Finishing*, **82**(11), pge.58 (1995)

33. KEDDAM, S. SENYARICH, H. TAKENOUTI, "A Composite Electrode for Studying Powdered electroactive Materials: Preparation and Performances", *Journal of Applied Electrochemistry*, **24**, pge.1037 (1994)

34. N. PERIENÉ, A. ČEŠUNIENÉ AND L. TAICAS, "Nickel Electrodeposits with Improved Hot Oxidation and Corrosion Resistance by Co-deposition of Submicron Powders", *Plating and Surface Finishing*, **80**(10), pge.73 (1993)

35. F. BECK, M. DAHLHAUS AND N. ZAHEDI, "Anodic Co-deposition of polypyrrole and Dispersed TiO_2", *Electrochimica Acta*, **37**(7), pge.1265 (1992)

36. J.W. GRAYDON AND D.W. KIRK, "Suspension Co-deposition in Electrowilling Cells: the Role of Hydrodynamics", *The Canadian Journal of Chemical Engineering*, **69**, pge.564 (1991)

37. J.W. GRAYDON AND D.W. KIRK, "Suspension Electrodeposition of Phosphorous and Copper", *Journal of the Electrochemical Society*, **137**(7), pge.2061 (1990)

38. J. SADOWSKA-MAZUR, M.E. WARWICK AND R. WALKER, "Electrodeposition and Properties of Tin-Nickel/Silicon Carbide Composite Coatings", *Transaction of the Institute of Metal Finishing*, **64**, pge.142 (1986)

39. C.A. ADDISON AND E.C. KEDWARD, "The Development of Chromium Based Electrodeposited Composite Coatings", *Transaction of the Institute of Metal Finishing*, **55**, pge.41 (1977)

40. E.C. KEDWARD, C.A. ADDISON AND A.A.B. TENNETT, "The Development of a Wear Resistant Electrodeposited Composite Coating for Use on Aero Engines", *Transaction of the Institute of Metal Finishing*, **54**, pge.8 (1976)

41. E.C. KEDWARD, A.I.M.F., "Electrodeposited Composite Coatings for Tribological Applications", *Metallurgia*, pge.225 (June, 1969)

42. E. GILLAM, K.M. McVIE AND M. PHILLIPS, "The Structure of Nickel Electrodeposited with Alumina Particles", *Journal of the Institute of Metals*, **94**, pge.228 (1966)